Samuel Timothy Cahill
Keble College

D.Phil Thesis
Trinity Term, 2017

Structural and Kinetic Studies on β-Lactamase Mechanism and Inhibition

β-Lactamases constitute one of the most prevalent identified mechanisms of bacterial resistance to the β-lactam antibiotics. These enzymes are broadly divided into two mechanistic subclasses, the serine-β-lactamases and the metallo-β-lactamases. The metallo-β-lactamases constitute an important subclass of β-lactamases on account of their ability to hydrolyse almost all classes of β-lactam, in particular the carbapenems, which are considered to be β-lactams of last resort. At present inhibitors of the serine-β-lactamases are clinically available for the treatment of resistant bacterial infections; these include clavulanic acid and related compounds, and more recently avibactam. However, there are currently no clinically validated inhibitors of the metallo-β-lactamases.

Structural and mechanistic study of the β-lactamases will aid in the development of novel inhibitor scaffolds with clinical potential in the treatment of resistant bacterial infections. In this work, the ability of the metallo-β-lactamases to promiscuously bind and employ transition metals, other than their native zinc, in catalysis is described in the context of ferrous iron. The effects of metal substitution on enzyme structure, mechanism and susceptibility to inhibitors are investigated. These studies demonstrate that the metallo-β-lactamases are able to employ iron, a transition metal of relatively high bioavailability, in catalysis with only small changes in catalytic efficiency.

In an increasing number of cases, bacteria are found to exhibit resistance to β-lactams mediated by both serine- and metallo-β-lactamases, simultaneously. With this likely to be an important issue in the future, the utility of developing molecules with the capability to inhibit both serine- and metallo-β-lactamases cannot be understated. In the work described herein, cyclic boronic acids were explored as a chemotype with inhibitory activity against the two mechanistic classes of β-lactamase and are shown to be potent inhibitors of both. Structural characterisation of the cyclic boronic acids in complex with β-lactamases reveals that their inhibitory activity likely derives from their mimicking of a tetrahedral anionic intermediate common to both mechanistic classes of β-lactamase. The activity of these molecules against clinically derived resistant bacterial strains is also explored.

While the metallo-β-lactamases are largely studied on account of their involvement in antibiotic resistance, the metallo-β-lactamase protein fold can facilitate a diverse range of chemistry from small molecule hydrolysis, to DNA and RNA processing, to oxidoreductase reactions. Moreover, a number of human enzymes share the metallo-β-lactamase fold. Thus the study of these human enzymes and development of activity assays for their functions will likely prove useful in the discovery of bacterial metallo-β-lactamase inhibitors with low toxicity in human patients. In this thesis, efforts made in the development of a novel high throughput assay for the unusual metallo-β-lactamase persulfide dioxygenase ETHE1 *via* the fluorescent detection of sulfite are described.

Overall, the work of this thesis explores the mechanism of β-lactamases as a framework for the discovery of novel β-lactamase inhibitors, and makes efforts in the development of novel assays for human metallo-β-lactamase fold enzymes to expedite the development of such molecules.

Firstly, heartfelt thanks go to my supervisor Prof. Christopher J. Schofield for allowing me to work in his lab, for his ongoing help and support, and for his never ending supply of ideas. I'm grateful for the environment of scientific freedom provided and the opportunity to try new things, even if they were doomed to failure.

An enormous debt is owed to Dr Jürgen Brem. Thank you for your ever present help, immensely broad knowledge of β-lactamases, and continued friendship that have, no doubt, helped to make these past three years a much smoother and more efficient experience.

Thanks are also due to Dr Anne Makena, for her help with metallo-β-lactamases, Dr Hanna Tarhonskaya, for her knowledge of stopped-flow kinetics, Dr Ilaria Pettinati for her assistance with cloning and all things ETHE1, and Dr Mike McDonough for his knowledge on, and assistance with, crystallography. Thanks to each of these for their continued friendship and support.

Thank you to my collaborators Dr James Spencer, and Dr David Wareham for their experimental support of my research and their help, opinions, and useful suggestions in the writing of publications.

I would also like to thank Dr Adam Hardy, Wendy Sobey and Manso Jubier Herminio for their lab management expertise and support of the CJS group, and indeed the entire CJS group for creating a supportive, friendly and inquisitive environment.

Thanks to the BBSRC and Keble College for funding and financial support over these four years spent in Oxford.

Finally, a huge thank you to my housemates of these past three years, Julia Busch, Andrea Lei Leston and Andra Necula, for your support, whenever necessary, and your heartfelt friendship, and to my mother, who, despite having no clue about what I've been up to these past four years, is an ever present source of loving encouragement.

A description of contributions from collaborators is present at the start of each chapter, and individual contributions are highlighted in the main text, where appropriate. All other experiments described in this thesis were carried out personally.

Abbreviations

(v/v)	Volume to volume ratio
(w/v)	Weight to volume ratio
2TY	2x Yeast tryptone medium
3-MST	3-Mercaptopyruvate sulfurtransferase
6-APA	6-Aminopenicillanic acid
7-ACA	7-Aminocephalosporanic acid
AA	L-α-aminoadipic acid
ACE	Angiotensin-converting enzyme
ACV	D-(L-α-aminoadipoyl)-L-cysteinyl-D-valine
AmpC	Class C serine-β-lactamase
AtETHE1	ETHE1 from *Arabidopsis thaliana*
ATP	Adenosine triphosphate
BcETHE1	ETHE1 from *Burkholderia cepacia*
BcII	*Bacillus cereus* β-lactamase II
Bla	β-Lactamase
BlaC	β-lactamase from *Mycobacterium tuberculosis*
CBS	Cystathionine-β-synthase
CcrA	Cefoxitin and carbapenem resistant metallo-β-lactamase
CD	Circular dichroism
CDO	Cysteine dioxygenase
Cm1A	Chloramphenicol biosynthesis enzyme
CMAH	Cytidine-5'-monophospho-*N*-acetyl-neuraminic acid hydroxylase
CphA	Carbapenem hydrolysing enzyme from *Aeromonas hydrophila*
CSA	Cysteine sulfenic acid
CSE	Cystathionine-γ-lyase
CSPF	Cleavage and polyadenylation specificity factor
CTX-M	Cefotaxime hydrolase from Munich
DCLRE	DNA cross-link repair enzyme
DMSO	Dimethyl sulfoxide
DNA	Deoxyribonucleic acid
dNTP	Deoxynucleoside triphosphate
EDTA	Ethylenediaminetetraacetic acid
EPR	Electron paramagnetic resonance
ESAC	Extended spectrum AmpC
ESBL	Extended spectrum β-lactamase

ESI-MS	Electrospray ionisation mass spectrometry
ETHE	Ethylmalonic encephalopathy
FEZ	*Fluoribacter gormanii* endogenous zinc β-lactamase
FprA	A-type flavoprotein
GIM	German imipenemase
GOB	*Chryseobacterium meningosepticum* β-lactamase
GSH	Glutathione
GSSH	Glutathione persulfide
hETHE1	ETHE1 from human
hMBL	Human metallo-β-lactamase fold enzyme
HPLC	High performance liquid chromatography
IC_{50}	50% inhibitory concentration
IMI	Imipenemase
ImiS	Imipenemase from *Aeromonas veronii bv. Sobria*
IMP	Metallo-β-lactamase imipenemase
IPNS	Isopenicillin N synthase
IPTG	Isopropyl β-D-1-thiogalactopyranoside
KPC	*Klebsiella pneumoniae* carbapenemase
L1	Labile enzyme from *Stenotrophomonas maltophilia*
LB	Luria-Bertani medium
λ_{em}	Emission Wavelength
λ_{ex}	Excitation wavelength
λ_{max}	Maximum absorbance wavelength
MBL	Metallo-β-lactamase
MIC	Minimum inhibitory concentration
MRSA	Multi-drug resistant *Staphylococcus aureus*
MS	Mass spectrometry
Mx2ETHE1	ETHE1 isoform 2 from *Myxococcus xanthus*
MxETHE1	ETHE1 isoform 1 from *Myxococcus xanthus*
NAPE-PLD	*N*-Acylphosphatidylethanolamine-hydrolysing phospholipase
NDM	New Delhi metallo-β-lactamase
NMR	Nuclear magnetic resonance
OD_{600}	Optical density at 600 nm
OXA	Oxacillinase
P99	β-lactamase from *E. cloacae* strain P99
PBP	Penicillin binding protein

Pce	Phosphorylcholine esterase
PCR	Polymerase chain reaction
PMSF	Phenylmethylsulfonyl fluoride
PNKD	Paroxysmal nonkinesiogenic dyskinesia protein
PpETHE1	ETHE1 from *Pseudomonas putida*
Q-TOF	Quadrupole time of flight
RA	Residual activity
RMSD	Root-mean-square deviation
RNA	Ribonucleic acid
ROO	Rubredoxin:oxygen reductase
SBL	Serine-β-lactamase
SDO	Sulfur dioxygenase
SDS-PAGE	Sodium dodecyl sulfate polyacrylamide gel electrophoresis
SEC-MALS	Size exclusion chromatography with multi-angle light scattering
Sfh	*Serratia fonticola* carbapenem hydrolase
SHV	Sulfhydryl reagent variable β-lactamase
SOC	Super optimal catabolite repression outgrowth medium
SPM	São Paulo metallo-β-lactamase
SPR	Surface plasmon resonance
SQR	Sulfide:quinone reductase
SUOX	Sulfite oxidase
TCEP	*Tris*(2-carboxyethyl)phosphine
TEM	Temoneira β-lactamase
TEMED	Tetramethyleneethylenediamine
T_m	50% Melting temperature
TMA	Thiomandelic acid
TST	Thiosulfate sulfur transferase
VIM	Verona integron-encoded metallo-β-lactamase

Chapter 2: Use of Ferrous Iron By Metallo-β-Lactamases

Chapter 3: Cyclic Boronates Inhibit All Classes of β-Lactamase

Chapter 1: General Introduction

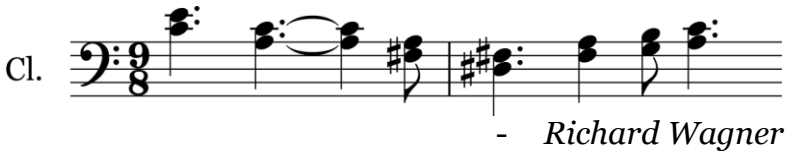

- *Richard Wagner*

Contents

1.1. Antibiotic Chemotherapy: *Eine Zauberkugel*

Throughout human history, infections have constituted an important threat to public health both in the form of contagious diseases or sepsis of wounds, acquired either through surgery or the general vicissitudes of life(1). The clinical introduction of antibiotics in the early 20th century, alongside increasing sanitation and the use of antisepsis has had an enormous impact on life expectancy(2), with estimates that global life expectancy may have increased by up to 10 years solely due to the introduction of antibiotics(3). Although often used interchangeably with antibacterials, the term antibiotic, first coined by Selman Waksman(4), originally referred to any metabolic product of one organism that antagonises the growth of another, with antibacterials, antifungals and antiparasitics constituting individual subclasses of antibiotics. Antibiotics may be further subcategorised based on their ability to either inhibit the growth of, or kill, microorganisms upon dosing, for example bactericidals kill bacteria, while bacteriostatics merely inhibit their ability to grow and divide, allowing bacterial cells to recover once the antibacterial has ceased to be administered(5).

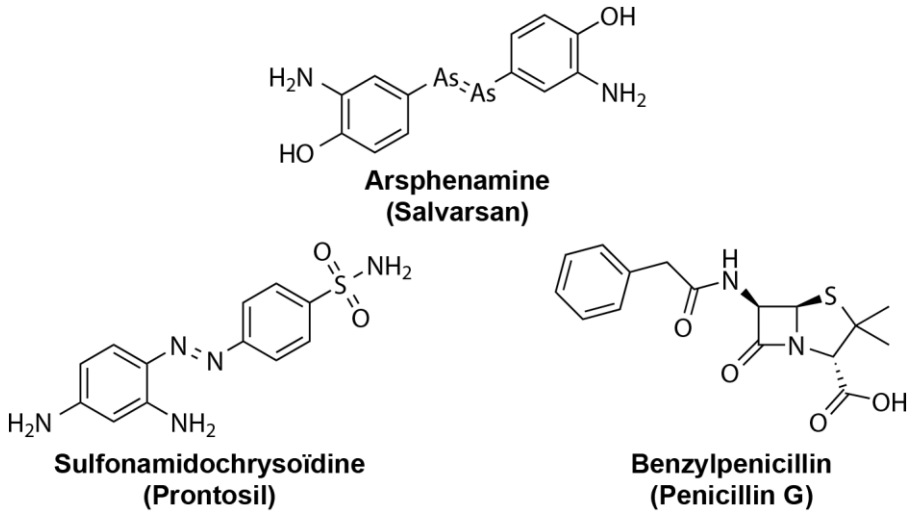

Figure 1.1: Chemical structures for examples from the first marketed classes of antibiotic. Their trade names are indicated in brackets.

Paul Ehrlich first pioneered the idea of chemotherapy in the form of a '*magic bullet*' as a method of treating infection, suggesting that, with strategic reasoning, chemistry might be aimed like a gun to specifically target a pathogen(6). Ehrlich's arsphenamine (marketed as Salvarsan, Figure 1.1) constitutes the first synthesised antibiotic agent used clinically for the treatment of syphilis and trypanosomal infections(7, 8). Arguably, given its noticeable toxicity in patients, Salvarsan was not the '*magic bullet*' that Ehrlich was shooting for. The first organic compound that demonstrated selective toxicity towards bacteria was sulfamidochrysoïdine (marketed by Bayer as Prontosil)(9). Prontosil exerts it effect as a dihydropteroate synthase inhibitor, blocking a key step in folate synthesis, so preventing

Gram-positive bacteria from synthesising nucleic acids(10). Importantly, folic acid is a human vitamin (vitamin B) and hence is acquired through diet and not metabolically synthesised. This allows Prontosil to selectively act on bacteria in infections, thus rendering it the first clinically used bacteriostatic antibacterial and a magic bullet much closer to Ehrlich's original intention.

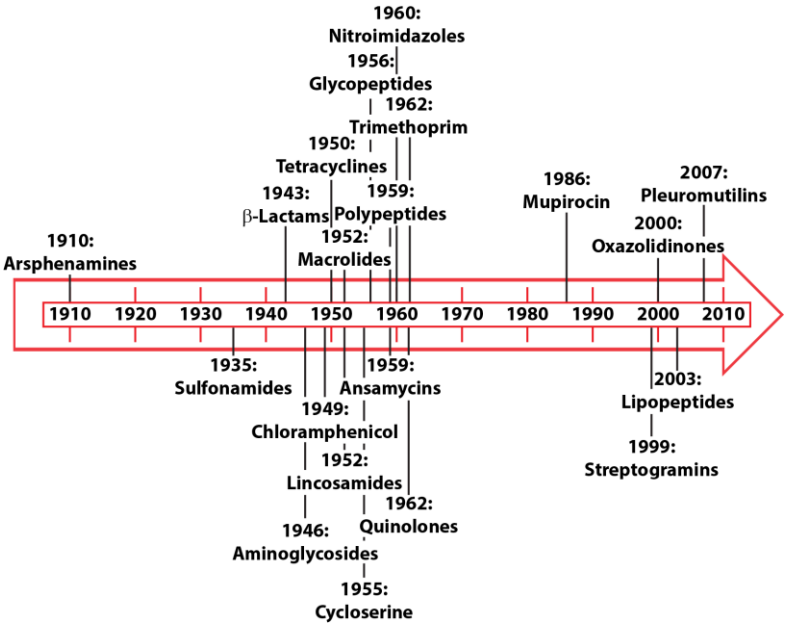

Figure 1.2: Timeline for the clinical introduction of novel classes of antibiotic. The lack of novel antibiotics between the early 1960s and late 1990s is made clear by the introduction of only one new class, mupirocin. While the introduction of four new classes, from 1999 to the present, reflect a rekindling of interest in antibiotic research.

Following the identification and successful application of sulfonamides in the 1930s, no fewer than 18 chemically distinct classes of antibacterial have been brought into clinical use(11-30). The structures of these compounds range from small molecules, like cycloserine(31-33) and the nitroimidazoles(34, 35), to the macrocyclic polyketide macrolides(36-39)(Figure 1.2), with molecular mechanisms ranging from inhibition of cell wall biosynthesis to that of protein and DNA/RNA synthesis(40). The substantial outpouring of new antibiotic classes between the 1940s and early 1960s lead some to declare man's victory over infectious disease(41), and the surfeit of available drugs lead the pharmaceutical industry to become disinterested in new antibiotic research, given the competition in this marketplace(42). Thus, with a couple of exceptions, any new antibiotics introduced from the 1970s to the 1990s were likely analogues of a pre-existing class, with little novelty in their mechanism of action(43). However the rise of antibiotic resistance as a global health concern(44, 45), with the potential to rival pre-antibiotic infectious disease(46), has more

recently rekindled interest, at least academically, in the need for new bactericidals, or, indeed, methods for the continued use of pre-existing classes(47, 48). Growth of 'unculturable' soil bacteria, as well as exploration of unusual bacterial ecosystems in recent years has resulted in the discovery of new antibiotics(49, 50), suggesting that sources of new antibiotics and new antibiotic classes are far from exhausted.

1.2. The β-Lactam Antibiotics

Among the various established classes of antibacterial, the β-lactams are arguably the most important, constituting around 60% of total worldwide antibiotic use(51, 52). The β-lactams are divided into four main subclasses, the penicillins (or penams), cephems, penems and monobactams, in order of their discovery. Despite being one of the first antibiotic classes to be discovered, the β-lactams remain a preferred class on account of their notable efficacy, general affordability, and low toxicity(53-55). The β-lactams are each characterised by a β-lactam ring (Figure 1.3), whose presence is crucial for antibacterial activity. The penams, cephems and carbapenems all exhibit a fused bicyclic core; the β-lactam ring may be fused to a thiazolidine ring, as in penams, to a dihydropyrrole or dihydrothiazole ring, for carbapenems or penems, respectively, or to a dihydrothiazine ring, as in cephalosporins and cephamycins.

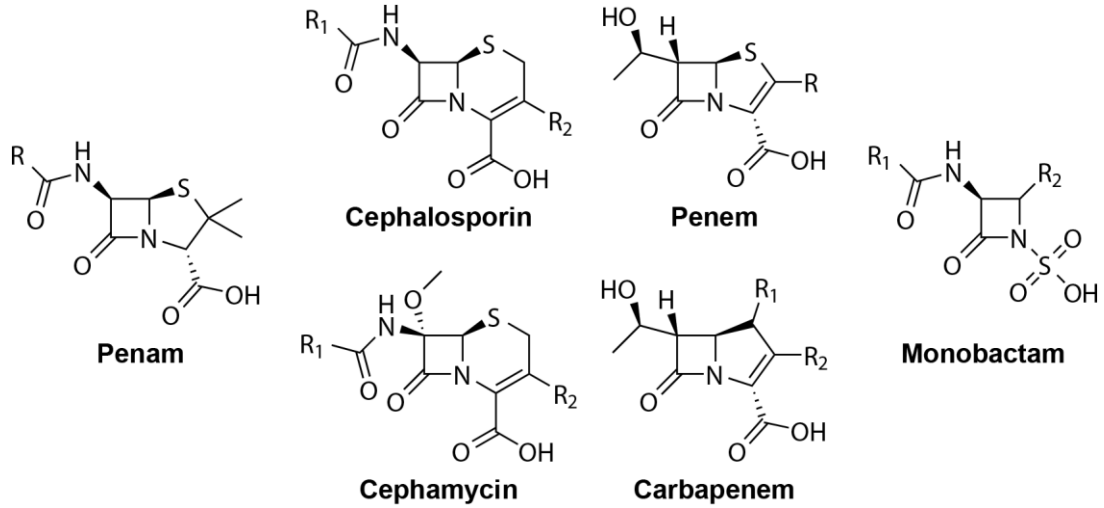

Figure 1.3: General structures of the major classes of β-lactam antibiotic. The four membered β-lactam ring, essential for function, is maintained in each of these classes.

1.3. A Brief History of β-Lactams

Although the discovery of penicillin is often credited to Sir Alexander Fleming(13), there are multiple accounts of inhibition of bacterial cell growth by *Penicillium* strains that predate his report(56, 57). In 1871, John Burdon Sanderson observed that *Penicillium* mould prevented bacterial growth both in culture fluid and in dissected guinea pig muscle(58). Around the

same time, Joseph Lister observed that the presence of *Penicillium* mould resulted in the growth of abnormal degenerate bacteria, or a complete absence of bacteria, in urine based cultures(59). Lister even went as far to suggest that *Penicillium* extracts might be used as an antiseptic against bacteria(60) and may have even used a crude extract in the treatment of an infected patient(61, 62), although Lister did not document this himself. Later observations made by William Roberts, led him to postulate on the possibility of antibiosis – either of one bacterial species against another, or between a fungus and bacteria – this is probably the first published statement on the subject(63). Similar work was published by John Tyndall and Thomas Henry Huxley(64), with Tyndall making the additional observation that the antibiotic effect of *Penicillium* was not apparent against a certain bacterial strain (likely *Pseudomonas sp.*). In France, Louis Pasteur and Jules Francois Joubert published observations of fungi inhibiting the growth of *Bacillus anthracis* in 1877(65), while in 1897 Ernest Duchesne successfully treated guinea pigs infected with typhoid using a culture of *Penicillium glaucum*(66).

Standing on the shoulders of these scientists, amongst others, Fleming made his observation of the bactericidal effect of *Penicillium notatum* (now *Penicillium chrysogenum*)(13). Arguably he was among the first to observe this phenomenon *and* attribute the correct cause to the effect, i.e. the release of some sort of toxic metabolite from the fungus, nominally penicillin, which was able to induce bacterial lysis.

Despite Fleming's report, the success of penicillin only became apparent once Howard Florey, professor of pathology in Oxford, took up the project. He, together with Ernst B. Chain and Norman Heatley successfully purified penicillin and demonstrated its antibacterial activity in mice infected with *Streptomonas pyrogenes*, *Staphylococcus aureus*, or *Clostridium septique*(67). An initial attempt at using partially purified penicillin to cure a patient with septicaemia resulted in marked improvement before subsequent deterioration due to a lack of enough of the drug(68, 69). However, the Oxford scientists failed to produce large quantities of highly purified penicillin. Efficient wartime collaboration with US industry lead to the use of a more productive *Penicillium chrysogenum* strain (isolated from a mouldy cantaloupe), the move to deep fermentation methods for growth of *Penicillium* fungus, and, crucially, more developed methods for the fermentation, recovery, and purification of penicillins with hydrophobic C-6 side chains, with the now high-yield drug being responsible for saving countless lives in World War II and even more with its subsequent introduction among civilian populations(70, 71). Continued work on penicillin revealed its β-lactam structure (Figure 1.4) in 1949 thanks to the work of Dorothy Hodgkin(72) and the subsequent total synthesis(73, 74) and isolation of 6-aminopenicillanic acid (6-APA, Figure 1.4) from fermentation liquor(75, 76) lead to the development of the semi-synthetic penicillins through the introduction of unnatural acetamido chains at the C-6

position (Figure 1.4), which collectively exhibited a broader spectrum of activity and increased bioavailability(77-79).

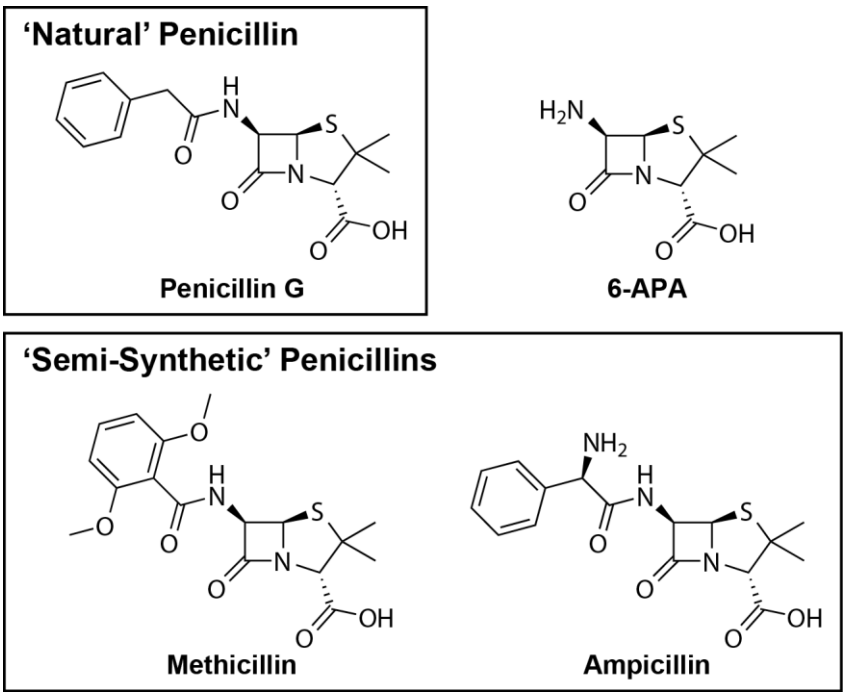

Figure 1.4: The structure of the 'natural' fermented penicillin, penicillin G, and its hydrolysed product 6-APA. Two examples of semi-synthetic penicillins, derived, by acylation of 6-APA are shown.

Alongside the success of the growing penicillin antibiotic family, there remained a keen interest in the discovery of novel antibiotics. Isolation of *Cephalosporium acremonium* from a sea water sample by Giuseppi Brotzu(80, 81) lead to the identification and purification of cephalosporin C by Guy Newton and Sir Edward Abraham in 1956(82). Cephalosporin C was observed to have generally lower, but broader, antibacterial activity (against both Gram-positive and Gram-negative bacteria) and was found to be more stable to acid and enzyme-mediated hydrolysis than the penicillins(82). Solution of the cephalosporin C structure revealed it to also be a β-lactam antibiotic, like the penicillins, but with an expanded dihydrothiazine ring (Figure 1.5)(83, 84). Similarly to the penicillins, isolation of the core 7-aminocephalosporanic acid (7-ACA) molecule enabled the synthesis of new generations of cephalosporin antibiotics through modification of the C-7 amino acyl side chain as well as alteration at the C-3 position, leading to multiple generations of cephalosporins with varied spectra of activity(85, 86).

Monocyclic β-lactams, produced by bacteria, were identified in the 1970s with the first, nocardicin A, being produced by *Nocardia uniformis*(Figure 1.5)(87). Similarly the monocyclic β-lactams, sulfazicin and formadicin, were isolated from *Pseudomonas acidophila* and *Flexibacter alginoliquefaciens*, respectively (88, 89). However, these

molecules only showed moderate antibacterial activity and it was not until the synthesis of aztreonam, with a 2-oxo-azetidine-1-sulfonic acid core, that a commercial monobactam became available(90). Aztreonam was followed by tigemonam(91) and carumonam(92, 93), although these latter monobactams are no longer marketed.

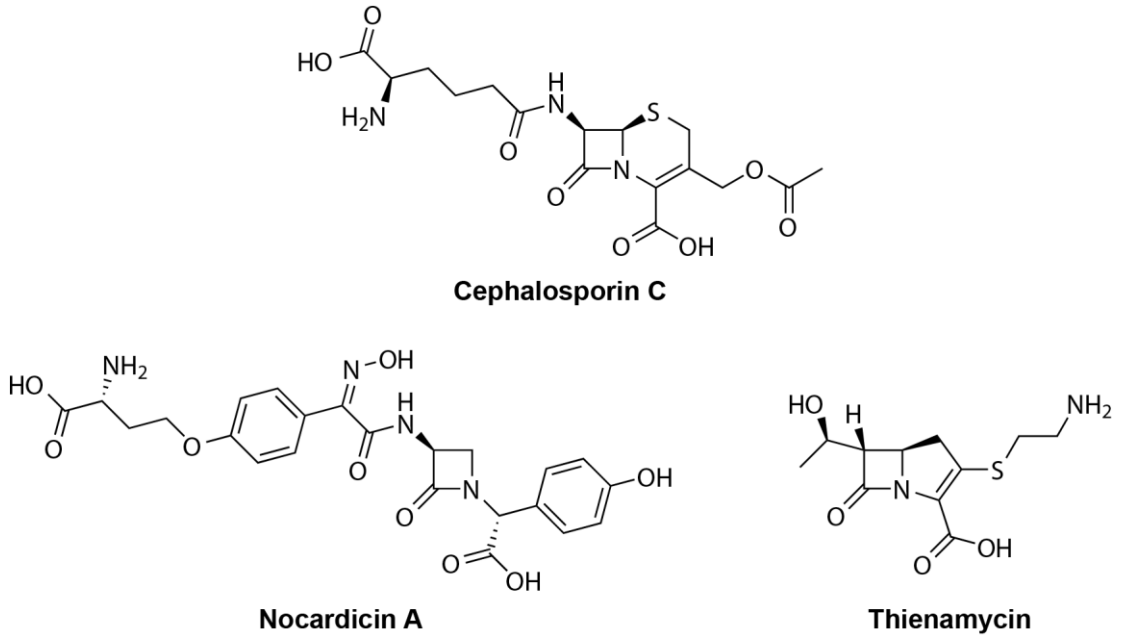

Figure 1.5: Chemical structures of the first isolated cephalosporin, cephalosporin C, monobactam, nocardicin A, and carbapenem, thienamycin.

In the 1980s, the carbapenem antibiotics were also isolated from β-lactam producing bacteria, with the first, thienamycin, being extracted from a fermentation broth of *Steptomyces cattleya* (Figure 1.5)(94, 95). This was followed up by a more chemically stable derivative, imipenem(96). Due to its rapid metabolism by the human dehydropeptidase enzyme, imipenem must be co-administered with the dehydropeptidase inhibitor cilastatin(97). Addition of a methyl substituent at the C-1 position of the carbapenem(98), as exemplified by meropenem(99), doripenem(100), and ertapenem(101), resulted in increased stability of these carbapenems to dehydropeptidase activity and removed the need for co-administration of cilastatin. Due to their high potency and broad spectrum of activity against both Gram-positive and Gram-negative bacteria, the carbapenems are often used as last resort antibiotics in resistant infections(102).

1.4. Mechanism of β-Lactam Antibacterials

The β-Lactam antibiotics exert their antibacterial effect through inhibiting bacterial cell wall synthesis(103). The β-lactam ring acts as an acylating agent to covalently modify the active site serine residues of the peptidoglycan transpeptidase penicillin-binding proteins

(PBPs)(104), which are responsible for cross-linking the peptide termini of peptidoglycan strands(105). This acylation is effectively irreversible (at least over the lifetime of a bacterial cell) and prevents the true peptidoglycan substrate from accessing the active site of the PBP(106). It is proposed that the β-lactam structure acts to mimic the D-Ala-D-Ala terminus of the incoming peptidoglycan strand(107), or, alternatively, the transition state for the initial acylation step of a PBP reacting with an incoming peptidoglycan strand (Figure 1.6)(108). Indeed, β-lactams that have been synthetically altered to mimic peptidoglycan to a greater extent can demonstrate enhanced activity against their targets(109, 110). The elucidation of further details on the mechanism of inhibition of PBPs by β-lactams represents ongoing work; however it is known that the inhibition of the PBPs results in interrupted cell wall synthesis, interrupted cell growth due to the cell wall becoming compromised, and, ultimately, lysis of the bacterium due to osmotic pressure(111-113). The lack of a direct homologue of the PBPs in humans is likely an important reason for the lack of toxicity in the treatment of bacterial infections with β-lactam antibiotics; the specificity of the β-lactam for its PBP targets prevents unwanted side reactions with human enzymes.

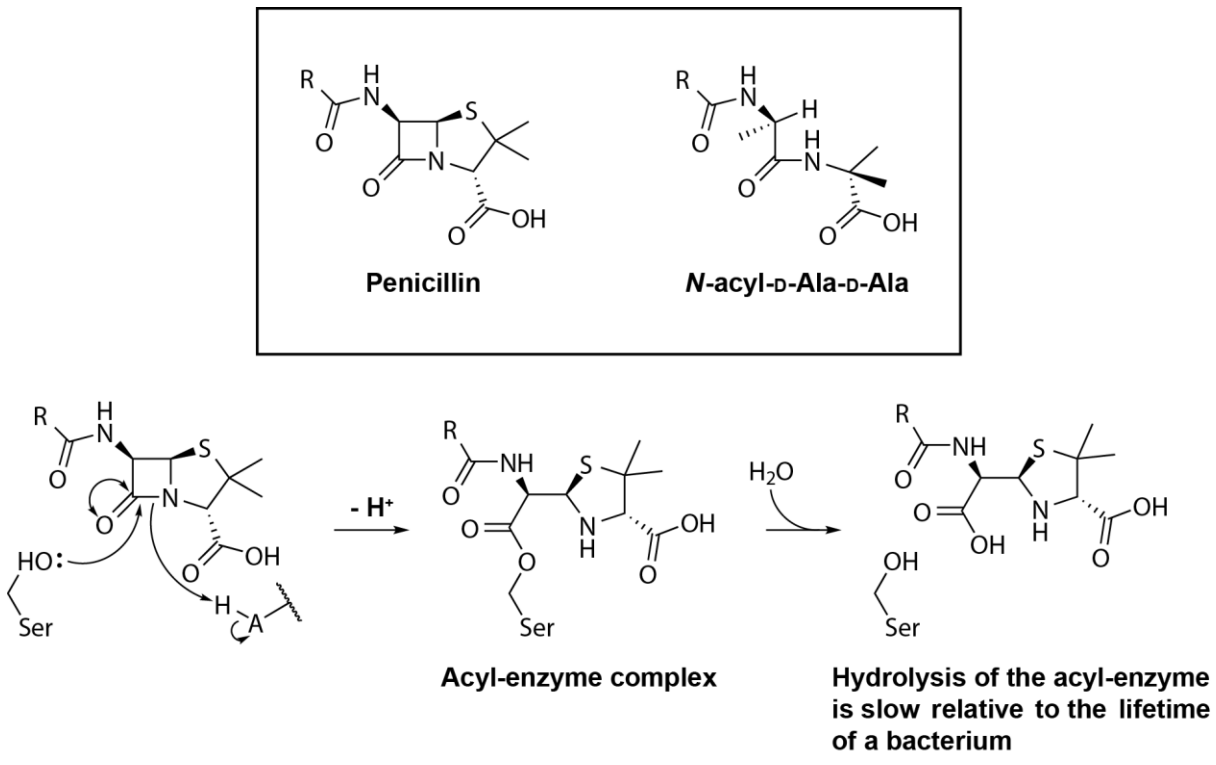

Figure 1.6: A. Comparison of the structures of penicillin and the D-Ala-D-Ala terminus of peptidoglycan strands reveals the possibility of β-lactams acting as mimics of the penicillin-binding proteins' native substrate. B. The mechanism of PBP inhibition by β-lactam antibiotics. Generation of a stable acyl-enzyme complex prevents binding of peptidoglycan strands and hence disrupts generation of peptidoglycan during bacterial growth.

1.5. Antibiotic Resistance and β-Lactamases

With β-lactams being produced by fungi and soil bacteria(2, 21), it is perhaps unsurprising that bacterial antibiotic resistance exists in environments free from clinical use of β-lactams, since bacteria would require mechanisms to counteract fungal-bacterial and bacterial-bacterial antibiosis, and indeed measures to stop any auto-inhibitory effect of their own produced antibiotics, in order to survive(4, 114); in fact, genetic studies suggest that some mechanisms of resistance have been present in bacteria for millions of years(115-117). Indeed, metagenomic analysis of bacterial samples from isolated microbiomes has revealed the prevalence of β-lactamase resistance mechanisms(118, 119). The dissemination of these resistance mechanisms via mobile gene elements, particularly amongst human pathogenic bacterial species, is a particularly worrisome aspect of antibiotic resistance(45, 120, 121).

Perhaps the best way to counteract bacterial resistance to one class of antibiotics is to treat with another distinct class with a different mode of action. However, as has already been stated, the loss of interest in antibiotic development from the 1970s onwards, even with a resurgence in academic interest more recently, has led to a depletion in the available arsenal of antibiotics that have not already been clinically employed in one way or another(122). With this being the case, the countering of emergent resistance mechanisms in a clinical setting can in some way be achieved by chemical modification of the antibiotics employed, thus creating generations of antibiotics based on the same core scaffold, as was successfully demonstrated by introduction of successive generations of penicillins and cephalosporins(123). This method does, however, pit the chemist in an arms race against the evolution of bacterial resistance mechanisms, a battle that, in all likelihood, is impossible to win(124). Where resistance takes the form of enzymatic modification of the incoming antibiotic, success has been had with co-administration of inhibitors(125-128), which has potentiated the use of previous generations of antibiotic against resistant bacteria, as described below.

Bacteria have evolved multiple mechanisms of antibiotic resistance, which may, or may not, be expressed simultaneously (Figure 1.7)(129-133). The mechanisms by which bacteria exhibit resistance to antibiotics include:

Modification of the antibiotic target. Acquired mutations to the active site of the target enzyme reduce the affinity for the antibiotic without compromising the catalytic efficiency of the enzyme with the result that the target is no longer inhibited in the presence of the drug. In the case of β-lactams, this is exemplified by the acquisition of *MecA*, which codes for a variant of PBP2 with a significantly lower affinity for penicillins(134). This is an important resistance mechanism in multi-drug resistant *Staphylococcus aureus* (MRSA).

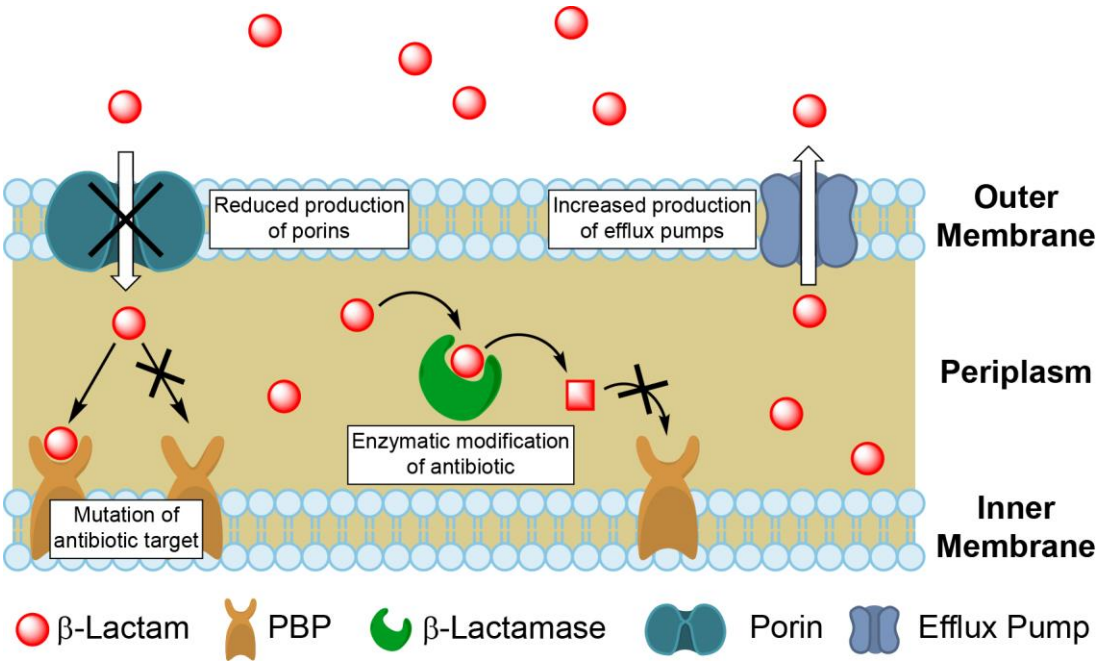

Figure 1.7: Cartoon illustration of the general mechanisms of resistance to antibacterials, including target modification, regulation of outer membrane permeability and modification of the incoming antibiotic. Note that the presence of two membranes, inner and outer, is only found in Gram-negative bacteria, but the same mechanisms of resistance apply in Gram-positive species.

Alteration of membrane permeability. Downregulation or alteration of porin channel proteins, as well as over expression of efflux pumps, helps to reduce the permeability of the bacterial cell membrane to antibiotics thus reducing their concentration in their site of action. Downregulated CarO or OprD porins are associated with carbapenem resistance in *Acinetobacter baumanii* and *Pseudomonas aeruginosa*, respectively(135-137). While efflux systems such as MexAB-OprM accept a broad range of β-lactam substrates for extrusion from *P. aeruginosa*(138, 139).

Enzymatic modification of the antibiotic. Chemical modification of the antibiotic produces a molecule that is no longer a successful inhibitor of its target. In the case of β-lactam antibiotics, this takes the form of hydrolysis by β-lactamases and is the most common and, arguably, the most important form of resistance to β-lactams(140).

The first identification of an enzyme able to hydrolyse penicillins, a serine β-lactamase (SBL), was made in 1940(141) by Abraham and Chain. Abraham and Sabbath identified both penicillinase and cephalosporinase activity in *Bacillus cereus*(142), with the latter activity being inhibited by treatment with ethylenediaminetetraacetic acid (EDTA)(143). This is likely the first reported identification of a metallo-β-lactamase (MBL). At the time of their

discovery, these β-lactamases were considered no more than a curiosity. However, despite the proximal introduction of penicillin into clinical use, the first penicillin-resistant *Staphylococcus aureus* infections began to plague hospitals in the mid-1940s(144). These first resistant *S. aureus* infections were expressing a β-lactamase to counteract treatment with penicillin(145). Since these first cases of resistance, the number of reported β-lactamases, including families, sub-families and sub-classes, now exceeds 1300(146, 147), with these enzymes cumulatively being able to hydrolyse all classes of β-lactam(140).

1.6. Serine-β-Lactamases

The serine-β-lactamases (SBLs) are so called since, much like the penicillin-binding proteins, they share a nucleophilic serine residue in their active site. In fact the SBLs are thought to be evolutionarily derived from the PBPs(148-150). Based on their sequence identity and substrate profiles, the SBLs are divided into three classes, Ambler classes A, C and D, corresponding to penicillinases, cephalosporinases and oxacillinases, respectively.

1.6.1. Class A Serine-β-Lactamases

Class A SBLs are the most widely studied SBLs. Class A enzymes include the Temoneira β-lactamase (TEM) and sulfhydryl reagent variable β-lactamase (SHV) enzymes, extended-spectrum SBLs (ESBLs) such as cefotaxime hydrolase from Munich (CTX-M) enzymes, which are able to hydrolyse later generation penicillins and cephalosporins, and carbapenemases including Imipenamase (IMI) and *Klebsiella pneumoniae* carbapenemase (KPC) enzymes. The class A SBLs exhibit a shared amino acid sequence identity of 40-60% between class members, and a much lower identity with members of other SBL classes (Figure 1.9). The class A SBLs are typically inhibited by β-lactam-based SBL inhibitors such as clavulanic acid(151), although KPC enzymes are an exception and some resistant TEM variants do exist(152, 153), as well as avibactam(154). There is some evidence to suggest that KPC-2 may hydrolyse avibactam via an initial desulfonation reaction(154, 155).

The first class A SBL to be structurally characterised was from *Bacillus licheniformis*(156). The structure of class A SBLs is characterised by two domains, one αβ domain characterised by a buried 5-stranded antiparallel β-sheet bound by three solvent-exposed α-helices, and one all a domain comprised of 8 α-helices (Figure 1.8). The active site cavity is located at the interface of these two domains(149).

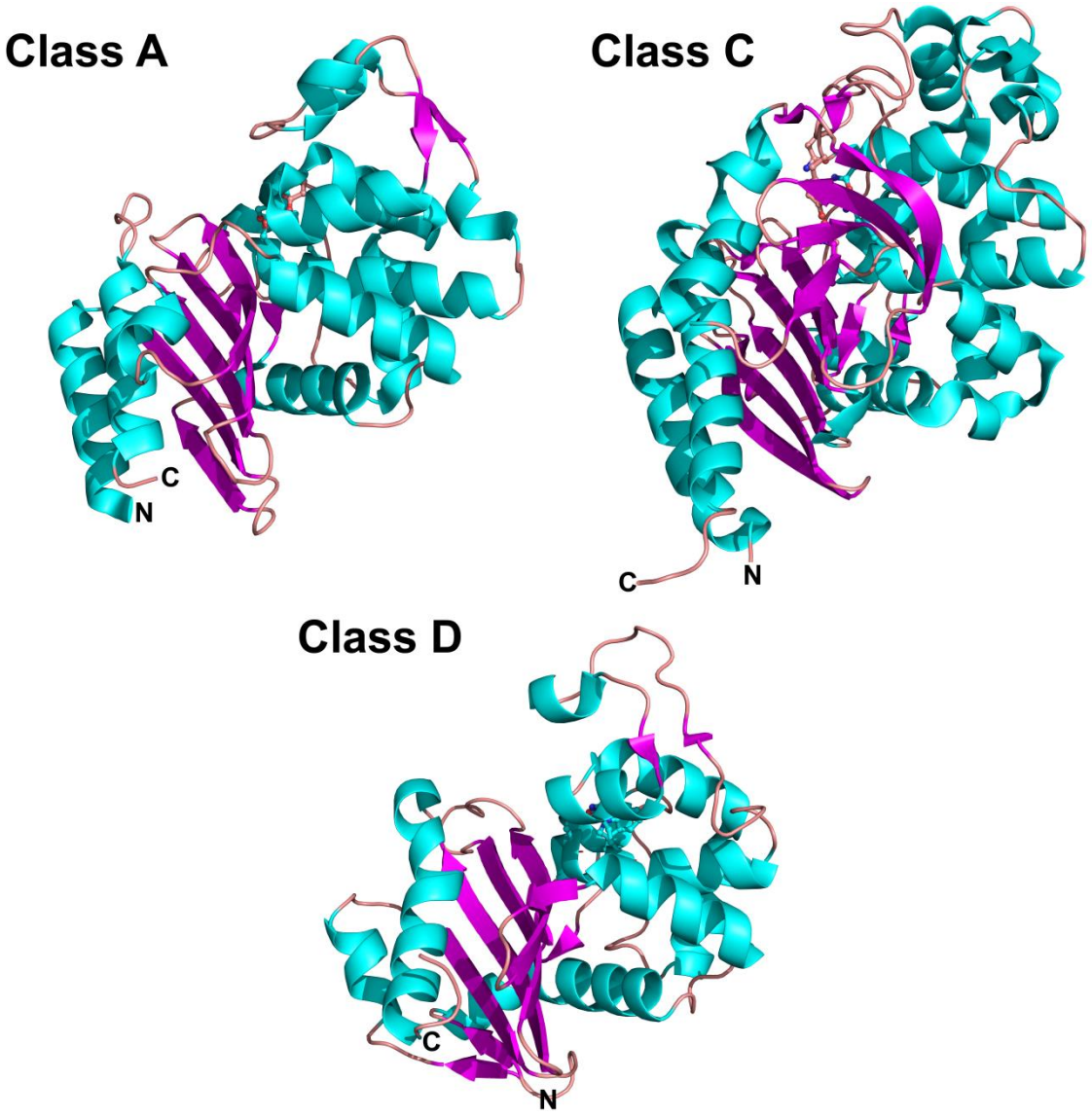

Figure 1.8: The structures of Ambler class A, C, and D serine-β-lactamases as exemplified by CTX-M-15(157), AmpC from *P. aeruginosa*(157), and OXA-10, respectively. Despite differences in sequence, the α/β and all α two-domain fold is largely conserved between classes. (PDB accession codes: 4HBT – CTX-M-15, 4GZB – AmpC, 2X02 – OXA-10).

	% Identity	A			C			D		
		SHV-1	TEM-1	CTX-M-15	Pa_AmpC	CMY-2	FOX-1	OXA-10	OXA-23	OXA-48
A	SHV-1	100	65	37	20	15	17	14	15	15
	TEM-1	65	100	36	18	13	15	12	13	13
	CTX-M-15	37	36	100	22	16	21	15	14	17
C	Pa_AmpC	20	18	22	100	42	54	14	12	13
	CMY-2	15	13	16	42	100	42	12	18	12
	FOX-1	17	15	21	54	42	100	13	18	14
D	OXA-10	14	12	15	14	12	13	100	35	47
	OXA-23	15	13	14	12	18	18	35	100	36
	OXA-48	15	13	17	13	12	14	47	36	100

Figure 1.9: Shared amino acid sequence identities of selected serine-β-lactamases. Grey boxes highlight the three Ambler classes, A, C, and D. Pa_AmpC indicates the AmpC enzyme from *P. aeruginosa*. Sequence alignments and identity calculations were performed using the Clustal Omega web service(158).

1.6.2. Class C Serine-β-Lactamases

Class C SBLs (AmpCs) are generally chromosomally mediated, although plasmid mediated class C enzymes do exist, and are found predominantly among the *Enterobacteriaciae*(159). These enzymes are able to hydrolyse penicillins, but are most active against cephalosporins and cephamycins, with some AmpC enzymes acting at the diffusion limit during cephalosporin hydrolysis(160). Class C enzymes are typically not inhibited by SBL inhibitors such as clavulanic acid (see below), although some are inhibited by sulbactam or tazobactam(161-163). They are, however, inhibited by aztreonam since they have a high affinity for this substrate but a poor rate of turnover(164). Extended spectrum AmpC (ESAC) enzymes, with a broader range of cephalosporin substrates, have also been characterised(165, 166). Production of ESACs in combination with porin loss has been associated with increased resistance to carbapenems in *E. coli*(167).

1.6.3. Class D Serine-β-Lactamases

Class D SBLs are comprised of the oxacillinase (OXA) enzymes which are able to confer resistance to penicillins, cephalosporins and, in some cases, carbapenems(168, 169). The OXA enzymes may be chromosomally or plasmid mediated and so some OXA variants are able to be transferred between pathogenic species(170). OXA enzymes are generally resistant to inhibition by SBL inhibitors but their activity is reduced in the presence of halide ions(171). The OXA enzymes undergo a non-enzymatic post-translation modification by reaction of an active site lysine (Lys70) with CO_2 to produce a lysine carbamylate residue that acts as a general acid/base in the catalytic mechanism of the enzyme(172). This modification is promoted by a nearby tryptophan residue (Trp154), which hydrogen bonds to and stabilises the carbamylated lysine residue(173).

1.7. Mechanism of Serine-β-Lactamases

The catalytic mechanism of SBLs is very similar to that of the PBPs from which they are derived(174). That is hydrolysis occurs via attack of the β-lactam carbonyl by a nucleophilic serine residue to form an acyl-enzyme intermediate, which is then subsequently hydrolysed by the addition of water (Figure 1.10). The ability of these enzymes to efficiently hydrolyse the acyl-enzyme intermediate produced by reaction with the β-lactam is what distinguishes them from the PBPs; no, or slow, hydrolysis of the acyl-enzyme intermediate in PBPs allows β-lactams to exert their antibiotic activity, while hydrolysis of this intermediate in the case of SBLs allows for efficient enzymatic degradation of the β-lactam before it can perform its function(175, 176).

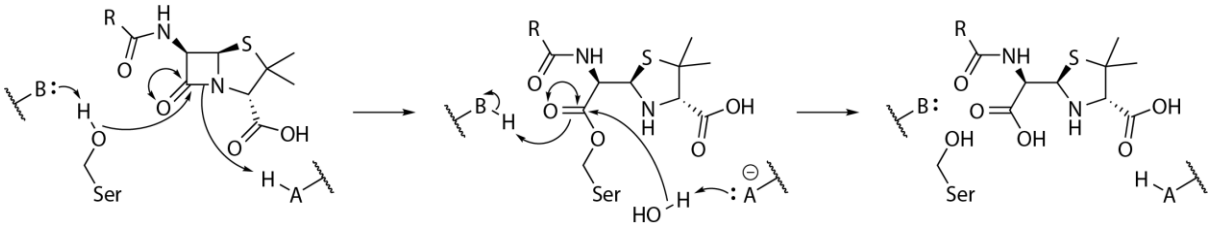

Figure 1.10: General mechanism for the hydrolysis of β-lactams by serine-β-lactamases. While the first reaction step is shared by the interaction of β-lactams with penicillin binding proteins, the second is exclusive to the serine-β-lactamases.

The identities of the general acid/base catalytic residues employed by SBLs are dependent on the class of enzyme being considered(175). In the class A SBLs, Glu166 acts as the general base to aid deprotonation of the serine nucleophile as well as the hydrolytic water in the turnover of the acyl-enzyme intermediate(177), although Lys73 and Ser130 are also implicated in proton shuttling during the reaction (Figure 1.11)(178, 179). In class C β-

lactamases, an extended active site hydrogen bonding network two has been implicated in fulfilling the role of the general base during catalysis(180). Among these residues both Lys67 (which is homologous to Lys73 in class A SBLs)(181, 182) and Tyr150(183) have both been put forward as critical in deprotonation events(184), although modelling suggests that Tyr150 may be the most important (Figure 1.11)(185, 186). As previously stated, the class D OXA β-lactamases undergo an interesting non-enzymatic post-translational modification by the reaction of an active site lysine residue (Lys70) with carbon dioxide (Figure 1.11)(187). The resulting lysine carbamylate takes the role of the general base to abstract a proton from the nucleophilic serine in the initial attack and in deprotonation of water during the hydrolysis of the acyl-enzyme intermediate(172).

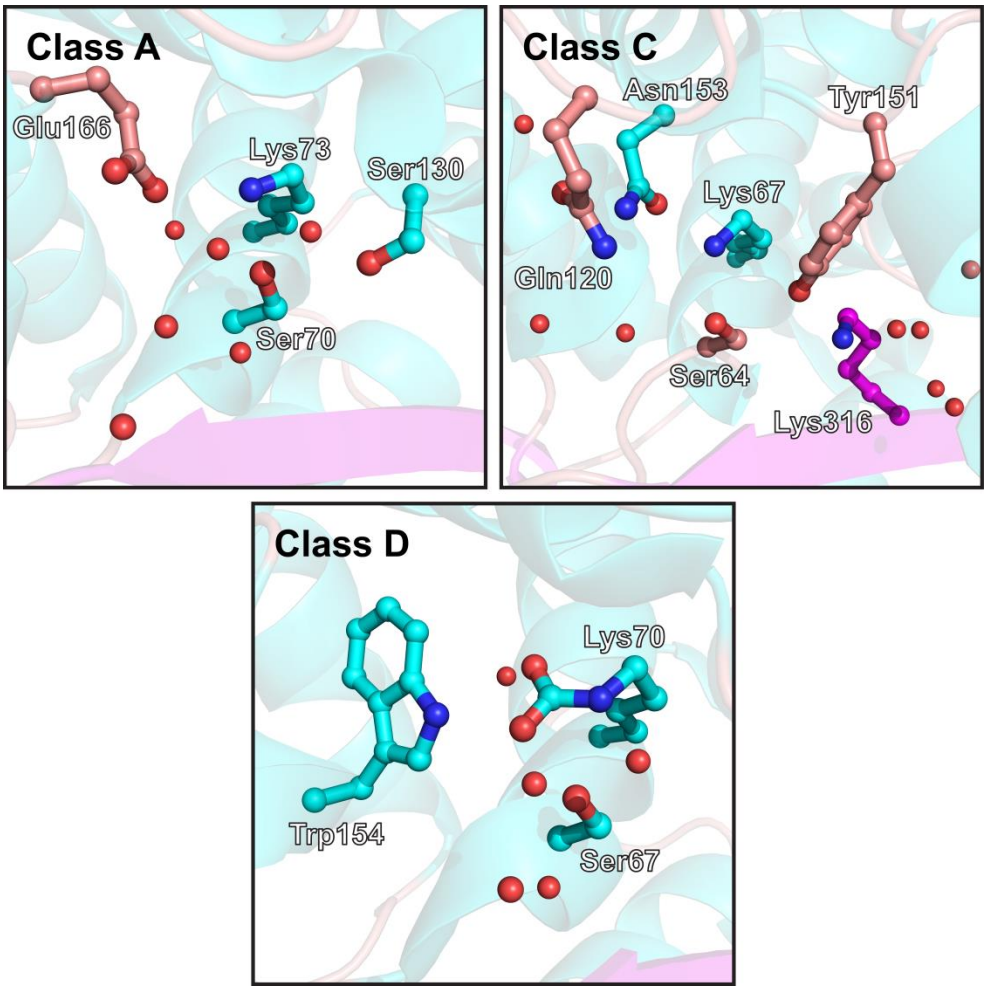

Figure 1.11: Active site views of Ambler class A, C, and D serine-β-lactamases as exemplified by CTX-M-15(157), AmpC from *P. aeruginosa*(157), and OXA-10, respectively. Amino acid residues implicated in the hydrolysis mechanism are rendered as balls and sticks. Red spheres represent water molecules within appropriate hydrogen bonding distances. (PDB accession codes: 4HBT – CTX-M-15, 4GZB – AmpC, 2X02 – OXA-10).

1.8. Serine-β-Lactamase Inhibitors

Historically, resistance from β-lactamases was combatted by the development of successive generations of penicillins and cephalosporins(123). Where this was not possible, the use of SBL inhibitors in combination therapy with β-lactams has been successful, particularly against class A SBL mediated infections(140, 188).

The first clinically used SBL inhibitor was clavulanic acid, which was isolated from *Streptomyces clavuligerus* in the late 1970s(189). Clavulanic acid is not dissimilar to penicillin, in possessing a bicyclic system with a β-lactam fused to a 5-membered heterocycle, however it differs in that the sulfur atom found in the penicillin is substituted by an oxygen, there is no aminoacyl side chain and the dimethyl substitution seen in penicillins is replaced by a β-hydroxyethylidine addition to the oxazolidine ring (Figure 1.12). Co-administered alongside amoxicillin, as Augmentin(190), or ticarcillin, as Timentin(191), clavulanic acid was shown to potentiate the use of penicillins against SBL-producing *S. aureus*, *K. pneumoniae*, and *E. coli* strains(192). Clavulanic acid was followed by the synthetic compounds sulbactam and later tazobactam(193), which are both penicillanic acid sulfones (Figure 1.12). Sulbactam is typically used in combination with ampicillin(194), while tazobactam is used in conjunction with piperacillin(195). These combinations are effective in the treatment of resistant *E. coli*, *S. aureus*, and *Klebsiella sp.* infections(196, 197). Although they themselves are not effective PBP inhibitors, the mechanism of SBL inhibition by clavulanic acid, sulbactam, and tazobactam is not dissimilar to the inhibition of PBPs by β-lactams. Structural, kinetic, and mass spectrometric studies indicate that inhibition starts by formation of an acyl-enzyme species, by reaction with the active site serine nucleophile, before complex on-enzyme fragmentation pathways involving cross-linking of active site residues to prevent further substrate turnover (Figure 1.13)(198-201).

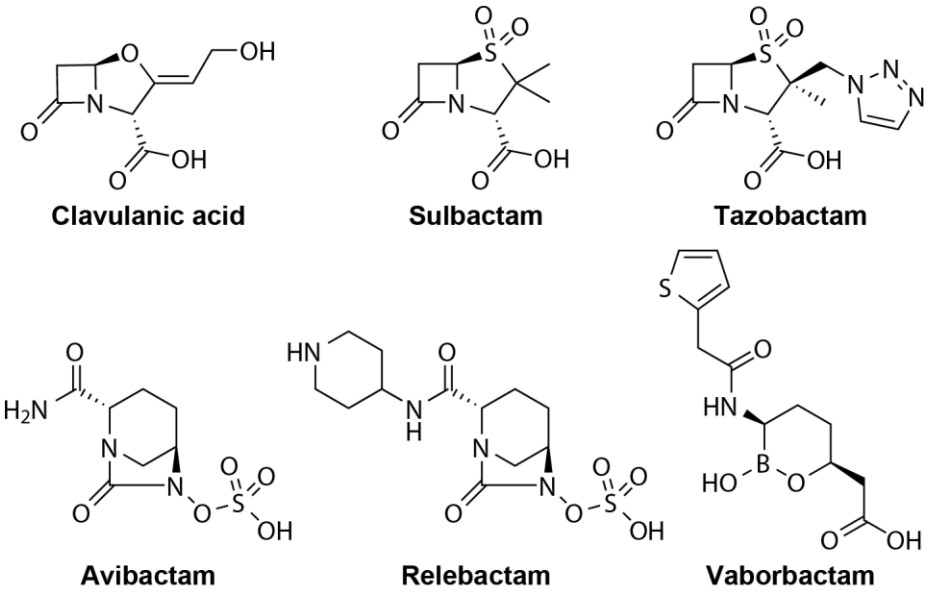

Figure 1.12: Clinically relevant serine-β-lactamase inhibitors. These compounds are either already in use, or are currently in clinical trials. Avibactam, relebactam and vaborbactam are examples of non-β-lactam β-lactamase inhibitors.

Although typically effective against class A enzymes, the β-lactam based SBL inhibitors are generally poor inhibitors of class C and D enzymes(202). The more recent inhibitor, avibactam(203), which is not a β-lactam, instead exhibiting a diazabicyclooctane scaffold (Figure 1.12), is able to inhibit class A, C and some class D SBLs(154). The inhibitor:β-lactam combination of avibactam and ceftazidime, Avycaz, has been approved for the treatment of complicated urinary tract and intra-abdominal infections(204). Although an important advance in the treatment of bacterial infections exhibiting resistance mediated by SBLs, avibactam in not an effective inhibitor of the class A KPC carbapenemases enzymes(152, 205), which are an important source of resistance particularly in the USA(206). In addition some MBLs have been shown to bind avibactam and catalyse slow hydrolysis of the inhibitor(207); although currently inefficient, the evolution of MBLs with an improved ability to turn over avibactam is a likely event in future and may prove important in cases where both SBLs and MBLs are produced in a single resistant infection.

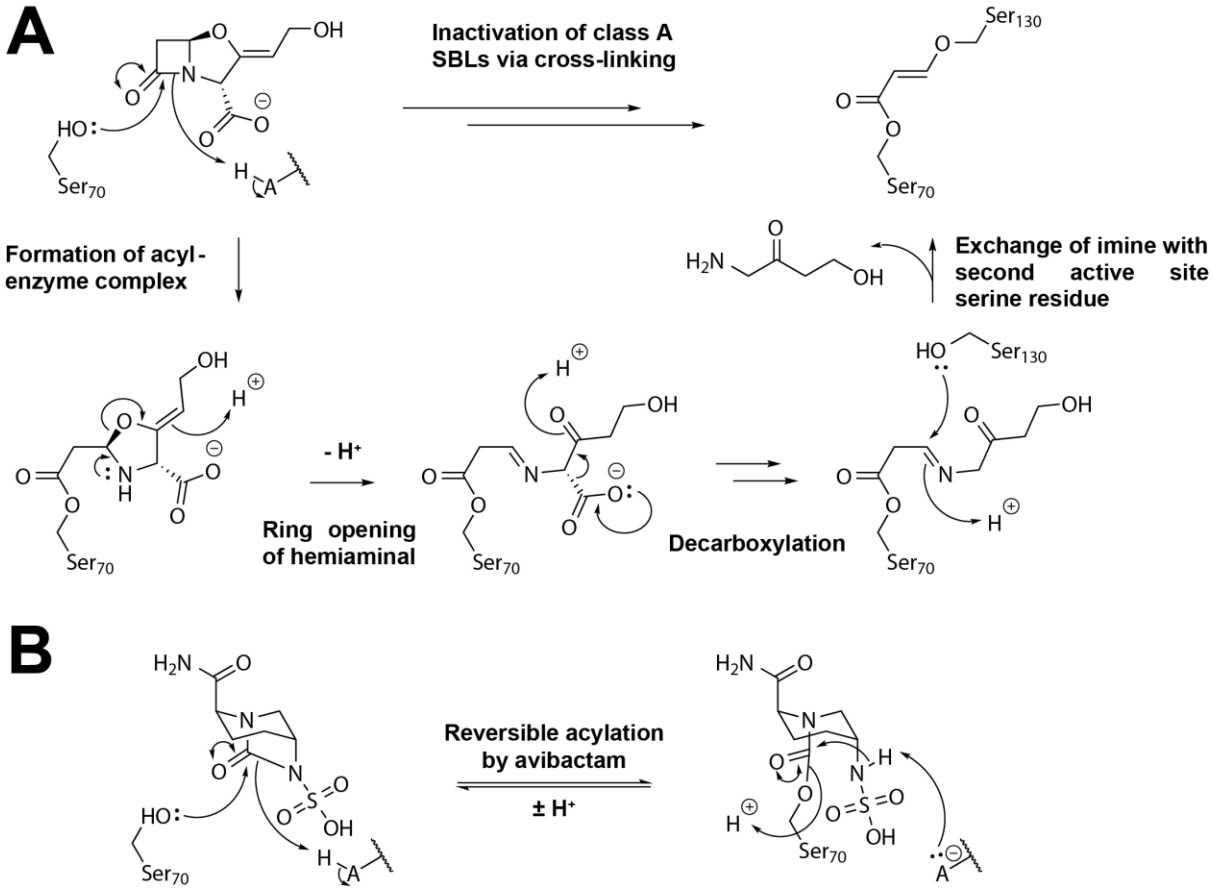

Figure 1.13: Covalent inhibition of serine-β-lactamases as illustrated by A. the 'suicide' inhibition of a class A enzyme by clavulanic acid and B. the reversible inhibition by avibactam. Note that avibactam can undergo slow hydrolysis in some cases(152, 205).

The avibactam derivative relebactam(208), which varies through the addition of a 4-aminopiperidine sidechain (Figure 1.12), is currently in clinical trials for treatment of KPC-mediated resistance by co-administration with imipenem/cilastatin(209-211), which is not treatable with Avycaz. Similarly, the boronic acid, vaborbactam (Figure 1.12)(212), in combination with meropenem (to be marketed as Carbavance)(213) has just passed phase III clinical trials as an effective treatment for SBL carbapenemase-mediated resistant infections. Unlike clavulanic acid, sulbactam and tazobactam, inhibition by avibactam derivatives or boronic acids is reversible via on-enzyme recyclisation of the inhibitor (Figure 1.13) or reversible formation of oxygen-boron covalent bonds, respectively(155, 214).

1.9. Metallo-β-Lactamases

The metallo-β-lactamase (MBL) fold superfamily constitutes a class (with >35000 members) of, predominantly, metallohydrolases that share a common pseudosymmetric αββα fold (Figure 1.15)(215-217). The various functions of the MBL fold enzymes include, but are not limited to, oxidoreductase enzymes, such as ethylmalonic encephalopathy 1 (ETHE1) and

cytidine-5'-monophospho-N-acetyl-neuraminic acid hydroxylase (CMAH)(218-220), small molecule hydrolases, including glyoxalase II(221, 222) and a bacterial phosphorylcholine esterase (Pce)(223, 224), and DNA/RNA modification or repair enzymes such as DNA cross-link repair enzyme 1 (DCLRE1) and cleavage and polyadenylation specificity factor 73 (CPSF73) (Figure 1.14)(225-227). The subgroup of the MBL fold enzymes that exhibit β-lactamase activity are often referred to as true β-lactamases and will be referred to as MBLs from hereon.

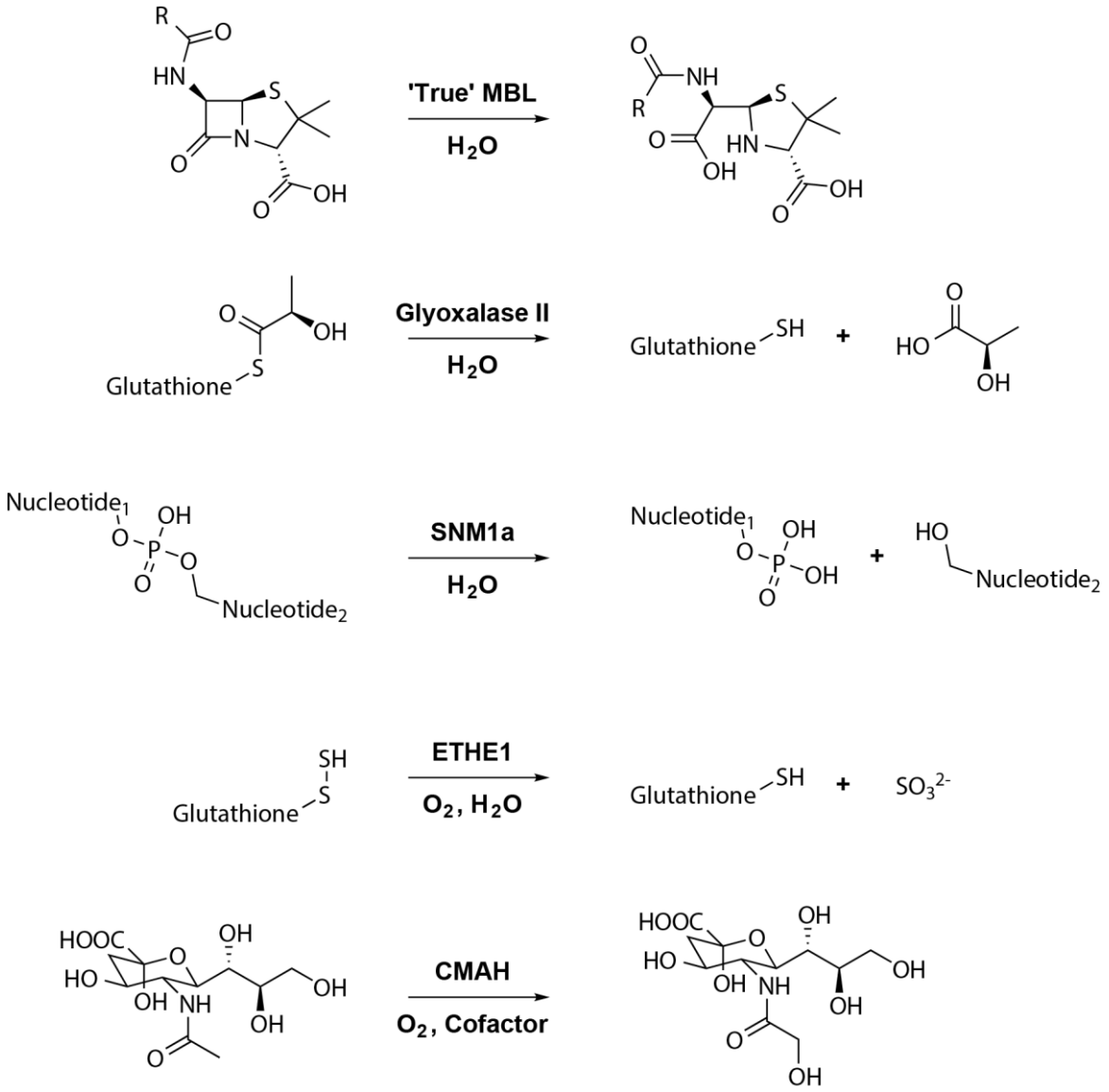

Figure 1.14: Example reactions catalysed by enzymes exhibiting a metallo-β-lactamase fold. These include both hydrolysis and oxidoreductase reactions.

The first evidence for an MBL came from Sabbath and Abraham who identified an enzyme, which co-purified with a known serine-β-lactamase, from *Bacillus cereus* that exhibited

cephalosporinase activity that could be inhibited by treatment with EDTA and restored by subsequent supplementation with zinc(II) ions(142, 143). With this enzyme, now known as *Bacillus cereus* β-lactamase II, BcII, being chromosomally mediated and present in a species of bacteria only implemented in rare opportunistic infections, the first MBL was only regarded as a biological curiosity(228). The same applied for other MBLs that were identified earlier in the study of these enzymes(229-231).

The clinical threat of MBLs became much more apparent with the identification of plasmid-mediated enzymes in the 1990s that were present in nosocomial species such as *P. aeruginosa*, and *Chryseobacterium meningosepticum*(232-234). Plasmid-mediated MBL genes have the capacity for efficient horizontal transfer amongst different bacterial species and this is most likely the dominant mechanism behind the ever-increasing reports of MBL-mediated resistance in pathogenic *Pseudomonas*, *Acinetobacter* and *Enterobacteriaciae* species(120, 146, 235-239). Non-infectious environmental bacterial species have also been implemented in horizontal transfer of MBL-encoding genes by acting as plasmid reservoirs and third parties for gene transfer between infectious species(240-242).

The increasing public health risk associated with the spread of MBLs is attributed to these enzymes' ability to hydrolyse all classes of β-lactam(243), with the exception of the monobactam aztreonam(244), including the carbapenems, which are often regarded as the antibiotics of 'last resort' in resistant bacterial infections(102). In addition the ability of MBLs to hydrolyse the β-lactam-based SBL inhibitors such as clavulanic acid, and bind and catalyse the slow turnover of the more recent non-β-lactam SBL inhibitor avibactam(207), has implications for the treatment of infections in which resistance mediated by both SBLs and MBLs is manifested – these types of infection are rare at present, but only likely to increase with time(245-247). In addition, mobile genetic elements encoding MBL genes may also contain genes that confer resistance to multiple other classes of antibiotic such as aminoglycosides and quinolones(248-250). This gives rise to multi-drug resistant bacterial strains that have very few therapeutic options for treatment.

1.10. Classification of Metallo-β-Lactamases

MBLs constitute Ambler class B of the β-lactamases(251) and are further divided into three subgroups, B1, B2, and B3, based on their sequences, structures as substrate profiles (Figure 1.15)(215, 216).

1.10.1 Subclass B1 Metallo-β-Lactamases

The B1 subclass constitutes the largest group of MBLs and includes BcII as well as Verona integron-encoded metallo-β-lactamase (VIM), New Delhi metallo-β-lactamase (NDM), and

MBL imipenemase (IMP) variants(252). In total the B1 subclass is comprised of greater than 14 enzyme families with a shared amino acid sequence identity of around 30% (Figure 1.16)(215). The majority of the B1 enzymes are encoded on mobile genetic elements and so are able to be rapidly transferred between pathogenic bacterial species(253). The B1 MBLs are able to hydrolyse penicillins, cephalosporins, and carbapenems, and thus are of high clinical relevance.

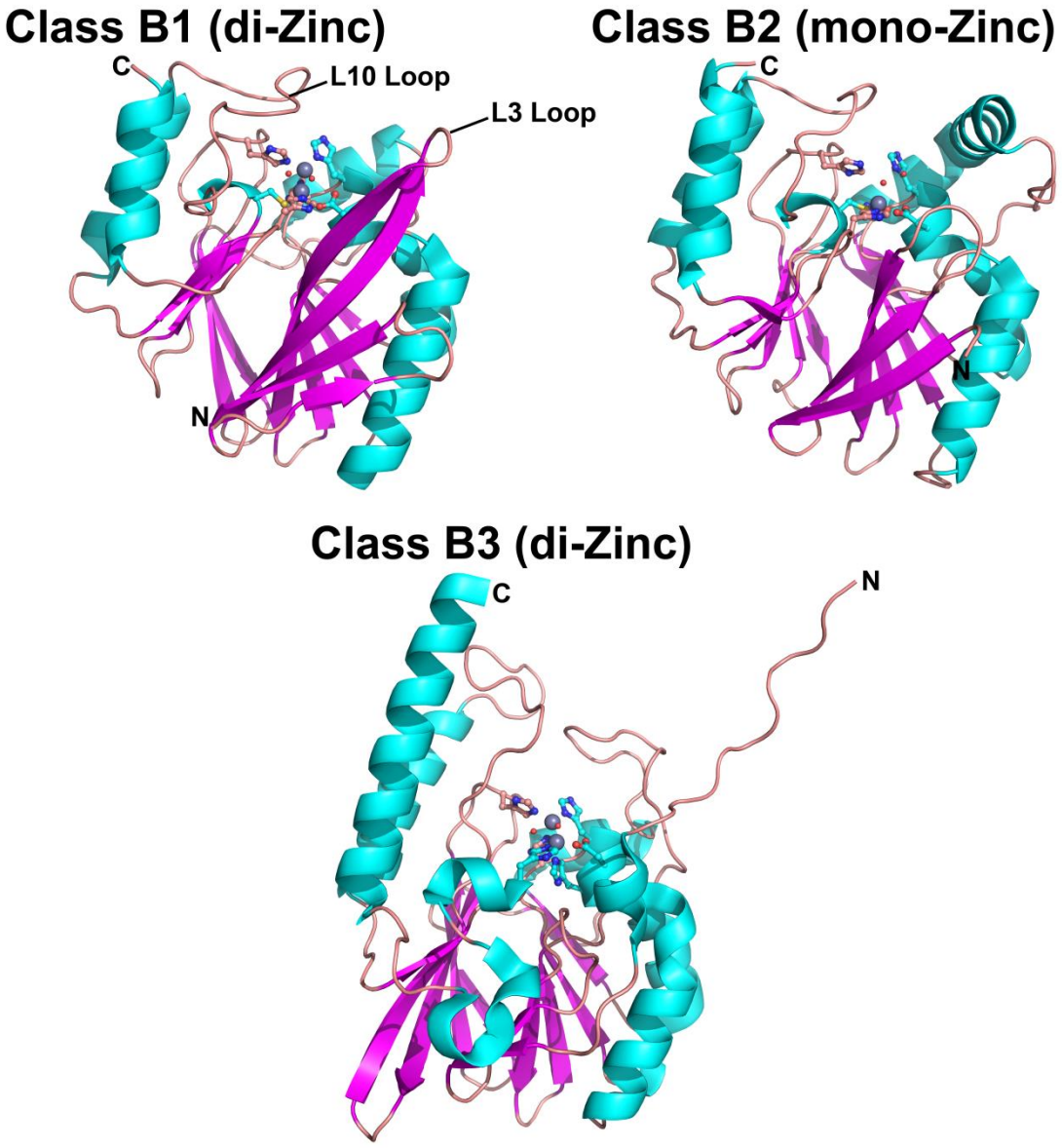

Figure 1.15: The structures of Ambler subclass B1, B2, and B3 metallo-β-lactamases as exemplified by BcII(254), CphA(255), and L1(256), respectively. Despite differences in sequence, the αββα is largely conserved between classes, however diversity is seen in the lengths of helices and loops. (PDB accession codes: 4C09 – BcII, 1X8G – CphA, 2FM6 – L1).

The first subclass B1 MBL, and indeed general MBL, structure to be elucidated was that of BcII, which was obtained initially in a mono-zinc(II), and later in a di-zinc(II) form. (It is now accepted that B1 MBLs require two metal ions for maximal activity)(257, 258). This revealed for the first time the pseudosymmetric αββα MBL fold, comprised of a dual β-sheet core surrounded by α-helices, with the metal-binding active site located in a solvent-exposed groove situated centrally on the pseudorotation axis (Figure 1.15).

The active site of the B1 MBLs is characterised by two metal binding centres, where one ion (Zn1) is coordinated by three histidine residues (the so called 3His site), His116, His118, and His196, while the second ion (Zn2) is coordinated by an aspartate, Asp120, a cysteine, Cys221, and a histidine, His263, residue (the DCH site, Figure 1.17). The coordination spheres of the two zinc ions are completed by two water molecules. Wat1 coordinates both zinc ions in a μ2 bridging mode, while Wat2 coordinates Zn only as an apical ligand making Zn1 tetrahedrally coordinated and giving Zn2 a trigonal pyramidal coordination sphere(259).

The B1 active site is flanked by two flexible loops the L3 loop between β-sheets 3 and 4, and the L10 loop between β-sheet 11 and α-helix 4 (Figure 1.15). These loops are implicated in substrate recognition and it is suggested that they contribute to the substrate selectivity of the enzymes(260-262). In B1 MBL structures the L3 loop is often poorly defined by the electron density map, suggesting a high flexibility for this loop even in a crystalline state. Comparison of apo and product-bound crystal structures show a tendency for the L3 loop to adopt a 'closed' conformation to increase interactions when a ligand is present in the active site(262, 263). Similarly the L10 loop contains residues that form key interactions with the substrate, such as Lys224/Arg228, which interact with the C3/C4 carboxylate of β-lactam substrates(215, 254).

1.10.2. Subclass B2 Metallo-β-Lactamases

The B2 subclass of MBL is a much smaller group and includes carbapenem hydrolysing enzyme from *Aeromonas hydrophila* (CphA), imipenemase from *Aeromonas veronii bv. Sobria* (ImiS), and *Serratia fonticola* carbapenem hydrolase (Sfh-I)(264, 265). The B2 MBLs have a smaller substrate range, with a much greater selectivity for carbapenems(266). The active site of B2 MBLs is structurally distinct from that of the B1 enzymes due to the mutation of His116 in B1 MBLs to Asn116 in B2 MBLs (Figure 1.17)(267). This has significantly reduced the affinity of the first metal binding site for zinc(II) so that the B2 enzymes only bind one metal ion in the second binding site in their most active form. In some cases excess zinc(II) in solution can encourage a second binding event, but this is inhibitory to B2 enzymes(268). The active site is characterised by one metal bound water molecule and a second positioned, by hydrogen bonding, between His118 and Asp120. An

extension in α-helix 3 in the B2 enzymes results in a narrower active site groove that likely gives rise to their selectivity for carbapenems(269).

% Identity		B1				B2		B3		
		BcII	VIM-2	NDM-1	IMP-1	CphA	Sfh-1	L1	GOB-1	FEZ-1
B1	BcII	100	35	29	35	29	25	17	16	13
	VIM-2	35	100	34	32	25	24	16	11	14
	NDM-1	29	34	100	33	23	19	17	14	16
	IMP-1	35	32	33	100	22	23	15	15	17
B2	CphA	29	25	23	22	100	55	18	16	17
	Sfh-1	25	24	19	23	55	100	16	20	13
B3	L1	17	16	17	15	18	16	100	24	32
	GOB-1	16	11	14	15	16	20	24	100	32
	FEZ-1	13	14	16	17	17	13	32	32	100

Figure 1.16: Shared amino acid sequence identities of selected metallo-β-lactamases. Grey boxes highlight the three subclasses, B1, B2, and B3. The B3 subclass is the most distinct, exhibiting the lowest shared sequence identity with both B1 and B2 enzymes. Sequence alignments and identity calculations were performed using the Clustal Omega web service(158).

1.10.3. Subclass B3 Metallo-β-Lactamases

The B3 subclass of MBLs is more significantly diverged from the B1 and B2 subclasses, with only 13% shared sequence identity in some cases, and the B3 enzymes are thought to have evolved independently of the other two classes (Figure 1.16)(270, 271). The B3 MBLs include the labile enzyme from *Stenotrophomonas maltophilia* (L1)(272), *Fluoribacter* (*Legionella*) *gormanii* endogenous zinc β-lactamase (FEZ-1)(273), and *Chryseobacterium meningosepticum* β-lactamase (GOB-1)(274). With the exception of GOB-1, which has now been shown to be active with one or two zinc(II) ions bound, the B3 enzymes are classified as di-zinc(II) enzymes(275, 276).

The active site of B3 MBLs is also different to B1 and B2 enzymes. Mutation of Cys221, present as a metal ligand in both B1 and B2 enzymes, to Ser221 in B3 enzymes has

negated the use of this amino acid as a metal ligand. However a new ligand His121 completes the coordination sphere of the second metal binding site(277). In the active site of GOB enzymes, there is a further mutation of His116 to a glutamine so that both metal binding sites are altered in GOB enzymes relative to B1 MBLs(275). The B3 enzymes exhibit the conserved αββα fold but with an additional β-strand in the first β-sheet as well as significant extension of loops flanking the active site(215). L1 is a further oddity among MBLs since it is tetrameric in solution unlike other MBLs, which are monomeric(278).

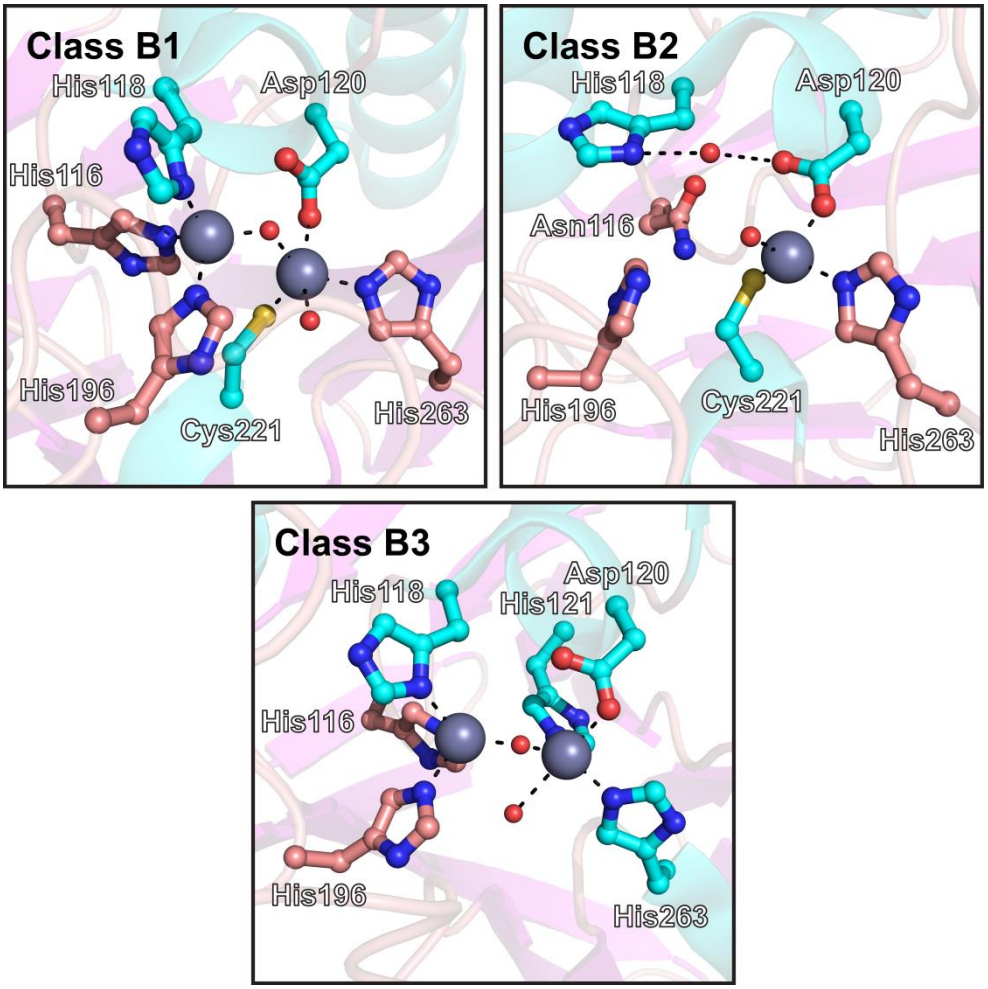

Figure 1.17: Active site views of subclass B1, B2, and B3 metallo-β-lactamases as exemplified by BcII(254), CphA(255), and L1(256), respectively. Amino acid residues ligating the metal ions are rendered as ball and stick. Red spheres represent water molecules, either coordinated to metal centres or within appropriate hydrogen bonding distances. (PDB accession codes: 4C09 – BcII, 1X8G – CphA, 2FM6 – L1).

1.11. Mechanisms of Metallo-β-Lactamases

The presence of zinc ions is critical for the activity of MBLs. Once bound in the active site, these zinc ions may have a number of beneficial effects for facilitating substrate hydrolysis(279), which include:

- Coordination and polarisation of the β-lactam carbonyl to facilitate attack of a nucleophile.
- Stabilisation of the oxyanion that would arise as a result of nucleophilic attack.
- Stabilisation of an amine anion that may result from expulsion of the leaving group in hydrolysis of the β-lactam ring.
- Coordination of a water ligand which can act as a nucleophile; the polarisation of water molecules by coordination to a transition metal can also encourage proton dissociation to produce a bound hydroxide ion that may be more nucleophilic than the parent water molecule.

Although the exact mechanism of MBLs is still a matter of debate, there is an agreed consensus that hydrolysis proceeds via attack of a metal-bound water/hydroxide onto the β-lactam carbonyl, followed by cleavage of the lactam carbon-nitrogen bond and subsequent protonation of the amine leaving group before release of the hydrolysed product.

The initial crystal structure solved for BcII revealed a mono-metallated enzyme, with one zinc ion in the 3His site(257). This lead to the proposal that hydrolysis proceeds by attack of a metal-bound water onto the β-lactam carbonyl and subsequent formation of a tetrahedral intermediate, which could be stabilised via coordination to the zinc ion. Asp120, free in the mono-metallated enzyme, was proposed to act as a general base/acid by abstracting from the proton from the tetrahedral anion to produce a dianionic species, stabilised by coordination to the zinc ion, and shuttling it to the amide nitrogen to give a protonated leaving group after collapse of the tetrahedral intermediate and cleavage of the carbon-nitrogen bond (Figure 1.18). Various aspects of this initial mechanistic proposal have been called into question, particularly since it is now agreed that BcII binds two zinc ions in its active site(258), resulting in a much reduced availability of Asp120 as a general acid/base, given its role as a metal ligand. Extensive characterisation of the MBLs via mutagenesis, crystallography, stopped-flow kinetics and EPR studies have increased our understanding of the mechanism of these enzymes.

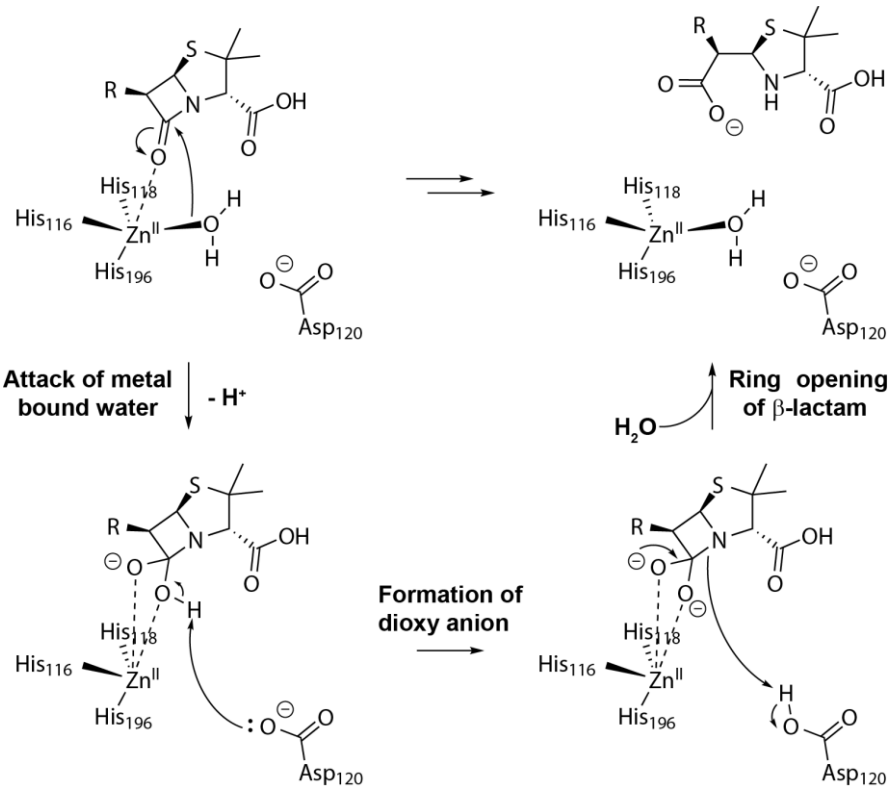

Figure 1.18: Initially proposed mechanism for the hydrolysis of β-lactams by metallo-β-lactamases. This mechanism was based on the observation of a monometallated enzyme in the first solved crystal structure of BcII.

1.11.1. The Catalytic Mechanism of B1 and B3 Metallo-β-Lactamases

The mechanisms of both B1 MBLs and the B3 enzyme, L1, have been studied in some detail. Steady-state and stopped-flow kinetics employing the reporter substrates CENTA, nitrocefin, and chromacef (Figure 1.19) as well as substitution of the spectroscopically inactive zinc(II) ions for cobalt(II), which also helps to reduce the rate of β-lactamase catalysis, have helped to identify various catalytic states of the enzyme as well as characterise transient small molecule species along the reaction pathway(280-284).

Stopped-flow analysis of Co(II)-BcII catalysed carbapenemase activity with imipenem conclude that both mono- and dimetallated BcII are catalytically active, however the greatest activity stems from the dimetallated enzyme(285). For dizinc MBLs, the substrate is proposed to bind initially via coordination to both zinc ions, with the β-lactam carbonyl coordinating Zn1 and the free carboxylate binding Zn2. This process will polarise the β-lactam carbonyl, thus facilitating attack of a nucleophile. The μ2 bridging water molecule likely has a lower pK_a due to coordination to two metal centres and consequently is proposed to exist as a hydroxide ion at relevant pH values(286). This hydroxide ion attacks the polarised β-lactam carbonyl to produce a transient tetrahedral anionic species(Figure 1.20)(287).

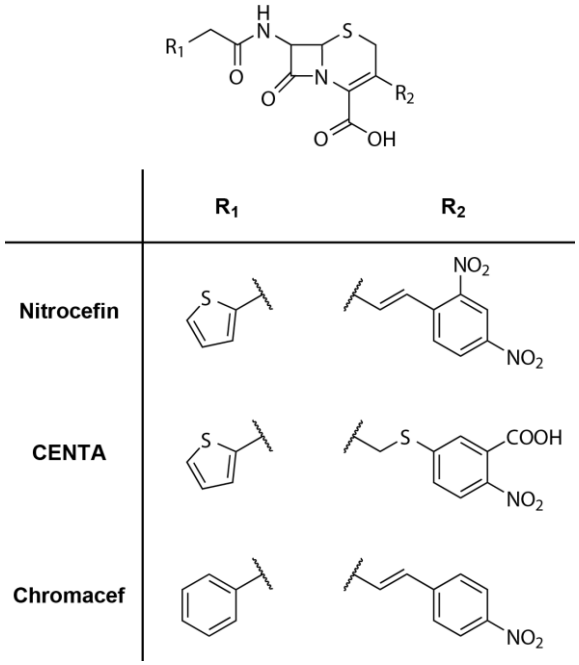

Figure 1.19: Reporter substrates routinely used to identify β-lactamase activity and to characterise the mechanisms of metallo-β-lactamases.

The exact nature of the collapse of this tetrahedral intermediate and subsequent protonation of the anion produced are contentious issues. If carbon-nitrogen bond cleavage were rate limiting, subsequent protonation of the amine leaving group would essentially be concomitant, whereas if the protonation itself were rate limiting, an anionic intermediate species resulting from the carbon-nitrogen bond cleavage should be detectable. Pre-steady state kinetic studies of the B1 cefoxitin and carbapenem resistant MBL (CcrA) revealed an intermediate species in nitrocefin hydrolysis, with a corresponding absorbance feature at 665 nm(288). This absorbance feature was shown to correspond to a deprotonated amine intermediate. Similar stopped-flow analyses with NDM-1 and the B3 enzyme, L1, have revealed this same species in nitrocefin hydrolysis, providing evidence for protonation of an anionic intermediate being rate determining(289, 290). However this feature is absent in nitrocefin hydrolysis catalysed by BcII and Bla2(281, 291). It has been argued that the extended conjugated system of nitrocefin, on account of its 2,4-dinitrostyryl substituent (Figure 1.19), is atypical compared to clinically employed cephalosporins(292), and that a greater potential for stabilisation of an anionic intermediate in this system leads to protonation being rate determining. This is supported by later work with L1, in which no detectable intermediate was present in the hydrolysis of cefaclor or meropenem and the carbon-nitrogen bond cleavage was determined to be rate determining(282). But intermediate species have been detected in the hydrolysis of imipenem by di-Co(II) BcII and meropenem by IMP-25 and both di-Zn(II) and di-Co(II) São Paulo MBL (SPM-1)(261, 285,

293). Thus the rate-determining step in the β-lactamase reaction is either carbon-nitrogen bond cleavage or protonation of the subsequent anionic species, and appears to be dependent on the enzyme and substrate combination employed in the study.

Following on from the mechanistic proposal developed based on the mono-metallated BcII structure, the results of mutational analysis suggest that Asp120 was not essential for protonation of an intermediate or activation of a nucleophile, ruling out its potential role as an acid/base catalyst(294, 295). Based on a co-crystal structure of NDM-1 in complex with hydrolysed ampicillin, it has also been proposed that the carboxylic acid formed on β-lactam hydrolysis is the proton source for protonation of the outgoing amine anion(296). The general consensus, however, is that the apical water coordinating Zn2 is the likely source of the proton during the β-lactamase reaction (Figure 1.20). Movement of this water molecule from an apical to a μ2 bridging position may help reduce its pK_a and thus making it more ready to act as a proton source(287).

1.11.2. The Catalytic Mechanism of B2 Metallo-β-Lactamases

Crystal structures of CphA and Sfh-I have revealed a monometallated enzyme with the sole zinc ion being present in the DCH site(255, 297). This ion has one water ligand at a coordination distance of 2.2 Å, consistent with a bound water rather than a hydroxide, while another water is held in the active site via interactions with His118 and Asp120. A co-crystal structure of CphA in complex with biapenem has led to the proposal that His196 may have a role in polarising the β-lactam carbonyl on substrate binding, while the carboxylate moiety of the molecule is coordinated to the zinc centre(255). It has also been suggested that, at least in the case of imipenem hydrolysis by Sfh-I, hydrolysis may proceed through an anionic intermediate, rendering protonation of this species the rate determining step in the reaction pathway(298).

Thus in the B2 MBLs, substrate binds by coordination to the zinc ion and via interaction with His196, His118 acts as a general base to deprotonate the adjacent water molecule which acts as the nucleophile to attack the β-lactam carbonyl (Figure 1.20). Collapse of the tetrahedral anionic intermediate produced gives rise to an anionic nitrogen species, which is stabilised via coordination to the zinc ion, and this is subsequently protonated by the metal bound water (Figure 1.20)(287). The observed inhibition of B2 MBLs by the binding of a second zinc ion supports this proposed mechanism(269), since binding of the metal in the second site would sequester both His196 and His118 as metal ligands and not leave them free to polarise the β-lactam carbonyl or deprotonate the hydrolytic water, respectively.

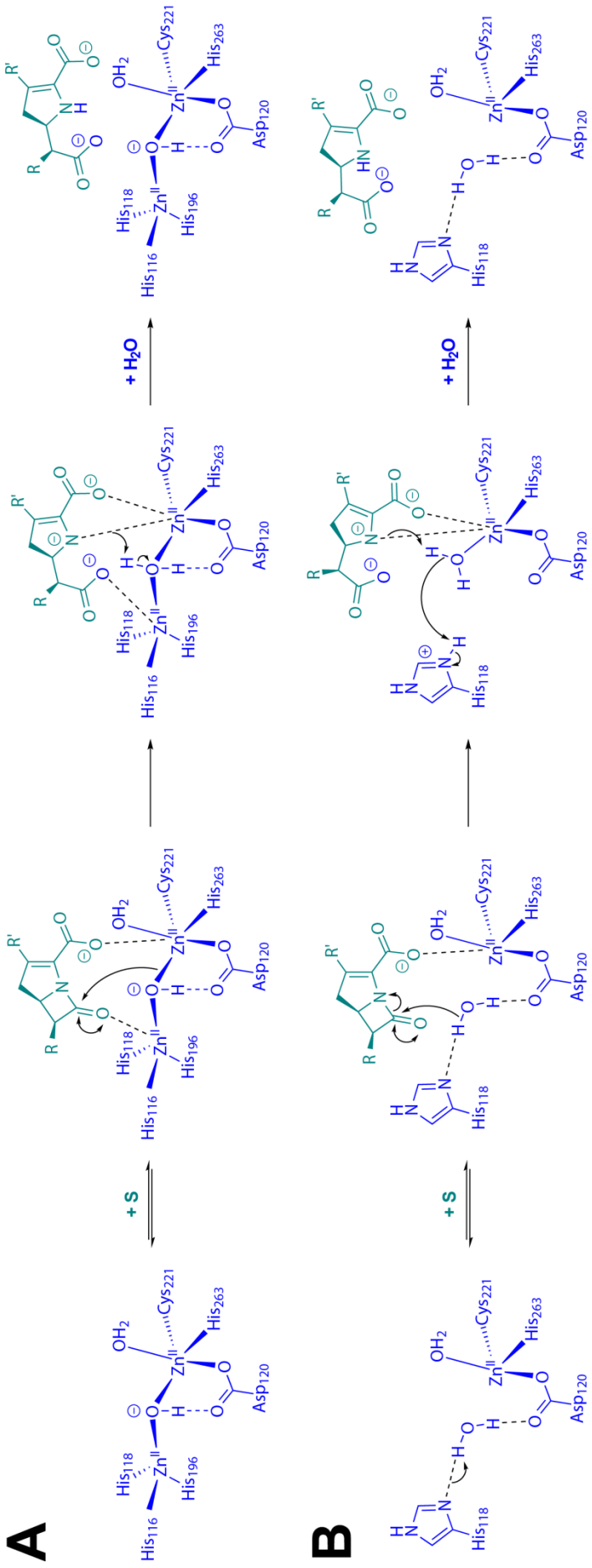

Figure 1.20: Reaction mechanism for hydrolysis of a carbapenem catalysed by A. a subclass B1 or B3 metallo-β-lactamase or B. a subclass B2 metallo-β-lactamase. The substrate is shown in green and the enzyme in blue. Dashed lines indicate metal coordination or hydrogen bonding interactions.

1.12. Inhibition of Metallo-β-Lactamases

Unlike the SBLs, the MBLs, to date, have no clinically available inhibitors(140). This may be in part due to the sequence and structural diversity exhibited by the different subclasses of MBL, as well as the differences in substrate selectivity and mechanism of individual enzymes(216). Despite this, a number of distinct classes of MBL inhibitor have been reported. These tend to be developed by initially focussing on chelation of the active site zinc ions. Many human proteins, potentially up to one third of the human proteome, are also metalloenzymes(299), thus metal chelation alone is not necessarily the best starting point for MBL inhibitors, since off-target human enzymes are also potential targets. As a result, increased selectivity through expansion of inhibitor chemistry to target conserved residues such as Arg228/Lys224, Asn233 and hydrophobic contacts with residues in the L3 loop is also critical in MBL inhibitor development(300, 301). Exploitation of mechanistic features conserved through all three subclasses of MBL is also a viable method of obtaining selectivity(302). A balance of breadth *versus* selectivity is, however, required to hit as many of the diverse clinically relevant enzymes (for example VIM, NDM and IMP types) as possible with a single compound. The breadth of MBL inhibitor chemotypes has been extensively reviewed(140, 280, 303, 304), and information on select examples of inhibitor subclasses is discussed below.

1.12.1 Metallo-β-Lactamase Inhibitors: Zinc Chelators

The initial identification of BcII as an MBL arose from the loss of activity that it exhibited when treated with EDTA(143). Hence, since their initial discovery, chelation of the active site metal ions has been a known method of inhibition. Typically MBLs inhibitors that act by zinc chelation exhibit one or more carboxylic acid or tetrazole rings.

The zinc chelators include biphenyl tetrazoles (Figure 1.21), which, when optimised, show mid-to-low micromolar IC_{50}s against IMP-1 and the CcrA from *Bacteroides fragilis*(305). Substituted succinic acid derivatives (Figure 1.21) show IC_{50} values as low as 2.7 nM against IMP-1 and have shown some success at potentiating meropenem against IMP-1 producing *E. coli* using *in vitro* growth assays(306, 307). Crystal structures with IMP-1 show that the molecules bind via the carboxylates chelating the active site zinc ions, one ion per carboxylate, and displace the bridging water in a binding mode that mimics the binding of hydrolysed β-lactam products(259). Linear and cyclised succinic acids have also been shown to inhibit L1 and exhibit a similar mode of binding in this B3 enzyme(256). Pyridine dicarboxylates and the corresponding thioacid natural products, which both arguably mimic the structure of hydrolysed cephalosporins, exhibit low micromolar IC_{50}s against CcrA, CphA and L1(308, 309). Other zinc-chelating chemotypes include trifluoromethyl ketones/alcohols, phthalic acid derivatives, and hydroxamic acids(310-312).

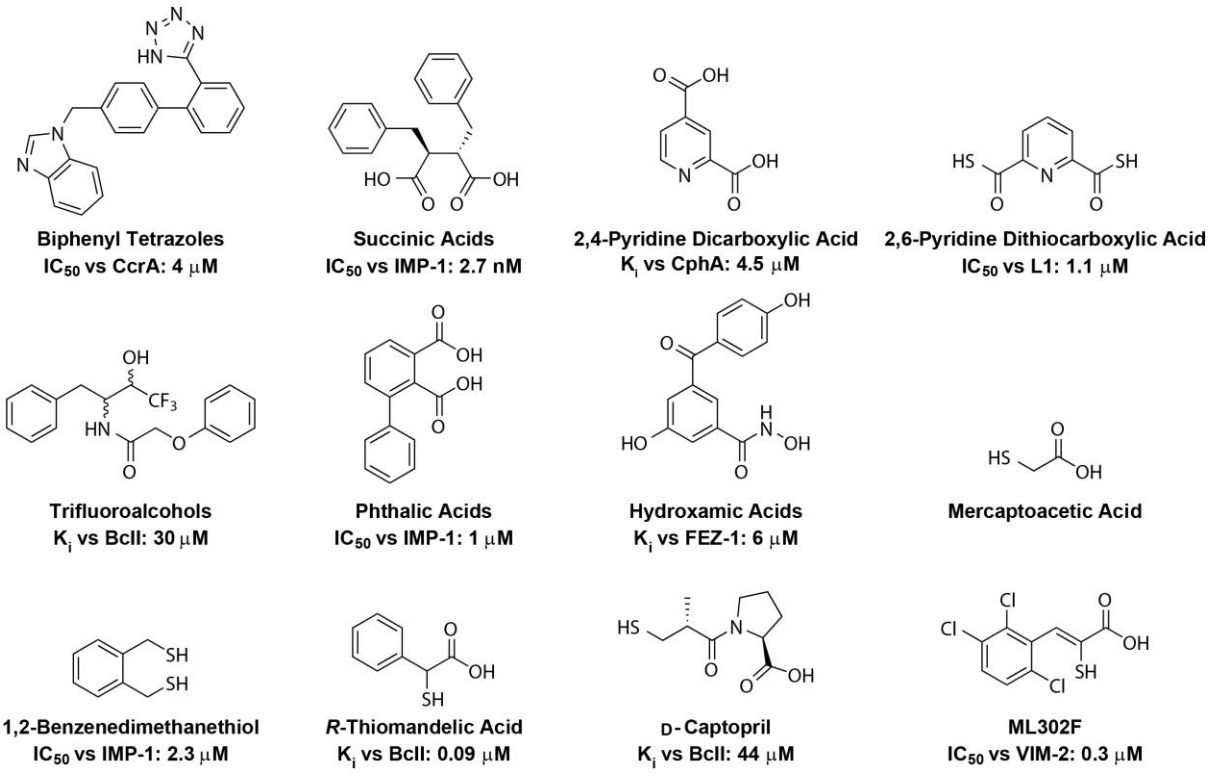

Figure 1.21: Representative structures for different classes of metallo-β-lactamase inhibitor. Reported IC_{50}/K_i values are also provided.

1.12.2. Metallo-β-Lactamase Inhibitors: Thiols

While thiol inhibitors also largely exhibit a mode of binding involving zinc chelation, a distinction is made for these inhibitors since the free sulfide group typically adopts a bridging position between the two zinc ions and hence mimics the binding of the hydrolytic water in the uninhibited enzyme (Figure 1.20)(313). Inhibitors in this class include simple thiols such as *N*-benzoyl-D-cysteine and 1,2-benzenedimethanethiol (Figure 1.21)(300, 314), which have been shown to inhibit L1 and IMP-1, respectively, or may include another acid group such as a carboxylic acid or phosphate group as in 3,5-bis(sulfanylmethyl)benzoic acid, and thiomandelic acid(300, 315, 316).

The angiotensin-converting enzyme (ACE) inhibitor L-captopril is able to inhibit enzymes from all three subclasses of MBL. The D-captopril isomer has been shown to be more potent against some B1 enzymes as well as CphA(300). Structural characterisation of B1 enzymes in complex with captopril stereoisomers suggests that the increased potency of D-captopril stems from the positioning of the carboxylate moiety, which is able to form a salt bridge with the conserved Lys224/Arg228 active site residue(254, 317). The thioenolate compound ML302F is a highly potent inhibitor of B1 MBLs(318). The altered relative positions of the thiol and carboxylate on account of the adjacent carbon-carbon double bond allows for an interesting binding mode whereby the thiol bridges the two zinc ions while the

carboxylate simultaneously binds to the second zinc ion. This mode of binding is likely what gives rise to the potent inhibition by this molecule.

Mercaptoacetic acid thiol esters have been shown to behave as 'mechanism-based' inhibitors(319). These molecules provide a source of mercaptoacetic acid, likely generated by hydrolysis in the active site, which is able to react with Cys221, one of the metal ligands in the second metal (DCH) binding site, to form a stable disulfide that obstructs binding of the second metal ion.

1.12.3. Metallo-β-Lactamase Inhibitors: Substrate Analogues

Since both SBLs and MBLs accept the same general substrate, it stands to reason that substrate mimics might act as a source of dual action inhibitors, with inhibitory activity against both classes of enzyme. This form of inhibitor may be useful in future, should coproduction of by SBLs and MBLs by resistant bacterial pathogens become prevalent.

6-(mercaptomethyl)-penicillanic acids (Figure 1.22) have been shown to inhibit both SBLs and MBLs, including TEM-1, BcII, and L1, and to increase the potency of piperacillin against *P. aeruginosa* strains producing MBLs(320). 8-thioxocephalosporins (Figure 1.22) have been shown to be weak inhibitors of BcII, while their hydrolysis products, as well as the hydrolysis products of normal cephalosporins are more potent, with IC_{50} values in the mid-to-low micromolar range(321, 322). 6-alkylidene-2-substituted penam sulfones (Figure 1.22) have also been identified as inhibitors of β-lactamase 2 (Bla2) with IC_{50} values as low as 1 μM(323). Reverse hydroxamate variants of cephalosporins (Figure 1.22) have also been shown to exhibit sub-micromolar IC_{50} values against the German imipenemase (GIM-1) MBL(324). β-methylcarbapenems, particularly those with dithiocarbamate, benzothienythio, or pyrrolidinylthio substituents at the C-2 position (Figure 1.22) have been shown to inhibit MBLs, with low to sub-micromolar IC_{50} values, as well as inhibiting class A and C SBLs.

Cyclobutanones represent a class of non-hydrolysable substrate mimics, since they lack a nitrogen atom in their four-membered ring (Figure 1.22). These molecules have been shown to inhibit both SBLs and MBLs, although potency against MBLs is modest, at best(302, 325).

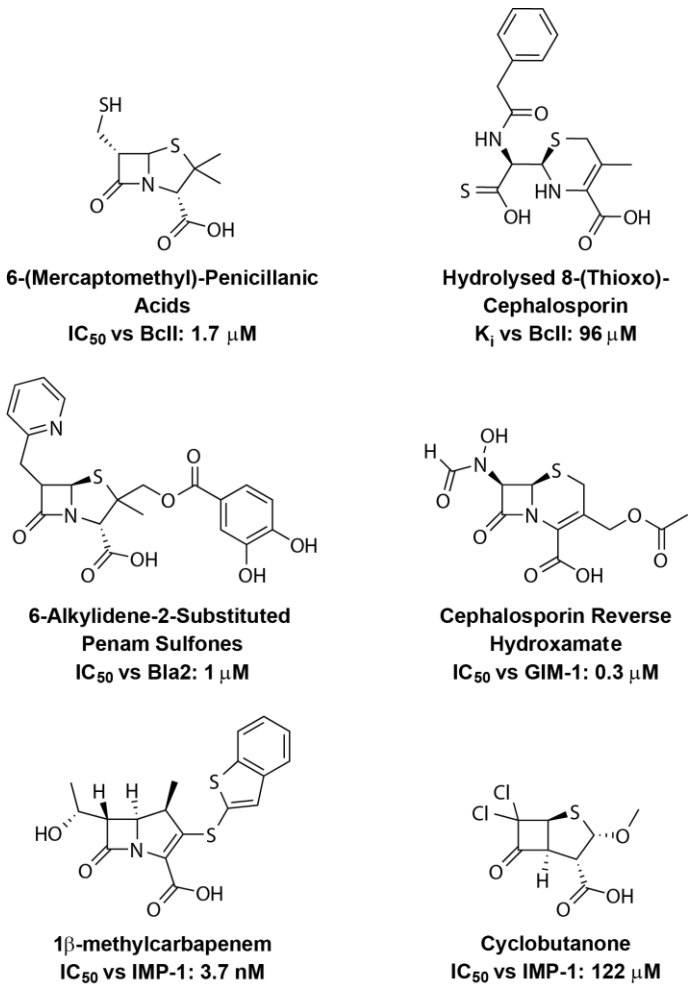

Figure 1.22: Representative structures for different substrate analogue based inhibitors of metallo-β-lactamases. Reported IC_{50}/K_i values are also provided.

1.13. Summary

Combined, the serine and metallo-β-lactamases constitute a diverse array of enzymes with the ability to hydrolyse β-lactam antibiotics. Although divided into two families that exhibit conserved folds, the SBLs and MBLs show large variation in the length of loops surrounding their active sites, substrate preferences, metal requirements and mechanisms (in the case of MBLs), and, importantly, in their response to inhibitors. Despite their age, β-lactams still constitute the largest portion of antibiotics used to treat bacterial infections worldwide. Thus, while their effectiveness may ultimately be outlasted by resistant bacteria, the continued study of β-lactamase enzymes and the development of β-lactamase inhibitors can continue to potentiate the use of β-lactams as effective drugs in the years to come.

Resistant bacterial infections mediated by the production of SBLs have multiple treatment possibilities, including the co-administration of clavulanic acid, sulbactam and tazobactam, as well as the non-β-lactam SBL inhibitors, avibactam, perhaps soon relebactam, and vaborbactam, alongside a β-lactam antibiotic. However to date there are no

clinically available MBL inhibitors. The treatment methods for SBL-mediated resistant infections do however provide precedence for the possibility of combination therapy involving a MBL inhibitor and a β-lactam, and thus the continued study of MBLs and their mechanisms, and the development of potential MBL inhibitors, are not unimportant areas of research. Perhaps of an even greater clinical interest would be 'dual-action' inhibitors with potency against both SBLs and MBLs. Molecules such as these may prove necessary as reports of resistant bacteria co-producing both SBLs and MBLs continue to rise, and with the possibility that the usefulness of avibactam be challenged by the evolution of MBLs with the capability of hydrolysing this molecule.

1.14. Research Objectives

The research detailed in this thesis followed three main objectives. Firstly, to elucidate more mechanistic detail about the true MBLs, particularly with reference to their metal requirements. Secondly, to achieve new chemotypes of MBL inhibitors, in particular to investigate the possibility of achieving dual inhibitors of both MBLs and SBLs, and to characterise their potency and mechanisms of binding and inhibition. And thirdly, to develop new assays, with moderate to high throughput, for human MBL fold enzymes with the view to developing counter screens of true MBL inhibitors in order to expedite future clinical inhibitor development.

Chapter 2: Use of Ferrous Iron by Metallo-β-Lactamases

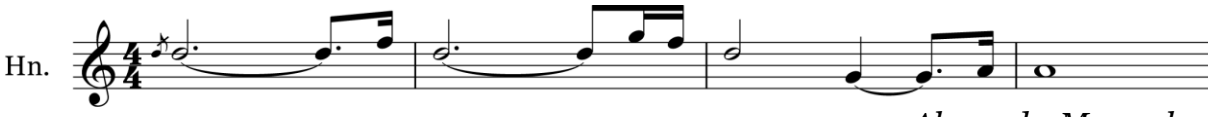

- *AlexanderMmosolov*

Contents

The work in this chapter was carried out in conjunction with Drs Jürgen Brem, who obtained MBL-encoding plasmids and advised on protein purification, Hanna Tarhonskaya, who advised on stopped-flow enzyme kinetics, and Michael McDonough, who advised on crystallography. The inhibitors, thiomandelic acid and ML302F, used in inhibition studies were synthesised by Dr Anna Rydzik. The majority of the work described herein has been reported in academic literature(326). *The structure of BcII in complex with ferrous ions is deposited in the Protein Data Bank with accession code 5FQA.*

2.1. Introduction

As discussed in the General Introduction, the true metallo-β-lactamases (MBLs) bind one or two zinc(II) ions in their active site to aid in their catalysis of β-lactam hydrolysis. The ability of the MBLs to utilise a number of transition metal ions in place of their native zinc(II) ions is well documented(327), with the metallo-β-lactamase from *Bacillus cereus* (BcII) exhibiting activity when substituted with cadmium(II), cobalt(II) or manganese(II) ions. Similarly the class B1 Verona integron-encoded MBL (VIM-2) and the B3 labile enzyme from *Stenotrophomonas maltophilia* (L1) have been shown to be active with similar transition metal substitutions(328). Indeed, cobalt-substituted BcII and VIM-2 have been used routinely in pre-equilibrium kinetic studies of MBL-catalysed reactions due to the spectroscopic visibility of cobalt(II) ions in electron paramagnetic resonance (EPR) studies(283, 285), where zinc(II) ions are not visible. Similarly, analysis of the cobalt(II)-bound B2 imipenemase from *Aeromonas veronii bv. sobria* (ImiS) has been used to inform about the metal binding sites of the enzyme(329). The ability to use multiple transition metals is highly beneficial for a bacterium producing MBLs since, even in situations of low zinc(II) ion availability, the use of other available transition metal ions can facilitate β-lactam hydrolysis.

A notable exception is iron ions. Although the activity of an assigned FeZn L1 enzyme has been demonstrated(330), and there are multiple documented instances of MBLs co-purifying with iron(221, 331, 332), no or negligible levels of activity have been reported with enzymes binding solely iron as a cofactor(275, 328, 333, 334). This is, perhaps, unusual considering that neighbouring transition metals in the same period *are* able to reconstitute β-lactamase activity and the role of iron availability in host-pathogen interactions(335, 336). Thus, these reported results may reflect a lack of control over the oxidation state of the iron employed, since solutions of ferrous iron salts have a tendency to rapidly oxidise in solutions with sufficient dissolved oxygen or exposed to air.

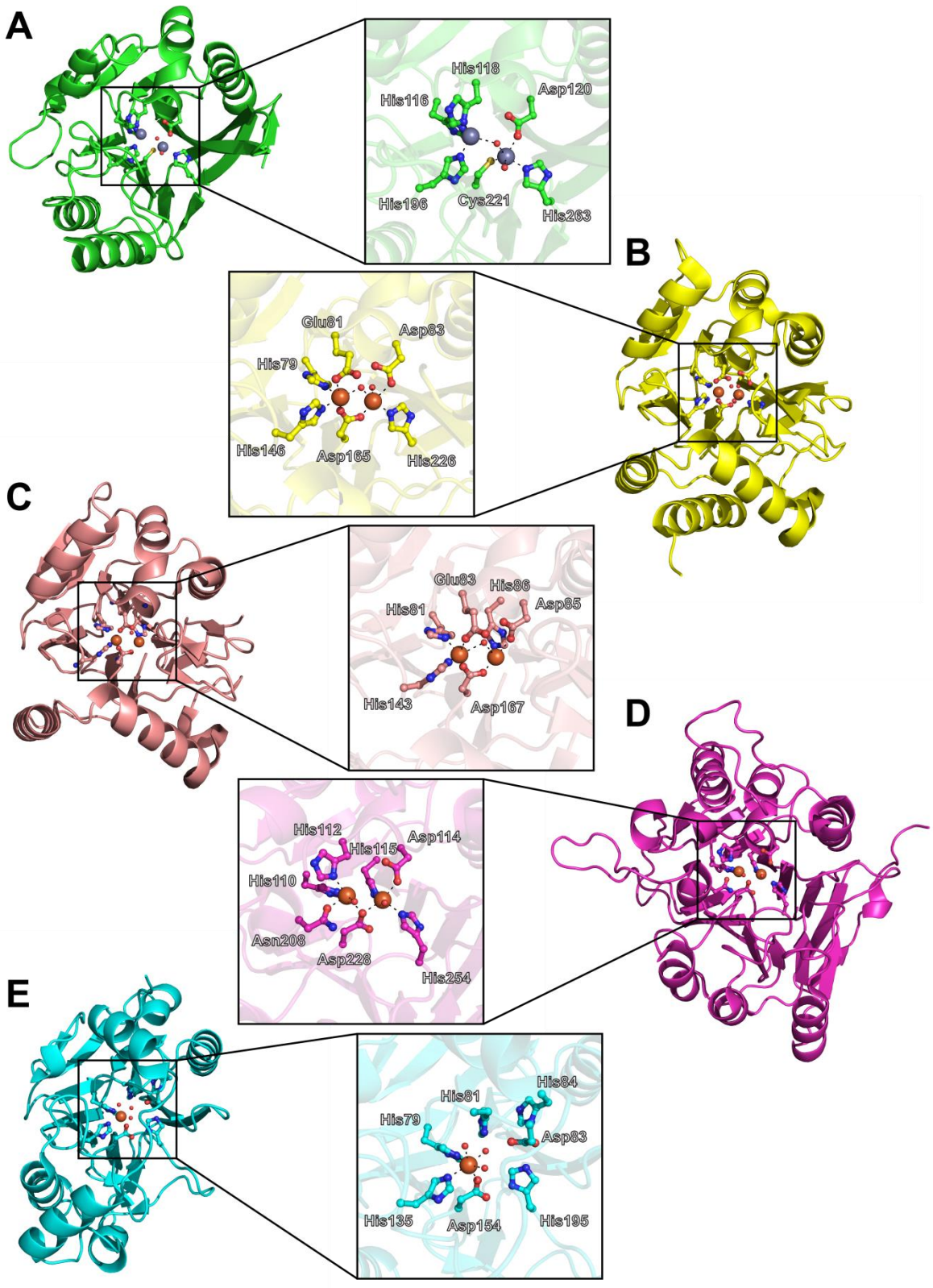

Figure 2.1: Crystal structures of selected metallo-β-lactamase fold proteins that are reported to use iron ions for catalysis. The conserved metallo-β-lactamase fold is exemplified for each enzyme alongside a view of the active site residues. The structure of the true metallo-β-lactamase, NDM-1 (A.) is provided for comparison. B. ROO C. FprA D. Pce E. ETHE1. Red spheres represent metal coordinated water molecules.

The MBL fold is, nevertheless, able to at least accommodate both mono- and di-ferrous iron binding, exemplified not only by co-purification with true MBLs(221, 331, 332), but also by members of the MBL fold superfamily(220, 223, 224, 337-339). MBL fold proteins that bind iron are known to exhibit either oxidoreductase or hydrolase activities. Oxidoreductase MBL fold enzymes include the di-iron rubredoxin:oxygen reductase (ROO) from *Desulfovibrio gigas* and A-type flavoprotein (FprA) from *Moorella thermoacetica*(337, 338) the mono-iron dioxygenase ethylmalonic encephalopathy 1, ETHE1(220, 340), and the di-iron oxygenase chloramphenicol biosynthesis enzyme, (Cm1A)(341). Studies have also revealed that the phosphorylcholine esterase (Pce) from *Streptococcus pneumoniae* is an MBL-fold hydrolase employing a di-Fe(II)-bound active site(223, 224). The latter enzyme is of particular note since it has a requirement for ferrous and not ferric iron, yet is located on the outer surface of the bacterial membrane(224), in what is considered to be an oxidising environment(342, 343), much like the β-lactamases(344). Structural and activity summaries of MBLs interacting with iron are presented in Figure 2.1 and Table 2.1.

Enzyme	Metall Content	Function	Reported as…(Ref)
L1	Zn(II)-Fe(II)	β-Lactamase	Active(330)
NDM-1	Zn(II)-Fe(II)	β-Lactamase	Inactive(334)
	Fe(II)-Fe(III)	β-Lactamase	Inactive(334)
GOB-18	Fe(II)-Fe(II)	β-Lactamase	Inactive(276)
	Fe(III)-Fe(III)	β-Lactamase	Inactive(276)
Glyoxalase II (*H. sapiens*)	Zn(II)-Fe(II)	Hydrolase	Inactive(331)
Glyoxalase II (*A. thaliana*)	Zn(II)-Fe(II)	Hydrolase	Inactive(339)
ElaC	Fe(II)-Fe(II)	Phosphodiesterase	Inactive(332)
ROO	Fe(III)-Fe(III)	Oxygen Reductase	Inactive(337)
	Fe(II)-Fe(II)	Oxygen Reductase	Active(337)
FprA	Fe(II)-Fe(II)	Nitric Oxide Reductase	Active(338)
ETHE1	Fe(II)	Persulfide Dioxygenase	Active(220)
Cm1A	Fe(II)-Fe(III)	Hydroxylase	Active(341)
Pce	Fe(II)-Fe(II)	Hydrolase	Active(223)

Table 2.1: Summary of reported interactions of metallo-β-lactamase fold proteins with iron ions.

2.2. Chapter Objectives

With limited knowledge on iron-substituted MBL activity, the goal of this chapter's work was to investigate whether iron ions are able to reconstitute the activity of MBL apo-enzymes. Further to this we aimed to characterise any effects of metal substitution on the mechanism of β-lactam hydrolysis, to examine any structural differences between metal-substituted MBLs, and to assess how the effects of known MBL inhibitors might be altered. A particular characteristic of MBLs is their ability to hydrolyse carbapenem antibiotics. Thus, in these

studies two substrates were employed to test for β-lactamase activity, the chromogenic reporter substrate, nitrocefin, and the clinically used 'last-resort' carbapenem, meropenem (Figure 2.2).

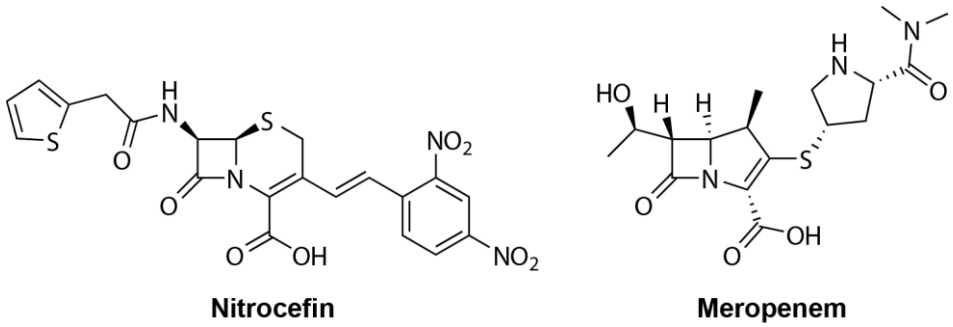

Figure 2.2: Chemical structure of the chromogenic reporter substrate, nitrocefin (a cephalosporin), and the clinically employed carbapenem, meropenem.

2.3. Production and Purification of Enzymes

Recombinant BcII was produced using the previously reported S31→K257 pET-9a encoded construct(345) in *E. coli* BL21(DE3) pLysS cells and purified by ion exchange using an SP Sepharose column, as described in the general methods. Recombinant VIM-2, with an *N*-terminal hexahistidine tag, was produced using the previously reported V27→E266 pOPINF encoded construct(346) in *E. coli* BL21(DE3) pLysS cells and purified by immobilised metal ion affinity chromatography followed by size exclusion chromatography before removal of the *N*-terminal tag by 3C protease digestion, as described in the general methods. At each stage in the purification of these enzymes, their purity was determined by sodium dodecyl sulfate polyacrylamide gel electrophoresis (SDS-PAGE) (Figure 2.3), and once purification was complete, their molecular weights were confirmed by electrospray ionisation mass spectrometry (ESI-MS), and their extent of folding by circular dichroism spectroscopy (Figure 2.4 & Table 2.2). The apo-forms of these two enzymes were generated by dialysis treatment with ethylenediaminetetraacetic acid (EDTA) as described in the General Methods.

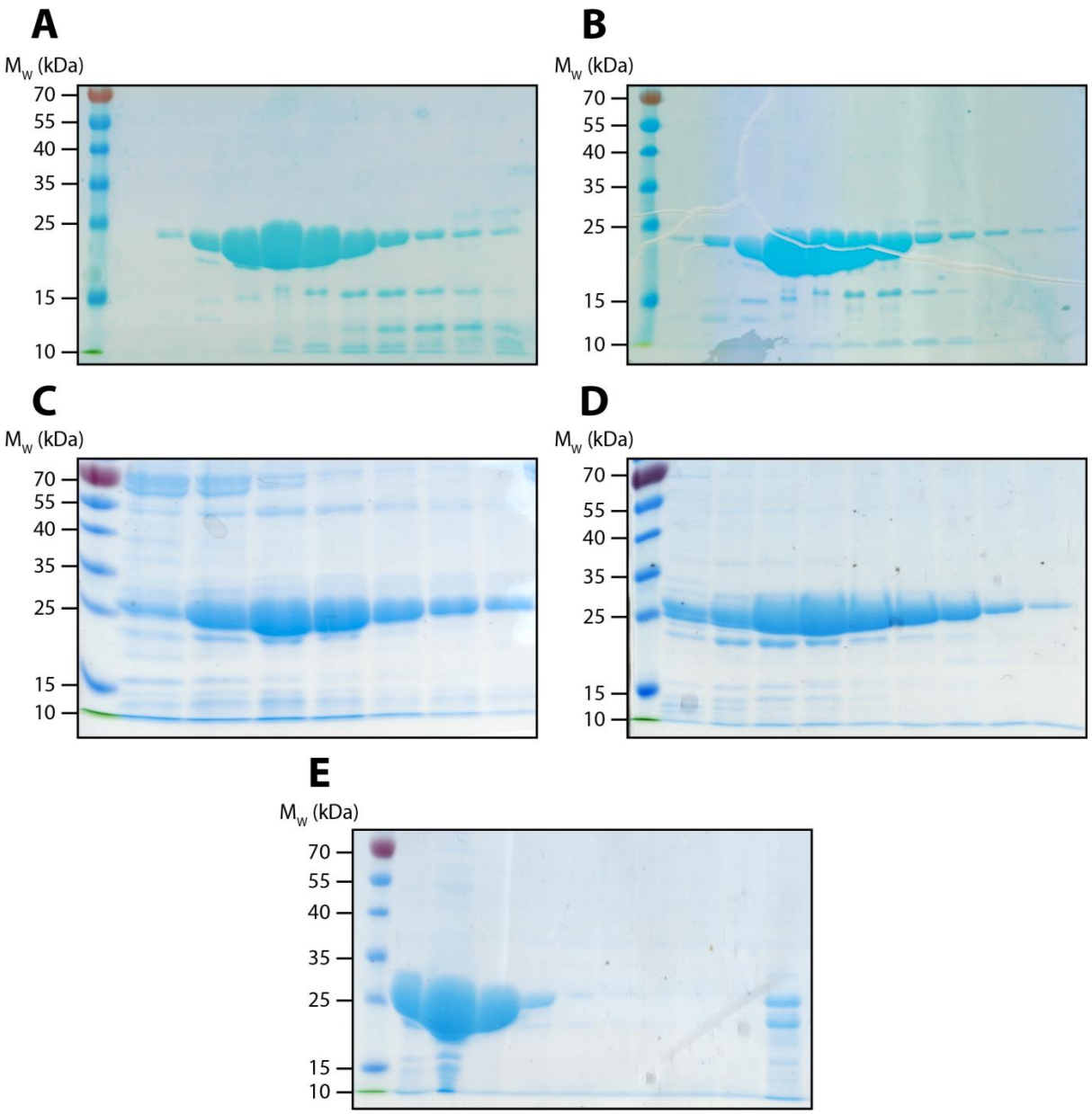

Figure 2.3: SDS-PAGE Gels of A & B. BcII after one or two rounds, respectively, of ion exchange purification by elution from an SP-sepharose column with a gradient of 0-1 M NaCl at pH 6.5. C, D & E. VIM-2 after successive rounds of metal ion affinity purification by elution from an immobilised nickel column with a gradient of 0-0.5 M imidazole, size exclusion chromatography using a Superdex 200 column, and 3C protease incubation followed by nickel ion affinity rebinding, respectively. All enzyme purification steps were carried out at 4 °C.

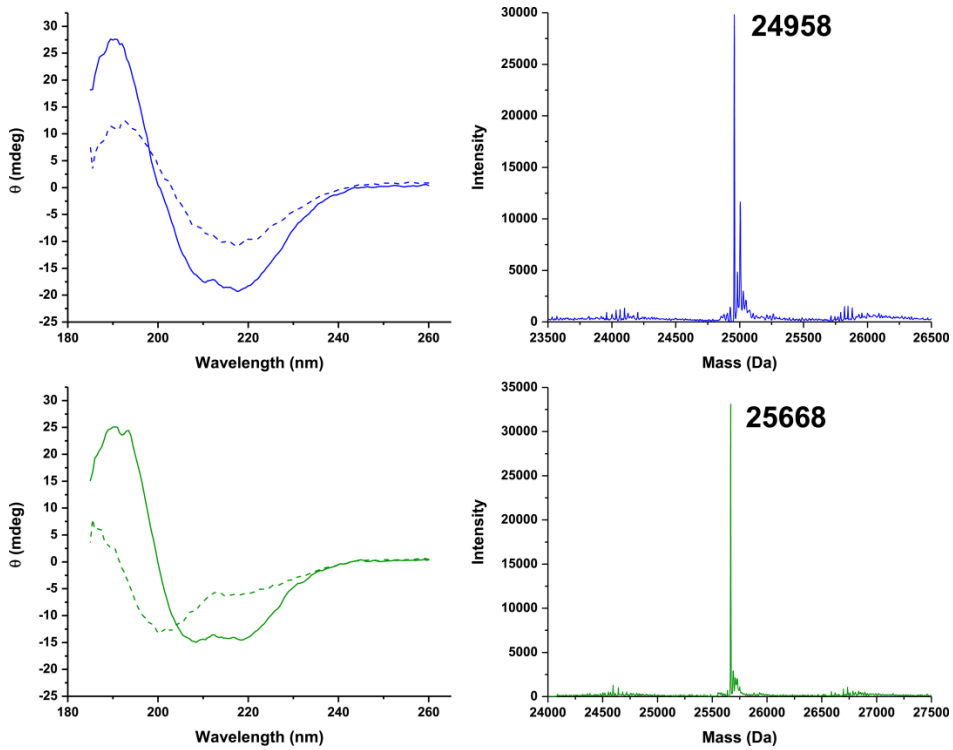

Figure 2.4: Circular dichroism and mass spectra for purified BcII (blue) and VIM-2 (green). Solid lines in circular dichroism spectra represent measurements at 10 °C, while dashed lines represent those at 85 °C. Enzymes were assayed at 0.2 mg mL^{-1} in 10 mM sodium phosphate buffer, pH 7.5.

Enzyme	Predicted Mass (Da)	Measured Mass (Da)
BcII	24952	24958
VIM-2	25670	25668

Table 2.2: Masses of BcII and VIM-2 as determined by denaturing mass spectrometry. The predicted masses, based on amino acid sequence, are also provided.

2.4. Determining the Feasibility of Metal Substitution

To verify that there was no significant loss in activity of the purified MBLs after metal removal and reconstitution, the ability of the purified enzymes and reconstituted di-Zn(II) apo-enzymes to hydrolyse nitrocefin was determined (Figure 2.5 & Table 2.3). Despite some variation in k_{cat} and K_m values when compared to literature reports with freshly prepared enzymes, both BcII and VIM-2 showed little loss in their ability to hydrolyse nitrocefin, as demonstrated by little (less than two-fold) variation in determined affinity constants (k_{cat}/K_m). This verified that the procedure for generating and reconstituting apo-enzymes was not detrimental to the enzymes' catalytic activities.

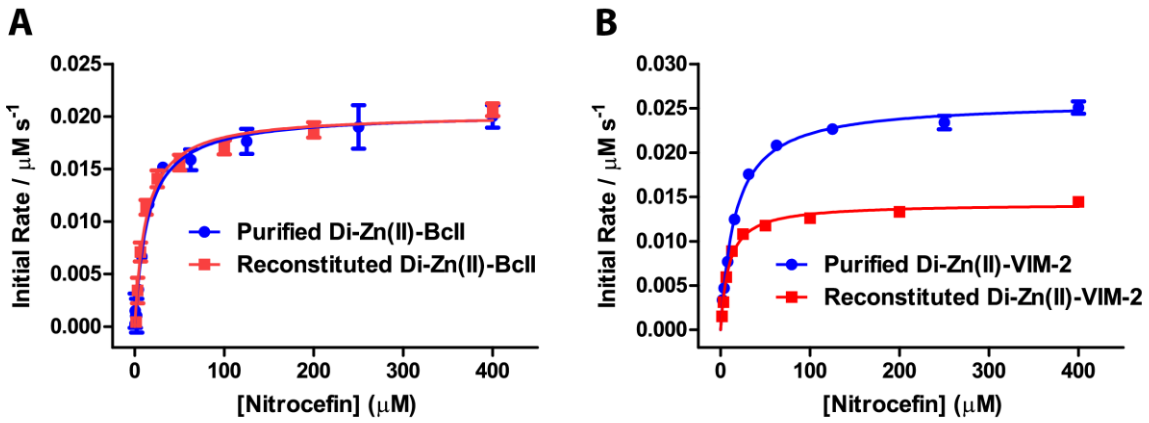

Figure 2.5: Kinetics of A. purified and zinc(II)-reconstituted apo- BcII and B. purified and zinc(II)-reconstituted apo- VIM-2 with nitrocefin. The initial rate of hydrolysis is plotted against substrate concentration. Solid lines indicate the Michaelis-Menten curves fitted in GraphPad Prism(347).

Enzyme	Form	[E] (nM)	k_{cat} (s^{-1})	K_m (μM)	k_{cat}/K_m ($\mu M^{-1} s^{-1}$)
BcII	Purified Di-Zn(II)	1	19.3 ± 0.5	14 ± 2	1.37
BcII	Reconstituted Di-Zn(II)	2	11.2 ± 0.4	11 ± 2	1.02
VIM-2	Purified Di-Zn(II)	0.1	257 ± 3	14 ± 1	18.4
VIM-2	Reconstituted Di-Zn(II)	0.1	162 ± 3	10 ± 1	16.2

Table 2.3: Fitted Michaelis-Menten kinetic constants for the hydrolysis of nitrocefin by purified and zinc(II)-reconstituted apo- BcII and VIM-2.

2.4.1. Assessing Activity with Iron

Having established this, it was ascertained as to whether β-lactamase activity could be restored to apo-BcII and apo-VIM-2 by the provision of iron ions. This restoration was provisionally verified by a visual test of nitrocefin hydrolysis (Figure 2.6). Addition of 10 equivalents of Fe(II), in the form of ammonium iron(II) sulfate, under low oxygen conditions restored efficient β-lactamase activity to apo-BcII, while no nitrocefin hydrolysis by either the apo-enzyme or the salt alone was observed.

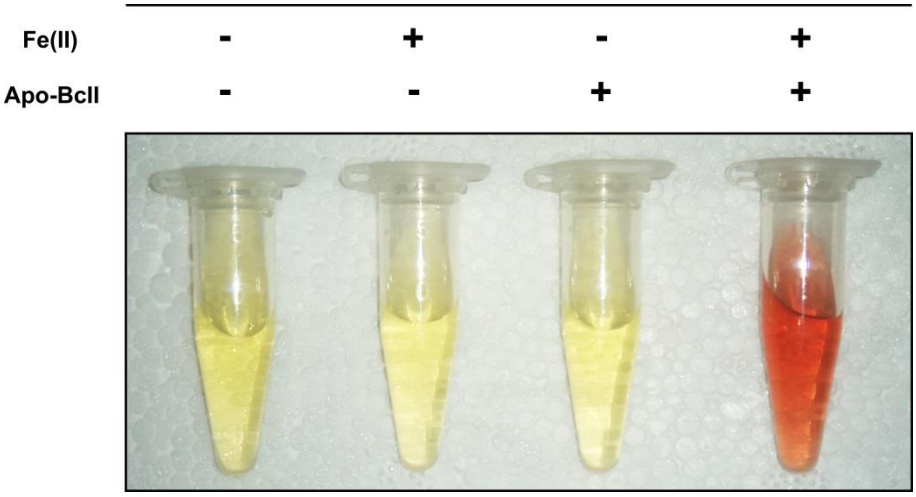

Figure 2.6: Activity of Fe(II)-substituted BcII as exemplified by nitrocefin hydrolysis. Left to right: 100 μM nitrocefin in buffer, 100 μM nitrocefin with 10 μM Fe(II) salt, 100 μM nitrocefin with 10 μM apo-BcII, and 100 μM nitrocefin with 10 μM Fe(II)-substituted BcII. These tests were performed at 25 °C and pH 7.5.

2.4.2. Determining Minimal Metal Requirements

Since the B1 MBLs have two metal binding sites and mono-metallation is a possibility, non-denaturing mass spectrometry (MS) was used to investigate the concentration of metal salts required to produce a di-metallated enzyme as the dominant species (Figure 2.7). This would allow for the activity of the metal-substituted enzymes to be assessed with a minimal excess of metal salt in solution, which might have the potential to interfere with the enzymatic β-lactamase activity. MS analysis confirmed that apo-BcII (measured as 24952 Da) could be reconstituted to its di-Zn(II) form with two equivalents of metal salt or higher (measured as 25082 Da, +130 Da mass shift). A similar result was obtained using Fe(II) salt, with the dominant form of the enzyme being di-Fe(II) after addition of two equivalents of metal (measured as 25064 Da, +112 Da mass shift). Interestingly, different behaviour was seen upon addition of either Zn(II) or Fe(II) salts; with Zn(II), the enzyme transitioned directly from apo-BcII to di-Zn(II) BcII with no detectable mono-metallated enzyme, in contrast a mono-Fe(II) enzyme (measured as 25008 Da, +56 Da mass shift) was seen as the dominant species upon addition of a half or one equivalent of Fe(II) salt. This suggested the possibility of differently metallated β-lactamases demonstrating differing catalytic behaviour, since the enzyme showed variability in its interaction with different metals.

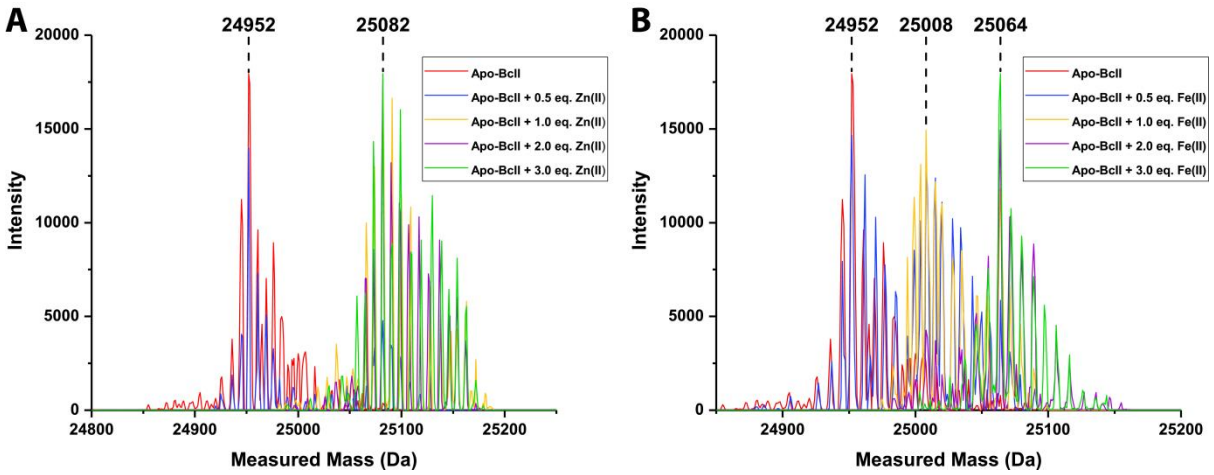

Figure 2.7: Mass spectra of A. 100 μM apo-BcII titrated with increasing equivalents of Zn(II) salt and B. 100 μM apo-BcII titrated with increasing equivalents of Fe(II) salt. All samples were buffer exchanged into, or dissolved in 15 mM ammonium acetate, pH 7.5. A mono-metallated species is visible in the Fe(II) titration that is not seen with the addition of zinc. In both cases the di-metallated enzyme is the dominant species after the addition of two equivalents of metal or higher.

In order to ensure that di-metallated enzymes were the major component in solution, it was decided that 3.5 equivalents of metal salt would be used to reconstitute the apo-MBLs. In addition, since oxidation of the active site Cys221 ligand is precedented both in apo-MBLs as well as in metallated forms of these enzymes(348), it was decided to supplement the enzyme with two equivalents of *tris*(2-carboxyethyl)phosphine (TCEP) prior to addition of metal salts.

2.5. Steady-State Kinetics with Iron-Substituted MBLs

Iron typically exhibits two oxidation states (+2 and +3) with a tendency for iron(II) salt solutions to oxidise in air, forming less soluble iron(III) salts. In previous reports concerning the use of iron by MBLs no attempt to control for the oxidation of the metal ions was reported(328, 333). This may, indeed, be the reason that no β-lactamase activity is seen, since Fe(II) solutions will rapidly oxidise to Fe(III), which may not facilitate catalysis. Thus, in assessing whether iron salts could reconstitute de-metallated MBLs, it was required to determine the effects of both Fe(II) and Fe(III) salts independently. This was achieved by carrying out kinetic assays in a glove-box (Belle Technology) at oxygen concentrations of < 10 ppm, using deoxygenated solutions, in order to significantly reduce the likelihood of iron oxidation.

Using a minimum amount of metal salt to restore di-metallated enzymes, as discussed above, the ability of di-Zn(II)-BcII, di-Fe(II)-BcII, di-Fe(III)-BcII, di-Zn(II)-VIM-2, di-Fe(II)-VIM-2, and di-Fe(III)-VIM-2 to hydrolyse both the reporter substrate,

nitrocefin, and the clinically used carbapenem, meropenem was investigated by measuring changes in absorbance at 485 nm or 295 nm (corresponding to hydrolysed nitrocefin or intact meropenem, respectively, Figure 2.8 & Tables 2.4 & 2.5). Substitution with Fe(III) salts under the same conditions did not produce any measurable β-lactamase activity. In the case of BcII, both di-Zn(II)- and di-Fe(II)-BcII were able to hydrolyse nitrocefin and meropenem with highly comparable specificity constants 0.82 and 1.2 μM^{-1} s^{-1}, respectively, for nitrocefin hydrolysis and 0.4 and 0.17 μM^{-1} s^{-1}, respectively, for meropenem hydrolysis. With VIM-2, hydrolysis of both nitrocefin and meropenem was seen with Fe(II) substitution, however this was less efficient in both cases, with an 11-fold drop in k_{cat}/K_m (from 16 to 1.4 μM^{-1} s^{-1}) with nitrocefin, and a comparable 8-fold drop (from 0.24 to 0.03 μM^{-1} s^{-1}) with meropenem.

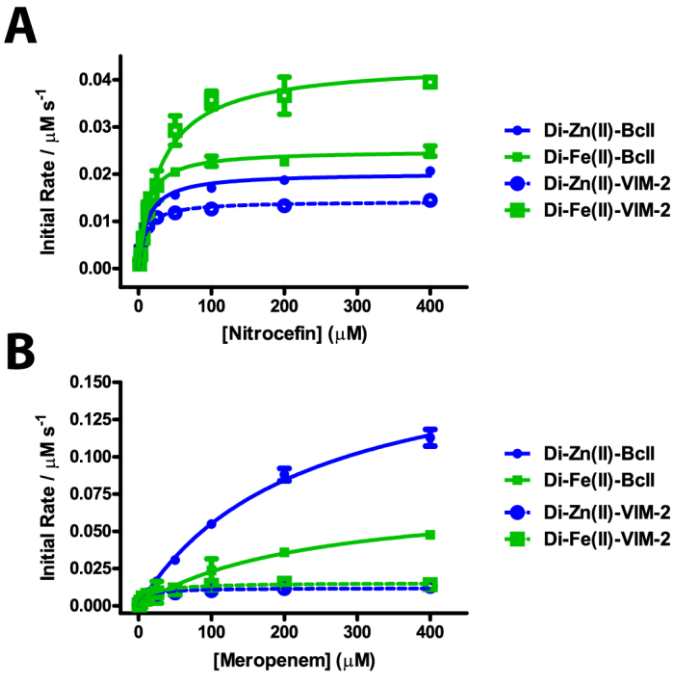

Figure 2.8: Kinetics of di-Zn(II)- and di-Fe(II)- BcII and VIM-2 with A. nitrocefin and B. meropenem. The initial rate of hydrolysis is plotted against substrate concentration. Hydrolysis data were collected at 25 °C and pH 7.5. Solid lines indicate the Michaelis-Menten curves fitted for BcII and dashed lines indicate curves fitted for VIM-2. Curves were fitted using GraphPad Prism(347).

Enzyme	Metal	[E] (nM)	k_{cat} (s^{-1})	K_m (μM)	k_{cat}/K_m (μM^{-1} s^{-1})
BcII	Zn(II)	2	10.1 ± 0.4	12 ± 2	0.82
BcII	Fe(II)	2	12.5 ± 0.4	11 ± 2	1.2
VIM-2	Zn(II)	0.1	143 ± 3	9 ± 1	16
VIM-2	Fe(II)	1	44 ± 2	32 ± 5	1.4

Table 2.4: Fitted Michaelis-Menten kinetic constants for the hydrolysis of nitrocefin by di-Zn(II)-and di-Fe(II)-BcII and VIM-2. Hydrolysis data were collected at 25 °C and pH 7.5.

Enzyme	Metal	[E] (nM)	k_{cat} (s^{-1})	K_m (μM)	k_{cat}/K_m ($\mu M^{-1} s^{-1}$)
BcII	Zn(II)	2	89 ± 3	220 ± 20	0.4
BcII	Fe(II)	2	38 ± 2	230 ± 30	0.17
VIM-2	Zn(II)	5	2.4 ± 0.1	10 ± 2	0.24
VIM-2	Fe(II)	30	0.5 ± 0.0	16 ± 2	0.03

Table 2.5: Fitted Michaelis-Menten kinetic constants for the hydrolysis of meropenem by di-Zn(II)-and di-Fe(II)- BcII and VIM-2. Hydrolysis data were collected at 25 °C and pH 7.5.

2.6. Other Metal Substitutions

As mentioned previously, the activity of the MBLs with a number of metal substitutions has been reported(327). Alongside work with iron, the ability of BcII and VIM-2 to hydrolyse nitrocefin and meropenem, when substituted with limiting quantities of different transition metal ions was investigated (Table 2.6). To gain information about each metal's ability to stabilise the MBL fold, melting temperatures for each metal substituted variant were also obtained (Figure 2.9 & Table 2.7).

Subtrate	Enzyme	Metal	[E] (nM)	k_{cat} (s^{-1})	K_m (μM)	k_{cat}/K_m ($\mu M^{-1} s^{-1}$)
Nitrocefin	BcII	Zn(II)	2	10.1 ± 0.4	12 ± 2	0.82
		Fe(II)	2	12.5 ± 0.4	11 ± 2	1.2
		Co(II)	2	6.8 ± 0.2	78 ± 6	0.087
		Mn(II)	4	1.47 ± 0.05	41 ± 5	0.035
	VIM-2	Zn(II)	0.1	143 ± 3	9 ± 1	16
		Fe(II)	1	44 ± 2	32 ± 5	1.4
		Co(II)	4	11.8 ± 0.6	26 ± 5	0.45
		Mn(II)	8	60 ± 1	172 ± 8	0.35
Meropenem	BcII	Zn(II)	2	89 ± 3	220 ± 20	0.40
		Fe(II)	2	38 ± 2	230 ± 30	0.17
		Co(II)	4	51 ± 9	400 ± 100	0.13
		Mn(II)	4	32 ± 5	160 ± 50	0.20
	VIM-2	Zn(II)	5	2.4 ± 0.1	10 ± 2	0.24
		Fe(II)	30	0.5 ± 0.0	16 ± 2	0.03
		Co(II)	250	0.38 ± 0.4	30 ± 10	0.013
		Mn(II)	250	1.27 ± 0.05	250 ± 20	0.0051

Table 2.6: Fitted Michaelis-Menten kinetic constants for the hydrolysis of nitrocefin and meropenem by transition metal substituted BcII and VIM-2. Hydrolysis data were collected at 25 °C and pH 7.5. The values from tables 2.4 and 2.5 are included for comparison.

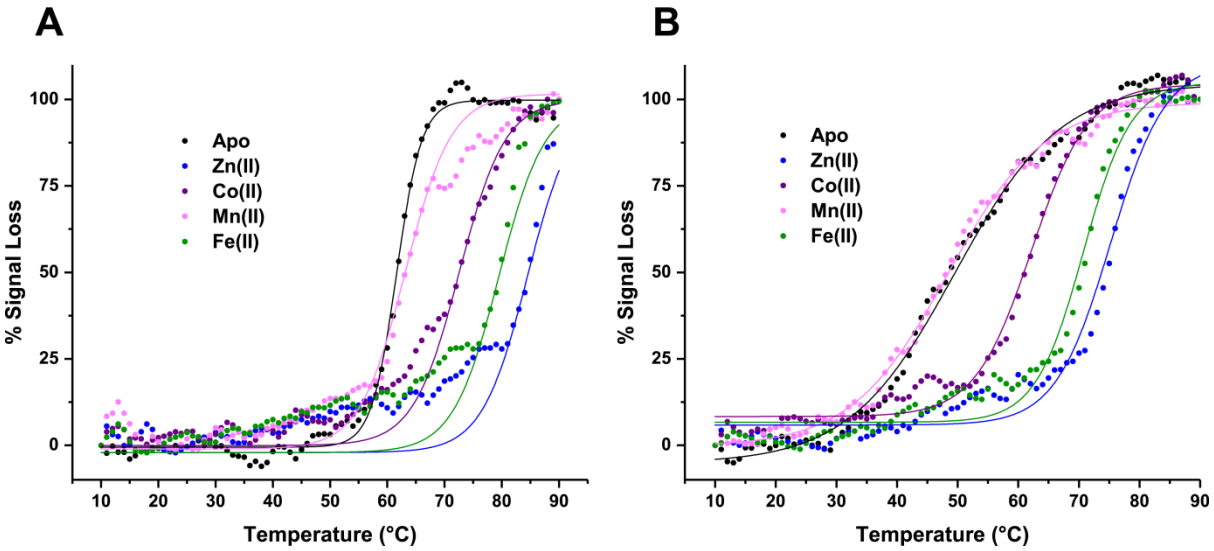

Figure 2.9: Melting curves for transition metal substituted the metallo-β-lactamases, A. BcII and B. VIM-2, as determined by circular dichroism spectroscopy. Enzymes were assayed at 0.2 mg mL^{-1} in 10 mM sodium phosphate buffer, pH 7.5. Curve fitting was performed using OriginPro(349).

Enzyme	Metal	Tm (°C)
BcII	Apo	61.6 ± 0.1
	Zn(II)	~ 85
	Fe(II)	79 ± 1
	Co(II)	73.4 ± 0.3
	Mn(II)	63.7 ± 0.3
VIM-2	Apo-	49.5 ± 0.3
	Zn(II)	75.2 ± 0.5
	Fe(II)	70.7 ± 0.4
	Co(II)	62.2 ± 0.2
	Mn(II)	48.3 ± 0.3

Table 2.7: Melting temperatures for transition metal substituted metallo-β-lactamases, as determined by circular dichroism spectroscopy. Enzymes were assayed at 0.2 mg mL^{-1} in 10 mM sodium phosphate buffer, pH 7.5.

Substitution of BcII with cobalt(II) or manganese(II) resulted in a 10 to 20-fold lower catalytic efficiency for the hydrolysis of nitrocefin, when compared to zinc(II) or iron(II) substitution, but only a four-fold reduction for meropenem hydrolysis (0.4 μM^{-1} s^{-1} *versus* 1.3 μM^{-1} s^{-1} for Zn(II) and Co(II), respectively). In both cases Mn(II) ions gave a lower value, and this may be a result of poor binding of the metal ions at this pH and concentration, as reflected by the low stabilisation of the metal-substituted enzyme relative to the apo form (T_m values of 63.7 ± 0.3 and 61.6 ± 0.1 °C for Mn(II)-substituted and apo BcII, respectively, Table 2.7). A similar pattern is seen with VIM-2, where Mn(II) and Co(II) substitution gave

poorer efficiencies for the hydrolysis of both nitrocefin and meropenem, relative to zinc(II) and iron(II). Once again, the calculated melting temperature suggests that Mn(II) is poorly bound by VIM-2 under these conditions, with no stabilisation of the protein relative to the apo-enzyme (T_m values of 48.3 ± 0.3 and 49.5 ± 0.3 °C for Mn(II) substitution and apo-VIM-2, respectively).

Interestingly, substitution of both enzymes with Fe(II) stabilises the enzymes most comparably to the Zn(II)-substituted counterparts. Thus, it seems likely that the affinity of the MBL active site for ferrous ions is closer to the affinity for zinc(II) when compared to Mn(II) or Co(II). This result may be the reason for the comparable activities of Zn(II) and Fe(II)-substituted enzymes under the assay conditions employed.

2.7. Stopped-Flow Kinetics with Iron-Substituted MBLs

Having established that MBLs were active when substituted with Fe(II), and given that they potentially respond differently to Zn(II) and Fe(II), at least in the case of binding (Figure 2.7), it was investigated whether the mechanism of nitrocefin hydrolysis by MBLs was altered upon substitution of Zn(II) for Fe(II). To investigate this, stopped-flow absorption spectroscopy kinetics were employed to monitor the reaction of di-Zn(II) and di-Fe(II) BcII and VIM-2 in a 1:1 ratio with nitrocefin. Nitrocefin absorbs at 390 nm, and the hydrolysed nitrocefin product absorbs at 485 nm. In some experiments an additional feature at 665 nm has been characterised, which is attributed the formation of an anionic intermediate in the hydrolysis reaction(282, 289, 290, 292). This intermediate has been characterised in the VIM-2 catalysed reaction with a similar substrate, chromacef(283), but is reportedly absent in the BcII-catalysed hydrolysis of nitrocefin(281). Variation in BcII activity as a function of pH has previously been observed(327). Therefore, BcII- and VIM-2-catalysed hydrolysis of nitrocefin was investigated at pH values of 5.5, 6.5 and 7.5.

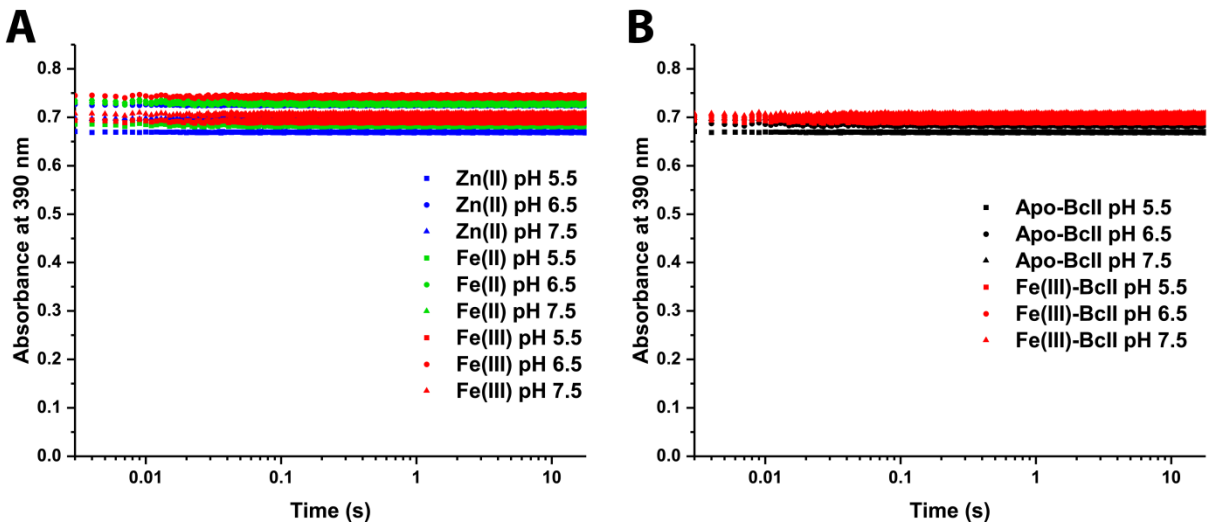

Figure 2.10: Spectral changes seen at 390 nm when 100 μM nitrocefin is mixed with buffer at pH 5.5, 6.5, or 7.5, supplemented with A. 100 μM metal salt or B. 100 μM apo-, or Fe(III)-substituted, BcII. Stopped-flow experiments were carried out at 5 °C. In this control experiment, no substrate hydrolysis is seen over the typical time course of an enzyme catalysed reaction.

2.7.1. Spectral Data Analysis

No hydrolysis of the substrate was observed in metal salt supplemented buffers over the course of the enzyme-catalysed reaction (Figure 2.10). The time taken for complete reaction of the nitrocefin substrate was similar for both di-Zn(II) and di-Fe(II) BcII, but substantially longer for di-Fe(II) VIM-2 when compared to di-Zn(II) VIM-2, which likely reflects the differences in the second order Michaelis-Menten rate constants (k_{cat}/K_m) seen in the steady-state kinetics.

As precedented by previous reports(281, 283), spectral changes corresponding to substrate depletion (390 nm) and product accumulation (485 nm) were observed with both di-Zn(II) and di-Fe(II) BcII and VIM-2 enzymes (Figures 2.11 – 2.13). Di-Zn(II) BcII showed no detectable intermediate while a clear feature with a maximum absorbance wavelength (λ_{max}) at 665 nm was observed with di-Zn(II) VIM-2. Both of these observations are in agreement with the literature(281, 283).

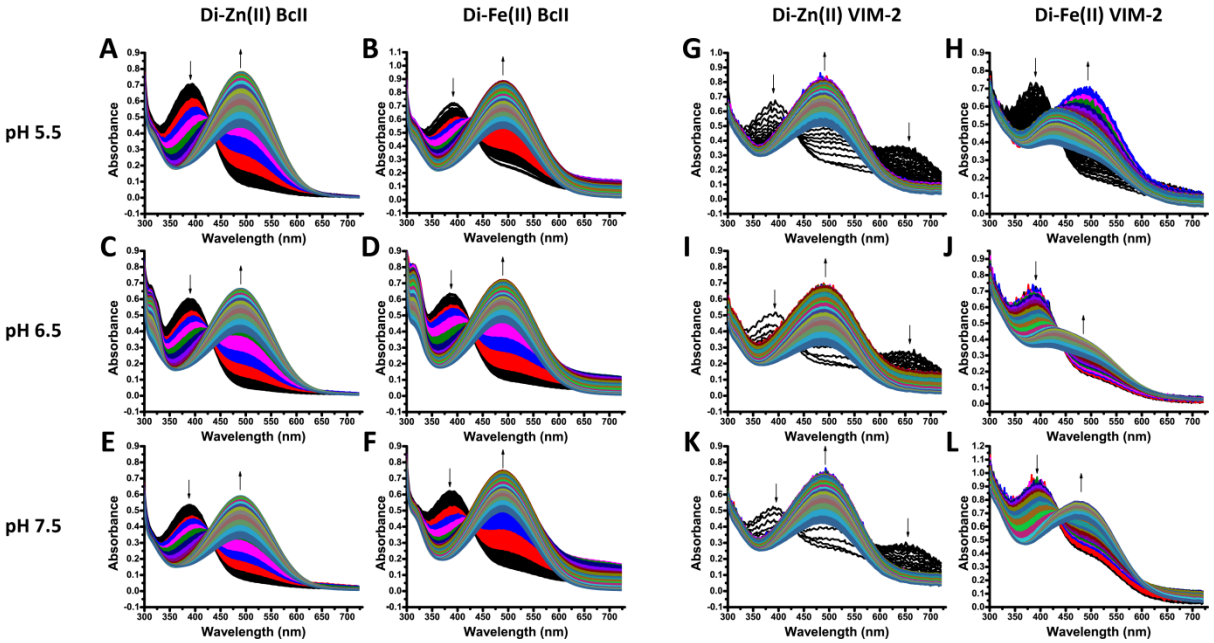

Figure 2.11: pH-Dependent spectral changes seen during the reaction of the specified enzyme at 50 μM with 50 μM nitrocefin in a 1:1 ratio at 5°C. A. Di-Zn(II) BcII, pH 5.5. B. Di-Fe(II) BcII, pH 5.5. C. Di-Zn(II) BcII, pH 6.5. D. Di-Fe(II) BcII, pH 6.5. E. Di-Zn(II) BcII, pH 7.5. F. Di-Fe(II) BcII, pH 7.5. G. Di-Zn(II) VIM-2, pH 5.5. H. Di-Fe(II) VIM-2, pH 5.5. I. Di-Zn(II) VIM-2, pH 6.5. J. Di-Fe(II) VIM-2, pH 6.5. K. Di-Zn(II) VIM-2, pH 7.5. L. Di-Fe(II) VIM-2, pH 7.5.

With di-Fe(II) BcII, no clear feature (as compared to the spectra obtained with di-Zn(II) VIM-2 (Figure 2.11)) was observed around 665 nm in the normal absorbance spectra. However difference spectra, which employed the absorbance spectrum at an intermediate time point in the reaction as a baseline, revealed a decaying feature with a λ_{max} of 665 nm (Figure 2.12). Although it is possible this feature might have been the result of an extended shoulder to the absorbance feature at 485 nm, the demonstration that the 665 nm decays while the 485 nm simultaneously grows confirms that the 665 nm feature corresponds to an independent species. A similar difference spectrum obtained from the di-Zn(II) BcII catalysed reaction showed no feature like this, as expected. This feature at 665 nm also appeared to be pH dependent, with a more substantial absorbance seen at pH 7.5, a reduced absorbance at pH 6.5, and again at pH 5.5.

On substitution of VIM-2 with iron, the apparent intermediate previously seen at 665 nm was no longer present, with negligible changes at 665 nm, even in difference spectra (Figure 2.13). Thus the observation of a reaction intermediate in nitrocefin hydrolysis at 665 nm appears to be dependent, not just on the enzyme catalyzing the reaction, but on the particular metal-enzyme combination employed.

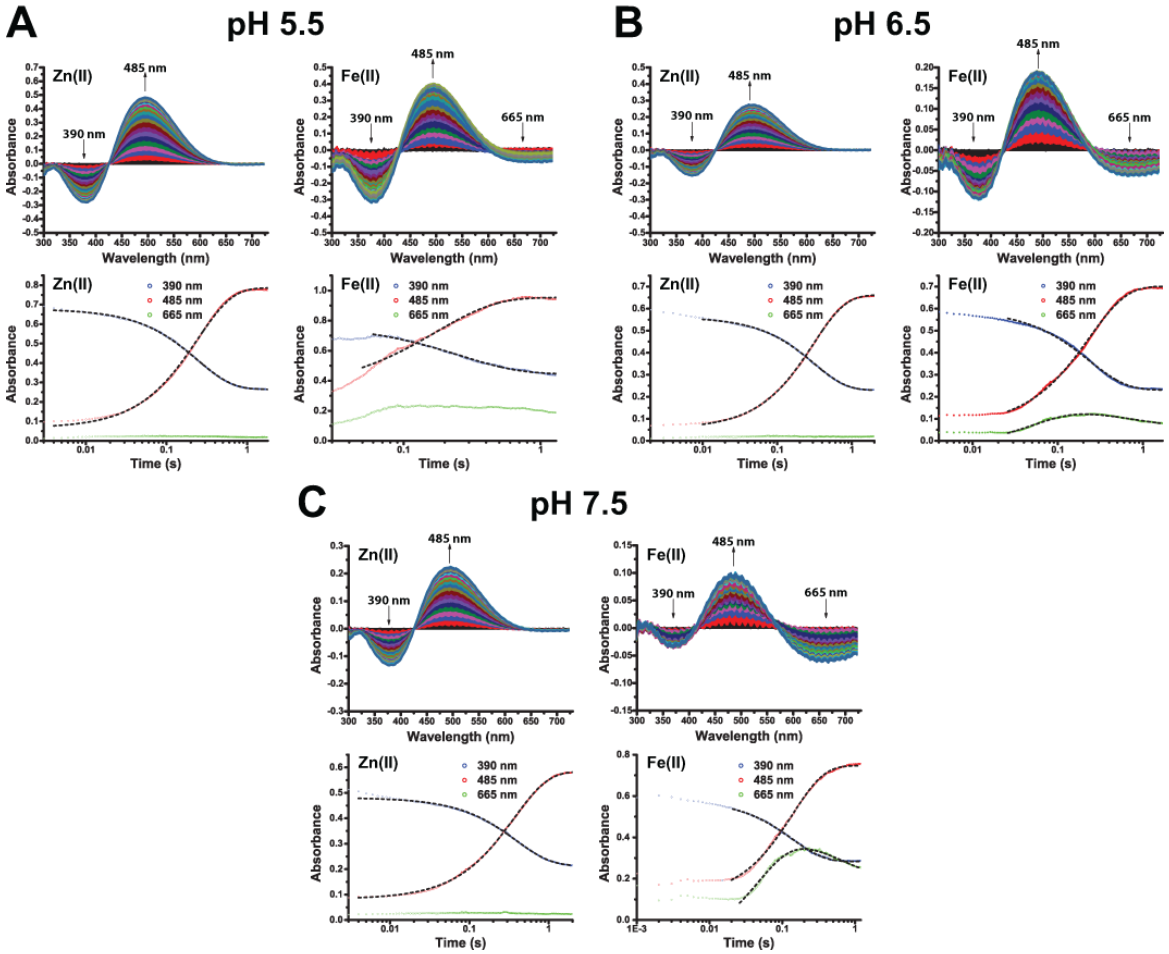

Figure 2.12: Stopped-flow kinetics of BcII catalysed nitrocefin hydrolysis at A. pH 5.5, B. pH 6.5 and C. pH 7.5. Spectral changes during the reaction of 50 μM di-Zn(II) BcII, or di-Fe(II) BcII, respectively, with 50 μM nitrocefin in a 1:1 ratio at pH 7.5 and 5°C. Difference spectra of absorbance wavelengths 300-750 nm from 0.3–1.2 s using absorbance at 0.3 s as a baseline. Arrows indicate growth or decay of peaks and λ_{max} values. Absorbance traces at 390, 485 and 665 nm over the reaction time course are also shown with dashed lines indicate fitting curve traces.

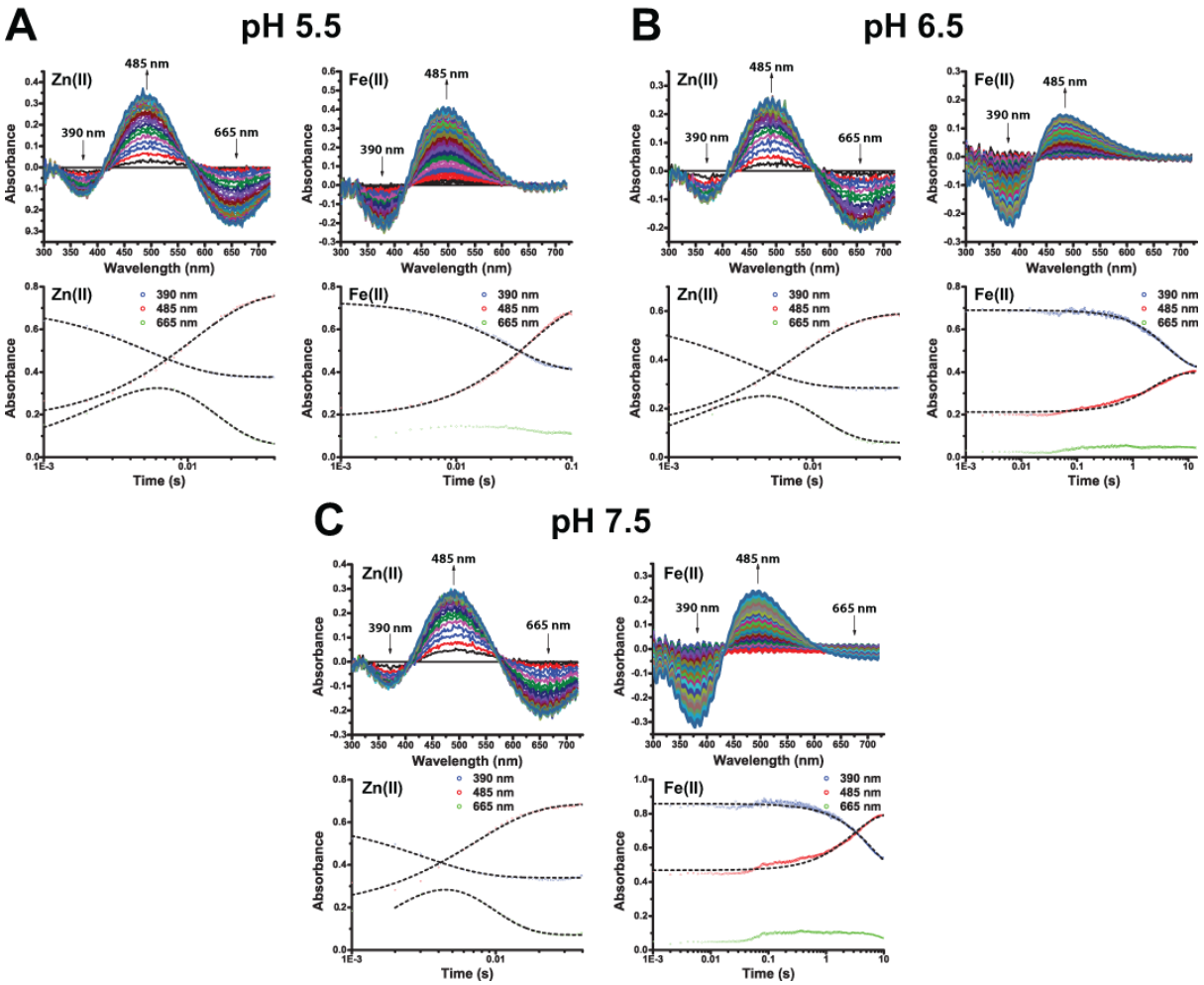

Figure 2.13: Stopped-flow kinetics of VIM-2 catalysed nitrocefin hydrolysis at A. pH 5.5, B. pH 6.5 and C. pH 7.5. Spectral changes during the reaction of 50 μM di-Zn(II) VIM-2, or di-Fe(II) VIM-2, respectively, with 50 μM nitrocefin in a 1:1 ratio at pH 7.5 and 5°C. Difference spectra of absorbance wavelengths 300-750 nm from 0.3–1.2 s using absorbance at 0.3 s as a baseline. Arrows indicate growth or decay of peaks and λ_{max} values. Absorbance traces at 390, 485 and 665 nm over the reaction time course are also shown with dashed lines indicate fitting curve traces.

2.7.2. Fitting of Kinetic Traces

Fitting of stopped-flow kinetic traces was carried out using OriginPro software(349). Kinetic traces for the di-Zn(II) BcII and di-Zn(II) VIM-2 reaction time courses, corresponding to substrate depletion (λ_{max} of 390 nm) and product accumulation (λ_{max} of 485 nm) were successfully fitted by a single exponential function at all pH values (Figure 2.12). The changes in absorbance at 665 nm, corresponding to production and depletion of an intermediate species, were fitted by a double exponential function for di-Zn(II) VIM-2 at all pH values and di-Fe(II) BcII at pH 7.5 and 6.5. It was not possible to fit the 665 nm absorbance trace for di-Fe(II) BcII at pH 5.5 (Figure 2.13) in the same manner. This is likely due to the shallow gradient of this trace on account of low changes in the absorbance at 665

nm. The fitting constants obtained for the BcII and VIM-2 catalysed reactions are shown in Tables 2.8 & 2.9, respectively.

Metal	pH	Substrate Decay (s^{-1})	Intermediate Growth (s^{-1})	Intermediate Decay (s^{-1})	Product Growth (s^{-1})
Zn(II)	5.5	4.16 ± 0.01	-	-	4.13 ± 0.01
Zn(II)	6.5	3.24 ± 0.01	-	-	3.29 ± 0.01
Zn(II)	7.5	2.55 ± 0.01	-	-	2.75 ± 0.01
Fe(II)	5.5	3.88 ± 0.01	Not Fitted	Not Fitted	5.78 ± 0.01
Fe(II)	6.5	5.25 ±0.01	18.31 ± 0.01	1.2 ± 0.1	4.27 ± 0.01
Fe(II)	7.5	7.25 ± 0.01	20.32 ± 0.01	1.4 ± 0.1	7.20 ± 0.01

Table 2.8: Analysis of the reaction of Zn(II)- and Fe(II)-substituted BcII, 50 μM, with 50 μM nitrocefin in a 1:1 ratio. Fitting constants are obtained from analysis of reaction time courses seen in Figures 2.12. Substrate Decay, Product Accumulation and Intermediate Accumulation and Decay correspond to absorbance features at 390, 485 and 665 nm, respectively.

Metal	pH	Substrate Decay (s^{-1})	Intermediate Growth (s^{-1})	Intermediate Decay (s^{-1})	Product Growth (s^{-1})
Zn	5.5	189.75 ± 3.55	220.75 ± 19.65	123.76 ± 9.64	92.94 ± 2.28
Zn	6.5	292.40 ± 11.76	315.46 ± 80.09	168.07 ± 34.36	128.70 ± 3.84
Zn	7.5	322.58 ± 25.14	359.71 ± 125.16	182.48 ± 46.88	140.06 ± 5.38
Fe(II)	5.5	35.05 ± 0.73	-	-	23.43 ± 0.50
Fe(II)	6.5	0.24 ± 0.01	-	-	0.44 ± 0.01
Fe(II)	7.5	0.15 ± 0.01	-	-	0.35 ± 0.01

Table 2.9: Analysis of the reaction of Zn- and Fe(II)-substituted VIM-2, 50 μM, with 50 μM nitrocefin in a 1:1 ratio. Fitting constants are obtained from analysis of reaction time courses seen in Figures 2.13. Substrate Decay, Product Growth and Intermediate Growth and Decay correspond to absorbance features at 390, 485 and 665 nm, respectively.

2.7.3. Mechanism of the Di-Fe(II)-MBL Reaction

In the case of di-Zn(II) BcII catalysed nitrocefin hydrolysis, the fitting constants for substrate decay and product accumulation match well and are consistent with a mechanism in which there is no reaction intermediate.

In contrast, a spectral feature at 665 nm is seen in the di-Fe(II) BcII catalysed reaction, which, given the wavelength of the absorbance, likely corresponds to an anionic intermediate (Figure 2.15)(350). This observation of an intermediate at 665 nm is correlated with pH, with a larger change in absorbance amplitude at pH 7.5 compared to that seen at pH 6.5 and 5.5 of (0.25, 0.15 and 0.05 absorbance units, respectively). The decay of this feature is slower than product accumulation, suggesting that di-Fe(II) BcII might employ a

branched reaction pathway as an alternative to the typically proposed linear pathway proceeding through an anionic intermediate (Figure 2.15).

Data fitting using the KinTek Explorer package(351) was unable to distinguish between linear and branched pathways (Figure 2.14), but in both fittings the decay of the intermediate species was identified as the rate-limiting step (k_3 and k_4 in Tables 2.10 & 2.11, respectively). Intermediate decay is rate limiting, yet a negligible amount of intermediate is seen at pH 5.5. This may be explained either by a branched pathway, in which the branch with no intermediate is favoured by lower pH, or by a linear pathway in which the rate of decay of the intermediate rises with a decrease in pH thus preventing an observable accumulation of intermediate.

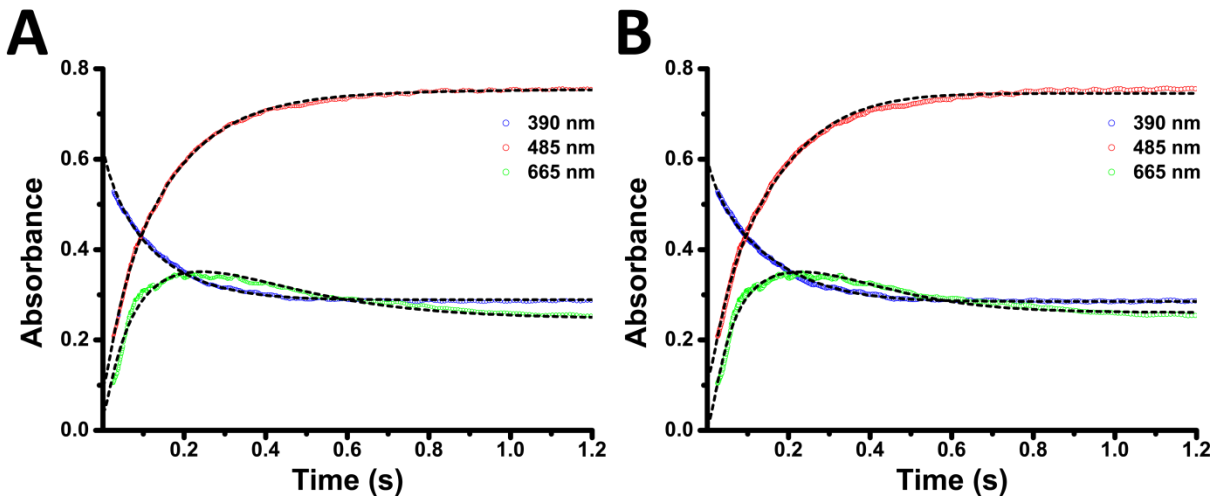

Figure 2.14: Spectral changes during the reaction of 50 µM di-Fe(II) BcII with 50 µM nitrocefin in a 1:1 ratio at pH 7.5 and 5°C. Dotted lines show the results of data fitting using KinTek Explorer(352). A. Fitting of data using a linear mechanism. Fitting constants can be found in Table 2.10. B. Fitting of data using a proposed branched mechanism. Fitting constants can be found in Table 2.11 C. Outline of the two mechanisms used to fit the data as well as associated kinetic constants.

Variable	Fitted Value	% Error
k_1	225000 M^{-1} s^{-1}	0.73
k_{-1}	0.000000403 s^{-1}	ND
k_2	82.7 s^{-1}	3.62
k_3	7.2 s^{-1}	0.98
k_4	100000000 s^{-1}	fixed
ε_S	6319 M^{-1} cm^{-1}	fixed
ε_P	12600 M^{-1} cm^{-1}	fixed
ε_{I+S}	13820 M^{-1} cm^{-1}	fixed
ε_{I+P}	4999 M^{-1} cm^{-1}	fixed
$Offset_S$	0.2851	fixed
$Offset_P$	0.116	fixed
$Offset_I$	0.01078	fixed

Table 2.10: Kinetic constants obtained from fitting the reaction of 50 μM di-Fe(II) BcII with 50 μM nitrocefin in a 1:1 ratio at pH 7.5 and 5°C using a linear mechanism. Data fitting was carried out using KinTek Explorer(352). Fixed values were first allowed to float from initial variables before fixing. ND – Not determined.

Variable	Fitted Value	% Error
k_1	239000 M^{-1} s^{-1}	0.84
k_{-1}	0.0000001 s^{-1}	ND
k_2	46 s^{-1}	6.59
k_3	73.4 s^{-1}	5.79
k_4	4.18 s^{-1}	1.9
k_5	100000000 s^{-1}	fixed
ε_S	6700 M^{-1} cm^{-1}	fixed
ε_{S+P}	13200 M^{-1} cm^{-1}	fixed
ε_P	10600 M^{-1} cm^{-1}	fixed
ε_{I+S}	13500 M^{-1} cm^{-1}	fixed
ε_{I+P}	4180 M^{-1} cm^{-1}	fixed
$Offset_S$	0.289	fixed
$Offset_P$	0.0966	fixed
$Offset_I$	0.0377	fixed

Table 2.11: Kinetic constants obtained from fitting the reaction of 50 μM di-Fe(II) BcII with 50 μM nitrocefin in a 1:1 ratio at pH 7.5 and 5°C using a branched mechanism. Data fitting was carried out using KinTek Explorer(352). Fixed values were first allowed to float from initial variables before fixing. ND – Not determined.

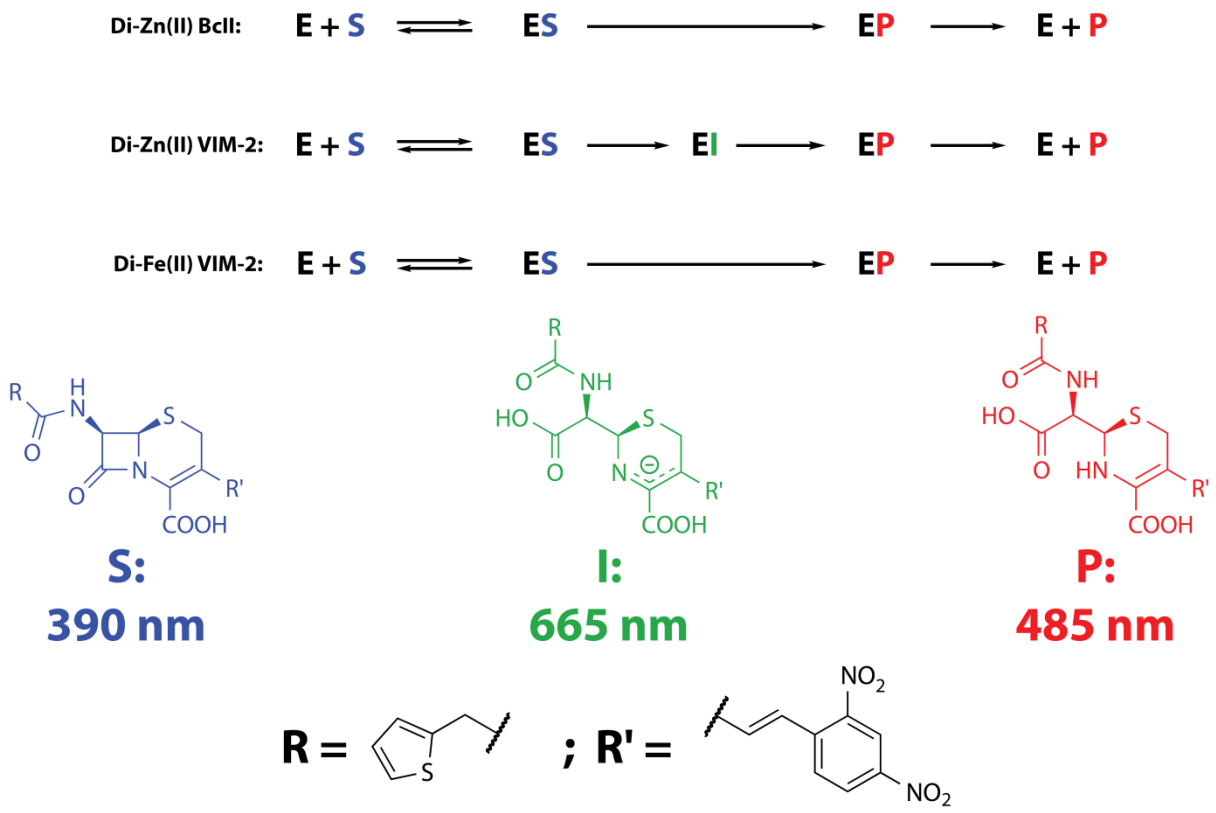

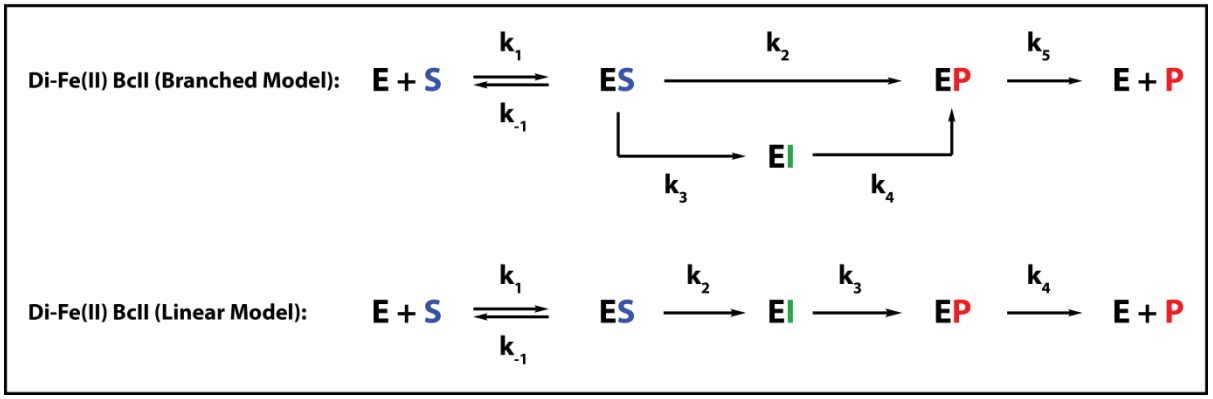

Figure 2.15: Proposed possible reaction schemes for differently metal-substituted BcII and VIM-2. Di-Zn(II) BcII exhibits no observable intermediate, while the hydrolysis of nitrocefin by di-Fe(II) BcII is best described by a branched mechanism. Di-Zn(II) VIM-2 exhibits an on pathway intermediate that is not observed with di-Fe(II) VIM-2. The corresponding species, S, I and P, and their absorbance wavelengths, are also shown.

It should be noted that two different trends in pH dependency are seen with di-Zn(II) and di-Fe(II) BcII. With di-Zn(II) BcII, the rate of substrate decay is highest at pH 5.5 and lowest at pH 7.5 (2.55 s^{-1} and 4.16 s^{-1}, respectively). In contrast, the opposite trend is seen with di-Fe(II) BcII, which exhibits the highest rate of substrate decay at pH 7.5 (7.25 s^{-1} at pH 7.5 vs 3.88 s^{-1} at pH 5.5). The reverse of these two trends is seen with VIM-2. Di-Zn(II) VIM-2 is more active at higher pH (substrate decay of 320 s^{-1} at pH 7.5 vs 190 s^{-1} at pH 5.5) while di-

Fe(II) VIM-2 shows the opposite effect, with a very low rate of substrate depletion at both pH 7.5 and 6.5 (0.15 and 0.24 s^{-1}, respectively) compared to that at pH 5.5 (35 s^{-1}).

In general for VIM-2, fitting values for the di-Zn(II) enzyme, in whose reaction an intermediate at 665 nm was seen, give good support to an on pathway intermediate as observed in studies with a similar substrate, chromacef, which is similar to nitrocefin(283), whereas there is no appreciable change in absorbance at 665 nm with di-Fe(II) enzyme at all pH values. Thus, nitrocefin hydrolysis by di-Zn(II) VIM-2 proceeds through an anionic intermediate which is no longer apparent upon substitution with Fe(II) (Figure 2.15).

Collectively, these results reveal that the mechanism of nitrocefin hydrolysis by an MBL may be changed upon substitution of the native zinc for iron(II), as demonstrated by the observable presence or absence of an intermediate species and by the potential introduction of a branched reaction pathway (Figure 2.15). Differing rates of reaction with different enzyme, metal, and pH combinations indicate that the optimum pH conditions for β-lactam hydrolysis are both metal- and enzyme-dependent, which is a result consistent with literature reports on MBLs(327, 353, 354).

2.8. Inhibition of Iron-Substituted MBLs

Since MBL inhibition is a current target for medicinal chemistry(140, 280), and given the differences observed in the metal-binding and kinetic properties of di-Fe(II) BcII and VIM-2 compared to their di-Zn(II) enzymes, it was investigated as to whether the two metal-substituted BcII enzymes might respond differently to known MBL inhibitors (Tables 2.12 & Figure 2.16). Of particular interest was the response of these two enzyme forms to thiol-based MBL inhibitors, since these compounds exert their inhibitory effect via their thiol sulfur bridging between the two metal centres as an analogue of the bridging water during inhibition(254, 355). Residual β-lactamase activity, through the hydrolysis of nitrocefin, was measured *via* absorbance of the hydrolysed product (λ_{max} = 485 nm) for a range of inhibitor concentrations. All measurements were performed at 25 °C and pH 7.5. The di-Zn(II) and di-Fe(II) enzymes were pre-incubated for 10 minutes with inhibitors before the addition of the substrate. EDTA was used to investigate the ability of BcII to bind the two transition metals, and two thiol inhibitors – thiomandelic acid (TMA)(316), which is a broad spectrum inhibitor of MBLs, and the thioenolate ML302F, which has been shown to be a potent inhibitor of B1 MBLs(318), were tested.

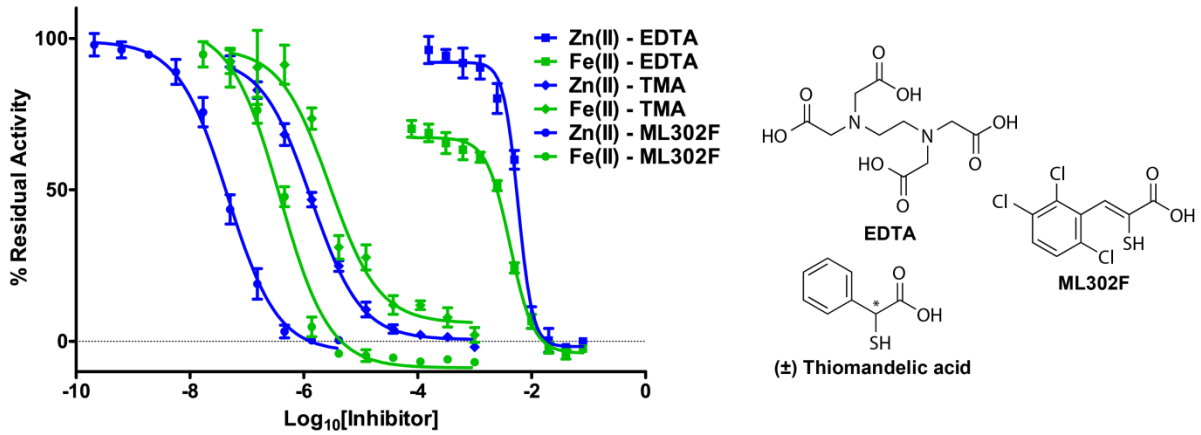

Figure 2.16: IC_{50} traces for metal-substituted BcII with TMA (diamonds), EDTA (squares) and ML302F (circles). Residual hydrolysis of nitrocefin was followed at 485 nm. Inhibition assays were carried out at 25 °C and pH 7.5. Blue lines indicate di-Zn(II) BcII and green lines di-Fe(II) BcII. The chemical structures of the inhibitors employed are provided.

Inhibitor	Metal	IC_{50} (μM)
EDTA	Zn(II)	7500 ± 300
	Fe(II)	4700 ± 100
Thiomandelic Acid	Zn(II)	1.3 ± 0.3
	Fe(II)	2.8 ± 0.8
ML302F	Zn(II)	0.046 ± 0.001
	Fe(II)	0.38 ± 0.08

Table 2.12: IC_{50} values for inhibitors of metal-substituted BcII, obtained from fitting of residual activity plots using GraphPad Prism(347). Inhibition assays were carried out at 25 °C and pH 7.5.

The measured IC_{50} value for inhibition by EDTA for was similar for the two differently metallated enzymes (i.e. 7.5 and 4.7 mM for di-Zn(II) BcII and di-Fe(II) BcII, respectively). Since the affinity of EDTA for Zn(II) is higher than that for Fe(II)(356), these data demonstrate that the MBL active site has a greater affinity for Zn(II) ions than for Fe(II) ions, a result which is consistent with work characterising Zn(II) ions as, the preferred MBL metal in an endogenous setting(357). Similarly, the IC_{50} values for inhibition by thiomandelic acid were very close for the different metal-substituted forms of BcII. This result may be in contrast to that which is expected given the high affinity of Zn(II) for sulfur ligands(357). However, around a 10-fold difference in IC_{50} was obtained for inhibition by ML302F, an inhibitor which employs a bidentate binding mode in which a sulfur atom bridges the two metal centres, substituting for the bridging water ligand, while the adjacent carboxylate binds to the metal in site 2 (Figure 2.17)(318). This difference may arise as a consequence of the observed structural differences between the di-Zn(II) and di-Fe(II) bound BcII enzymes. (Note that, although attempts to obtain crystal structures of

thiomandelic acid and ML302F with di-Fe(II) BcII were made, via both co-crystallisation and soaking, these were unsuccessful).

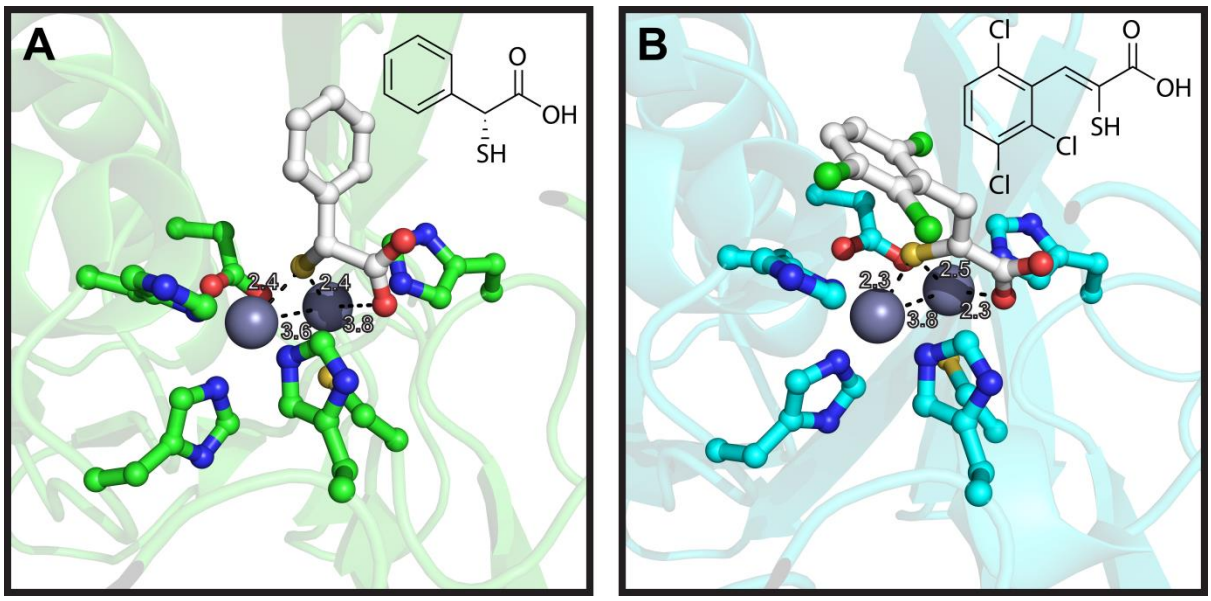

Figure 2.17: Comparison of structures of BcII complexed with A. R-Thiomandelic acid and B. ML302F. Metal-inhibitor coordination distances are shown in Å. The intermetallic distance is also shown. Note that the coordination distance of the carboxylate is much reduced in the ML302F co-crystal when compared to the thiomandelic acid co-crystal, which may account for the greater potency of ML302F against subclass B1 metallo-β-lactamases. The chemical structures of the inhibitors are inset.

These inhibition studies reveal that, in some instances, it is possible for the same inhibitor to exhibit a differing potency against Zn(II)- and Fe(II)-substituted BcII (Table 2.12), with the potent inhibitor ML302F exhibiting a higher IC_{50} against di-Fe(II) BcII than against di-Zn(II) BcII. With this in mind, if there is any possibility that ferrous iron substituted MBLs constitute a minor population of the enzymes produced in a resistant infection, it may be prudent to test MBL inhibitors in clinical development against both Zn(II)- and Fe(II)-bound MBLs, in order to ascertain if they are potent against both metallated forms.

2.9. Structural Characterisation of Iron-Bound BcII

Having established the activity of di-Fe(II) BcII and VIM-2, the alterations to the catalytic mechanism that metal substitution may induce, and the possibility for differences in the inhibition of Zn(II)- and Fe(II)-bound BcII, it was investigated as to whether these differences could be explained structurally.

Using glovebox based crystallographic techniques previously employed in the group to study iron(II)-dependent oxygenases(358), Fe(II)-substituted BcII was successfully crystallised under low oxygen conditions. In addition an apo-preparation of BcII also was

crystallised, whose resolved structure revealed a lack of metal, in line with a previously reported apo-enzyme structure (PDB accession code: 3I0V)(359) and validating the metal-free MBL preparations. Diffraction data were integrated and scaled using iMosflm and AIMLESS(360, 361), and initial phases were obtained by molecular replacement using a reported structure for BcII in complex with two zinc ions (PDB accession code: 4C09)(254) as a search model. This was followed by iterative rounds of refinement and model fitting using PHENIX and Coot(362, 363). Statistical information on data collection and refinement can be found in Table 2.13. (The di-Zn(II) BcII structure (4C09) was used in structural comparisons, since the data are of a comparable quality and resolution to the di-Fe(II) data and were obtained under similar crystallisation conditions.)

Data Set	Diferrous-BcII
Data Collection	
Source	Diamond Light Source I02 Beamline
Wavelength (Å)	0.9795
Resolution Range (Å)	14.18 – 1.1 (1.139 – 1.1)[a]
Space Group	$C\ 2_1$
Unit Cell Parameters	
a, b, c (Å)	53.1, 61.1, 69.4
α, β, γ (°)	90.0, 93.1, 90.0
Unique Reflections	87857 (4468)[a]
Completeness (%)	97.48 (92.67)[a]
Redundancy	6.1
R_{merge}	0.065 (0.10)[a]
$\langle I/\sigma(I)\rangle$	16.9 (4.9)[a]
Refinement	
R_{work}/R_{free}	0.1173/0.1395
RMSD	
Bonds (Å)	0.012
Angles (°)	1.568
Average B-factor for protein atoms ($Å^2$)	16.6
Ramachandran Plot	
Most Favoured Geometry (%)	96
Additionally Allowed (%)	4
Outliers (%)	0

Table 2.13: Crystallographic data and refinement statistics for di-Fe(II) BcII. [a]Values for the highest resolution shell.

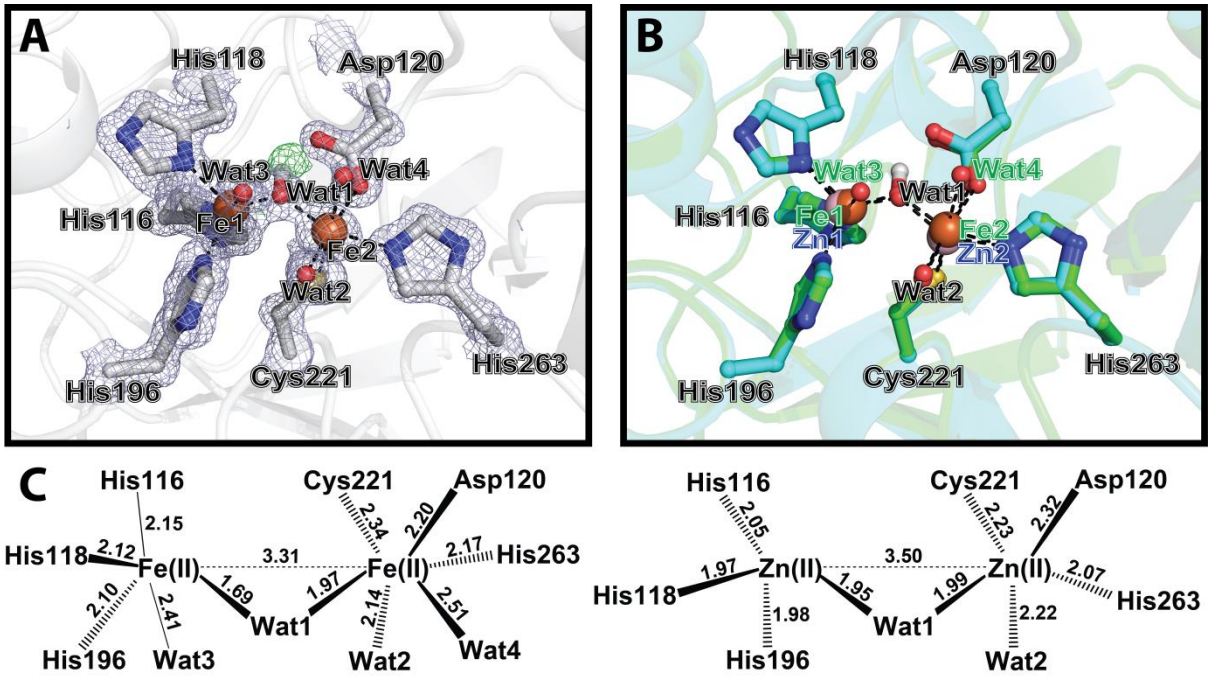

Figure 2.18: Comparison of the active site geometries of di-Fe(II) BcII (1.1 Å resolution) and di-Zn(II) BcII (1.2 Å resolution). A. Active site of di-Fe(II) BcII structure is shown with representative electron density (3.0 σ mF$_o$-DF$_c$ OMIT, blue mesh). The position of the modelled hydrogen atom associated with the bridging hydroxide ion and its representative electron density are shown (3.0 σ mF$_o$-DF$_c$ OMIT, green mesh). B. Comparison of di-Fe(II) (green) and di-Zn(II) BcII (cyan, PDB Code: 4C09). The amino acid residues occupy very similar positions in both structures but there are clear shifts in the positions of the metal ions. In addition each of the two ferrous ions binds a further water molecule (labelled in green). BBL numbering is used throughout. C. Stereoviews of the active sites of A. Di-Fe(II) BcII complex (1.1 Å resolution) and B. di-Zn(II) BcII (PDB code: 4C09, 1.2 Å resolution). Numbers shown represent distances in Å.

The overall structure of di-Fe(II) BcII is near identical to that of the di-Zn(II) enzyme with an RMSD of 0.084 Å over backbone carbon atoms (227 residues). Analysis of the active site of the di-Fe(II) structure clearly reveals the binding of two metal centres and that the overall active site structure is retained (Figure 2.18). Of note, the bridging water molecule between the two metal centres, as described in almost all reported di-Zn(II) MBL structures, is also retained. The refined metal occupancies were 1.00 for Fe1 and 0.60 for Fe2. Additional density in the mF$_o$-DF$_c$ map of the di-Fe(II) structure, seen during refinement around the cysteine metal ligand, led us to model a small population of Cys221 as a doubly-oxidised sulfur (sulfinic acid) residue (20% population), a chemical modification precedented by previous work with BcII(359), alongside the cysteine residue which formed the major population (80 %) (Figure 2.19). Further, additional mF$_o$-DF$_c$ density seen between the typical site of the bridging water molecule and Asp120 led to modelling the bridging water

ligand, Wat1, as a hydroxide ion with the hydrogen positioned between its oxygen and the side chain oxygen of Asp120, as shown in Figure 2.18.

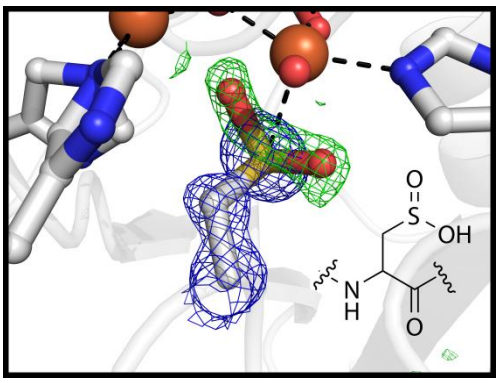

Figure 2.19: View of active site residue Cys221 of di-Fe(II)-BcII structure with representative electron density (3.0 σ mFo-DFc OMIT, blue mesh). During refinement additional density seen in the mF_o-DF_c map (green mesh) was apparent. This was modelled as a doubly oxidised sulfur (sulfinic acid). Similarly oxidised cysteine residues have been reported with MBLs, e.g. PDB Accession Codes 3I0V and 3I14 (359). Inset the chemical structure of cysteine sulfinic acid as found in the polypeptide chain.

In the active site, the positions of the metal ligands in di-Fe(II) BcII are near identical to those of the di-Zn(II) enzyme (PDB accession code: 4C09) with a model RMSD of 0.068 Å over the active site side chain atoms. However, there are significant changes in the relative positions of the metal centres when compared to the di-Zn(II) structure. The iron ions are shifted by 0.2 Å in site 1 and by 0.4 Å in site 2, relative to the Zn positions in the 4C09 model. Additionally, both of the ferrous ions have an additional water ligand when compared to the di-Zn(II) structure making site 1 pentacoordinate with a distorted trigonal bipyramidal geometry and site 2 hexacoordinate with a near perfect octahedral coordination sphere. The intermetallic distance in the di-Fe(II) BcII structure is 3.3 Å compared to the 3.5 Å distance observed for the di-Zn(II) structure 4C09. Further, the distance between the first metal centre and the bridging water molecule is shortened from 1.95 Å in di-Zn(II) BcII to 1.69 Å in di-Fe(II) BcII (Figure 2.18).

The strong similarity between the structures of di-Zn(II) BcII and di-Fe(II) BcII supports the similar steady-state kinetic data obtained with the two differently metallated enzymes, although it makes explanation of the observation, or lack, of an intermediate more difficult. This mechanistic feature might therefore be derived from the differing charge densities of Fe(II) and Zn(II), although one would expect Zn(II) to better stabilize an anionic intermediate given its higher charge density, or different geometric constraints the two metals put on their surrounding ligands. The differences seen in the inhibition of di-Zn(II) and di-Fe(II) BcII by ML320F may arise, at least in part, as a consequence of the shortened

intermetallic distance and more tightly bound water in the di-Fe(II) BcII structure (Figure 2.18 C); indeed the alternate position and geometry of the bridging water, Wat1, may make it more difficult for some sulfur ligands to bind in an analogous manner, for steric reasons.

2.10. Discussion

The results in this chapter reveal that the class B1 metallo-β-lactamases are able to bind Fe(II) and, in contrast to previous reports(275, 328, 330, 333), are active when their Zn(II) ions are replaced by Fe(II) ions, under conditions of low oxygen. Fe(II)-bound BcII and VIM-2 are able to hydrolyse both the chromogenic substrate, nitrocefin, and the clinically employed carbapenem antibiotic, meropenem. Despite differences in the metallochemistry of Zn(II) and Fe(II), differences in the overall catalytic efficiencies of di-Zn(II) and di-Fe(II) enzymes are small for BcII, while di-Fe(II) VIM-2 exhibits around a 10-fold drop in catalytic efficiency, when compared to the di-Zn(II) enzyme, with both of the tested substrates. Differences between the results presented here and previous reports observing a lack of activity for MBLs with bound iron likely result from oxidation of the ferrous iron in the reported experiments.

Reported stopped-flow kinetics employing nitrocefin, and the related substrate chromacef, as a substrate has identified an intermediate, absorbing at 665 nm, corresponding to the deprotonated delocalised anion. Such an intermediate has been observed in reactions catalysed by MBLs including VIM-2, IMP-1, New Delhi metallo-β-lactamase 1 (NDM-1) and L1(262, 282, 283, 289, 290, 293, 350). Stopped-flow studies of reconstituted di-Fe(II) BcII with nitrocefin revealed an additional absorbance feature with a λ_{max} of 665 nm, likely corresponding to this same anionic intermediate. Such a feature was not visible in the di-Zn(II) BcII reaction spectrum, as has been previously reported(281), suggesting that di-Fe(II) BcII may employ a different mechanism for β-lactam hydrolysis (Figure 2.15). In contrast, the on-pathway intermediate seen in nitrocefin hydrolysis by di-Zn(II) VIM-2, which has been previously reported(283), is no longer apparent on substitution with Fe(II).

The crystallographic results reveal that the overall geometry of the BcII active site is retained on metal substitution with Fe(II), including the presence of a bridging water molecule (Figure 2.18). However, there are changes in the positions of the metal centres resulting in different coordination distances and angles between both the metal ligands and the bridging water. Although it would be premature to propose any mechanistic consequences of the shifted metal binding sites, the results at least raise the possibility that changes in metal position may occur in catalysis and indeed inhibition; emerging evidence with non-haem Fe(II)-dependent oxygenases suggest that changes in metal position in some enzymes may have been underestimated to date(364-367). In the di-Fe(II) BcII structure,

the presence of extra mF_o-DF_c density beside the bridging oxygen lead us to model the bridging species as a hydroxide ion with its hydrogen projecting towards Asp120. In addition to the essential metal ligation, Asp120 has been proposed to play additional roles in MBL catalysis including orientating a zinc-bound bridging water to protonate the anionic intermediate(287). These results suggest that Asp120 may also play a role in positioning the bridging hydroxide to attack the β-lactam carbonyl in the enzyme-substrate complex.

It has previously been reported that a number of MBL enzymes can co-purify with iron ions in the active site(221, 223, 331, 334). This is unsurprising given the promiscuous ability of these enzymes to bind and exhibit catalysis with a number of transition metal ions. Indeed there are members of the MBL superfamily that bind Fe(II) in their native forms to carry out their catalytic functions(220, 223, 337, 338). Iron is a relatively bioavailable metal, although not necessarily in its reduced ferrous form, giving rise to the possibility that Fe(II)-substituted MBLs may constitute a proportion of the active enzyme population, especially under conditions of relatively low Zn(II) or high Fe(II) availability(368, 369). This possibility is supported by the finding that Pce, an Fe(II)-dependent MBL-fold hydrolase is an extracellularly located protein(223, 224). That there already exists a bacterial di-Fe(II)-binding MBL fold enzyme that exhibits extracellular activity lends credence to the proposal that di-Fe(II)-bound true MBLs might constitute a biologically relevant population.

Stopped-flow and crystallographic work using Fe(III) salts produced no positive data, in that apo-enzymes supplemented with Fe(III) were inactive or crystallised in an apo form despite the presence of the metal ions. This may be explained by a greater affinity of the MBL active site for ions in the +2 oxidation state *versus* the +3 state, but makes it harder to explain the purification of iron-containing, but inactive MBLs. One possibility is that these MBLs have initially bound ferrous ions that have subsequently oxidized in the active site, yet do not dissociate due to a kinetic barrier. Alternatively, the enzymes may contain Fe(II), but this might constitute too small of a population for observable activity, di-Fe(II) VIM-2 is, after all, 10 times less active than its di-Zn(II) counterpart. What few reports there are give varying results on the activity of Zn(II)-Fe(II) MBLs, with L1 characterised as active and NDM-1 as inactive(330, 334). This may again reflect the variability in the activity of iron bound MBLs observed in this study, with the general heterogeneity of the MBLs giving rise to some metal-enzyme combinations that are better than others on a case by case basis.

The inhibitor studies reveal that in some, but not all cases, it is possible for the same inhibitor to behave differently with Zn(II)- and Fe(II)-substituted BcII (Table 2.12), a result consistent with the altered active site metallo-chemistry between the di-Zn(II) di-Fe(II) forms. The potent inhibitor ML302F exhibited a higher IC_{50} with di-Fe(II) BcII than di-Zn(II) BcII(318). Thus, it may be prudent to test MBL inhibitors that are in clinical development against both Zn(II)- and Fe(II)-bound MBLs, in order to identify inhibitors

potent against both metallated forms. Further, given the known promiscuity of the MBL fold, it is possible that substitution of Zn(II) for other metals may alter catalytic properties in a manner relevant to the development of resistance. In this regard it is of interest that a recent report has highlighted the effects of different active site metals on native compared to promiscuous reactions as catalysed by MBL fold proteins(328).

Chapter 3: Cyclic Boronates Inhibit All Classes of β-Lactamase

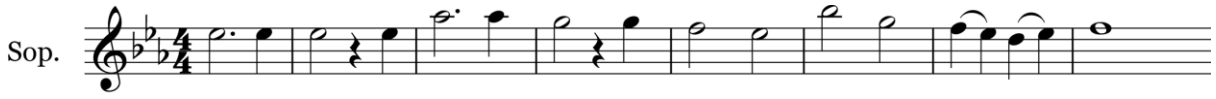

- *Gustav Mahler*

Contents

The work in this chapter was carried out in conjunction with Drs Jürgen Brem, who obtained MBL-encoding plasmids and advised on protein purification, Michael McDonough, who advised on crystallography, and Christopher Lohans, who assisted with NMR data collection. The cyclic boronates were synthesised by Dr Ricky Cain, under the supervision of Professor Colin Fishwick, University of Leeds. Studies employing clinical isolates were performed in conjunction with Dr David Wareham, Queen Mary University of London. The majority of the work described herein has been reported in the academic literature(370, 371).

3.1. Introduction

As discussed in the General Introduction, while there are multiple inhibitors of the serine-β-lactamases (SBLs), in the form of clavulanic acid, sulbactam, tazobactam, and, more recently, avibactam and vaborbactam (Figure 3.1)(140, 203, 212), there are no clinically available inhibitors of the metallo-β-lactamases (MBLs)(304). On account of this, the development of MBL inhibitors is of increasing clinical relevance, particularly with increased dissemination of the plasmid-borne MBLs amongst pathogenic bacteria, and is the subject of continuing research.

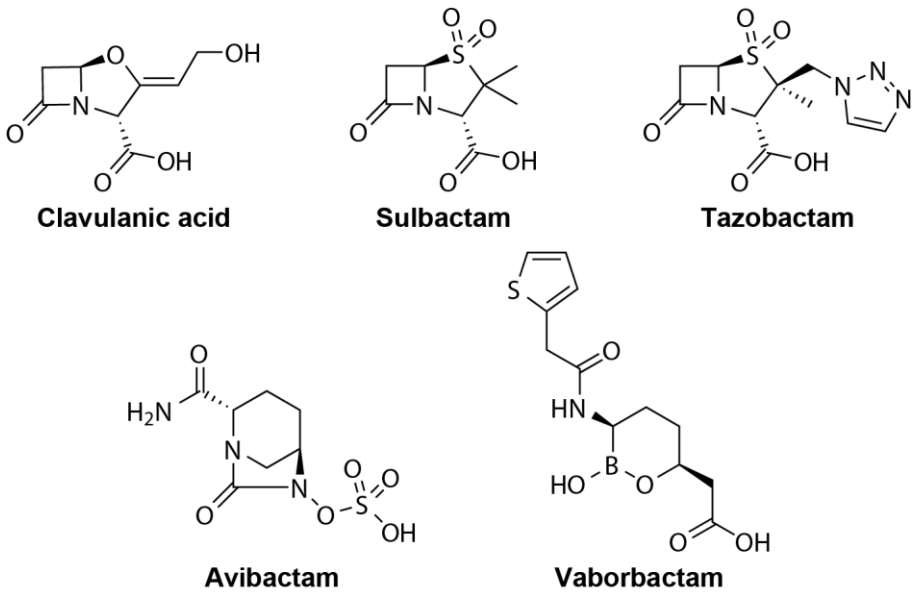

Figure 3.1: Clinically relevant serine-β-lactamase inhibitors. Clavulanic acid, sulbactam, and tazobactam are inhibitors based around the β-lactam scaffold, while avibactam, and vaborbactam are examples of non-β-lactam β-lactamase inhibitors.

The emergence of pathogenic bacteria exhibiting resistance mediated by both SBLs and MBLs, simultaneously, poses a significant threat to the use of β-lactams in treating resistant infections. While clavulanic acid, and the mechanistically related inhibitors sulbactam and

tazobactam, are successful against many Ambler class A SBLs, they are generally poorer inhibitors of class C and D enzymes and, in addition, are readily hydrolysed by metallo-β-lactamases(140). The non-β-lactam SBL inhibitor, avibactam, has a broader range of inhibitory activity, being able to inhibit class A, C, and some class D enzymes(154). While avibactam has been approved for use in combination with the cephalosporin, ceftazidime, and has been effective in treating resistant infections mediated by SBLs(204), there are already reports of resistance to this drug combination. In addition, since avibactam is not an inhibitor of MBLs, this combination is ineffective against MBL-mediated resistant infections, as the ceftazidime counterpart is still readily hydrolysed. Similarly, the combination of vaborbactam (Figure 3.1) and meropenem, which has just successfully passed through phase III clinical trials, will likely encounter comparable problems, since vaborbactam is only an inhibitor of class A and C SBLs and not of MBLs(212, 213). Aztreonam is exceptional among the β-lactams, on account of it not being hydrolysed by MBLs, the combination of avibactam and aztreonam has been shown to be effective against *Enterobacteriaciae* producing MBLs alone or in combination with various classes of SBL(372-375), and is currently in phase III clinical trials. This combination is effective since it inhibits SBLs, while bypassing MBLs, but it is not successful against all bacterial species, for example against *Acinetobacter baumannii*(373). In addition, a report demonstrating that MBLs are able to bind and turnover avibactam, albeit slowly(207), is worrying for the future use of this drug combination; the SBL, KPC-2, and its variants, are able to slowly inactivate avibactam via a desulfonation mechanism(205, 376), thus it is not unreasonable to suggest that continued use of avibactam/aztreonam, once approved, would provide enough of a selection pressure to encourage evolution of efficient avibactam-hydrolysing MBL variants.

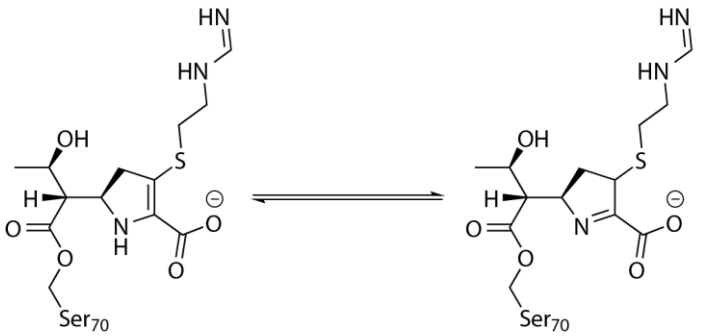

Δ^2-Pyrroline Tautomer Δ^1-Pyrroline Tautomer

Figure 3.2: Possible tautomers of the imipenem-serine-β-lactamase acyl-enzyme intermediate. The deacylation rate of the Δ^1 tautomer is significantly lower than that of the Δ^2 tautomer, giving rise to the inhibitory effect of carbapenems against class C serine-β-lactamases. Note the stereochemistry of the Δ^1 tautomer is not defined.

With this in mind, the development, not only of MBL inhibitors, but of dual action inhibitors with the ability to act against both SBLs and MBLs could have an enormous clinical impact.

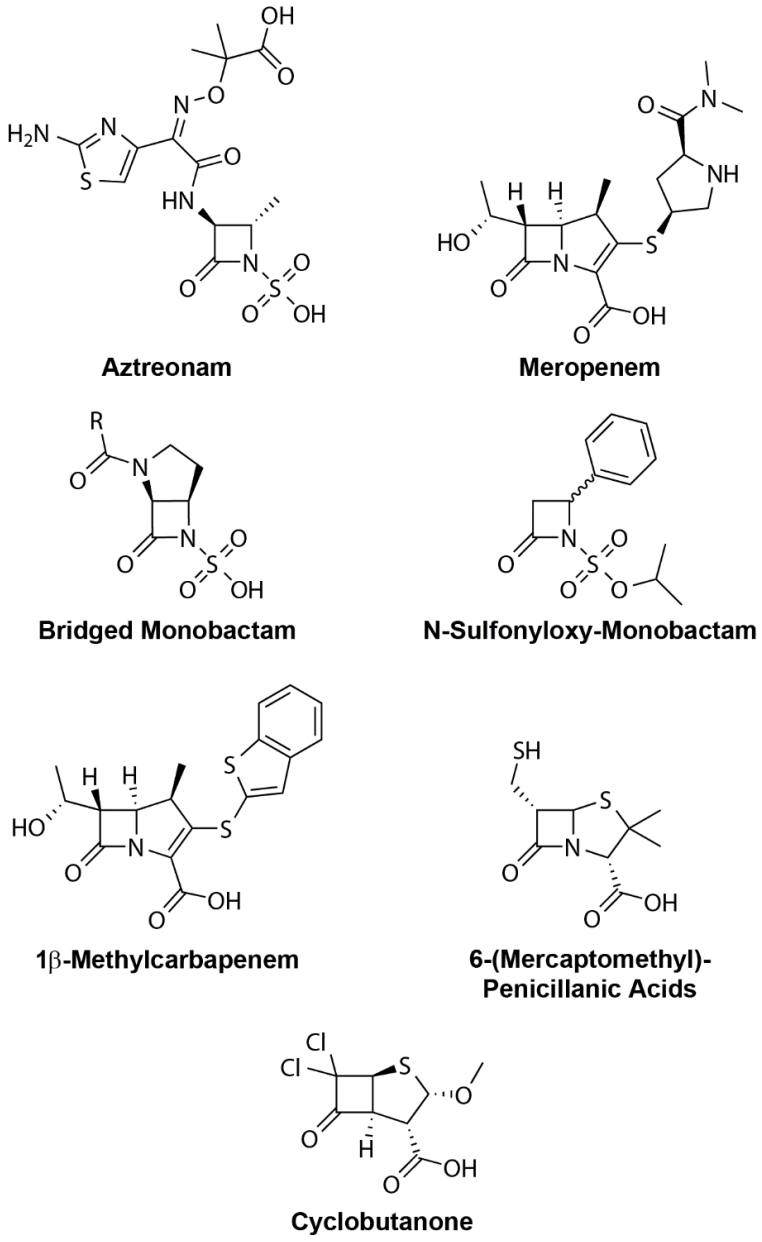

Figure 3.3: Example non-clinically used mechanism-based inhibitors of the serine- and metallo-β-lactamases. These molecules all share a core β-lactam-based scaffold, or a close analogue.

3.1.1. Mechanism-Based Inhibitors of the Serine-β-Lactamases

As discussed in the General Introduction, the β-lactam-based SBL inhibitors, clavulanic acid, sulbactam, and tazobactam, are mechanism-based inhibitors of the SBLs; initially these molecules react to form an acyl-enzyme intermediate by nucleophilic attack of the active site serine, before undergoing a fragmentation process that results in an inactivated enzyme with

a cross-linked active site(198-200). These molecules are, however, not the only β-lactam derivatives with the ability to inhibit the SBLs.

Although serine carbapenemases, such as the Ambler class A *Klebsiella pneumoniae* carbapenemase (KPC) and imipenemase (IMI) enzymes(377), and the class D oxacillinases (OXAs) OXA-23 and OXA-48 type enzymes(378), are known, many of the SBLs are inhibited by carbapenems. The inhibitory activity of the carbapenems is attributed to a number of mechanisms. The ability of the carbapenem acyl-enzyme to exist in two different pyrroline tautomers (Figure 3.2) is one possibility for the observed inhibitory effect, since it has been established that the Δ^1 tautomer hydrolyses at around a 10-fold slower rate than the Δ^2 tautomer(379). Co-crystal structures of Temoneira β-lactamase 1 (TEM-1) and a class C serine-β-lactamase (AmpC) with imipenem, as well as the sulfhydryl reagent variable β-lactamase 1 (SHV-1) with meropenem, show that a portion, or the entire population of the complexed β-lactam is positioned such that the ester carbonyl oxygen is not placed in the oxyanion hole(380-382), this may result in slow hydrolysis due to a lesser stabilisation of the transient tetrahedral anionic intermediate produced in the hydrolysis of the acyl-enzyme(383, 384). Hydrogen bonding of the hydrolytic water with the C-6 α-hydroxyethyl substituent, as seen in co-crystal structures of SHV-1 and OXA with meropenem, may reduce its nucleophilicity or hold it in an incorrect position for optimal attack on the acyl-enzyme ester carbonyl(382, 385). Alternatively, reaction with a β-lactam may exclude water molecules from the active site entirely, thus preventing acyl-enzyme hydrolysis(386).

The monobactam, aztreonam, has some inhibitory activity against the class C SBLs (e.g. the K_i for the β-lactamase from *E. cloacae* strain P99 (P99) is 1.9 nM) due to a very slow rate of deacylation after its initial reaction with the enzyme(164, 387, 388). Structural studies suggested that rotation around the C3-C4 bond was required to render the acyl-enzyme intermediate susceptible to hydrolysis, and that this resulted in the slow deacylation observed(389, 390). Synthesis of monobactams, with a bridge between C3 and C4 to limit rotation (Figure 3.3), produced potent inhibitors of AmpC enzymes from *C. freundii* and *P. aeruginosa*, but these showed little inhibition of class A enzymes where this rotation of the acyl-enzyme intermediate is not thought to be required for hydrolysis(391, 392). Modification of the monobactams at the β-lactam nitrogen, such as in the production of N-sulfonyloxy-β-lactam derivatives (Figure 3.3) has also produced inhibitors of class A SBLs with acyl-enzyme intermediates that are resistant to hydrolysis(393).

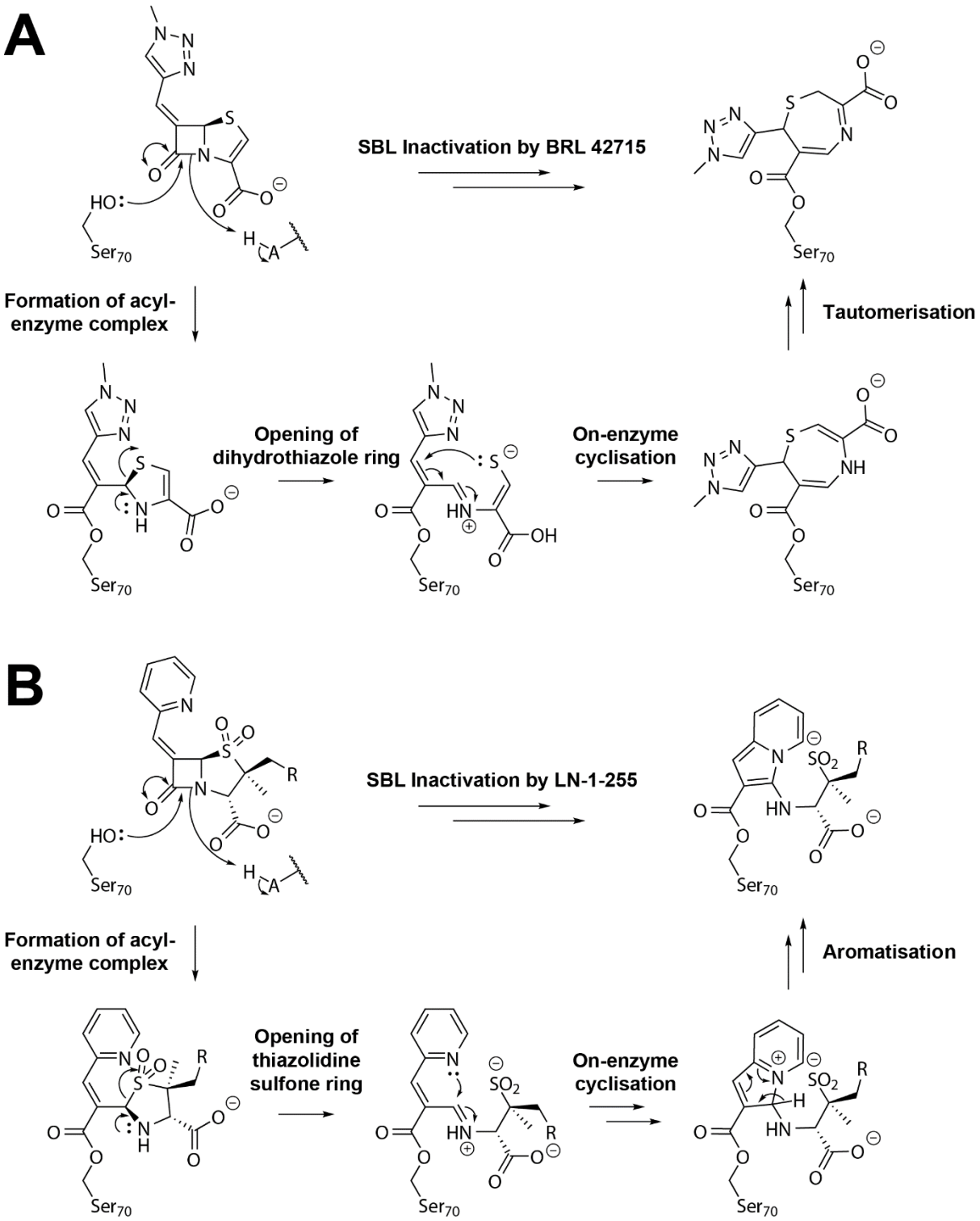

Figure 3.4: Mechanism for the inhibition of serine-β-lactamases by A. 6-methylidene substituted penems and B. 6-methylidene substituted penam sulfones as exemplified by BRL 42715(394) and LN-1-255(395), respectively. Inhibition proceeds by acylation, subsequent ring opening, and further on-enzyme rearrangements.

6-methylidine penems and penam sulfones are potent inhibitors of many members of the three classes of SBL(394, 396). Much like clavulanic acid derivatives, these compounds exert their inhibitory activity by undergoing an on-enzyme ring opening with further intramolecular reactions (Figure 3.4)(394-399). The resultant acyl-enzyme species is thought to be stable to hydrolysis due the steric exclusion of the hydrolytic water from, or displacement of the hydrolytic water within, the active site(395, 400). These molecules are, however, potential substrates of the MBLs(396).

3.1.2. Dual Action Inhibitors of the Serine- and Metallo-β-Lactamases

1-β-Methylcarbapenems (Figure 3.3) have been shown to inhibit both MBLs, with sub-micromolar K_i vales for MBL imipenemase 1 (IMP-1), cefoxitin and carbapenem resistant metallo-β-lactamase (CcrA), and labile enzyme from *Stenotrophomonas maltophilia* (L1), and class A and C SBLs, with K_i values of 2.5 μM and 37 nM for TEM-1 and AmpC from *E. cloacae*, respectively. These molecules behave as very slow substrates for the β-lactamases with between 1-8% of the hydrolysis rate of imipenem for the MBLs and <1% of the hydrolysis rate of cephaloridine for the SBLs(401). Similarly penicillin derivatives functionalised with a C-6-mercaptomethyl substituent (Figure 3.3) have been shown to inhibit both class A and C SBLs and the MBLs, BcII and L1 (IC_{50} values of 6.8 and 10.5 μM for TEM-1 and p99, respectively, and 1.4 and 0.1 μM for BcII and L1, respectively). These compounds have also been shown to increase the susceptibility of MBL-producing *E.coli* and *P. aeruginosa* strains to piperacillin(320). Finally, cyclobutanones (Figure 3.3) have been shown to inhibit all four classes of β-lactamase, although potency against class A and C enzymes is much greater than that seen against the MBLs and OXA enzymes(325).

3.1.3. Boronic Acids as Serine-β-Lactamase Inhibitors

In all of the above cases it is argued that the use of the β-lactam scaffold, which should be recognized and bound by both SBLs and MBLs, is the key factor that allows for the targetting of two functionally different classes of enzyme. However work in the early 1970s showed that the SBL from *Bacillus cereus* was inhibited by borate ions in a reversible manner(402). Along with a confirmation of this result, it was subsequently demonstrated that the same enzyme was inhibited by phenylboronic acid and 3-aminophenylboronic acid, although with a slightly lower potency(403). Boronic acids are known inhibitors of the serine proteases with a tetrahedrally coordinated boron mimicking a tetrahedral intermediate in the enzyme-catalysed reaction(404-406).

Boronic acids behave as good tetrahedral intermediate mimics or transition-state analogues of hydrolytic reactions since they adopt the same coordination geometry as seen in

the enzyme-catalysed reaction, the lengths of boron-carbon and boron-oxygen bonds, 1.57 and 1.48 Å, respectively, are highly comparable to carbon-carbon and carbon-oxygen bonds, 1.54 and 1.43 Å, respectively(407), and, unlike in, for example, sulfonamides, which are also successful transition-state analogues(408), the net charge of the intermediate is also maintained, although centered on boron rather than oxygen (Figure 3.5)(409).

Since the initial observation, boronic acids have been shown to inhibit all three classes of SBL to varying degrees(410-416), and exhibit a similar mode of inhibition to that seen with the serine proteases, i.e. formation of a tetrahedrally coordinated boron centre by reaction with the active site serine residue(413, 414, 416, 417). Of particular note, and as mentioned previously, the boronic acid compound, vaborbactam (Figure 3.1), has recently passed phase III clinical trials and is successful in combatting infections with resistance mediated by class A SBLs(213).

It should also be noted that the dipeptide boronic acid, Bortezomib (Figure 3.6), is a known and clinically employed proteasome inhibitor(418). This molecule is approved for the treatment of multiple myeloma and mantle cell lymphoma(419, 420). Bortezomib exerts its effect by reaction of the boron centre with the active site threonine residue of the 26s proteasome, thus preventing proteolytic activity(421).

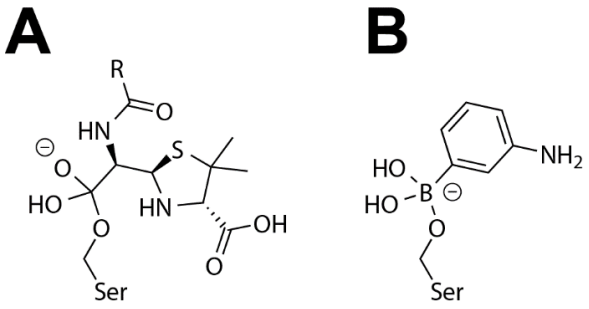

Figure 3.5: Comparison of A. the tetrahedral anionic intermediate in the hydrolysis of an SBL-penicillin acyl-enzyme complex and B. a boronic acid, as exemplified by 3-aminophenylboronic acid, coordinated by an active site serine. Bond lengths, angles and the net charge are all similar between these two systems. However the localisation of charge on oxygen in structure A and boron in structure B sets the two apart to some extent.

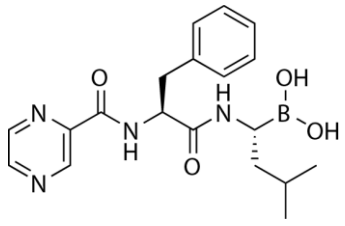

Figure 3.6: Chemical structure of the 26S proteasome inhibitor, Bortezomib.

3.1.4. Boronic Acids as Serine- and Metallo-β-Lactamase Inhibitors

Boronic acids are not only inhibitors of enzymes that utilise a serine nucleophile to catalyse hydrolysis. The boronic acid chemotype has also been successfully employed in the inhibition of metalloenzymes such as arginases and carbonic anhydrases(422-426).

A structural comparison of the binding modes of boronic acids to an SBL, an arginase, and a carbonic anhydrase is shown in Figure 3.7. In each of these three enzyme-inhibitor structures, the boron centre is tetrahedrally coordinated through a carbon-boron, and three oxygen-boron, bonds. In the SBL (Figure 3.7 A), the boron centre is coordinated by two hydroxide moieties and the third oxygen is provided by covalent bonding with the active site serine residue (Ser70). It is this covalent bond that gives rise to the strong potency of boronic acids against SBLs and other serine proteases(427). In the case of the arginase complex (Figure 3.7 B), the boron is coordinated by three hydroxide groups. Arginases bind two manganese(II) ions in their active site that are responsible for coordinating the substrate and a hydrolytic water molecule, which bridges the two metal centres in a manner reminiscent of the MBLs(428). When coordinated to a boronic acid inhibitor, one of the boronate oxygens replaces the bridging water molecule to adopt a μ2 bridging position between the two centres, while the other two oxygens each coordinate one of the Mn(II) ions. Finally, the co-crystal structure of a carbonic anhydrase II in complex with a boroxazole inhibitor (Figure 3.7 C) reveals that the endocyclic boronate binds to the zinc centre via two coordination interactions, one from a terminal hydroxide moiety and the other from the endocyclic oxygen. Notably, even though there is a possibility for ring opening of the boroxazole in an aqueous environment, via exchange with water, the complexed molecule shows a closed ring. It should also be pointed out that promiscuous binding of the boroxazole chemotype was observed in the carbonic anhydrase II study, where surface binding of the molecules was also seen via coordination to free histidine residues (Figure 3.7 D). This result may raise questions regarding the selectivity of these types of boron-based inhibitors.

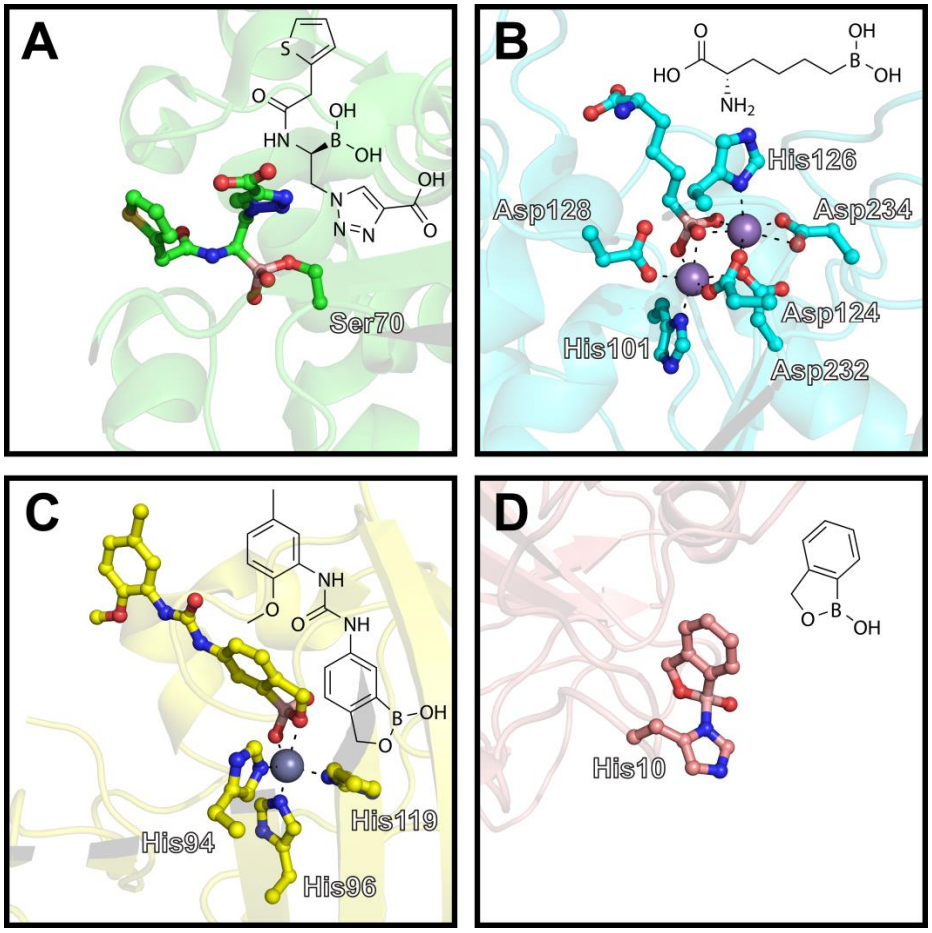

Figure 3.7: Structural comparison of the binding modes of boronic acid inhibitors to A. a serine-β-lactamase (PDB accession code: 5EEC)(429), B. an arginase (PDB accession code: 1D3V)(422), and C. a carbonic anhydrase II (PDB accession code: 5LMD)(426). D. Surface binding of a boroxazole to carbonic anhydrase II via a histidine residue is also shown. Chemical structures of the inhibitors are inset.

Since boronic acids have had success in inhibiting both serine and metalloenzymes, it is not unreasonable to posit that they might be employed in the inhibition of *both* serine and metallo-β-lactamases – particularly given that there is evidence for boronic acids inhibiting both mono and dimetallated enzymes similar to those seen in the B1+B3 and B2 MBL subfamilies. A side by side comparison of the mechanisms of the SBLs and B1+B3 MBLs (Figure 3.8) shows that the proposed tetrahedral intermediate EI[1] is conserved between both hydrolysis reactions. Thus it is likely that boronic acids mimicking this intermediate species will have the greatest chance of success in inhibiting both types of β-lactamase. A similar result has already been suggested in patent literature, indicating that boronic acids in which the boron is held in a six-membered ring can manifest inhibitory activity against metalloenzymes(202).

3.2. Chapter Objectives

Boronic acids are known inhibitors of the serine-β-lactamases. Given that some success has been had in inhibiting metalloenzymes with this chemotype(422-426), and that there is some evidence for inhibition of the metallo-β-lactamases in patent literature(202), the objective of this work was to investigate as to whether boronic acids, particularly the cyclic boronic acids, have the capacity to inhibit both SBLs and MBLs and to assess their impact on the growth of bacteria exhibiting resistance to β-lactams through the production of these enzymes. Further objectives included assessment of any selectivity that these compounds might have for the different classes of SBL or subclasses of MBL, their binding modes to the β-lactamases, and kinetics of binding and inhibition. *Note, with the presence of the VenatoRx compound, VNRX-5113 (structure not yet released), reported to be an inhibitor of all β-lactamase classes, in phase I clinical trials, the medicinal potential of an all class β-lactamase inhibitor cannot be understated.*

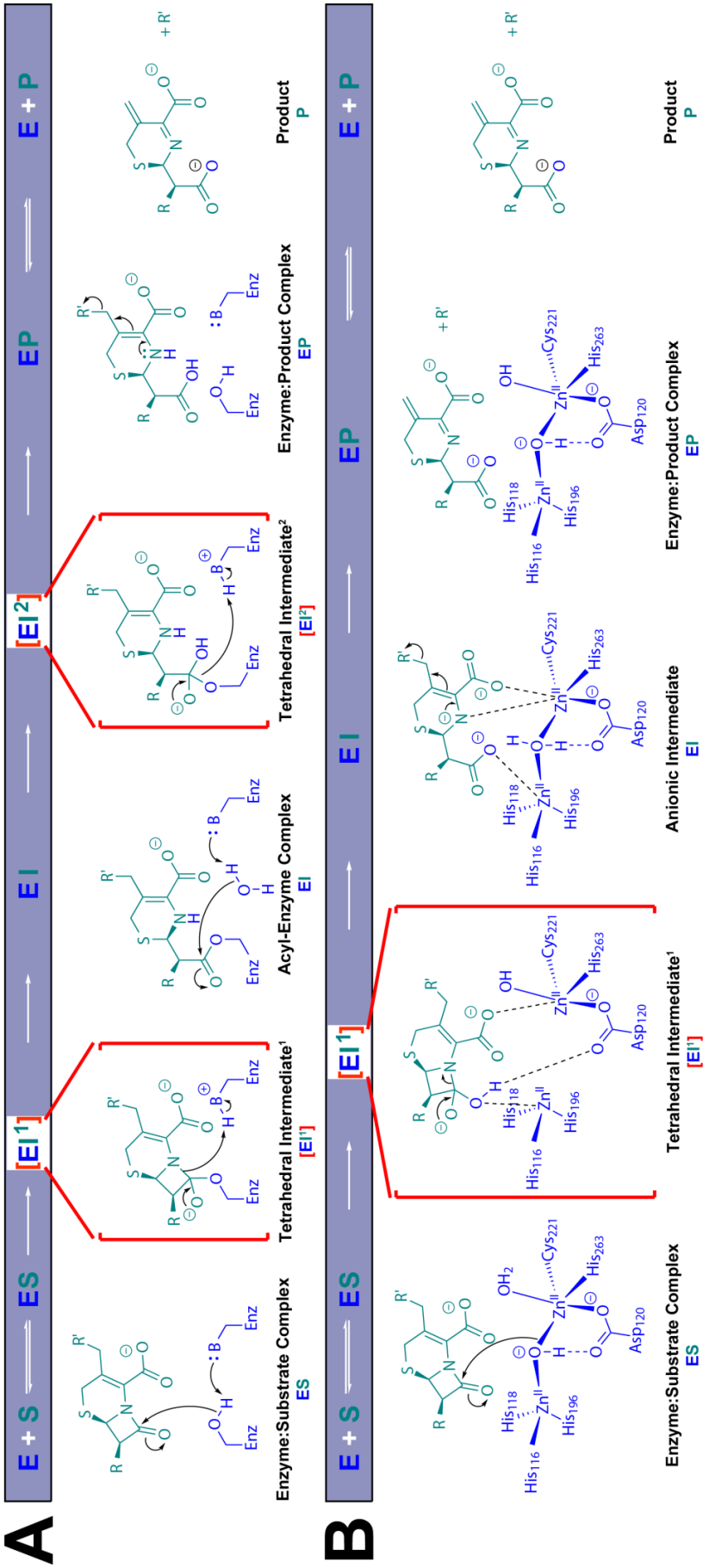

Figure 3.8: Outline mechanism for the hydrolysis of a cephalosporin by A. a serine-β-lactamase and B. a metallo-β-lactamase. Proposed tetrahedral intermediates are indicated by red brackets. The intermediate EI^1 is arguably the most similar between the two different mechanisms due to the bicyclic structure of the substrate remaining closed in both reactions.

3.3. Synthesis of Cyclic Boronic Acids

The cyclic boronic acids used in this study (Figure 3.9) were synthesised by Dr Ricky Cain under the supervision of Prof. Colin Fishwick, University of Leeds. A synthetic outline is provided in Figure 3.9.

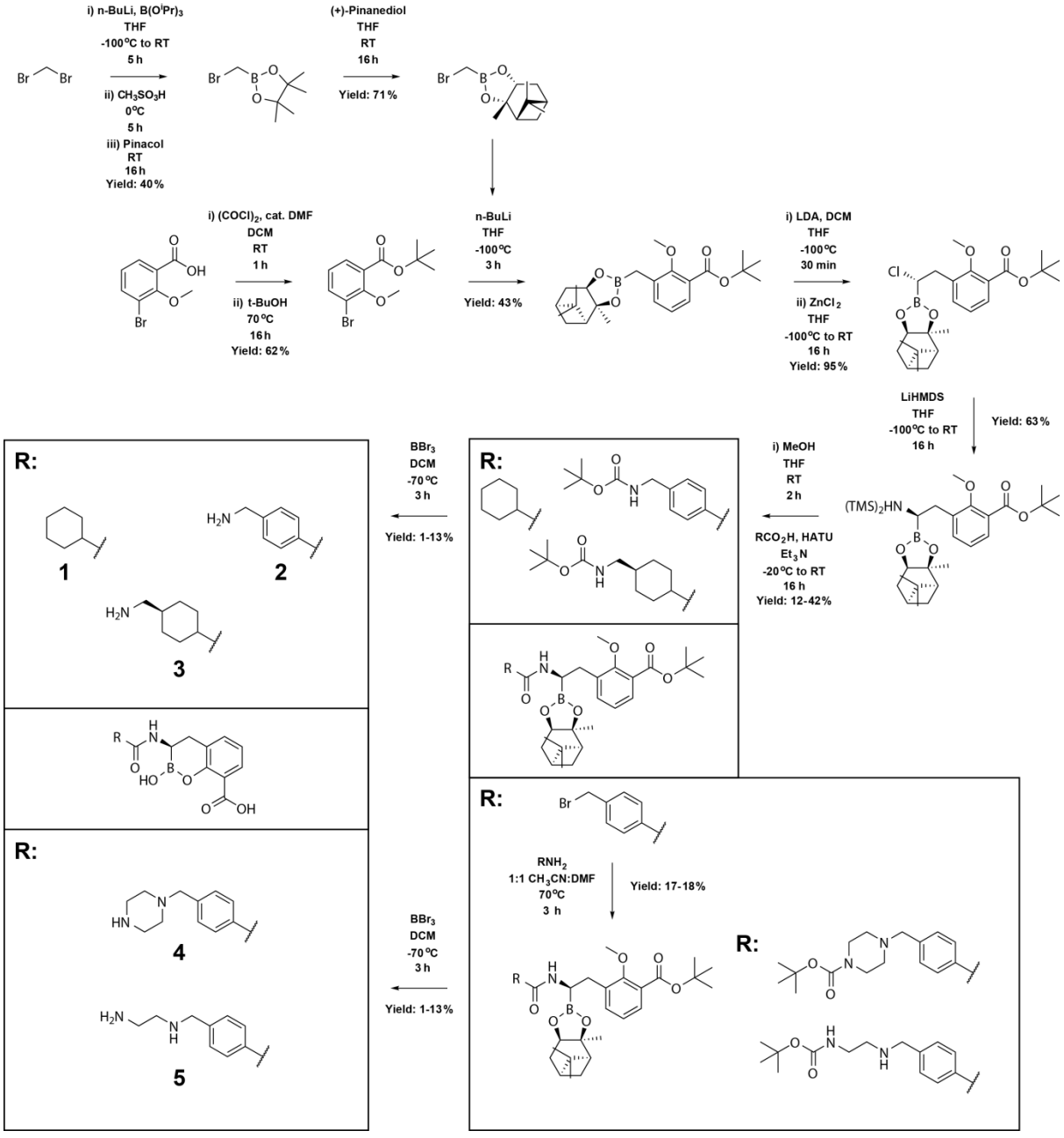

Figure 3.9: Structures and synthetic scheme for the production of the cyclic boronates employed in this study.

3.4. Production and Purification of Enzymes

Recombinant *Bacillus cereus* β-lactamase II (BcII)(345) and Verona integron-encoded metallo-β-lactamase 2 (VIM-2)(346) were produced as described in Chapter 2 and the General Methods. Recombinant carbapenem hydrolysing enzyme from *Aeromonas hydrophila* (CphA) as a pET9a construct(430), a gift from Dr Moreno Galleni, University of Liège, and IMP-1 as the previously reported pET-26b construct(431), a gift from Dr James Spencer, University of Bristol, were produced in *E. coli* BL21(DE3) pLysS cells and purified by ion exchange using an SP Sepharose column (followed by size exclusion chromatography for IMP-1), as described in the General Methods. Recombinant New Delhi metallo-β-lactamase 1 (NDM-1)(432), São Paulo metallo-β-lactamase 1 (SPM-1)(433), cefotaxime hydrolase from Munich 15 (CTX-M-15), β-lactamase from *Mycobacterium tuberculosis* (BlaC), AmpC from *Pseudomonas aeruginosa*, OXA-23, and OXA-48, each with an *N*-terminal hexahistidine tag, and VIM-1 with a *C*-terminal hexahistidine tag(346), were produced, using pOPINF constructs lacking the *N*-terminal signal peptides, in *E. coli* BL21(DE3) cells, and purified by immobilised metal ion affinity chromatography followed by size exclusion chromatography before removal of the *N*-terminal tag by 3C protease digestion, as described in the General Methods. (Constructs for CTX-M-15, BlaC, AmpC, OXA-23, and OXA-48 were kindly supplied by Dr James Spencer, University of Bristol.) Recombinant TEM-1, with an *N*-terminal His-tag(434), was produced from a pQE30 construct in *E. coli* BL21(DE3) cells and purified by immobilised metal ion affinity chromatography as described in the general methods. Recombinant OXA-10 as a pET22b construct(173) was produced in *E. coli* BL21(DE3) cells and purified by ion exchange chromatography using a Q Sepharose column as described in the General Methods. Penicillin binding protein 3 (PBP3) as a pOPINF construct(435) was produced in *E. coli* Rosetta *p*LysS (DE3) and purified by immobilised metal ion affinity chromatography followed by size exclusion chromatography as described in the General Methods. Recombinant penicillin binding protein 5 (PBP5) as a pET28b construct(434) was produced in *E. coli* BL21(DE3) and purified by immobilised metal ion affinity chromatography as described in the General Methods.

At each stage in the purification of these enzymes, their purity was determined by SDS-PAGE (Figure 3.10), and once purification was complete, their molecular weights were confirmed by ESI-MS, and their extent of folding by circular dichroism spectroscopy (Figures 3.11-3.12 & Tables 3.1-3.2). Note that CphA, NDM-1, IMP-1, SPM-1, VIM-1, TEM-1, PBP3, and PBP5 were produced in conjunction with Dr Jürgen Brem.

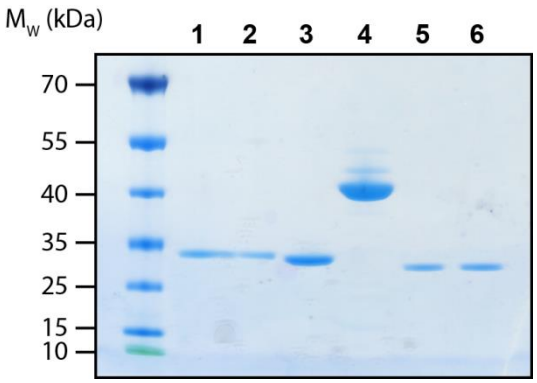

Figure 3.10: SDS-PAGE of purified enzymes newly produced during this study. 1 & 2. CTX-M-15. 3. BlaC. 4. AmpC from *Pseudomonas aeruginosa*. 5. OXA-23. 6. OXA-48

Enzyme	Predicted Mass (Da)	Measured Mass (Da)
CTX-M-15	28262	28260
BlaC	28526	28524
AmpC	40834	40827
OXA-23	28299	28301
OXA-48	28301	28300

Table 3.1: Masses of enzymes newly purified in this study as determined by denaturing mass spectrometry. Enzymes were assayed at 0.2 mg mL^{-1} in 10 mM sodium phosphate buffer, pH 7.5. The predicted masses, based on amino acid sequence, are also provided.

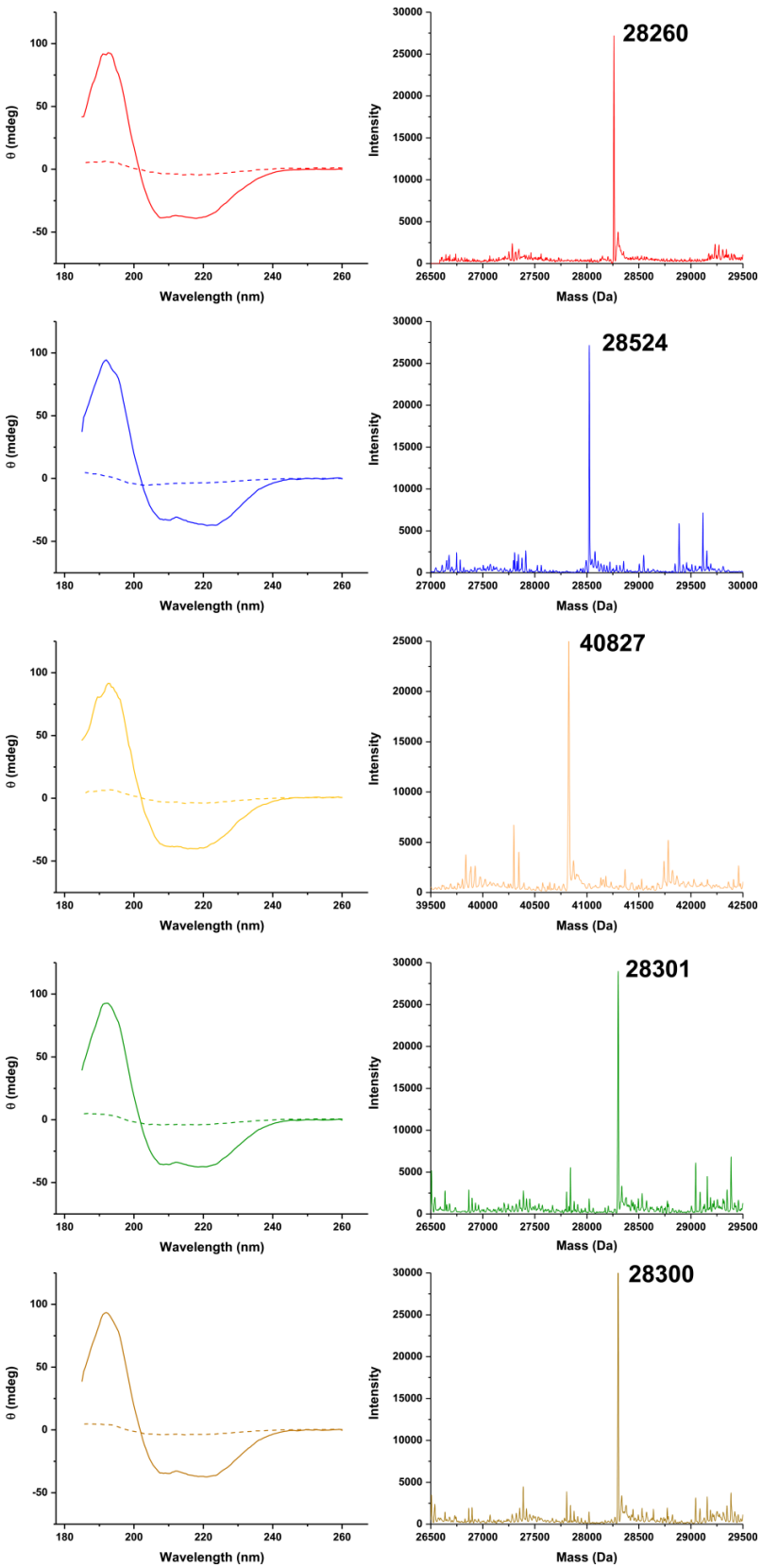

Figure 3.11: Circular dichroism and mass spectra for enzymes newly produced during this study. Solid lines in circular dichroism spectra represent measurements at 10 °C, while dashed lines represent those at 85 °C. Enzymes were assayed at 0.2 mg mL^{-1} in 10 mM sodium phosphate buffer, pH 7.5. Red: CTX-M-15. Blue: BlaC. Yellow: AmpC. Green: OXA-23. Brown: OXA-48.

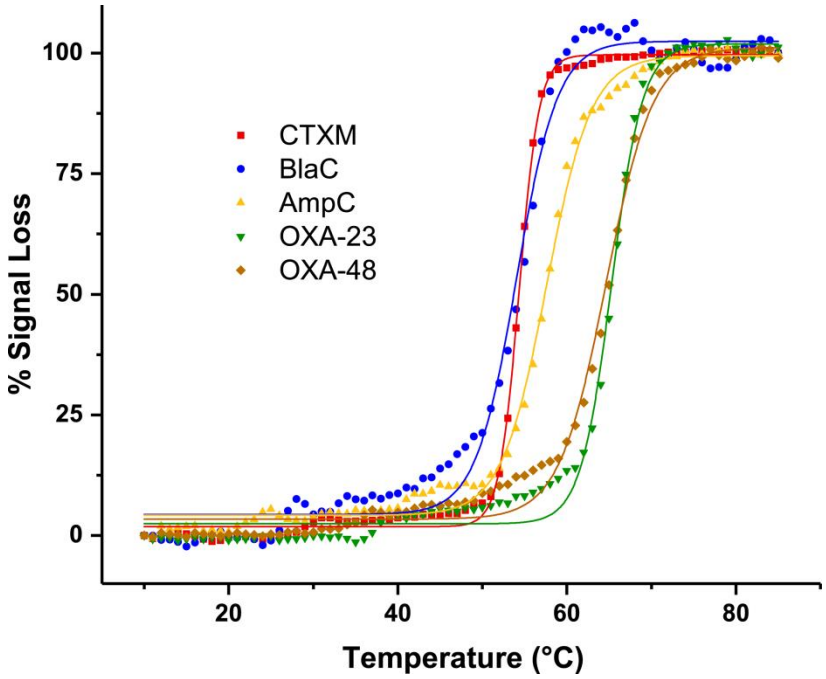

Figure 3.12: Melting curves for enzymes newly purified in this study as determined by circular dichroism spectroscopy. Enzymes were assayed at 0.2 mg mL^{-1} in 10 mM sodium phosphate buffer, pH 7.5. Curve fitting was performed using OriginPro(349).

Enzyme	T_m (°C)
CTX-M-15	54.3 ± 0.1
BlaC	54.1 ± 0.2
AmpC	57.6 ± 0.1
OXA-23	65.3 ± 0.1
OXA-48	64.6 ± 0.2

Table 3.2: Melting temperatures of enzymes newly purified in this study as determined by circular dichroism spectroscopy. Enzymes were assayed at 0.2 mg mL^{-1} in 10 mM sodium phosphate buffer, pH 7.5.

3.5. Steady-State Kinetics with Newly Purified Enzymes

Since this work was the first instance of producing CTX-M-15, BlaC, AmpC from *P. aeruginosa*, OXA-23 and OXA-48, in the Schofield group, steady state kinetics were first performed with the chromogenic reporter substrate, nitrocefin(292), and the fluorescent reporter, FC5 (Figure 3.13 & Table 3.3)(433), in order to assess activity of the purified enzymes and the suitability of FC5 for use in inhibition assays.

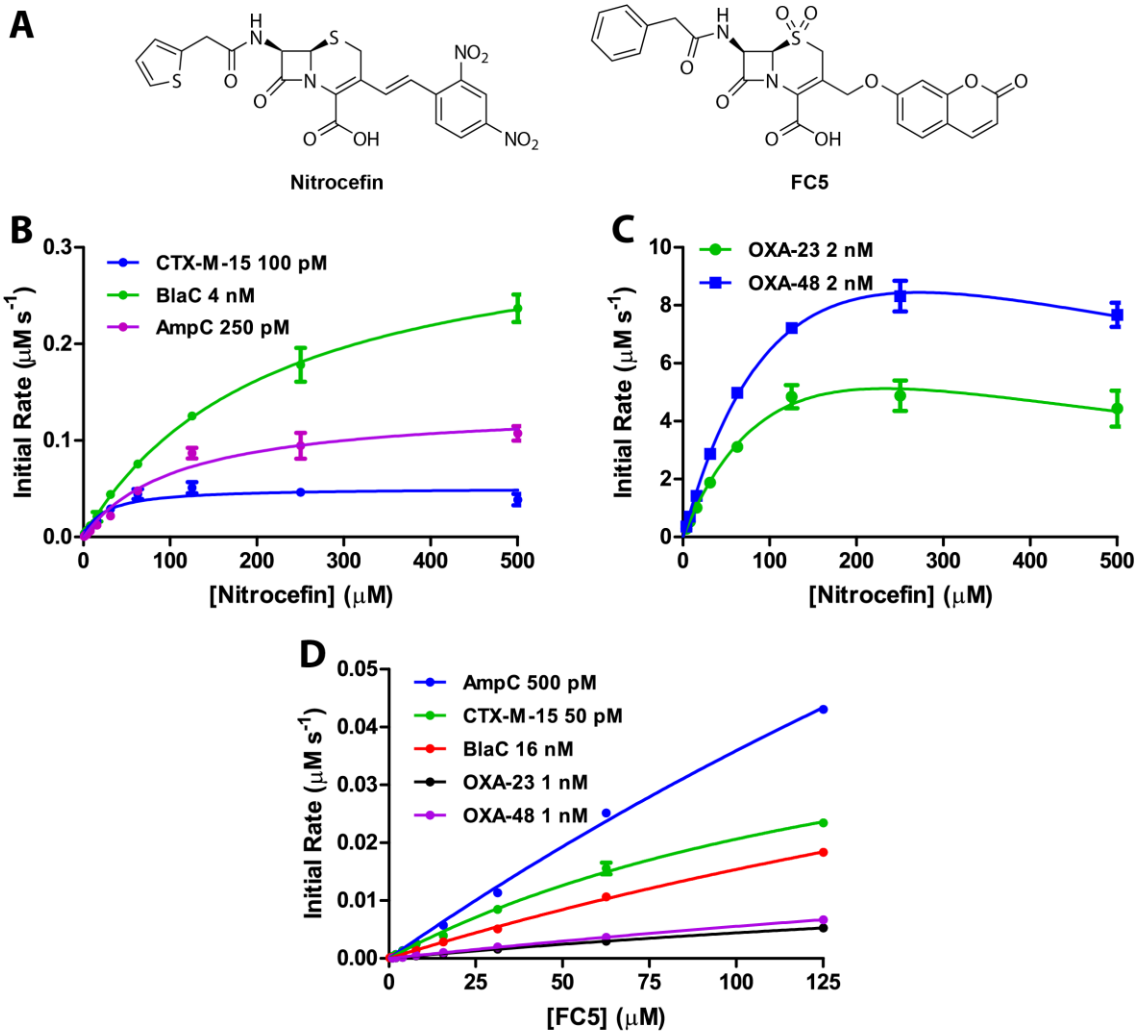

Figure 3.13: A. Chemical structures of the β-lactamase reporter substrates, nitrocefin and FC5. Kinetics of B. the hydrolysis of nitrocefin as catalysed by CTX-M-15, BlaC, and AmpC, C. the hydrolysis of nitrocefin as catalysed by OXA-23 and OXA-48, D. the hydrolysis of FC5 as catalysed by CTX-M-15, BlaC, AmpC, OXA-23, and OXA-48, are shown. Hydrolysis data were collected at 25 °C and pH 7.5. The initial rate of hydrolysis is plotted against substrate concentration. The concentration of enzyme used in the assay is indicated. Solid lines indicate the Michaelis-Menten curves fitted in GraphPad Prism(347).

In each case, the measured specificity constant for nitrocefin is greater than for FC5 by up to three orders of magnitude (e.g. k_{cat}/K_m values for OXA-23 with nitrocefin and FC5 are 56 and 0.076 μM s^{-1}, respectively). This generally comes as a result of a reduced k_{cat} and an increased K_m, i.e. both a poorer affinity and a lower turnover rate. It should be noted that some degree of substrate inhibition was observed for the OXA enzymes and nitrocefin. In addition, for each of the enzymes tested, it was not possible to reach the limiting initial rate of hydrolysis with FC5. Thus fitting values for both k_{cat} and K_m from GraphPad Prism typically have a greater degree of error with FC5 than with nitrocefin and should be taken with a little caution.

Enzyme	Substrate	[E] (nM)	k_{cat} (s^{-1})	K_m (μM)	k_{cat}/K_m (μM s^{-1})
CTX-M-15	Nitrocefin	0.1	1000 ± 120	80 ± 14	13
	FC-5	0.05	1100 ± 100	170 ± 20	6.5
BlaC	Nitrocefin	4	84 ± 1	220 ± 10	0.38
	FC-5	16	5.4 ± 0.7	460 ± 70	0.012
AmpC	Nitrocefin	0.25	540 ± 40	100 ± 20	5.4
	FC-5	0.5	500 ± 160	600 ± 220	0.83
OXA-23	Nitrocefin*	2	2800 ± 200	50 ± 9	56
	FC-5	1	38 ± 7	500 ± 130	0.076
OXA-48	Nitrocefin*	2	4800 ± 200	62 ± 8	77
	FC-5	1	28 ± 2	420 ± 50	0.067

Table 3.3: Fitted Michaelis-Menten kinetic constants for the hydrolysis of nitrocefin or FC5 by CTX-M-15, BlaC, AmpC from *P. aeruginosa*, OXA-23, and OXA-48. Hydrolysis data were collected at 25 °C and pH 7.5. Asterisks indicate experiments in which substrate inhibition was observed.

3.6. Inhibition of β-lactamases by Cyclic Boronates

Using an FC5-based fluorogenic assay(433), the cyclic boronates were initially screened for inhibitory activity against the SBLs TEM-1 and OXA-10, class A and D enzymes, respectively. Residual β-lactamase activity, through the hydrolysis of FC5, was measured *via* fluorescence of the hydrolysed product (λ_{ex} = 380 nm, λ_{em} = 460 nm) for a range of inhibitor concentrations. All measurements were performed at 25 °C and pH 7.5. Enzymes were incubated with the inhibitor for 10 minutes before initiation of the reaction through the addition of substrate. The compounds were also screened against the non-essential penicillin-binding protein, PBP5 (dacA) from *E. coli*, and the essential penicillin-binding protein, PBP3, from *P. aeruginosa*, since these are enzymes that are evolutionarily related to the SBLs (Figure 3.14 & Table 3.4)(149, 150).

The initial results confirmed that the synthesised cyclic boronates were inhibitors of the SBLs, as expected from the academic literature. However potency against the class A enzyme, TEM-1, was generally much greater than against the class D enzyme, OXA-10, with low nanomolar IC_{50} values against the former and low micromolar values against the latter. Variability was also seen between the cyclic boronates tested, suggesting that a greater potency could be achieved against OXA-10 by investigating further variations of the sidechain. Although no inhibition was seen against the essential PBP3, inhibition of the non-essential PBP5 was seen by all boronates, with a determined apparent IC_{50} of 1.99 nM for boronate **2**. This result suggests that cyclic boronates might have some utility, not only in potentiating β-lactams against infections exhibiting resistance mediated by SBLs, but, with further refinement, might also have the potential to act as antibiotics themselves by inhibiting PBPs in the same manner as the β-lactams. Having established the activity of these compounds against SBLs, it was investigated as to whether the cyclic boronates also

inhibited MBLs. Thus, the cyclic boronates were screened for inhibitory activity against a panel of MBLs, including the clinically relevant B1 enzymes NDM-1, IMP-1, VIM-2 and SPM-1, the model MBL, BcII, and the B2 subclass enzyme CphA from *Aeromonas hydrophilia* (Figure 3.15 & Table 3.5).

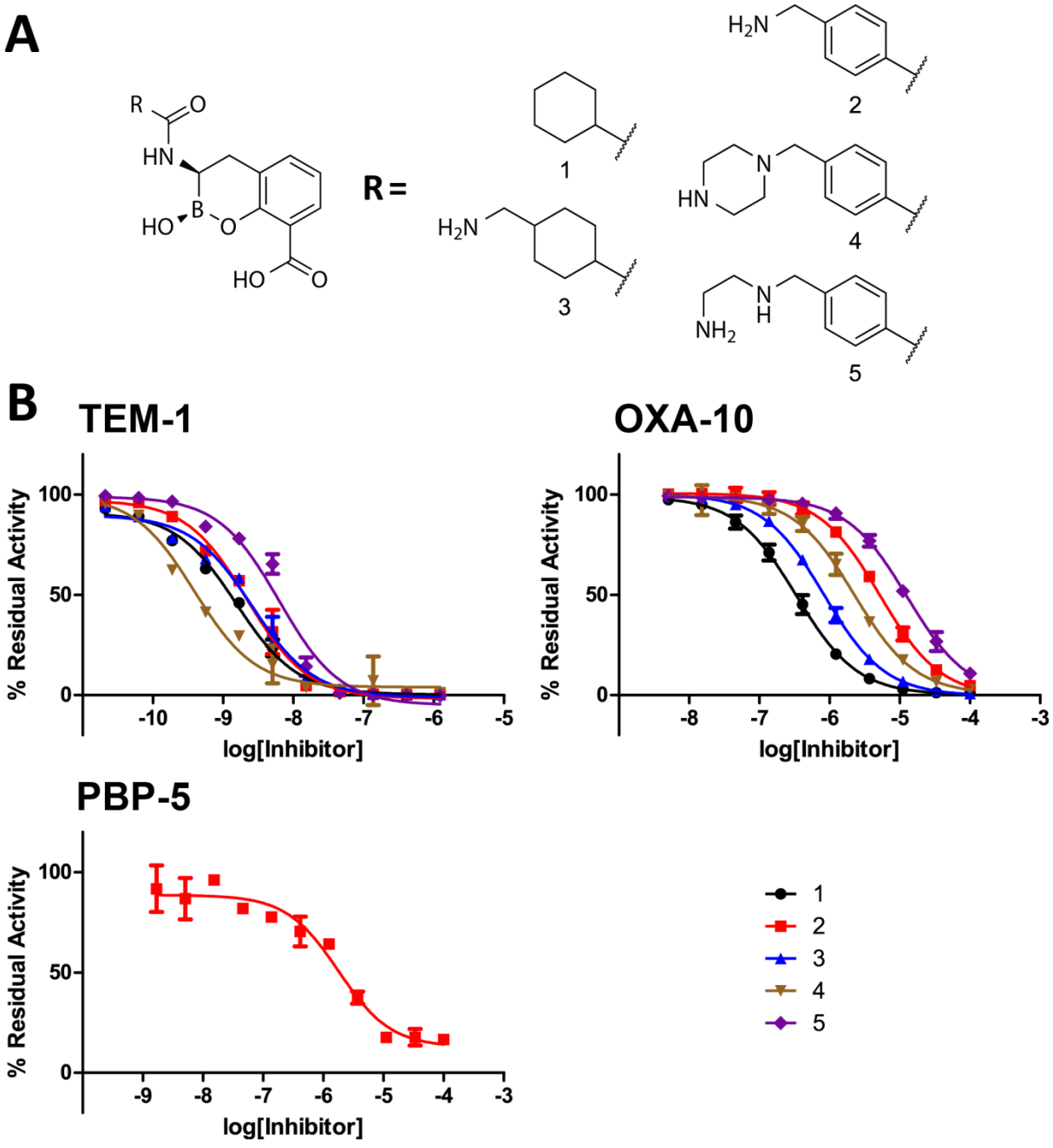

Figure 3.14: A. Chemical structures of the cyclic boronates 1 to 5 used in these inhibition studies. B. IC_{50} traces for the inhibition of serine-β-lactamases and penicillin-binding proteins by cyclic boronates. Residual hydrolysis of FC5 (TEM-1 and OXA-10) was followed by fluorescence (λ_{ex} = 380 nm, λ_{em} = 460 nm), while residual hydrolysis of nitrocefin (PBP-5) was followed by absorbance at 390 nm. Inhibition assays were carried out at 25 °C and pH 7.5.

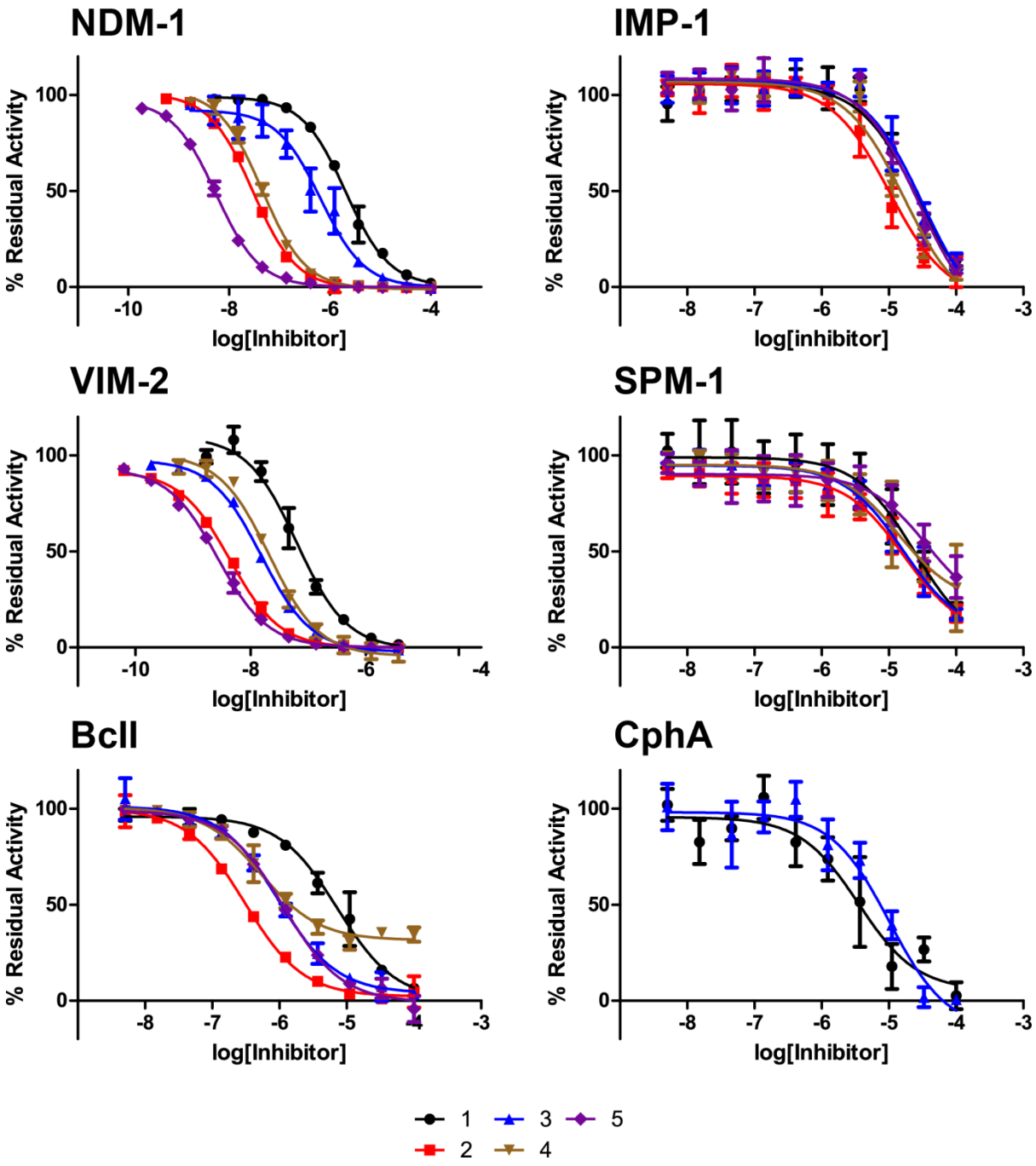

Figure 3.15: IC_{50} traces for the inhibition of metallo-β-lactamases by cyclic boronates. Residual hydrolysis of FC5 was followed by fluorescence (λ_{ex} = 380 nm, λ_{em} = 460 nm). Inhibition assays were carried out at 25 °C and pH 7.5. Note that curves for 2, 4, and 5 with CphA are not shown due to minimal inhibition at the tested inhibitor concentrations.

	IC_{50} for Cyclic Boronate (nM)				
Enzyme	1	2	3	4	5
TEM-1	1.25 ± 0.06	3.98 ± 0.02	3.16 ± 0.01	0.40 ± 0.02	7.94 ± 0.01
OXA-10	398 ± 1	6310 ± 20	1000 ± 2	2510 ± 10	12600 ± 100
PBP3	NI	NI	NI	NI	NI
PBP5	ND	1990 ± 10	ND	ND	ND

Table 3.4: IC_{50} values for the inhibition of serine-β-lactamases and penicillin-binding proteins by cyclic boronates. Inhibition assays were carried out at 25 °C and pH 7.5. NI – No inhibition seen. ND – Not determined.

	IC_{50} for Cyclic Boronate (μM)				
Enzyme	1	2	3	4	5
NDM-1	2.04 ± 0.01	0.029 ± 0.001	0.68 ± 0.01	0.04 ± 0.01	0.004 ± 0.001
IMP-1	1.44 ± 0.04	1.00 ± 0.02	1.50 ± 0.04	1.21 ± 0.03	1.41 ± 0.04
VIM-2	0.051 ± 0.001	0.003 ± 0.001	0.011 ± 0.001	0.014 ± 0.001	0.002 ± 0.001
SPM-1	24.1 ± 0.8	16.7 ± 0.4	16.0 ± 0.3	13.9 ± 0.5	36 ± 2
BcII	7.27 ± 0.07	0.30 ± 0.01	0.96 ± 0.01	0.52 ± 0.02	1.14 ± 0.01
CphA	4.4 ± 0.1	>100	20 ± 1	>100	>100

Table 3.5: IC_{50} values for the inhibition of metallo-β-lactamases by cyclic boronates. Inhibition assays were carried out at 25 °C and pH 7.5.

These results demonstrated that the cyclic boronates were able to inhibit not only the SBLs, but also the MBLs, as predicted based on consideration of the enzymes' mechanisms. Potencies of inhibition were, however, variable, with IC_{50} values ranging from >100 μM against CphA to 2 nM against VIM-2 (Table 3.5). The inhibition data suggest that the inclusion of an aromatic sidechain in the position analogous to the C6/7 aminoacyl side chains of penicillins or cephalosporins give rise to more potent inhibition of the B1 MBLs, while decreasing potency against the B2 enzymes (IC_{50} values for inhibition of CphA by boronates 2, 4, and 5 are all greater than 100 μM). In general, the potencies against CphA and SPM-1, a B1/B2 hybrid enzyme(261), were lower than for the other MBLs tested, suggesting that further optimization would be required to achieve strong inhibition against the B2 subclass MBLs.

3.6.1. Examining Time Courses of Inhibition by Cyclic Boronates

To investigate whether the cyclic boronates would inhibit a broader range of β-lactamase targets, such as class C β-lactamases as well as important class A ESBL and class D carbapenemase targets, the same FC5-based fluorogenic assay(433) was used to screen cyclic boronates **1** and **2** against TEM-1, CTX-M-15 (class A), AmpC from *Pseudomonas aeruginosa* (class C), OXA-23 and OXA-48 (class D), collectively representing all classes of

β-lactamase. The time-dependency, if any, of the inhibition of these enzymes by the cyclic boronates as well as against two B1 MBLs, BcII and VIM-1 was also examined. As a benchmark to the potency of the cyclic boronates, the clinically used SBL inhibitors avibactam (MedChemexpress LLC) (154, 203), sulbactam (436, 437), and BLI-489, a potent inhibitor of class D enzymes (140, 438, 439) were also screened. Against MBLs the broad-spectrum thiol-based MBL inhibitors, L-captopril (254, 317) and (racemic) thiomandelic acid (316, 355) were used for comparison. It was attempted to examine the effect of pH on the inhibition of the MBLs, however this proved troublesome, most likely due to the known instability of VIM-1 and the possibility of quenching of the fluorescent reporter when assays were conducted at lower pH, thus, only data for both MBLs at pH 7.5 and BcII at pH 6.5 are shown. The extent of inhibition was tested at five time points over a six hour period and inhibition data are shown in Figures 3.17-3.18 & Tables 3.6-3.7.

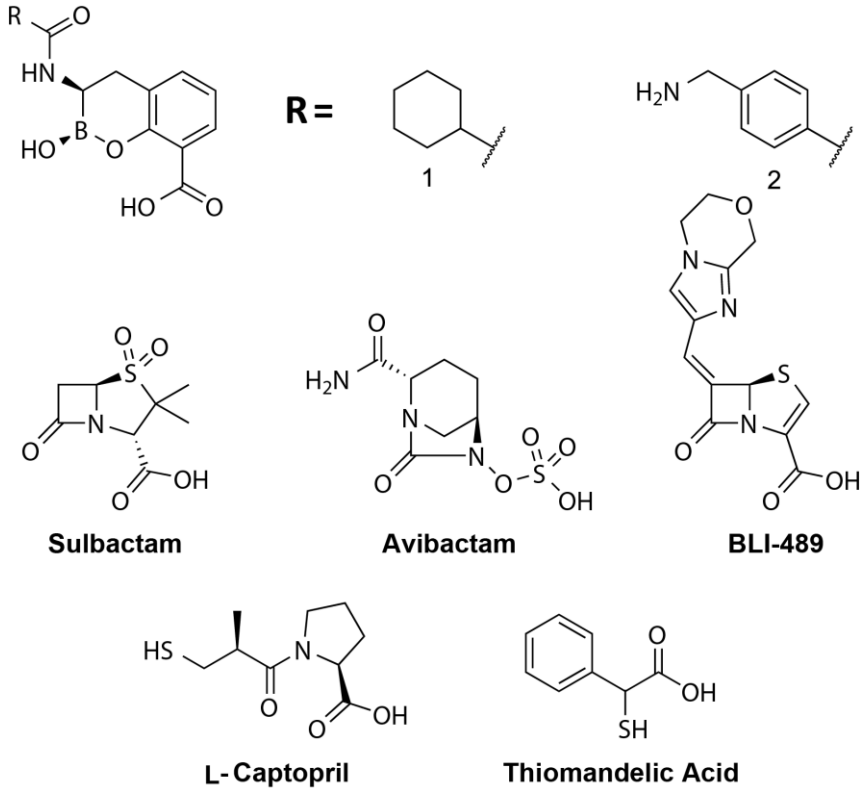

Figure 3.16: Chemical structures of inhibitors employed in inhibition time course studies with serine- and metallo-β-lactamases.

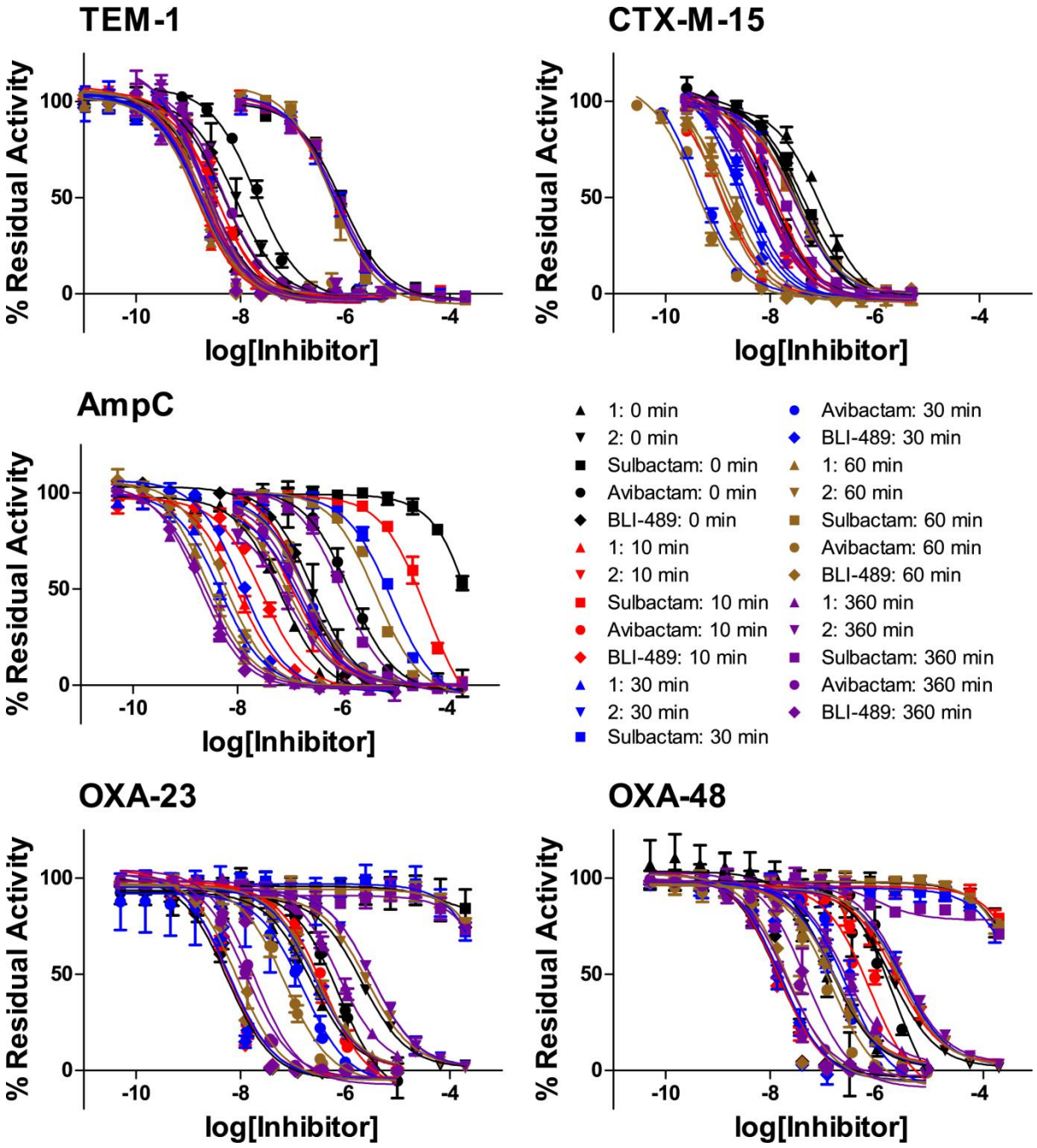

Figure 3.17: IC_{50} curves the time course of inhibition of serine-β-lactamases. Residual activities were calculated from initial rates of FC5 hydrolysis after incubation of the enzyme with the inhibitor for 0, 10, 30, 60 or 360 minutes. Inhibition assays were carried out at 25 °C and pH 7.5.

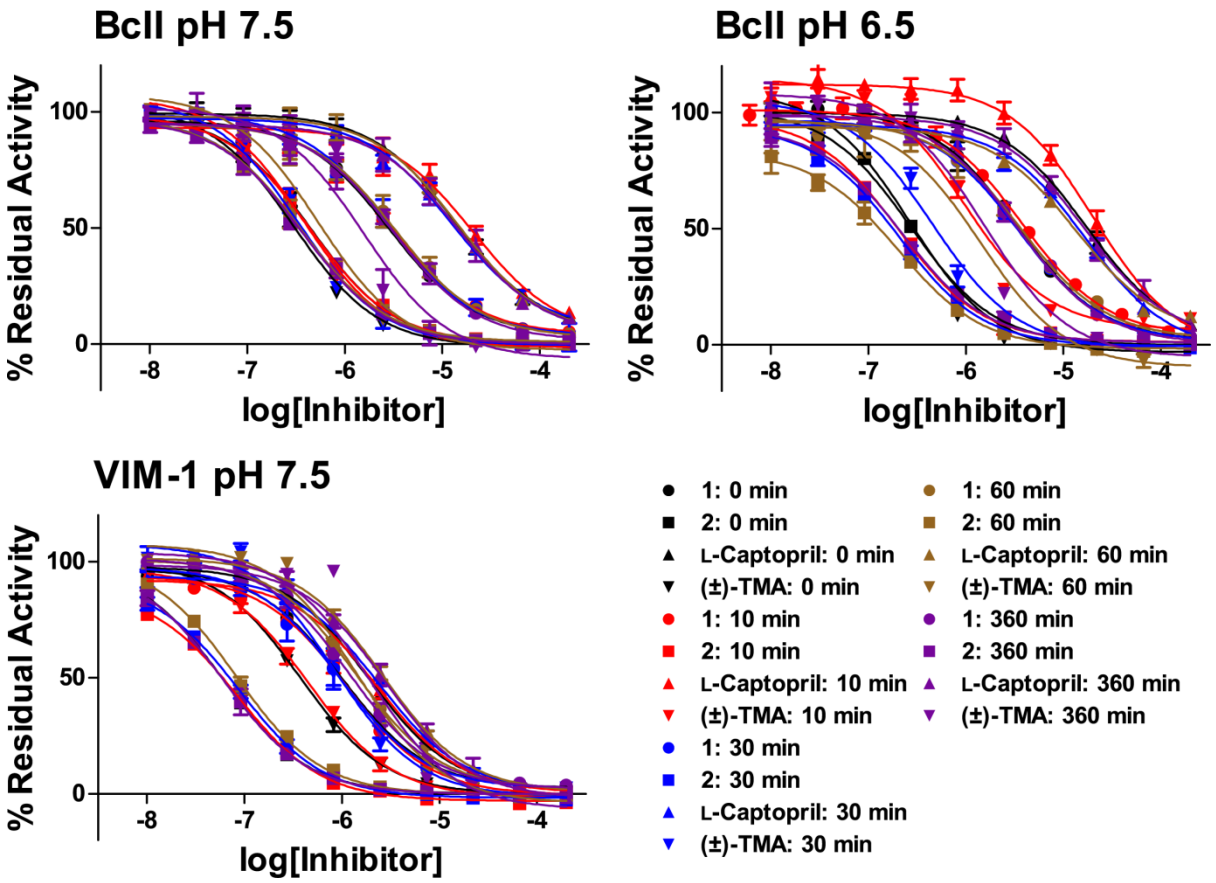

Figure 3.18: IC_{50} curves the time course of inhibition of metallo-β-lactamases. Residual activities were calculated from initial rates of FC5 hydrolysis after incubation of the enzyme with the inhibitor for 0, 10, 30, 60 or 360 minutes. Inhibition assays were carried out at 25 °C and pH 7.5.

Inhibitor	Pre-incubation Time (min)	TEM-1 IC_{50} (nM)	CTX-M-15 IC_{50} (nM)	AmpC IC_{50} (nM)	OXA-23 IC_{50} (nM)	OXA-48 IC_{50} (nM)
1	0	2.6 ± 0.1	92 ± 6	68 ± 3	220 ± 1	140 ± 1
	10	1.3 ± 0.1	13 ± 1	9.8 ± 0.3	250 ± 1	160 ± 1
	30	1.6 ± 0.1	3.7 ± 0.1	4.5 ± 0.1	260 ± 1	170 ± 1
	60	1.5 ± 0.1	1.7 ± 0.1	2.6 ± 0.1	270 ± 1	170 ± 1
	360	1.7 ± 0.1	4.0 ± 0.01	2.4 ± 0.1	730 ± 2	270 ± 1
2	0	8.1 ± 0.1	39 ± 2	270 ± 60	2000 ± 10	2000 ± 10
	10	3.4 ± 0.1	7.5 ± 0.3	120 ± 10	2600 ± 10	2600 ± 20
	30	2.6 ± 0.1	2.8 ± 0.1	150 ± 10	3300 ± 20	3400 ± 10
	60	2.6 ± 0.1	1.3 ± 0.1	100 ± 10	2600 ± 10	3000 ± 10
	360	2.1 ± 0.1	6.4 ± 0.1	96 ± 1	3300 ± 20	3300 ± 20
Sulbactam	0	860 ± 80	44 ± 1	$> 2 \times 10^5$	$> 2 \times 10^5$	$> 2 \times 10^5$
	10	600 ± 200	29 ± 1	42000 ± 2000	$> 2 \times 10^5$	$> 2 \times 10^5$
	30	600 ± 200	28 ± 7	8600 ± 600	$> 2 \times 10^5$	$> 2 \times 10^5$
	60	500 ± 200	32.0 ± 0.3	4400 ± 500	$> 2 \times 10^5$	$> 2 \times 10^5$
	360	700 ± 300	16.6 ± 0.1	1000 ± 400	$> 2 \times 10^5$	$> 2 \times 10^5$
Avibactam	0	19 ± 1	9.9 ± 0.2	1400 ± 400	770 ± 4	2500 ± 30
	10	3.4 ± 0.1	1.1 ± 0.1	190 ± 10	390 ± 1	810 ± 50
	30	2.2 ± 0.1	0.40 ± 0.06	200 ± 10	160 ± 2	300 ± 2
	60	2.0 ± 0.1	0.39 ± 0.01	200 ± 10	71 ± 1	150 ± 1
	360	4.3 ± 0.1	6.4 ± 0.1	150 ± 10	13 ± 1	20 ± 1
BLI-489	0	4.8 ± 0.2	32 ± 2	210 ± 20	5.6 ± 0.1	14 ± 1
	10	2.0 ± 0.1	6.9 ± 0.2	30 ± 1	5.6 ± 0.1	15 ± 1
	30	1.7 ± 0.2	2.2 ± 0.1	12.0 ± 0.4	6.2 ± 0.1	16 ± 1
	60	1.7 ± 0.1	0.94 ± 0.03	5.6 ± 0.1	8.6 ± 0.1	22 ± 1
	360	1.9 ± 0.1	8.0 ± 0.1	1.9 ± 0.1	18 ± 1	49 ± 1

Table 3.6. Time course for the inhibition of serine-β-lactamases (classes A, C and D) by cyclic boronates and selected covalent serine-β-lactamase inhibitors using FC5 as a substrate. IC_{50} values were taken after pre-incubation of the enzyme with the corresponding inhibitor for 0, 10, 30, 60 or 360 minutes prior to assay. Inhibition assays were carried out at 25 °C and pH 7.5. IC_{50} values were obtained from fitting of residual activity plots using GraphPad Prism(347).

Inhibitor	Pre-incubation Time (min)	BcII pH 7.5 IC_{50} (μM)	BcII pH 6.5 IC_{50} (μM)	VIM-1 pH 7.5 IC_{50} (μM)
1	0	2.8 ± 0.2	3.3 ± 0.1	1 ± 1
	10	3.0 ± 0.2	3.8 ± 0.2	1 ± 1.2
	30	2.8 ± 0.3	3.5 ± 0.1	1 ± 1.5
	60	3.4 ± 0.3	3.8 ± 0.2	1.4 ± 0.3
	360	3.1 ± 0.2	3.0 ± 0.2	1.2 ± 0.3
2	0	0.45 ± 0.02	0.27 ± 0.02	0.061 ± 0.001
	10	0.45 ± 0.02	0.20 ± 0.01	0.085 ± 0.002
	30	0.36 ± 0.02	0.20 ± 0.01	0.088 ± 0.001
	60	0.36 ± 0.01	0.20 ± 0.01	0.083 ± 0.002
	360	0.36 ± 0.03	0.23 ± 0.01	0.061 ± 0.001
L-Captopril	0	13.7 ± 0.3	17.4 ± 0.3	1.91 ± 0.06
	10	21 ± 1	20.4 ± 0.6	2.3 ± 0.2
	30	12.5 ± 0.5	16.8 ± 0.8	2.4 ± 0.2
	60	14.6 ± 0.4	13.7 ± 0.7	2.6 ± 0.1
	360	15 ± 1	16.3 ± 0.5	2.8 ± 0.2
(±)-TMA	0	0.30 ± 0.03	0.27 ± 0.06	0.38 ± 0.03
	10	0.39 ± 0.05	0.9 ± 0.1	0.45 ± 0.02
	30	0.33 ± 0.04	0.5 ± 0.1	0.8 ± 0.9
	60	0.5 ± 0.2	2 ± 1	1.4 ± 0.9
	360	2 ± 1	2 ± 1	2 ± 1

Table 3.7. Time course for the inhibition of metallo-β-lactamases (classes A, C and D) by cyclic boronates and selected thiol-based metallo-β-lactamase inhibitors using FC5 as a substrate. IC_{50} values were taken after pre-incubation of the enzyme with the corresponding inhibitor for 0, 10, 30, 60 or 360 minutes prior to assay. Inhibition assays were carried out at 25 °C and pH 7.5. IC_{50} values were obtained from fitting of residual activity plots using GraphPad Prism(347).

Both cyclic boronates, **1** and **2**, were able to inhibit the additional SBLs tested with IC_{50} values ranging from 250 to 2 nM (Table 3.6). Against TEM-1 and CTX-M-15, **1** and **2** exhibit a similar inhibition potency (1.5 ± 0.1 nM and 1.7 ± 0.1 nM, respectively, after 60 minutes pre-incubation). Against AmpC, **2** shows around 10-fold lower IC_{50} values than **1** (9.8 ± 0.3 nM vs 120 ± 10 nM, respectively, with 10 minutes pre-incubation) while, against the OXA enzymes, **1** exhibits 10- to 15-fold lower IC_{50}s than **2** (250 ± 1 nM and 2600 ± 100 nM, respectively, after 10 minutes incubation for OXA-23, and 160 ± 1 nM and 2600 ± 200 nM, respectively, after 10 minutes incubation for OXA-48). **1** and **2** show similar potency to avibactam and BLI-489 against the class A enzymes, with low to sub-nanomolar IC_{50} values. **2** shows a similar potency to avibactam against AmpC, while **1** exhibits up to 60-fold lower IC_{50} values than avibactam (9.8 ± 0.3 nM and 190 ± 10 nM at 10 minutes, respectively) and results comparable to those seen for BLI-489 (30 ± 1 nM at 10 minutes). Against the OXA enzymes, neither **1** nor **2** were able to achieve potency comparable with BLI-489, with IC_{50} values for **1** being around 10 to 20-fold higher and those for **2** being around 100 to 200-fold

higher, but IC_{50} values for **1** were comparable with those seen for avibactam, at least after up to 60 minutes of pre-incubation (270 ± 1 nM and 170 ± 1 nM for **1** against OXA-23 and OXA-48, respectively, and 71 ± 1 nM and 150 ± 1 nM for avibactam against OXA-23 and OXA-48, respectively, after 60 minutes incubation). In all cases the inhibition of the MBLs by **2** was around 10 times more potent than by **1** (Table 3.7). **1** exhibited IC_{50} values around two- to five-fold lower than those seen with L-captopril (2.8 ± 0.3 μM and 12.5 ± 0.5 μM, respectively, after 30 minutes incubation with BcII). **2** showed very similar potency to thiomandelic acid against BcII but showed five to 10-fold greater potency than thiomandelic acid against VIM-1.

The observation of time-dependency in inhibition varied depending on the particular inhibitor-enzyme combination being considered (Table 3.6). Where significant time dependency was observed, the largest decrease in IC_{50} generally occurred over the first 10 minutes of inhibition. Avibactam showed time-dependency in its inhibition of all the tested SBLs with the lowest IC_{50} value typically observed after 60 or 360 minutes pre-incubation. The IC_{50} values obtained with BLI-489 only showed substantial time-dependency with CTX-M-15 and AmpC, and the lowest IC_{50} values were seen after longer incubation times. The time-dependency of inhibition by the cyclic boronates, **1** and **2**, was similar to that observed for BLI-489, in that it was seen with CTX-M-15 and AmpC but not with TEM-1 or the OXA enzymes. Perhaps unexpectedly, a significant increase in the IC_{50} values for avibactam and BLI-489 against CTX-M-15 was observed between 60 and 360 minutes of incubation. This may be the result of slow hydrolysis of the inhibited acyl-enzyme to restore a population of the active enzyme. No time-dependency of MBL inhibition by either the cyclic boronates or thiol-based inhibitors was observed.

3.7. In Solution Studies of Cyclic Boronates and β-Lactamases

While crystallography is an important tool for characterizing the binding mode of inhibitors and subsequent structure-activity relationship (SAR) studies, in solution data can also help to produce a more dynamic picture of an interaction. Thus, the binding of cyclic boronates to SBLs and MBLs was explored using both nuclear magnetic resonance (NMR) spectroscopy and surface plasmon resonance (SPR).

3.7.1. NMR Studies on Binding of Cyclic Boronates to β-Lactamases

When in solution the boron centre of a boronic acid may exist as a trigonal planar neutral species or tetrahedral anion by coordination of an additional water molecule. ^{11}B NMR was employed to investigate the ratio of boron hybridization states in solution and how this might be affected by addition of a β-lactamase (Figure 3.19).

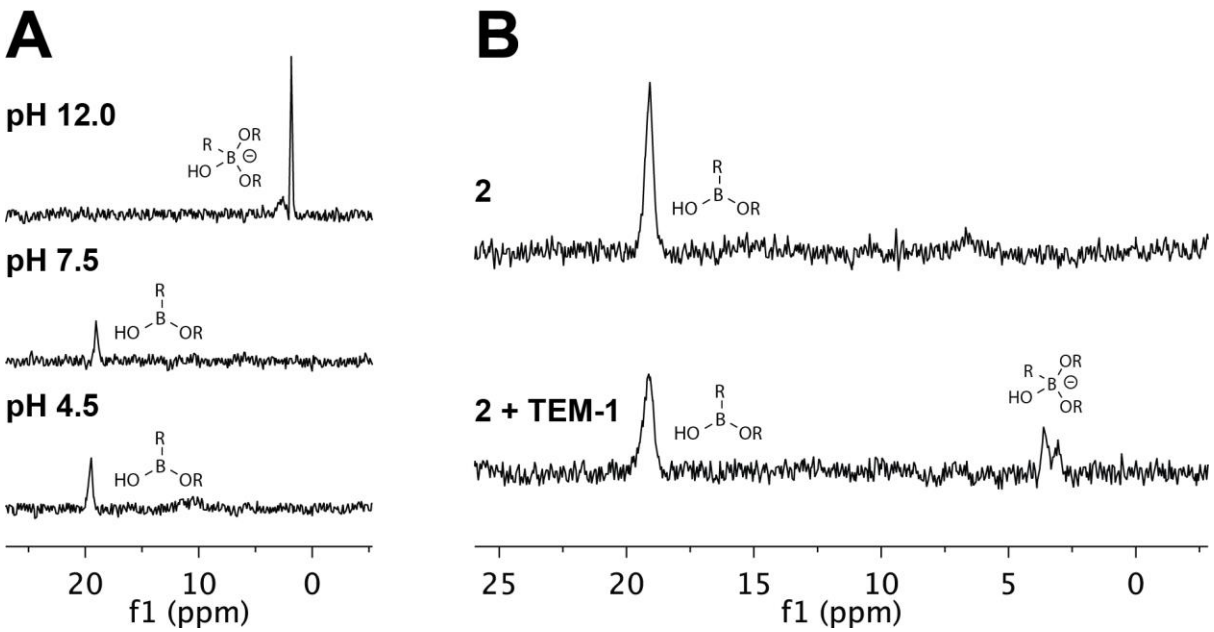

Figure 3.19. Impact of pH and enzyme on the ^{11}B-NMR spectrum of 2. A. ^{11}B-NMR spectra of 2 at varying pH. B. ^{11}B-NMR spectra showing the interaction of TEM-1 with 2 at pH 7.5. 2 was employed at a final concentration of 200 μM and TEM-1 was studied at 300 μM. Studies at pH 12.0 and 7.5 were carried out in 50 mM sodium phosphate supplemented with 10% D_2O. Studies at pH 4.5 were carried out in 50 mm sodium acetate supplemented with 10% D_2O.

At low to neutral pH values, cyclic boronate **2** gave rise to a shift at 20 ppm, while at higher pH (12.0) this shift was not apparent and a peak at 2 ppm was observed. The 20 ppm peak likely corresponds to a trigonal planar, tricoordinate boron centre, while the 2 ppm one corresponds to a tetrahedral anionic centre – the resultant negative charge on the boron giving rise to increased shielding(440). Note that an additional broad peak a shoulder to the 2 ppm shift is seen at pH 12.0. The origin of this peak is, as yet, unidentified but may correspond to an oligomeric state. On addition of TEM-1 to a sample of **2** at pH 7.5, the 20 ppm signal was reduced but not ablated and an additional signal was visible around 3 ppm. This additional signal comprised two peaks, which could correspond to ring closed and opened forms of **2**. The binding of a boronic acid to TEM-1 in an open configuration is precedented by X-ray crystallographic studies on a very similar compound to this series (Figure 3.20)(441). The additional peak could also correspond to binding at an alternative site, as precedented by surface binding of a benzoxaborole to histidines (Figure 3.7 D)(426), or may once again may represent an oligomeric state of **2**. Thus, addition of TEM-1 to a solution of **2** could result in a peak corresponding to a tetrahedral boronate species in both open and closed forms, with the additional ligand coordinating the boron likely being the active site nucleophilic serine residue. Further work using other β-lactamases has been proposed to confirm the identity of the species corresponding to each observed peak.

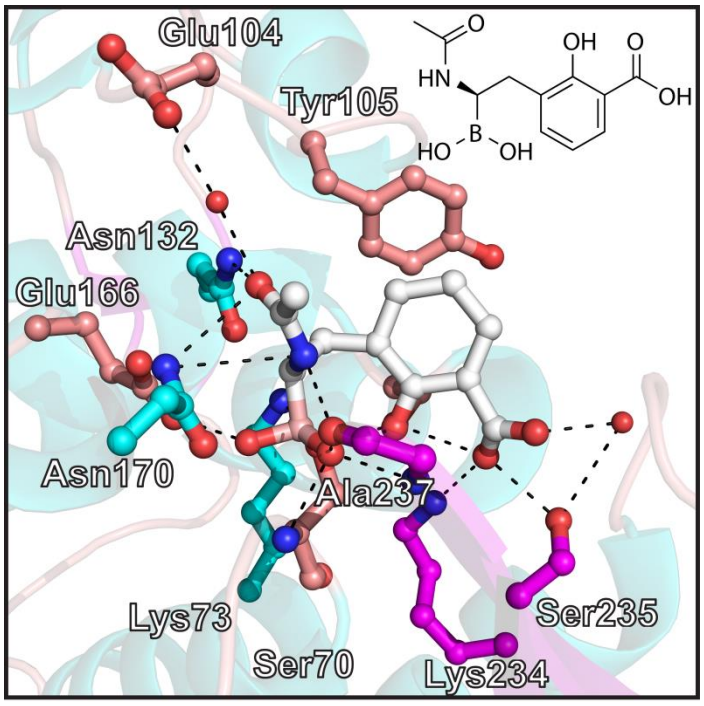

Figure 3.20: View from a crystal structure of a cyclic boronate (white) in complex with TEM-1. Although the ligand has the potential to cyclise in a similar manner to the compounds in this study, it has been refined in an open conformation(441). The chemical structure of the inhibitor is inset.

In the class D OXA SBLs, the reversible reaction of Lys70 with carbon dioxide(442), a post-translation modification critical for activity(172), can be manipulated to site specifically label the residue with ^{13}C(172). Thus, the binding of **1** to OXA-10 was monitored using ^{13}C NMR spectroscopy. Based on crystallographic studies with OXA enzymes, it has been proposed that the SBL inhibitor, avibactam, exerts its activity, in part, by encouraging lysine decarbamylation to activate the enzyme. Interestingly, the carbamylation of OXA-10 is maintained upon binding of **1**, however a shift of 6 ppm in the carbamylate signal is observed (Figure 3.21). This observed shift is substantial when compared to that reported upon binding of hydroxyisopropylpenicillanates, where only a 0 to 0.4 ppm shift is seen(172). The greater shift of the ^{13}C signal on binding of the boronate may reflect the different environment of the lysine carbamylate and the adjacent active site serine, being bound to an sp^3 anionic boron centre when complexed to cyclic boronate **1** as opposed to an sp^2 carbon center in the hydroxyisopropylpenicillanate complex.

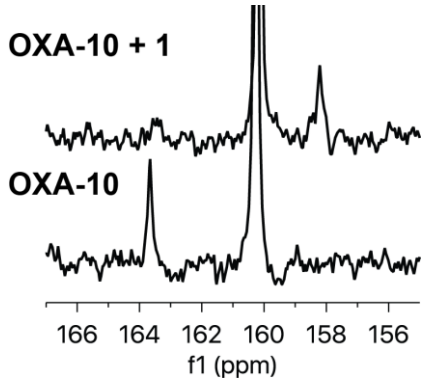

Figure 3.21: ^{13}C NMR spectra for OXA 10 with a ^{13}C labelled Lys70 carbamylate, formed by addition of 10 mM NaH$^{13}CO_3$ alone and after supplementation with 5 mM boronate 1. OXA-10 was present at 560 μM. All samples were supplemented with 10% D_2O. The large peak at 160.5 ppm corresponds to ^{13}C labelled sodium bicarbonate.

3.7.2. Kinetics of Cyclic Boronate Binding to β-lactamases

Surface plasmon resonance was employed to investigate the origins of the low IC_{50} values seen with the cyclic boronates and MBLs, in particular with VIM-2.

A fast binding rate, k_{on} = 1.25 x 10^5 M^{-1} s^{-1}, combined with a very slow dissociation rate, k_{off} = 5.74 x 10^{-4} s^{-1}, gives rise to a dissocation constant (K_d) of 4.6 nM. While this K_d value is in close agreement with the IC_{50} value of 3 nM determined previously (Table 3.5), it should be taken with caution since the low off rate of the inhibitor may limit the success of computational fitting of the SPR response traces. The most striking observation is the very low off rate of the inhibitor. This results in a response curve in which, after initial binding, the enzyme is saturated by **2** over the course of the experiment. This very slow off rate may come as a result of the non-chelating ionic interaction between a negatively charged tetrahedral boron centre and the positive metal ions.

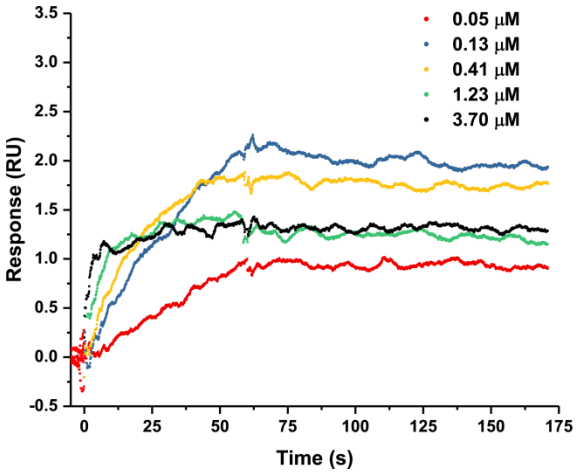

Contant	Fitted Value
k_{on}	0.125 $\mu M^{-1} s^{-1}$
k_{off}	5.74 x 10^{-4} s^{-1}
K_d	4.59 nM

Figure 3.22: Time course and fitted kinetic constants for the binding of varying concentrations of cyclic boronate 2 to VIM-2 as determined by surface plasmon resonance. Biotinylated VIM-2 was captured on the streptavidin coated chip surface by continuous flow of 100 μM enzyme until a stable response of 3000 RU was achieved. All measurements were recorded at 4 °C. Note that upon binding, 2 exhibits a very low off rate such that the enzyme remains saturated for the duration of the experiment. Fitting of traces was carried out using Biacore T200 software.

3.8. Structural Characterisation of Cyclic Boronates with β-Lactamases

Given the chemical structure of the synthesised cyclic boronate compounds, there are two obvious potential forms of the molecule, one in which the boron is part of a heterocycle (Figure 3.23) and the other in which it has been linearised due to exchange with water. (Both of these general forms can also adopt sp^2 and sp^3 coordinate states at the boron centre). A recent publication has demonstrated that a balance of two entropic effects, water release and intrinsic chain entropy, cause cyclic boronic acids in which the boron is contained within a five, six, or eight membered ring, to exist predominantly in a ring closed form, while seven membered rings favor an open conformation(443).

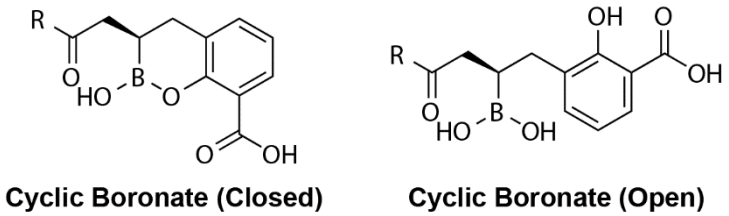

Figure 3.23: General chemical structures of the closed and open forms of the cyclic boronates used in the study. The latter can be obtained via exchange with water at the boron centre.

As already mentioned above, a crystal structure of a related cyclic boronate complexed with TEM-1 shows an open conformation rather than a six membered ring(441). However, co-

crystal structures of RPX-7009 (vaborbactam) with CTX-M-15 and AmpC reveal that the boron-containing ring remains closed (Figure 3.24)(212).

X-ray crystallography was employed to assess the mechanism of β-lactamase inhibition by the cyclic boronates, to investigate the preference for ring-opened/closed states in enzyme-boronate complexes, and to characterise the structures of the enzyme inhibitor complexes. Crystal structures were obtained for cyclic boronates in complex with CTX-M-15, AmpC from *P. aeruginosa*, OXA-10, BcII, and VIM-2, thus covering all four Ambler classes of β-lactamase, and a structure of a cyclic boronate complexed with PBP-5 was also obtained.

Data Set	CTX-M-15:1 Complex	AmpC:1 Complex	OXA-10:1 Complex	BcII:2 Complex	VIM-2:2 Complex	PBP-5:2 Complex
Data Collection						
Source	Rotating Anode	Diamond I04	Diamond I04	Rotating Anode	Diamond I04	Diamond I02
Resolution Range (Å)	21.68 – 1.95 (2.02 – 1.95)	60.3 - 2.06 (2.11 - 2.06)	15.42 - 1.50 (1.55 - 1.50)	21.64 - 1.90 (1.97 - 1.90)	28.89 - 1.45 (1.50 - 1.45)	28.14 - 2.52 (2.61 - 2.52)
Space Group	$P\ 2\ 2_1\ 2_1$	$P\ 2_1\ 2_1\ 2_1$	$P\ 2_1\ 2_1\ 2_1$	$C\ 2_1$	$C\ 2_1$	$P\ 2\ 2_1\ 2_1$
Unit Cell Parameters						
a, b, c (Å)	43.5, 76.1, 149.4	45.0, 75.3, 100.6	48.9, 103.1, 125.5	53.1, 61.1, 69.4	101.9, 79.2, 67.1	50.2, 61.6, 138.4
a, b, g (°)	90.0, 90, 90.0	90.0, 90, 90.0	90.0, 90, 90.0	90.0, 93.1, 90.0	90.0, 130.2, 90.0	90.0, 90, 90.0
Unique Reflections	36639 (3565)	20739 (1133)	102231 (10087)	17335 (1684)	71720 (7077)	14957 (1427)
Completeness (%)	99.07 (99.56)	96.3 (92.8)	99.90 (99.50)	93.38 (95.43)	99.40 (97.00)	99.90 (99.70)
Redundancy	5.3 (4.6)	4.8 (3.2)	5.9 (8.9)	3.7 (3.5)	4.4 (3.7)	6.4 (5.3)
R_{merge}	0.120 (0.100)	0.090 (0.120)	0.047 (1.100)	0.058 (0.088)	0.065 (0.582)	0.098 (0.593)
$\langle I/\sigma(I)\rangle$	5.3 (1.6)	5.2 (1.8)	5.6 (2.0)	17.8 (5.2)	11.0 (1.8)	13.5 (1.8)
Refinement						
R_{work}/R_{free}	0.2003/0.2341	0.2286/0.2762	0.1569/0.1806	0.1403/0.1807	0.1550/0.1852	0.2000/0.2334
RMSD						
Bonds (Å)	0.003	0.003	0.014	0.010	0.014	0.003
Angles (°)	0.61	0.68	1.34	1.25	1.41	0.56
Average B-factor for protein atoms ($Å^2$)	19.31	32.35	27.40	26.80	17.85	54.19
Ramachandran Plot						
Most Favoured Geometry (%)	98.0	96.3	97	98.0	96.0	98.0
Additionally Allowed (%)	1.1	3.4	2.4	1.3	4.0	2.0
Outliers (%)	0.4	0.3	0.6	0.7	0.0	0.0

Table 3.8: Data collection and refinement statistics for crystallised complexes of cyclic boronates with serine-β-lactamases, metallo-β-lactamases, and penicillin binding proteins. Bracketed values correspond to data for the highest resolution shell.

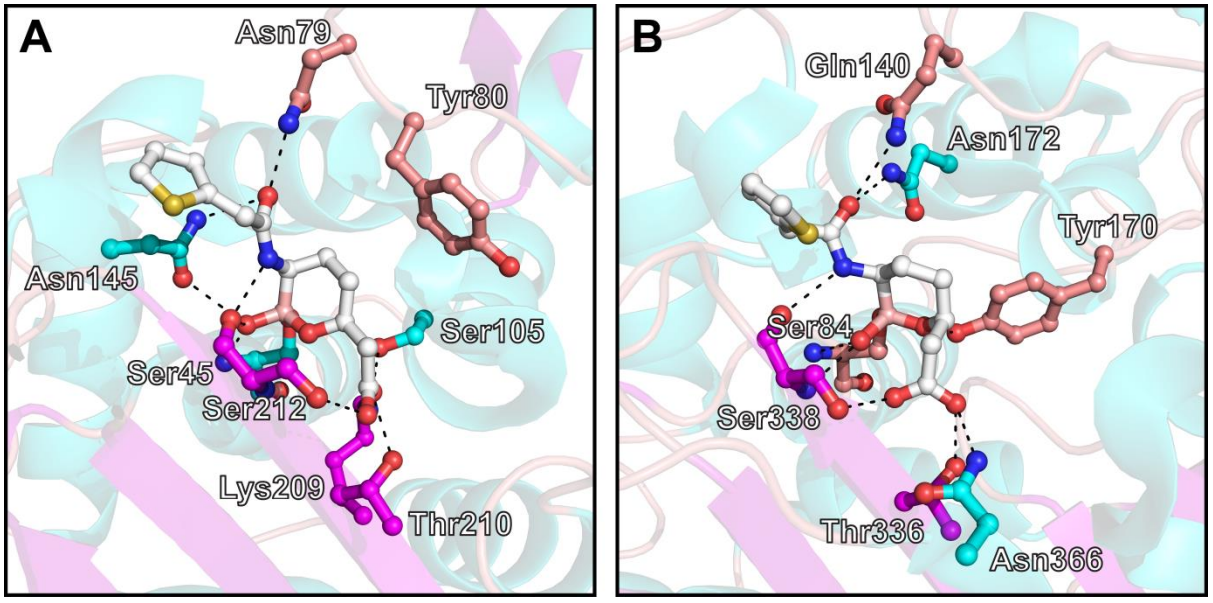

Figure 3.24: Views from co-crystal structures of vaborbactam with A. CTX-M-15 (PDB accession code: 4XUZ) and B. AmpC (PDB accession code: 4XUX)(212). In both structures the compound adopts a closed ring configuration. Interestingly the boron containing ring adopts a different ring flip conformation between the two structures, with the amino acyl side chain being axial in CTX-M-15 and equatorial in AmpC.

3.8.1. Structures of Cyclic Boronates in Complex with Serine-β-Lactamases

Crystal structures of SBLs in complex with cyclic boronate **1** (Figure 3.25) were obtained via co-crystallisation experiments. A structure of the CTX- M-15:**1** complex was solved to 1.95 Å resolution by molecular replacement, using a reported structure of the apo-enzyme (PDB accession code 4HBT)(157) as a search model. (Crystallographic data are provided in Table 3.8). Comparison of the structure of the boronate complex with that of the apo-enzyme shows little change in the overall conformation of the enzyme upon binding the inhibitor, with a root-mean-square deviation (RMSD) of 0.194 Å over backbone carbon atoms. Electron density in the active site clearly reveals that **1** is bound *via* reaction with the side chain of the nucleophilic serine, Ser73, and provides clear evidence for a tetrahedral coordination of the boron centre (Figure 3.26 A). The carboxylate of **1** is positioned to form a salt bridge interaction with Lys237 as well as hydrogen bonding interactions with Thr238, Ser240 and a water molecule, while the acetamido side chain can form hydrogen bonds with Asn107, Asn135 and the main chain carbonyl of Ser240 (Figure 3.26 B). The aromatic ring of the central core of **1** is positioned to make an aromatic/hydrophobic interaction with Tyr108. Importantly, the electron density demonstrates unequivocally that the boron centre is maintained within a closed six membered ring. (Figure 3.26 A)

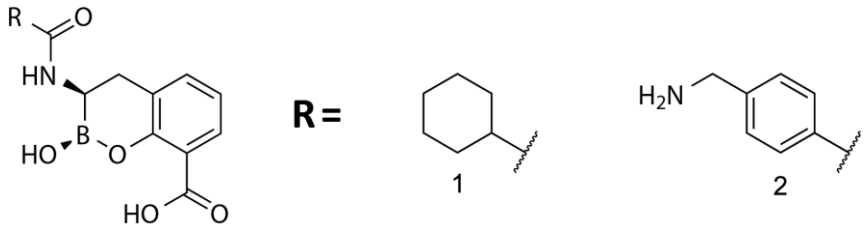

Figure 3.25: Chemical structures of the cyclic boronates employed in crystallographic studies with serine- and metallo-β-lactamases and penicillin binding proteins.

A structure of AmpC in complex with **1** was solved to 2.06 Å resolution by molecular replacement using a previous apo-enzyme structure (PDB accession code: 4GZB)(157) as a search model. In a similar manner to that described for the CTX-M-15:**1** complex, the electron density reveals the boron to be covalently linked to the active site serine, Ser90, tetrahedrally coordinated, and housed within a closed six membered ring (Figure 3.26 C). As above, the carboxylate moiety of **1** is positioned to form salt bridge interactions with Lys342 and Arg376 as well as potential hydrogen bonds with Thr343, Ser345, and Asn373, while the acetamido side chain forms hydrogen bonds with Gln146, Asn179 and the main chain carbonyl of Ser345.

A structure of OXA-10 in complex with **1** was determined to 1.5 Å resolution by molecular replacement using an apo-enzyme structure (PDB accession code: 1FOF)(444) as a search model. Comparison of the structures of apo-OXA-10 with that of the enzyme in complex with a cyclic boronate reveals minimal changes in the overall structure of the enzyme, with an RMSD of 0.19 Å over backbone carbon atoms. In the active site, Lys70, which is carbamylated in catalytically active OXA enzymes, is observed to be carbamylated in the enzyme-inhibitor complex (Residue KCX70 in Figure 3.26 F). As for the class A and C enzymes above, electron density around the boron centre demonstrates that the inhibitor is bound by covalent attachment to the nucleophilic serine residue, Ser67. Further, the electron density clearly demonstrates that the boron centre is tetrahedrally coordinated, and that the boron is located within a closed six-membered ring (Figure 3.26 E). The carboxylate of **1** is positioned to form a salt bridge with Arg250, while the acetamido side chain is positioned to hydrogen bond with the main chain carbonyl of Phe208. Finally, the cyclohexyl side chain makes hydrophobic contacts with Met99 and Trp102.

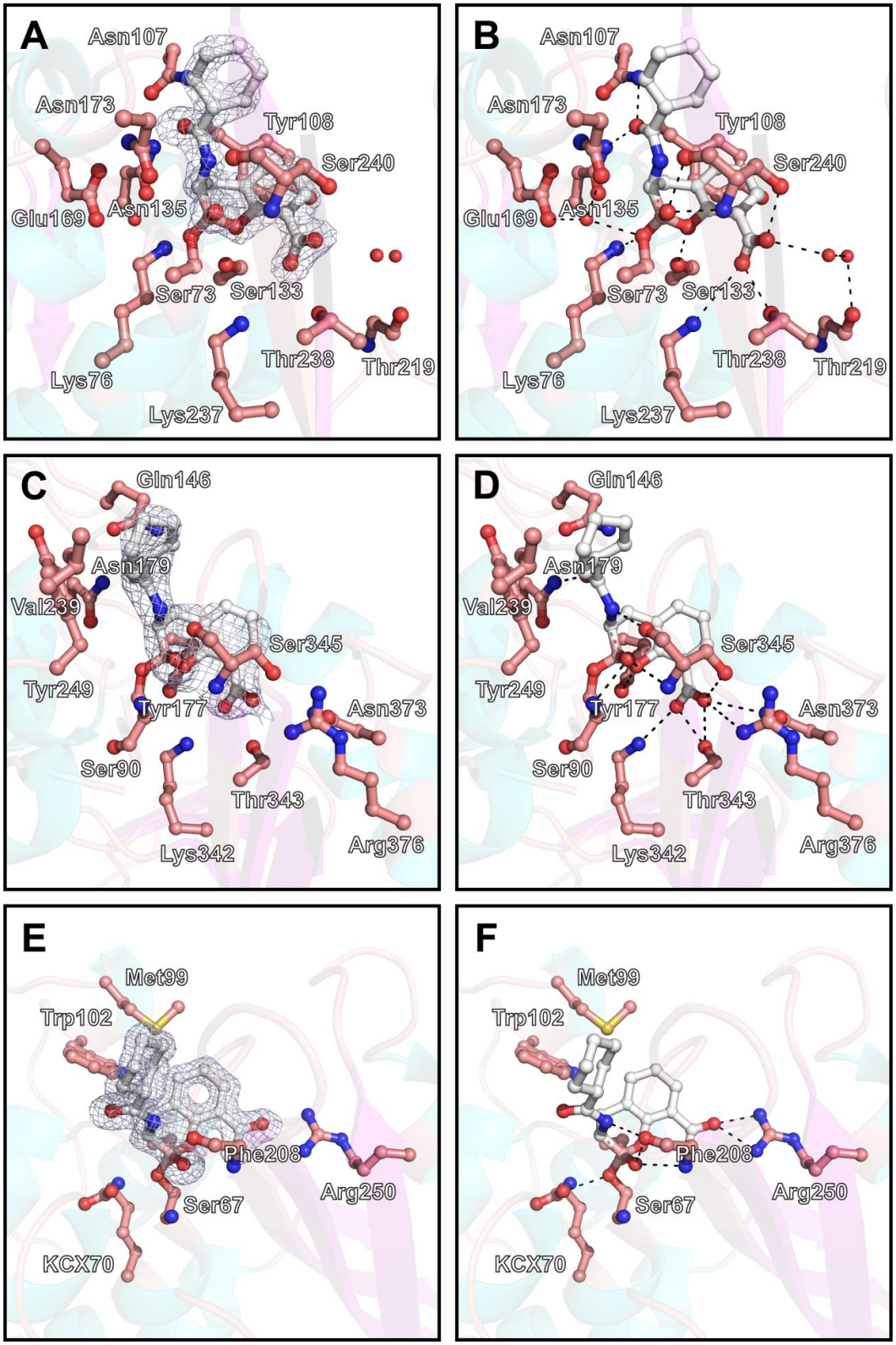

Figure 3.26: Co-crystal structures of cyclic boronates with serine-β-lactamases. A & B. CTX-M-15:1. C & D. AmpC:1. E & F. OXA-10:1. Representative density for the ligands is shown (3.0 σ mF_o-DF_c OMIT, grey mesh). Dashed lines indicate potential hydrogen bonding interactions. Water molecules are represented by red spheres.

Taken together, these results show that the cyclic boronates inhibit SBLs via covalent reaction with their active site nucleophilic serine. A closed conformation of the boron-containing ring is seen in all three structures, which supports the conclusions drawn from boron and carbon NMR. This suggests that these compounds mimic the first tetrahedral anionic intermediate in β-lactam hydrolysis, EI^1 in Figure 3.8 A. Further evidence for the cyclic boronates mimicking β-lactam substrates can be obtained from overlaying structures of, for example, OXA-10:1 and a catalytically inactive OXA-10 mutant in complex with benzylpenicillin (PDB accession code: 2WGL)(173). Comparison of these two structures shows analogous placement of the carboxylate and acetamido side chains, while the endocyclic oxygen of **1** is well placed to mimic the nitrogen of the penicillin thiazolidine ring in its interaction with Ser115 (Figure 3.27).

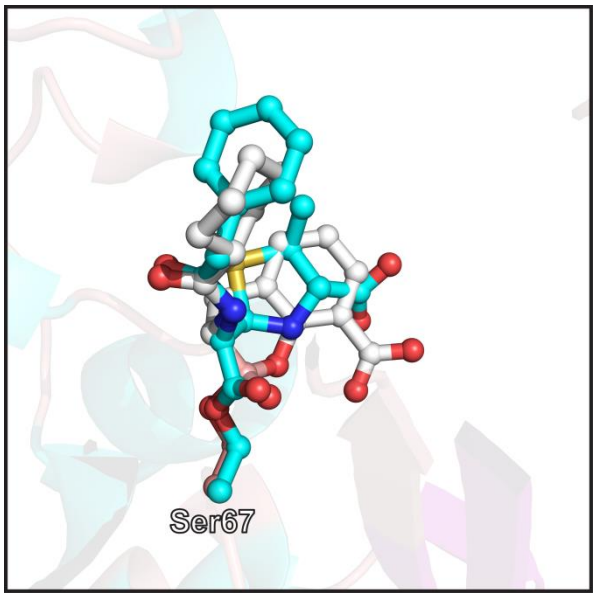

Figure 3.27: Structural overlay of OXA-10:1 (white) and an OXA-10 K70C benzylpenicillin complex (PDB accession code: 2WGI, cyan)(173). Note the similar placements of the carboxylates and acetamido side chains, and how the endocyclic oxygen of 1 may mimic the thiazolidine nitrogen in the penicillin.

3.8.2. Structure of a Cyclic Boronate in Complex with PBP5

As stated previously, the cyclic boronates have been shown to inhibit the non-essential penicillin binding protein, PBP5, with an apparent IC_{50} of 1.99 nM for inhibition by **2** (Table 3.4). The SBLs are believed to be evolutionarily related to the PBPs and the two enzyme classes demonstrate similarity in both their protein fold and the use of an active site nucleophilic serine residue for catalysis. Thus, it would be expected that the binding mode of the cyclic boronates to PBPs would be similar to that seen with SBLs. To investigate this, PBP5 was co-crystallised with **2** and the structure of the complex was solved to 2.5 Å resolution.

As with the SBLs, the electron density of the ligand revealed covalent binding **2** to the active site serine residue, Ser44, via the boron centre, a tetrahedral coordination of the boron atom and a closed six membered ring (Figure 3.28 A). In many structures of PBP5 in complex with β-lactams, little to no electron density is observed for the C-6/C-7 side chains of the ligand(445-447).

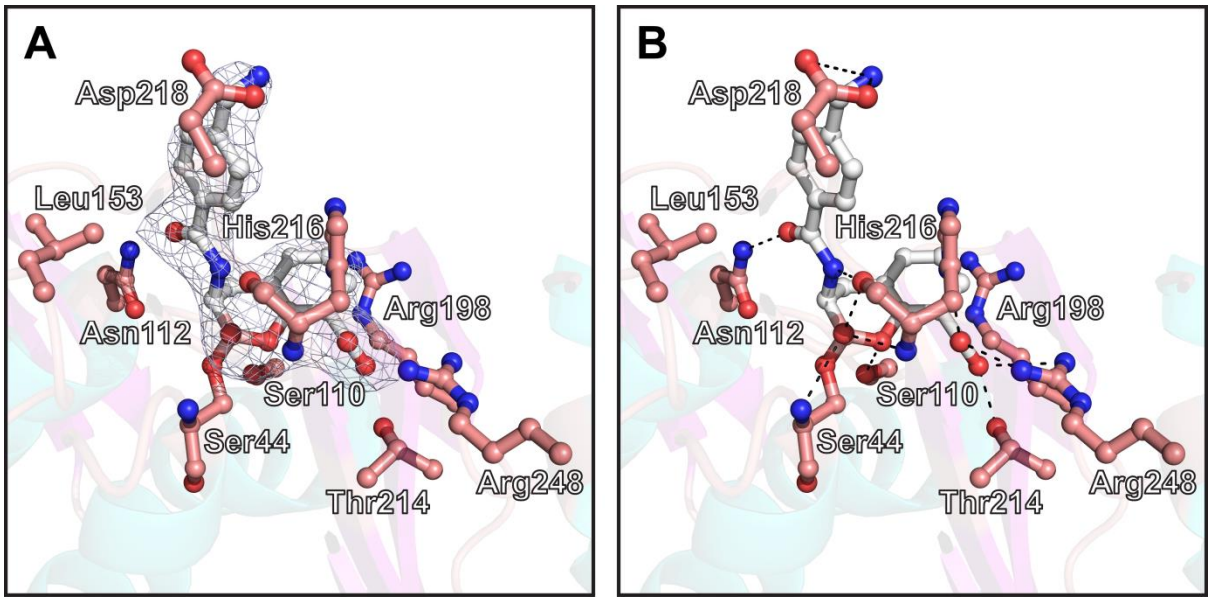

Figure 3.28: Co-crystal structure of cyclic boronate 2 with penicillin-binding protein 5. Representative density for the ligand is shown (3.0 σ mF_o-DF_c OMIT, grey mesh). Dashed lines indicate potential hydrogen bonding interactions.

In the PBP5:**2** structure, this is not the case, with clear electron density for the side chain revealing hydrogen bonding interactions with Asn112, Asn218, and the main chain carbonyl of His216, as well as a hydrophobic contact with Leu153 (Figure 3.28 B). His216 has moved 3.5 Å when compared to its location in an apo-enzyme structure(448) suggesting that its interaction with the carboxylate of **2** may mimic a crucial interaction in PBP5 substrate recognition. In the core of **2**, the endocyclic oxygen is positioned to hydrogen bond to Ser110, while the carboxylate forms salt bridge/hydrogen bonding interactions with Arg198, Arg248, and Thr214. With the exception of a tetrahedral boron centre versus a trigonal planar carbon centre, many features of the binding mode of **2** are mimicked in a crystal structure of the PBP5:cloxacillin acyl-enzyme intermediate (PDB accession code: 3MZD, Figure 3.29 B)(446).

Interestingly comparison of the PBP5:**2** structure with that of the apo-enzyme or the enzyme in complex with hydrolysed imipenem shows that the Ω-like loop, which is conserved in PBPs and class A SBLs and likely has a role in substrate recognition(449), adopts a 'closed' conformation, as opposed to the 'open' conformation seen in the apo- and

product-bound structures (Figure 3.29 A). As with the SBL:**1** complexes, the closed six membered ring and tetrahedral coordination of the boron centre suggest that **2** is mimicking a tetrahedral intermediate in the reaction of β-lactams with PBP5 that precedes the formation of an acyl-enzyme species.

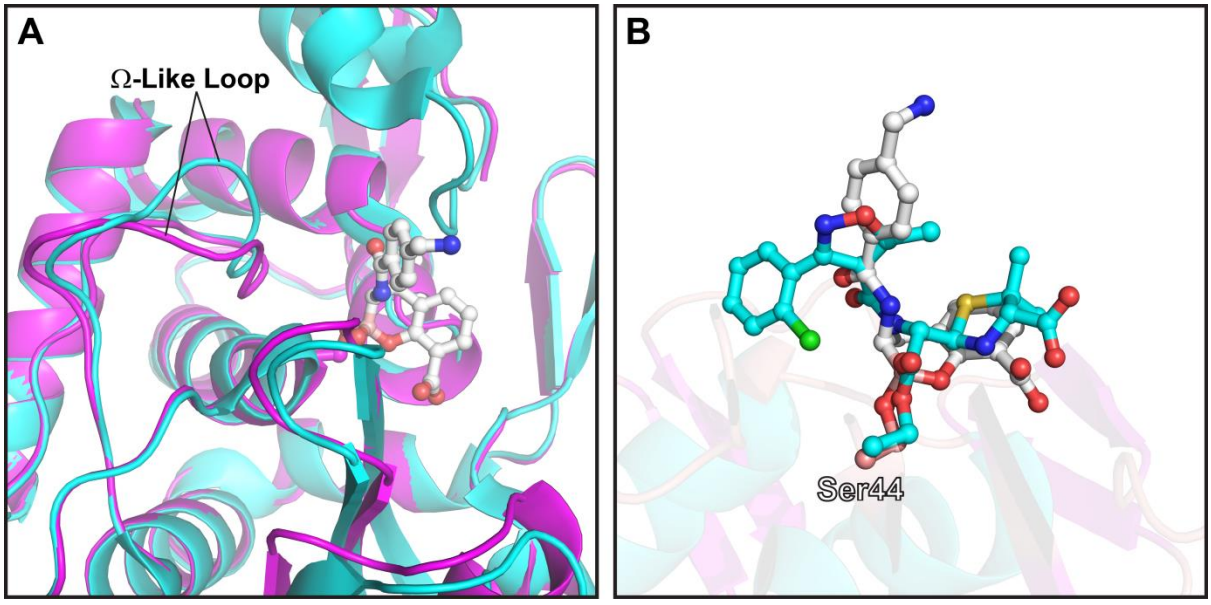

Figure 3.29: A. Comparison of the Ω-like loop conformations in apo-PBP5 (PDB accession code: 1NZO, cyan)(448) and the PBP5:2 complex (magenta). B. Overlay of the PBP5:2 (white) and PBP5:cloxacillin acyl-enzyme (PDB accession code: 3MZD, cyan)(446) structures. The Conformation of 2 in complex with PBP5 appears to mimic that of complexed cloxacillin.

3.8.3. Structures of Cyclic Boronates in Complex with Metallo-β-Lactamases

High resolution crystal structures were obtained for the subclass B1 MBLs, VIM-2 and BcII, in complex with cyclic boronate **2** to 1.5 and 1.9 Å resolution, respectively. In both of these structures electron density for the boronate reveals a tetrahedral sp^3 boron centre (Figure 3.30 A & C). The boron centre of **2** is observed to bind to Zn1 in a bidentate manner via two terminal hydroxide oxygen atoms, with one of these effectively replacing the bridging nucleophilic water.

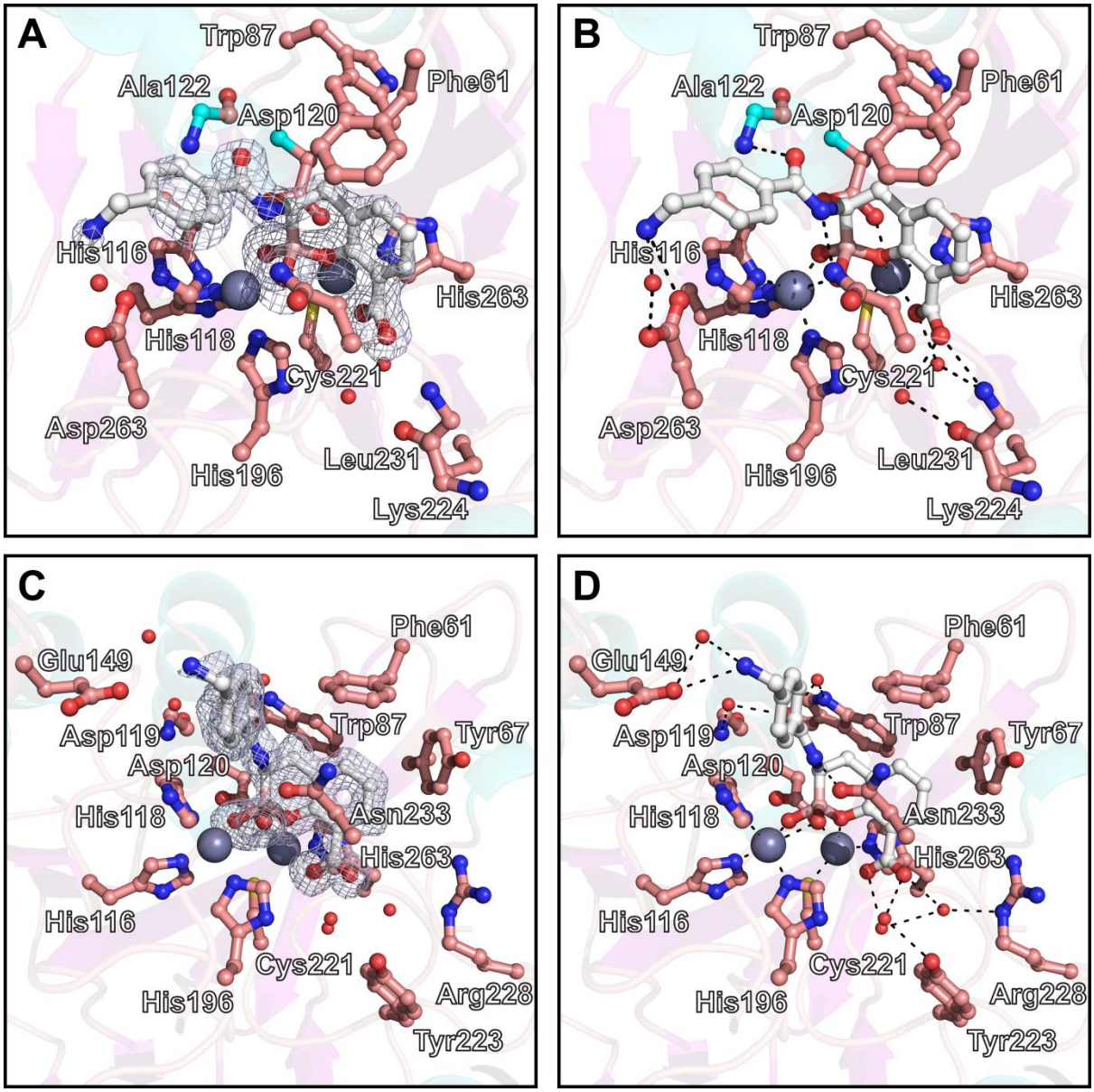

Figure 3.30: Co-crystal structures of cyclic boronates with metallo-β-lactamases. A & B. BcII:2. C & D. VIM-2:2. Representative density for the ligands is shown (3.0 σ m*Fo*-D*Fc* OMIT, grey mesh). Dashed lines indicate potential hydrogen bonding interactions. Water molecules are represented by red spheres.

The binding mode of **2** mimics that of hydrolysed β-lactams in complex with MBLs in a number of respects(259). Firstly, the carboxylate of **2** is oriented to interact with Lys224 of BcII or Arg228 of VIM-2 and coordinates to Zn2 in much the same way as the C-3/C-4 carboxylate of hydrolysed penicillins/cephalosporins has been shown to. Secondly, the aromatic ring of **2** is positioned to make hydrophobic contacts with Phe61 and Trp87, as well as Tyr67 in VIM-2, in a similar manner to the dihydrothiazine ring of hydrolysed cephalosporins (or analogous ring in penicillins and carbapenems). Thirdly, the side chain of **2** adopts a binding mode very similar to that of the C-7 acetamido side chain of cephalosporins such that the amide carbonyl is positioned to hydrogen bond with the main

chain amide nitrogen of Ala119 or Asp119 in BcII or VIM-2, respectively. Fourthly, binding of the two exocyclic, boron-bound oxygen atoms to Zn1 mimics the proposed binding mode of the oxyanion intermediate(450). Hydrogen bonding of Asn233 to the pro-(*S*) oxygen of the boron centre supports the proposal that this residue is involved in the stabilization of the oxyanion intermediate in β-lactam hydrolysis.

3.9. Susceptibility of Clinical Isolates to Cyclic Boronates

In the *in vitro* screening of the cyclic boronates against the purified enzymes, **2** was observed to be the more potent inhibitor of the B1 MBLs when compared to **1**. Since there are multiple clinically available inhibitors of the SBLs, potency against the MBLs, particularly against the clinically relevant B1 MBLs, is, arguably, a more highly desirable characteristic in the design of MBL/SBL dual inhibitors. Thus **2** (10 μg/mL), in combination with a number of β-lactams, was tested against a variety of Gram-negative clinical isolates characterized as producing multiple β-lactamases across all four Ambler classes (Tables 3.9-3.10). Those selected included *Enterobacteriaceae* (*E. coli* ST 131, *Klebsiella pneumoniae* ST 258, *Providencia stuartii*) producing class A ESBLs (CTX-M-15, CTX-M-27, SHV-5, VEB-1), serine (KPC-2) and metallo-β-lactamases (VIM-1, VIM-2), plasmid mediated AmpC (CMY-2) and/or carbapenem-hydrolysing OXA-48-like oxacillinases (OXA-181, OXA-232) in various combinations. The activity against carbapenemase producing strains of *Pseudomonas aeruginosa* (VIM-2) and *Acinetobacter baumannii* (OXA-23) was also investigated.

Bacterial Isolate	β-Lactmases Produced (Ambler Class)	± 2 Supplement (10 mg/L)	MIC (mg/L) for β-Lactam													
			AMP	AMP/SUL	PIP	PIP/TAZ	TIM/CLAV	AZT	FAZ	CRO	CAZ	FEP	ERT	IMI	MEM	DOR
E.coli (EC107) ST 131	CTX-M-15 (A), OXA-1 (D)	-	>16	>16/8	>64	>128/4	>64/2	>16	>16	>16	>16	>32	<0.25	<0.5	<0.5	<0.5
		+	>16	>16/8	>64	>128/4	64/2	<1	8	<0.5	1	8	<0.25	<0.5	<0.5	<0.5
E.coli (EC114) ST 131	TEM-1 (A), CTX-M-15 (A), OXA-1 (D)	-	>16	>16/8	>64	>128/4	>64/2	>16	>16	>32	>16	>32	<0.25	<0.5	<0.5	<0.5
		+	>16	>16/8	>64	>128/4	>64/2	<1	8	<0.5	1	8	<0.25	<0.5	<0.5	<0.5
E.coli (EC86)	CTX-M-15 (A), CMY-4 (C), OXA-181 (D)	-	>16	>16/8	>64	>128/4	>64/2	>16	>16	>16	>16	>32	>8	>8	4	>4
		+	>16	>16/8	>64	>128/4	>64/2	8	>16	8	8	<4	4	4	1	2
E.coli (EC113) ST 131	CTX-M-27 (A)	-	>16	8/4	>64	<8/4	16/2	>16	>16	>32	8	>32	<0.25	<0.5	<0.5	<0.5
		+	<8	<4/2	<16	<8/4	<8/2	<1	4	<0.5	<1	<4	<0.25	<0.5	<0.5	<0.5
K. pneumoniae (KP15)	TEM-1 (A), SHV-11 (A), KPC-2 (A)	-	>16	>16/8	>64	>128/4	>64/2	>16	>16	>32	>16	>32	>8	>8	>8	>4
		+	>16	16/8	>64	>128/4	>64/2	>16	>16	1	4	<4	<0.25	<0.5	1	<0.5
K. pneumoniae (KP41)	TEM-1 (A), SHV-1 (A), -5 (A), -11 (A), CTX-M-15 (A), OXA-232 (D)	-	>16	>16/8	>64	>128/4	>64/2	>16	>16	>32	>16	>32	>8	>8	>8	>4
		+	>16	>16/8	>64	>128/4	64/2	>16	>16	>32	>16	32	>8	>8	>8	>4
K. pneumoniae (KP58)	SHV-11 (A), VIM-4 (B)	-	>16	>16/8	>64	>128/4	>64/2	>16	>16	>32	>16	>32	>8	>8	>8	>4
		+	>16	>16/8	>64	>128/4	>64/2	2	>16	1	2	>32	<0.25	2	<0.5	<0.5
P. stuartii (PS71)	TEM-1 (A), SHV-5 (A), VEB-1 (A), VIM-1 (B)	-	>16	>16/8	>64	>128/4	>64/2	>16	>16	>32	>16	>32	>8	>8	>8	>8
		+	>16	>16/8	>64	>128/4	>64/2	>16	4	16	>16	8	<0.25	>8	1	2
P. aeruginosa (PA12) ST 111	VIM-2 (B)	-	>16	>16/8	>64	128/4	>64/2	>16	>16	>32	>16	>32	>8	>8	>8	>4
		+	>16	>16/8	64	128/4	>64/2	16	>16	>32	>16	>32	>8	>8	>8	>4
A. baumannii (AB14)	OXA-23 (D), OXA-51 (D)	-	>16	>16/8	>64	>128/4	>64/2	>16	>16	>32	>16	>32	>8	>8	4	>4
		+	>16	>16/8	>64	>128/4	>64/2	>16	>16	>32	>16	32	>8	>8	4	>4

Table 3.9. MIC values of selected penicillins, cephalosporins, monobactams, and carbapenems against different bacterial strains with or without cyclic boronate, 2, supplementation. MIC values in black indicate resistance and those in red, susceptibility, according to current CLSI/EUCAST breakpoints. Blue values indicate where the MIC is reduced with 10 mg/L 2, but the MIC lies either outside of the susceptible range or there is no agreed breakpoint for the drug/organism combination. AMP: ampicillin; AMP/SUL: ampicillin/sulbactam; PIP: piperacillin; PIP/TAZ: piperacillin/tazobactam; TIM/CLAV: ticarcillin/clavulanate; AZT: aztreonam; FAZ: cefazolin; CRO: ceftriaxone; CAZ: ceftazidime; FEP: cefepime; ERT: ertapenem; IMI:imipenem; MEM: meropenem;

Bacterial Isolate	β-Lactmases Produced (Ambler Class)	Synergy When Combined with (2): Fixed 2:1 µg Ratio																	
		CAR	PRL	TZP	KF	C/T	TEM	MEL	CTX	CAZ	SAM	CPT	FEP	AZT	IPM	CAZ/AVI	AUG	ERT	FOX	MEM
E.coli (EC107) ST 131	CTX-M-15 (A), OXA-1 (D)	N	Y	N	N	N	Y	N	Y	Y	N	Y	Y	Y	N	N	N	N	Y	N
E.coli (EC114) ST 131	TEM-1 (A), CTX-M-15 (A), OXA-1 (D)	N	Y	N	N	N	Y	N	Y	Y	N	Y	Y	Y	N	N	N	N	Y	N
E.coli (EC86)	CTX-M-15 (A), CMY-4 (C), OXA-181 (D)	N	N	Y	N	Y	N	N	N	N	N	N	N	Y	N	N	N	N	N	N
E.coli (EC113) ST 131	CTX-M-27 (A)	N	Y	N	Y	N	N	N	Y	Y	N	Y	Y	Y	N	N	Y	N	N	N
K. pneumoniae (KP15)	TEM-1 (A), SHV-11 (A), KPC-2 (A)	N	Y	Y	N	Y	Y	Y	Y	N	N	N	Y	Y	Y	N	N	Y	Y	Y
K. pneumoniae (KP41)	TEM-1 (A), SHV-1 (A), -5 (A), -11 (A), CTX-M-15 (A), OXA-232 (D)	N	N	N	N	Y	N	N	N	N	N	N	N	N	N	N	N	N	N	N
K. pneumoniae (KP58)	SHV-11 (A), VIM-4 (B)	N	Y	Y	N	Y	Y	Y	Y	N	N	N	Y	Y	Y	N	N	Y	N	Y
P. stuartii (PS71)	TEM-1 (A), SHV-5 (A), VEB-1 (A), VIM-1 (B)	N	Y	N	N	Y	N	N	Y	N	N	N	Y	Y	N	N	N	N	N	N
P. aeruginosa (PA12) ST 111	VIM-2 (B)	N	Y	Y	N	Y	N	N	N	N	N	N	N	Y	N	N	N	N	N	N
A. baumannii (AB14)	OXA-51 (D), OXA-23 (D)	N	N	N	N	N	N	N	N	N	N	N	Y	N	N	N	N	N	N	N

Table 3.10: Synergy in Disc Diffusion Assays between 2 and β-lactams: CAR: Carbenacillin; PRL: Piperacillin; TZP: Piperacillin/Tazobactam; KF: Cephalothin; C/T: Ceftolozane/Tazobactam; TEM: Temocillin; MEL: Mecillinam; CTX: Cefotaxime; CAZ: Ceftazidime; SAM: Ampicillin/Sulbactam; CPT: Ceftaroline; FEP: Cefepime; AZT: Aztreonam: IPM: Imipenem; CAZ/AVI: Ceftazidime/Avibactam; AUG: Amoxicillin/Clavulanate; ERT: Ertapenem; FOX: Cefoxitin; MEM: Meropenem.

Susceptibility of the examined isolates to penicillins was generally not affected by supplementation with **2**, with the exception of CTX-M-27 producing *E. coli* which was

rendered susceptible to ampicillin, piperacillin and ampicillin/sulbactam. Susceptibility to the monobactam aztreonam (AZT) was either increased or completely restored to strains producing CTX-M-1-like (CTX-M-15, CTX-M-27) enzymes and *K. pneumoniae* producing the MBL, VIM-4. Carbapenem usage was potentiated by **2** against *P. stuartii* producing VIM-1 and *K. pneumoniae* producing VIM-4.

Success was also had in increasing the susceptibility of *E. coli* producing the carbapenemase OXA-181, but not against *K. pneumoniae* producing OXA-232, presumably due to the sheer number of β-lactamases being produced by this strain (note, also, that OXA-181 and OXA-232 are OXA-48 like enzymes and purified OXA-48 was not so potently inhibited **2** in the *in vitro* studies, Table 3.6). While a *K. pneumoniae* strain producing three different class A β-lactamases was rendered susceptible to all carbapenems on supplementation with **2**. **2** also potentiated the use of all four cephalosporins, most notably ceftriaxone, ceftazidime, and cefepime, against a number of the strains examined. No effects were seen on the carbapenem susceptibility of either VIM-2 producing *P. aeruginosa* or *A. baumannii* with OXA-23 upon supplementation with **2**. Once again, at least in the latter case, this may come as a result of the reduced potency of the cyclic boronates against class D enzymes.

The effects of **2** on susceptibility to 19 diverse β-lactam compounds was also assessed in Kirby-Bauer disc diffusion tests(451). Screens in which **2** was added in a fixed ratio against the same strains revealed synergy with a number of β-lactams, illustrating its potential as an inhibitor (Table 3.10 and Appendix 1). The largest extent of enhancement by **2** was seen in the activity of piperacillin, ceftolozane/tazobactam, cefotaxime, cefepime, and aztreonam. Synergy with both ertapenem and meropenem was clearly observed for the VIM-4 producing *K. pneumoniae* strain at the 2:1 ratio.

Susceptibility screening of a further 134 *Enterobacteriaciae* species to **2** in combination with meropenem was investigated by Drs Ali Aboklaish and Jonathan Tyrell in the laboratory of Prof. Timothy Walsh, Cardiff University. These included *C. freundii*, *Enterobacter sp.*, *E. coli*, and *K. pneumoniae* strains expressing both serine and metallo-β-lactamases (Tables 3.11-3.12). Supplementation with **2** increased the susceptibility of a substantial number of the isolates tested, with susceptibility of MBL bearing isolates increasing from 10% to 59% upon addition of **2**. Between a 4- to 8-fold increase in susceptible MBL bearing strains was seen for each of the main species tested (Figure 3.31). **2** was also able to render strains producing both SBLs and MBLs susceptible to meropenem, reflecting the ability of **2** to inhibit both distinct classes of enzyme (Table 3.12).

Genotype	MEM ± 2	MIC Distribution (μg mL^{-1})											
		≤0.06	0.125	0.25	0.5	1	2	4	8	16	32	64	>64
NDM (n=66)	-	-	-	-	1	-	5	5	13	7	12	9	14
	+	1	4	4	4	7	17	4	9	1	2	3	10
NDM + VIM (n=1)	-	-	-	-	-	-	-	-	1	-	-	-	-
	+	-	-	-	1	-	-	-	-	-	-	-	-
NDM + OXA (n=36)	-	-	-	-	-	-	-	2	3	7	21	2	1
	+	-	-	1	2	10	13	-	2	2	4	1	1
NDM +CTX-M-15 (n=1)	-	-	-	-	-	-	-	1	-	-	-	-	-
	+	-	-	-	1	-	-	-	-	-	-	-	-
VIM (n=26)	-	-	-	-	1	-	3	3	3	3	7	4	1
	+	2	3	2	1	2	1	2	1	2	2	6	2
VIM + OXA (n=2)	-	-	-	-	-	1	-	-	-	-	-	1	-
	+	-	-	-	-	1	-	-	-	-	-	1	-
IMP (n=1)	-	-	-	-	-	-	1	-	-	-	-	-	-
	+	-	-	-	1	-	-	-	-	-	-	-	-
OXA (n=1)	-	-	-	-	-	1	-	-	-	-	-	-	-
	+	-	-	-	-	1	-	-	-	-	-	-	-

Table 3.11: Minimum inhibitory concentration values of meropenem against bacterial strains with or without cyclic boronate, 2, supplementation. Strains are distributed by species.

Species	MEM ± 2	MIC Distribution (μg mL^{-1})											
		≤0.06	0.125	0.25	0.5	1	2	4	8	16	32	64	>64
C. freundii (n=8)	-	-	-	-	-	-	1	-	5	1	1	-	-
	+	-	-	-	1	2	2	-	1	-	-	-	2
Enterobacter spp . (n=21)	-	-	-	-	1	1	3	4	1	3	4	3	-
	+	-	2	2	2	4	5	2	3	1	-	-	-
E. coli (n=25)	-	-	-	-	-	-	2	4	3	6	3	5	-
	+	-	2	3	1	5	5	2	2	1	-	3	1
K. pneumoniae (n=78)	-	-	-	-	1	2	3	2	10	7	31	8	14
	+	3	3	1	4	12	19	2	6	3	8	7	10
M. morganii (n=1)	-	-	-	-	-	-	-	-	-	-	-	1	-
	+	-	-	-	-	-	-	-	1	-	-	-	-
S. marcescens (n=1)	-	-	-	-	-	-	-	-	-	-	1	-	-
	+	-	-	-	1	-	-	-	-	-	-	-	-
Total (n=134)	-	-	-	-	2	3	9	11	20	17	40	16	16
	+	3	7	7	8	23	31	6	12	5	8	11	13

Table 3.12: Minimum inhibitory concentration values of meropenem against bacterial strains with or without cyclic boronate, 2, supplementation. Strains are distributed according to the β-lactamases expressed.

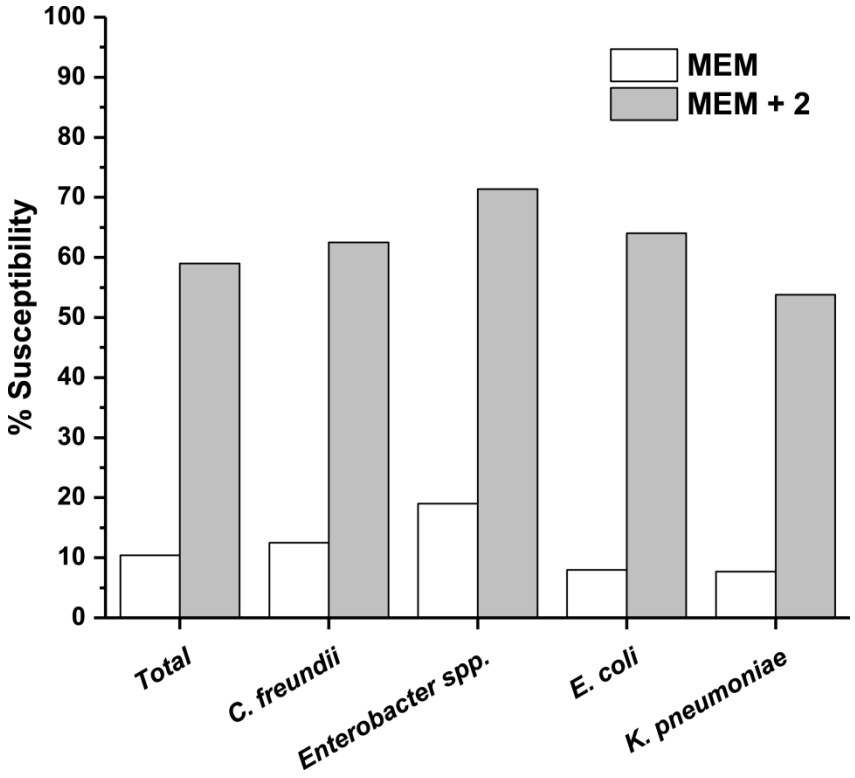

Figure 3.31: Susceptibility of metallo-β-lactamase expressing clinical isolates to meropenem (MEM) with or without cyclic boronate 2 supplementation. The susceptibilities of all screened isolates and individual species are shown.

3.10. Discussion

Collectively, these results reveal that cyclic boronates are able to inhibit all classes of β-lactamase, including clinically important B1 MBLs, class D OXA carbapenemases and extended spectrum β-lactamases such as CTX-M-15 with the potential for low micromolar to low nanomolar IC_{50}s (Tables 3.4-3.7). The inhibitors manifested nanomolar levels of inhibition against NDM-1, VIM-2, TEM-1, CTX-M-15, and AmpC, but were less potent against the OXA enzymes and B2 or B1/B2 hybrid MBLs. This suggests that, while an excellent starting point, more optimisation of the inhibitor scaffold is required to achieve maximal potency against all variants of β-lactamase.

^{13}C NMR studies on OXA-10 point to only a single closed species in the enzyme-inhibitor complex (Figure 3.21), as seen in the crystallographic studies presented here. However NMR data acquired with TEM-1 suggest that the cyclic boronates may be able to bind to SBLs in open and closed ring forms (Figure 3.19), an observation supported by previous literature(441). Unlike the TEM-1:boronic acid complex illustrated above (Figure 3.20)(441), the cyclic boronates in this study appear to adopt closed ring conformations whether complexed to SBLs, MBLs, or PBPs (a result supported by NMR studies on cyclic boronates of varying ring sizes)(443). An overlay of the cyclic boronate conformation in each

crystal structure obtained shows that the conformation of the fused bicyclic boronate ring system is remarkably conserved in all cases, while only minor changes are seen in the conformation of the C-7 acetamido side chain (Figure 3.32). The fact that the boron ring remains closed in all structures is supportive of the proposal that the molecules are inhibiting both SBLs and MBLs by mimicking the first tetrahedral anionic intermediate in β-lactam hydrolysis, EI[1] in Figure 3.8 A and 3.8 B, respectively, in which the β-lactam ring has not yet opened. Further to this, comparison of the small molecule energy minimized structure of the tetrahedral species produced by addition of a hydroxide ion onto the β-lactam carbonyl of cefalexin reveals a strong structural similarity between it and the enzyme-bound cyclic boronates (Figure 3.32).

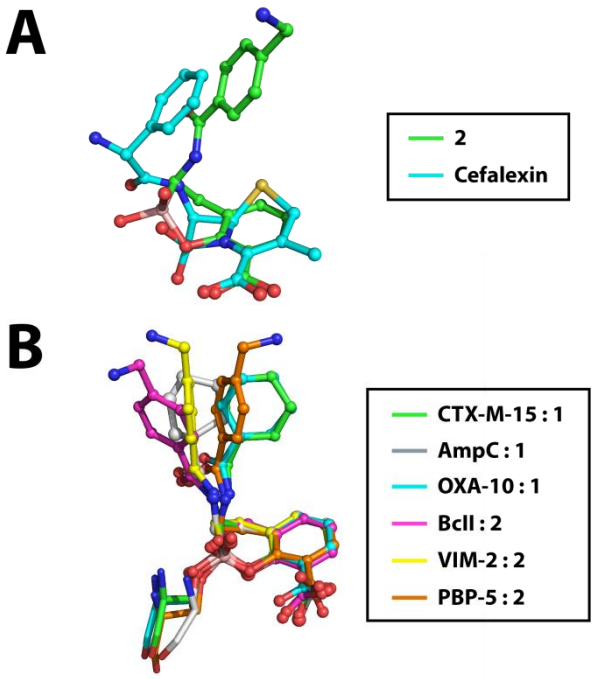

Figure 3.32: A. Overlay of 2 in complex with BcII and the energy minimized small-molecule species defined by addition of a hydroxide ion onto the β-lactam carbonyl of cephalexin. Energy minimisation was carried out using the MM2 energy minimisation function in ChemBio3D Ultra(452). B. Overlay of cyclic boronates 1 and 2 in complex with serine-β-lactamases, metallo-β-lactamases and penicillin binding protein 5. Note that, despite variation in the position of the aminoacyl side chains, the structure and conformation of the fused bicyclic ring system is highly conserved.

Cyclic boronate **2** potentiated the activity of all four classes of β-lactam against Gram-negative clinical isolates (Table 3.9). Co-administration of **2** alongside the clinically used SBL inhibitors, clavulanic acid, sulbactam, and tazobactam, was able to further potentiate the activity of penicillins against some *E. coli* strains compared to co-administration with SBL

inhibitors alone. **2** also increased the effectiveness of both cephalosporins and carbapenems against VIM-producing *K. pneumoniae* strains, although this result is not apparent with KP41, possibly due to the sheer number of β-lactamases (six) being produced in this organism (Table 3.9). Activity against VIM-2 producing *P. aeruginosa* was limited, likely on account of production of AmpC as well as upregulated efflux. An increased susceptibility to ceftolozane was a common finding regardless of the number or class of β-lactamases produced, except in *A. baumanii*. Ceftolozane is a fifth generation cephalosporin, recently developed for use in combination with tazobactam(453). The results presented here suggested that ceftolozane, partnered with a cyclic boronate, could be an attractive combination to pursue in future.

The combined results reveal that cyclic boronates can act as dual inhibitors of SBLs and MBLs, two enzyme classes with highly distinct mechanisms, by mimicking a shared tetrahedral intermediate. Further, the inhibition of PBP5 suggests that these molecules not only represent a promising line of investigation in the development of β-lactam/β-lactamase inhibitor combinations, but also in the development of new antibiotic chemotypes with activity against the penicillin-binding proteins. Structural data obtained in this study allow for the further optimisation of the cyclic boronate scaffold to increase potency, particularly against OXA and B2 enzymes, but also provide important structural and mechanistic insights into the nature of transient species in β-lactam hydrolysis that have yet to be structurally characterised.

With the first cyclic boronate drug, tavaborole(454), approved for clinical use in the topical treatment of fungal infections, the use of the linear boronic acid, Bortezomib, as an anti-cancer drug(455), and further cyclic boronates in the pipeline as anti—inflammatory and anti-bacterial treatments(456, 457), the further use of this molecular scaffold in future drug candidates seems inevitable. The ability of these molecules to mimic tetrahedral intermediates in enzyme-catalysed hydrolysis pathways may prove to be highly useful in the inhibition of mechanistically diverse enzymes, particularly in cancer treatments where it may be desirable to inhibit different classes of functionally related proteases(458). Notably, there are no reports of acyclic boronates inhibiting MBLs, suggesting that conformationally restrained analogues may be a promising line of enquiry. In addition to boronates, cyclic phosphonates, sulfonates, and sulfonamides have yet to be extensively explored and may prove to be a fruitful source of future inhibitors.

Chapter 4: Further Inhibitors Targeting Serine and Metallo-β-Lactamases

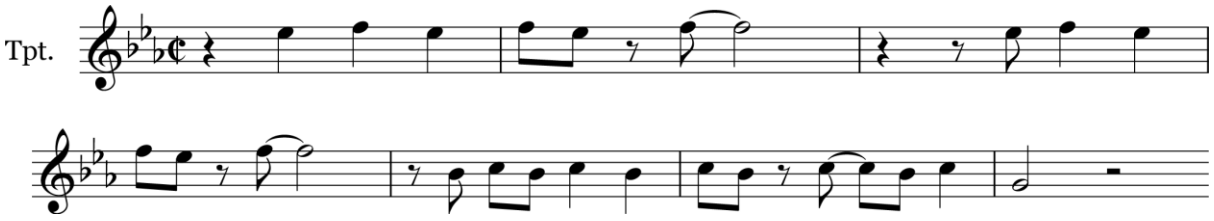

- *Thomas Wright 'Fats' Waller*

Contents

The work in this chapter was carried out in conjunction with a number of other researchers. The thiol carboxylate inhibitors were synthesised by Dr Ricky Cain, under the supervision of Prof. Colin Fishwick, University of Leeds. The crystal structure of a thiol carboxylate in complex with VIM-2 was obtained by Mr David Zollman. The inhibitory activity of thioenolates has been reported in the academic literature(318). Crystal structures of thioenolates were obtained in conjunction with Dr Jürgen Brem. Further thioenolates discussed in this study were synthesised by Dr Anna Rydzik and Mr Dong Zhang, who also carried out some assays with some thioenolates. Squaramides and indole carboxylates were identified in collaborative work with the European Lead Factory, Dundee.

4.1. Introduction

In the previous chapter cyclic boronates were discussed as a chemotype that is able to inhibit both the serine- and metallo-β-lactamases (SBLs and MBLs, respectively). Since these compounds likely exert their inhibitory activity by mimicking a tetrahedral anionic intermediate common to the reaction mechanism of both enzyme classes (EI^1 in Figure 4.1), it stands to reason that other compounds believed to mimic a chemical species along the β-lactam hydrolysis pathway may also be able to inhibit both SBLs and MBLs. Chemical species sharing the highest structural similarity in the SBL and MBL catalysed β-lactam hydrolysis mechanisms are the first anionic intermediate, previously discussed in relation to the cyclic boronates, as well as the substrate and product, which should be identical for both enzymes. Thus, chemical scaffolds mimicking these species, should show the greatest inhibitory impact against both mechanistic classes of β-lactamase.

Aside from exploring enzyme inhibition as a method for verifying potential drug molecules for combatting antibiotic resistance, if an inhibitor is classified as mimicking a chemical species along an enzymatic pathway, structural features of its binding mode may provide useful information about the enzyme mechanism. For example, to date there are no available crystal structures of β-lactams in complex with MBLs (a structure of faropenem in complex with cadmium bound New Delhi metallo-β-lactamase 1 (NDM-1), PDB accession code: 4HKY, has been reported, but analysis of the electron density maps suggests that this structure may not be completely reliable). Likewise, tetrahedral anionic species in both SBL and MBL reactions (EI^1 and EI^2 in Figure 4.1) have yet to be structurally characterised. As discussed in the previous chapter, the cyclic boronates likely represent a mimic of EI^1, but it would be informative if inhibitors representing other species could be identified in order to clarify mechanistic details such as the mode of β-lactam binding to MBLs.

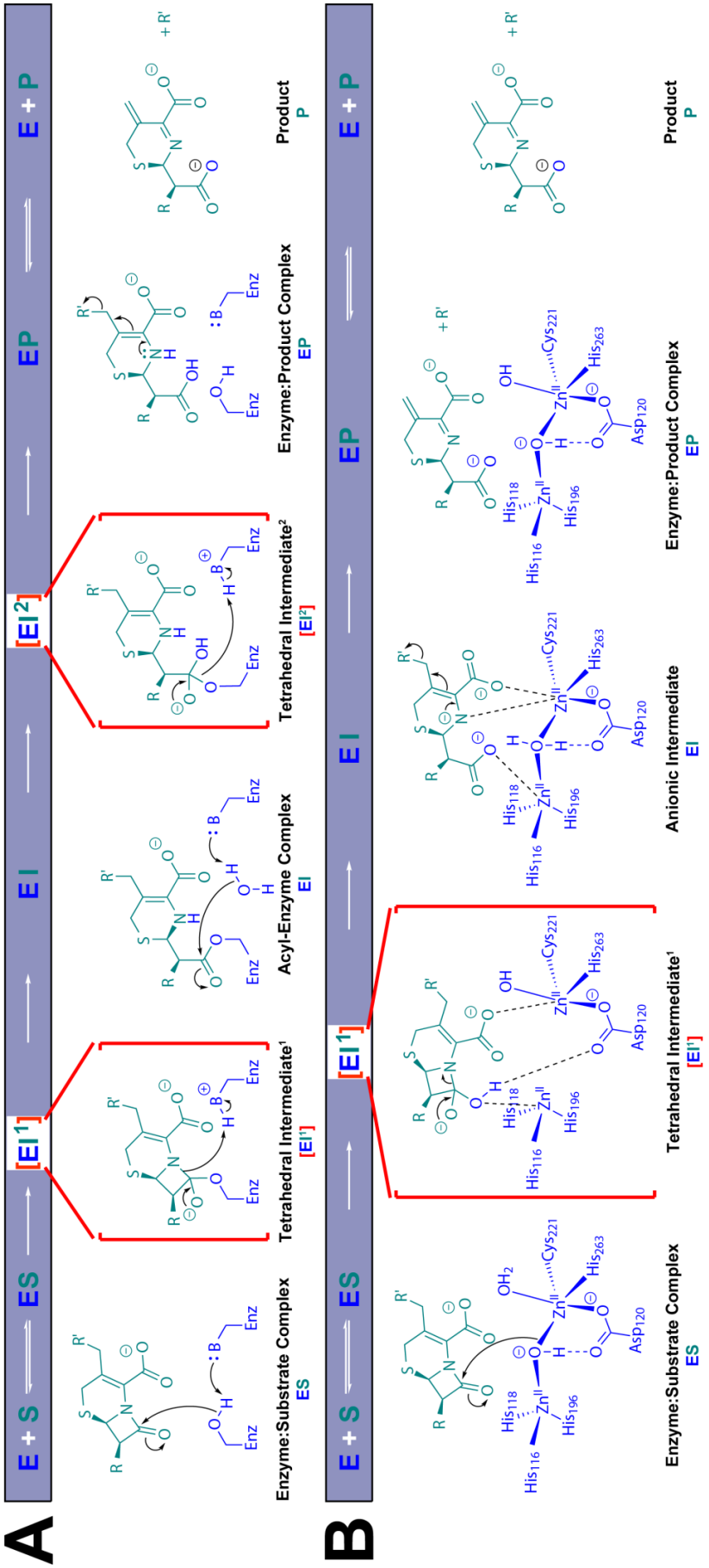

Figure 4.1: Outline mechanism for the hydrolysis of a cephalosporin by A. a serine-β-lactamase and B. a metallo-β-lactamase. Proposed tetrahedral intermediates are indicated by red brackets. Other than the substrate and product structures, the intermediate EI^1 is arguably the most similar between the two different mechanisms due to the bicyclic structure of the substrate remaining closed in both reactions.

4.2. Chapter Objectives

The work described in this chapter explores the activity of molecules with other chemotypes in the simultaneous inhibition of SBLs and MBLs. Structural and kinetic evaluation of these compounds' inhibition was investigated, and the information about β-lactamase mechanism discussed.

4.3. Squaramides

Squaramides represent promising pharmacophores in drug design since they comprise a planar aromatic scaffold with the ability to accept and donate multiple hydrogen bonds through their two set of carbonyl oxygen and amide nitrogen atoms(459-461). The biological effects of a number of molecules based on the squaramide scaffold have been reported with functions including the mimicking of phosphate groups in oligonucleotides, and of the arginine guanidinium ion in peptides(462-464), behaving as agonists for ATP-sensitive potassium channels(465, 466), and antagonists of chemokine receptors(467-469), and inhibition of cholera toxin binding to epithelial cell surface receptors(470-472). Their potential as a cancer treatment is also being explored(473-476), while their use as fluorescent probes for intracellular labelling in live cells has also been demonstrated(477). In addition, the role of this chemotype as a possible antibacterial has also been explored(478-481).

4.3.1. Inhibition of MBLs by Squaramides

The inhibition of metalloenzymes by squaric acids and squaramide derivatives is precedented by reports on the inhibition of matrix metalloproteins by such scaffolds(482, 483). Squaramides **6** and **7** (Figure 4.2) were identified as potential MBL inhibitors during a library screen conducted in conjunction with the European Lead Factory, Dundee(484).

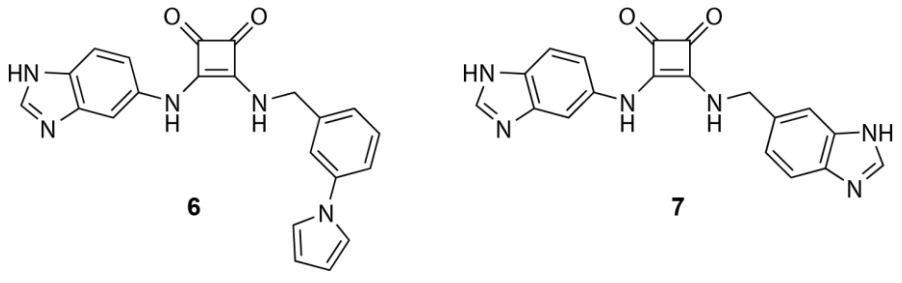

Figure 4.2: Chemical structures of the squaramides employed in this study.

The inhibitory activity of **6** and **7** was tested against three clinically important enzymes, NDM-1, Verona integron-encoded metallo-β-lactamase 2 (VIM-2) and MBL imipenemase 1 (IMP-1) (Table 4.1). Neither compound can be considered a potent MBL inhibitor, with IC_{50}

values in the moderate to high micromolar range, however **6** was general a better inhibitor compared to **7**. VIM-2 appears to be the most susceptible to inhibition by the squaramides (IC_{50} values of 10 ± 2 and 15 ± 4 μM for **6** and **7**, respectively), while little to no activity was seen against NDM-1 and IMP-1 with compound **7**.

Compound	IC_{50} vs NDM-1 (μM)	VIM-2 (μM)	IMP-1 (μM)
6	27 ± 2	10 ± 2	48 ± 2
7	>100	15 ± 4	>100

Table 4.1: IC_{50} values for the inhibition of B1 metallo-β-lactamases by squaramides 6 and 7. Inhibition assays were carried out at 25 °C and pH 7.5. Enzymes were incubated with the potential inhibitor for 10 minutes before initiation of the β-lactamase reaction by addition of FC5.

4.3.2. Inhibition of SBLs by Squaramides

The potency of the squaramides against SBLs was also investigated (Table 4.2). The residual activity of representative enzymes from each class of SBL, Temoneira β-lactamase 1 (TEM-1) and cefotaxime hydrolase from Munich (CTX-M-15) (class A), class C serine-β-lactamase (AmpC) from *Pseudomonas aeruginosa* (class C), and oxacillinase 10 (OXA-10) (class D) after incubation with **6** and **7** was determined. As with the MBLs, **6** was generally the more potent inhibitor across the SBL classes, with residual activities of 1.3 and 10% *versus* TEM-1 and OXA-10, respectively. **7** also showed potent activity against TEM-1, but not against the other lactamases.

Compound	% Residual Activity at 100 μM vs TEM-1	CTX-M-15	AmpC	OXA-10
6	1.3 ± 0.5	65 ± 3	67 ± 5	10 ± 4
7	3 ± 2	94 ± 10	99 ± 8	78 ± 7

Table 4.2: Residual activities for serine-β-lactamases after incubation with squaramides 6 and 7 at 100 μM. Residual activity measurements were carried out at 25 °C and pH 7.5. Enzymes were incubated with the potential inhibitor for 10 minutes before initiation of the β-lactamase reaction by addition of FC5.

4.3.3. Squaramides as Dual Action Inhibitors

Although not the most potent of MBL or SBL inhibitors, the squaramides represent a novel chemical scaffold for β-lactamase inhibitors and, importantly demonstrate the ability to find inhibitors of both the metallo and serine enzymes.

Attempts to achieve a crystal structure of a squaramide in complex with either a MBL or a SBL have, to date, not yielded results. However, in the case of the MBLs, inhibition likely arises from the ability of the squaric acid to form a dioxyanion which can mimic acidic

residues, such as those found in metal chelators. Although the possibility for bidentate binding of the scaffold to a single metal ion is likely limited on account of the wide angle between the two endocyclic carbonyls(485), the squaric acid dianion may be able to chelate to a bimetallic centre in a similar manner seen with the two carboxylates of a hydrolysed β-lactam(259). The mechanism of inhibition of SBLs is less clear, however it is likely that the dioxyanion interacts with the positively charged residue responsible for interacting with the C3/C4 carboxylate of a β-lactam substrate (Arg244 in TEM-1 or Arg250 in OXA-10)(444, 486).

4.4. Thiol Carboxylates

The inhibition of MBLs by thiol containing compounds is well documented(140, 280, 314), with inhibitors ranging from simple thiols to compounds exhibiting both thiol and carboxylic acid or phosphonate chemistries(300, 315, 317). A regular structural feature in the inhibition of MBLs by thiols is the substitution of the nucleophilic bridging water with the thiol sulfur in a similar μ2 bridging mode(313), while a carboxylate may bind to the zinc centres or else project towards Ly224/Arg228 to form a salt bridge interaction(254).

A series of thiol carboxylate inhibitors designed to utilise interactions with the zinc centres, Lys224/Arg228 and further hydrophobic/π-stacking interactions with Trp87, all believed to be crucial interactions in β-lactam binding and hydrolysis by MBLs, were designed and synthesised by Dr Ricky Cain, under the supervision of Prof. Colin Fishwick, University of Leeds (Compounds **8**-**11**, Figure 4.3).

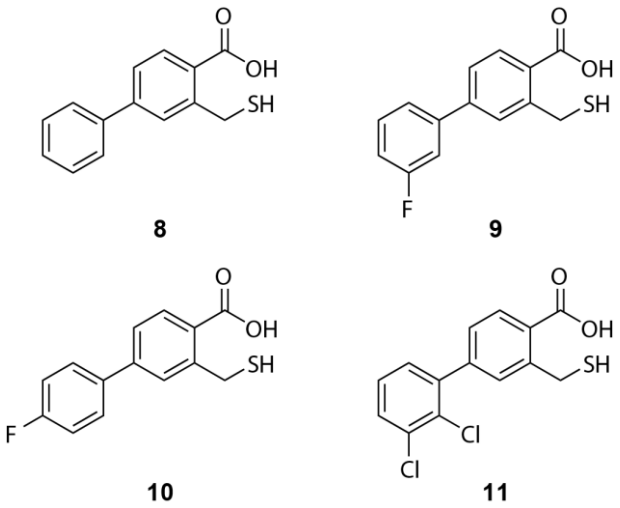

Figure 4.3: Chemical structures of the thiol carboxylates employed in this study. Note that further compounds have been synthesised, but only those inhibiting both metallo and serine-β-lactamases are shown here.

4.4.1. Inhibition of MBLs by Thiol Carboxylates

The unsubstituted lead compound, **8**, showed low to sub micromolar potency against the B1 MBLs (IC_{50} values of 5.59 ± 0.05, 0.23 ± 0.04 and 0.23 ± 0.04 μM *versus* NDM-1, VIM-2, and IMP-1, respectively), while fluorine substituted derivatives **9** and **10** showed around a 10-fold increase in potency against NDM-1 and the 2,3-dichloro compound, **1**, showed enhanced activity against VIM-2 (Table 4.3). The addition of electronegative substituents to the distal phenyl ring did not appear to make a difference to the potency of these compounds against IMP-1. Potencies against *Bacillus cereus* β-lactamase II (BcII) were lesser, however, since this enzyme does not represent a significant clinical target, this is not necessarily a concern.

Compound	IC_{50} vs			
	NDM-1 (μM)	VIM-2 (μM)	IMP-1 (μM)	BcII (μM)
8	5.59 ± 0.05	0.23 ± 0.04	0.23 ± 0.04	-
9	0.60 ± 0.03	0.21 ± 0.07	0.40 ± 0.09	-
10	0.71 ± 0.02	0.23 ± 0.03	0.31 ± 0.09	2.45 ± 0.08
11	1.16 ± 0.06	0.05 ± 0.03	0.38 ± 0.06	2.3 ± 0.1

Table 4.3: IC_{50} values for the inhibition of B1 metallo-β-lactamases by thiol carboxylates 8-11. Inhibition assays were carried out at 25 °C and pH 7.5. Enzymes were incubated with the potential inhibitor for 10 minutes before initiation of the β-lactamase reaction by addition of FC5.

A crystal structure of **8** in complex with VIM-2 was determined by Mr David Zollman (Figure 4.4). Analysis of the binding mode of **8** shows that the sulfur atom is positioned to replace the hydrolytic water and bridge the two zinc ions, as designed and precedented by work with other thiol inhibitors such as captopril and thiomandelic acid. Unexpectedly, the carboxylate moiety is not projected towards Arg228, as was predicted, but instead is positioned to interact with Asp117 via an adjacent water molecule. The distal phenyl group, positioned where the carboxylate might have been predicted to sit, forms a π stacking interaction with Tyr67 as well as an end on aromatic interaction with Arg228. The increased potency of the dichloro substituted compound, **11**, might be explained by the proximity of the distal ring to Arg228, since Arg228, likely positively charged, would interact favourably with the increased electron density supplied by the chlorine atoms.

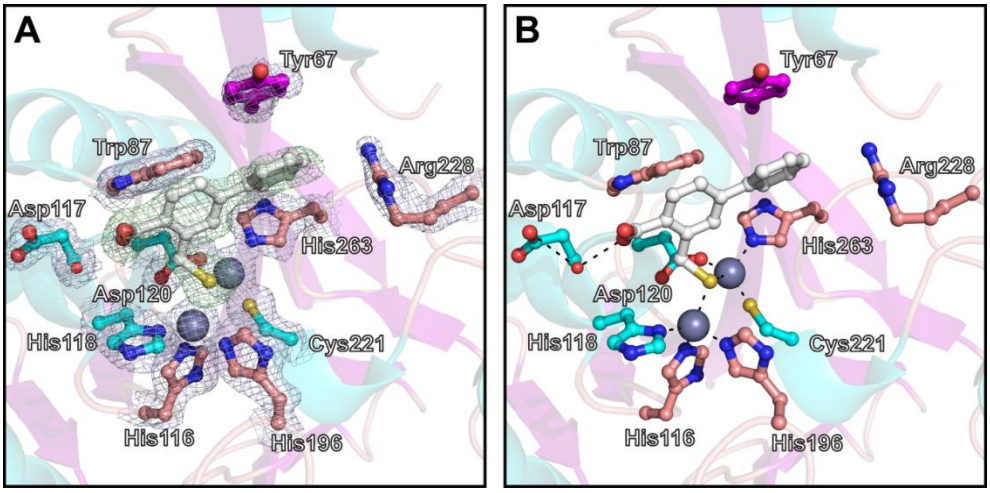

Figure 4.4: View from a crystal structure of the VIM-2:6 complex. A. Active site with representative electron density (3.0 σ *m*F_o-*D*F_c OMIT, blue mesh). Representative density for the ligand is also shown (3.0 σ *m*F_o-*D*F_c OMIT, green mesh). B. Interactions of 6 with active site residues. Dashed lines indicate metal coordination or potential hydrogen bonding interactions. Red spheres represent water molecules.

4.4.2. Inhibition of SBLs by Thiol Carboxylates

Having established the activity against of the thiol carboxylates against MBLs, their inhibitory activity towards SBLs was investigated (Table 4.4). Compounds **9**-**11** were screened against representative enzymes from each class of SBL, TEM-1 and CTX-M-15 (class A), AmpC from *Pseudomonas aeruginosa* (class C), and OXA-10 (class D).

Compound	IC_{50} vs			
	TEM-1 (μM)	CTX-M-15 (μM)	AmpC (μM)	OXA-10 (μM)
9	>100	>100	>100	>100
10	32.8 ± 0.3	>100	>100	>100
11	5.58 ± 0.04	>100	>100	37.3 ± 0.6

Table 4.4: IC_{50} values for the inhibition of serine-β-lactamases by thiol carboxylates 9-11. Inhibition assays were carried out at 25 °C and pH 7.5. Enzymes were incubated with the potential inhibitor for 10 minutes before initiation of the β-lactamase reaction by addition of FC5.

Generally, there was little inhibitory activity observed against the SBLs, and although some inhibition of CTX-M-15 and AmpC was seen, IC_{50} values against these enzymes could not be obtained with the inhibitor concentrations employed. However, **11** showed inhibitory effects against both TEM-1 and OXA-10, giving an IC_{50} value of 5.58 ± 0.04 μM, against the former.

4.4.3. Thiol Carboxylates as Dual Action Inhibitors

The thiol carboxylates represent moderately potent inhibitors of the MBLs and, to a lesser extent the SBLs. While the binding mode of **8** to an MBL has been structurally characterised, to date, there is no structural data for a thiol carboxylate in complex with an SBL. However, as with the squaramides, the inhibitor could be predicted to bind to SBLs such that its carboxylate moiety interacts with the basic residue (e.g. Arg244 in TEM-1 or Arg250 in OXA-10) in the active site.

Given the chemistry of the thiol carboxylates, these molecules are unlikely to be covalent inhibitors of the SBLs. Thus, an IC_{50} of 5.58 μM *versus* TEM-1 is not unremarkable and this may prove to be an interesting route towards the development of inhibitors of both MBLs and SBLs with a non-covalent binding mode.

4.5. Thioenolates

Rhodanines have previously been reported as inhibitors of both class A and C SBLs (TEM-1, from *E. coli*, and β-lactamase from *E. cloacae* strain P99 (P99) and AmpC, from *Enterobacter cloacae* and *Pseudomonas aerugin*osa, respectively)(487, 488) as well as against the penicillin binding proteins (PBPs) (PBP2x from *Streptococcus pneumoniae*, and PBP2 from *Neisseria gonnorhoea*)(489, 490). The rhodanine ML302 (Figure 4.5) had also been reported as a sub micromolar inhibitor of the class B1 MBLs, VIM-2 and IMP-1(487, 491).

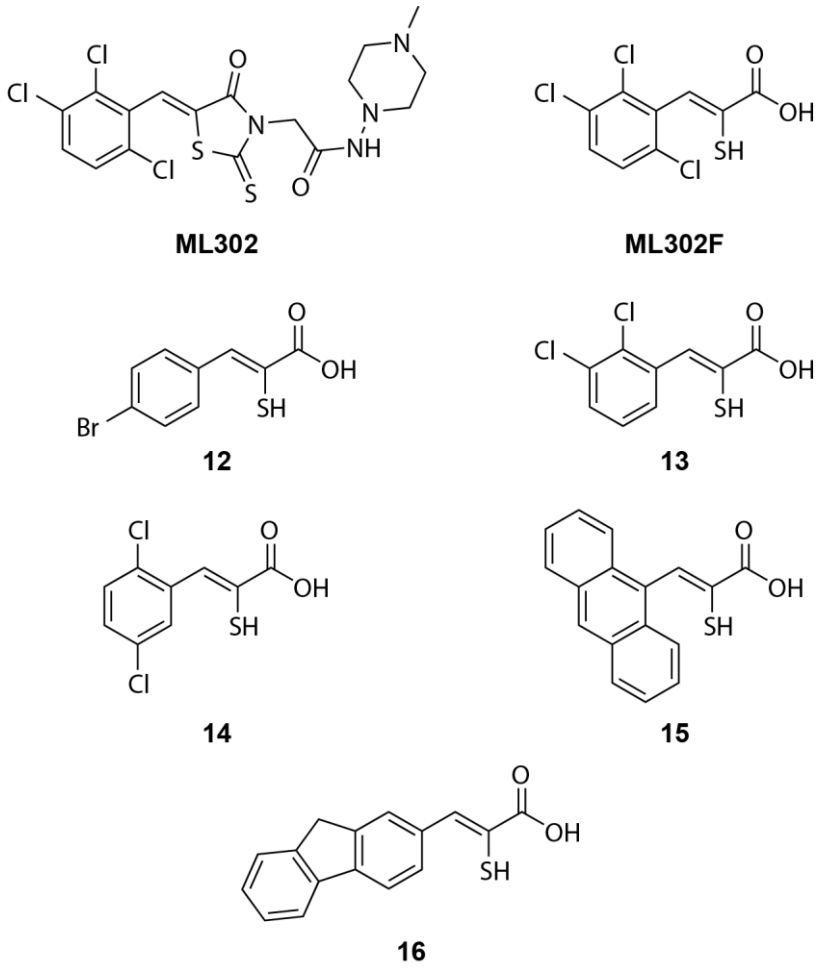

Figure 4.5: Chemical structures of the thioenolates employed in this study. The structure of the parent rhodanine, ML302, is also shown.

4.5.1. Inhibition of MBLs by Thioenolates

Crystallographic studies were undertaken to investigate the mechanism of MBL inhibition by **ML302**. Notably, a co-crystal structure of **ML302** with VIM-2 revealed two different binding modes of the inhibitor. In one chain of the asymmetric unit a thioenolate hydrolysis product of the **ML302** (**ML302F**, Figure 4.5) can be seen bound at the active site (Figure

4.6 B), while in the other chain an unexpected ternary complex was observed in which both the thioenolate and the parent rhodanine are bound (Figure 4.6 A).

In the binary complex, the thiol of **ML302F** bridges the two zinc ions, replacing the μ2 nucleophilic water, while the carboxylate is positioned to coordinate DCH zinc ion at a distance of 2.2 Å. The carboxylate can further interact with Arg228, both directly and *via* an adjacent water molecule. The aromatic ring is not situated coplanar, but rather orthogonal, to the carboxylate such that it is not conjugated, likely a steric effect of the di-*ortho*-chloro substitution. This allows the ring to form a π stacking interaction with His118 and further hydrophobic interactions with the side chain of Trp87 and the backbone atoms of Asp119 and Asn233 (Figure 4.6 B). The conformation of the **ML302F** molecule is unchanged in the observed ternary complex, while the rotation of the **ML302F** aromatic ring allows to engage in π stacking with the **ML302** molecule above it. The carbonyl oxygen of the **ML302** five membered ring is positioned to engage in a hydrogen bonding interaction with Asn233 (which is oriented differently when compared to the binary VIM-2:**ML302F** complex), while the rest of the **ML302** molecule is positioned to engage in further hydrophobic interactions with Phe61, Tyr67, and Trp87 (Figure 4.6 A).

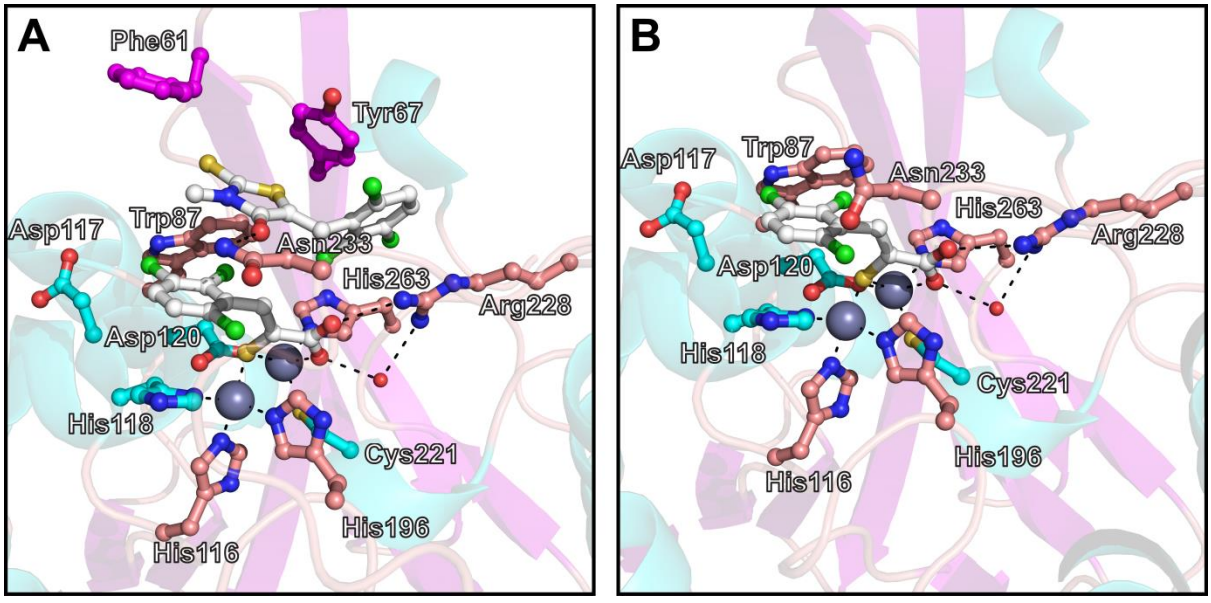

Figure 4.6: A. Crystal structure of the ternary complex formed by ML302 and ML302F binding to VIM-2 B. Crystal structure of ML302F in complex with VIM-2. Dashed lines indicate metal coordination or potential hydrogen bonding interactions.

Comparison of the binding mode of **ML302F** to VIM-2 with that observed in a crystal structure of hydrolysed benzylpenicillin bound to NDM-1 (PDB accession code: 4EYF)(259) shows some important similarities (Figure 4.7). Firstly, the thiol of **ML302F** bridges the two zinc ions, while the carboxylate coordinates the second zinc ion in the DCH site, analogously

the β-amine formed from the hydrolysis of the β-lactam ring in benzyl penicillin sits between the two zinc centres while the adjacent carboxylate coordinates the second zinc ion. Secondly, the carboxylate of **ML302F** interacts further with Arg228, just as the benzylpenicillin C-3 carboxylate interacts with the analogous Lys224 in NDM-1. Thirdly, **ML302F** makes a further interaction with Asn233 in a not identical, but similar, manner to the hydrogen bonding seen between Asn233 and the newly formed carboxylate of benzyl penicillin in the NDM-1 complex. Thus, it is likely that **ML302F** acts as a mimic of β-lactam hydrolysis products to inhibit MBLs.

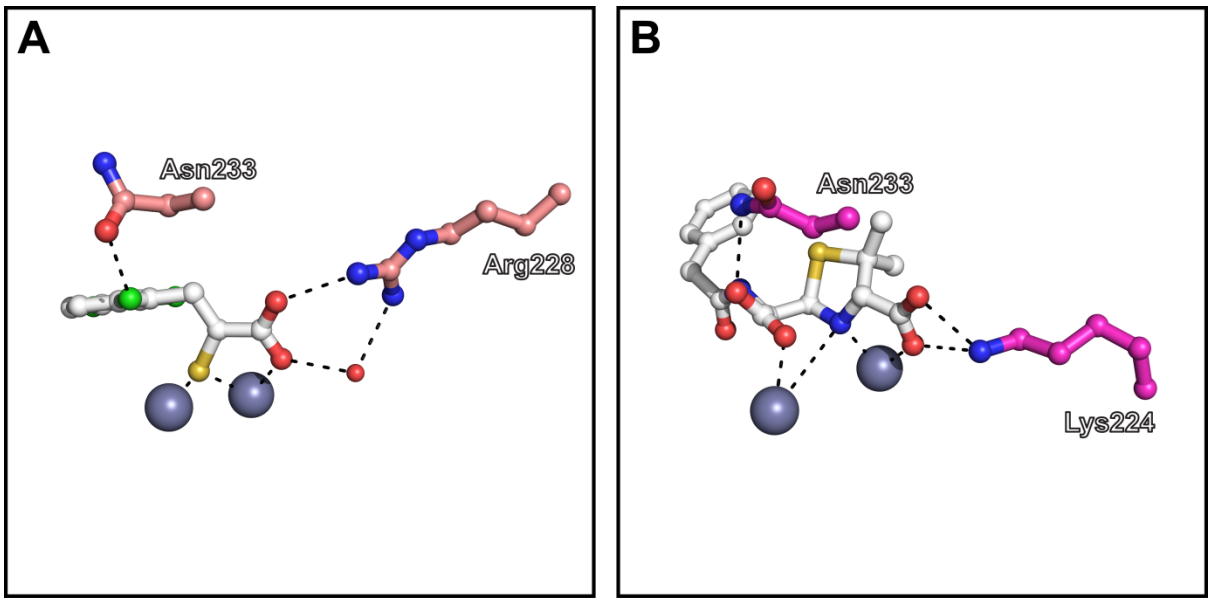

Figure 4.7: Comparison of the binding modes of A. ML302F to VIM-2 and B. hydrolysed benzylpenicillin to NDM-1. The orientation of the carboxylate to interact with a nearby basic residue, interaction with Asn233 and bridging of the two metal ions are all conserved.

Inspired by the crystallographically observed ternary complex, the inhibitory effects of **ML302**, **ML302F**, and their 1:1 mixture (**ML302M**) were tested against a variety of B1 MBLs, including against example enzymes from the three most clinically relevant families, NDM-1, VIM-2 and IMP-1 (Table 4.5). In each case the parent rhodanine, **ML302**, was a poorer inhibitor of the MBLs than the hydrolysis product, **ML302F**. IC_{50} values for **ML302F** were low to sub micromolar in all cases, with an especially high potency against IMP-1 (2.9 ± 5 nM). The inhibitor mixture, **ML302M**, was only observed to show increased potency against VIM-2, with a notable 20 fold lower IC_{50} compared to **ML302F** alone. Thus, the ternary complex formation observed with VIM-2 does not seem to be general for B1 MBLs.

Compound	IC_{50} vs			
	NDM-1 (μM)	VIM-2 (μM)	IMP-1 (μM)	BcII (μM)
ML302	9 ± 1	0.5 ± 0.2	0.17 ± 0.06	0.5 ± 0.2
ML302F	1.1 ± 0.3	0.30 ± 0.09	0.0029 ± 0.0005	0.02 ± 0.07
ML302M	0.5 ± 0.2	0.016 ± 0.004	0.06 ± 0.02	0.6 ± 0.2

Table 4.5: IC_{50} values for the inhibition of B1 metallo-β-lactamases by the rhodanine, ML302, its hydrolysis product, ML302F, and their 1:1 mixture, ML302M. Inhibition assays were carried out at 25 °C and pH 7.5. Enzymes were incubated with the potential inhibitor for 10 minutes before initiation of the β-lactamase reaction by addition of FC5.

4.5.2. Inhibition of SBLs by Thioenolates

Further thioenolates have been synthesised by Dr Anna Rydzik and Mr Dong Zhang to investigate the role of aromatic ring substitutions on inhibitory potency against the MBLs (Figure 4.5, Compounds **12-16**). Since the thioenolates likely exert their inhibitory effects by mimicking hydrolysed β-lactam products, structures common to the mechanism of both the MBLs and SBLs, it was investigated as to whether the thioenolates might inhibit SBLs.

Residual activities for thioenolates, and the parent rhodanine **ML302**, against the two class A SBLs, TEM-1 and CTX-M-15, the class C SBL, AmpC, and the class D enzyme, OXA-10, can be seen in Table 4.6. At 100 μM, compounds **12-16** showed some activity against the SBLs, with **15** and **16** showing notable potency against TEM-1 and moderate activity *versus* AmpC. Curiously, the lead thioenolate, **ML302F**, showed little to no activity against the tested enzymes, while the 2,3-dichloro compound, **13**, showed greater potency. The poorest activity is seen against the ESBL CTX-M-15, where none of the tested inhibitors could achieve a residual activity below 61%. This is interesting, given that it is a class A SBL like TEM-1, which is potently inhibited in some cases, and serves to highlight the diversity of the SBLs, even within a single class.

Compound	% Residual Activity at 100 μM vs			
	TEM-1	CTX-M-15	AmpC	OXA-10
ML302	63 ± 5	61 ± 4	54 ± 2	71 ± 2
ML302F	84 ± 6	103 ± 5	107 ± 5	105 ± 4
12	55 ± 5	92 ± 3	80 ± 4	87.0 ± 0.2
13	52 ± 2	86 ± 4	55 ± 2	60 ± 3
14	40 ± 9	95 ± 4	59 ± 2	92 ± 3
15	1.1 ± 0.7	65 ± 4	41 ± 3	47 ± 4
16	8.4 ± 0.8	83 ± 4	35 ± 6	43 ± 3

Table 4.6: Residual activities for serine-β-lactamases after incubation with thioenolates at 100 μM. Residual activity measurements were carried out at 25 °C and pH 7.5. Enzymes were incubated with the potential inhibitor for 10 minutes before initiation of the β-lactamase reaction by addition of FC5.

4.5.3. Thioenolates as Dual Action Inhibitors

Thus, while more potent against the MBLs, the thioenolates demonstrate inhibitory activity against both the MBLs and SBLs. This activity likely arises from their mimicking of a β-lactam hydrolysis product, as determined by crystallographic studies with the MBLs, which is common to the mechanisms of both enzymes (Figure 4.1). The increased potency of the thioenolates compared to the thiol carboxylates, presented previously, can likely be attributed to the bidentate zinc binding of the former through both its thiol and carboxylic acid moieties. At present, inhibitory activity against the SBLs is low. But with further modification of the scaffold, it may be possible to achieve appreciable activity against both mechanistic types of β-lactamase.

4.6. Indole Carboxylates

Indole carboxylates were identified as potent inhibitors after a high throughput screen carried out in conjunction with the European Lead Factory(484). Follow up structure activity relationship (SAR) studies were carried out by European Lead Factory, and European Gram-Negative Antibacterial Engine (ENABLE) chemists in the Schofield group, and led to the development of a library of compounds exhibiting this scaffold, example structures are provided in Figure 4.8.

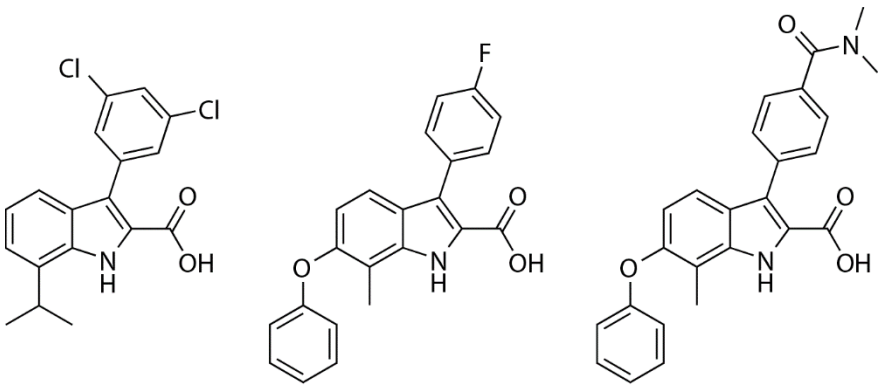

Figure 4.8: Chemical structures of the indole carboxylates employed in this study.

4.6.1. Inhibition of MBLs by Indole Carboxylates

The indole carboxylates have been identified as highly potent inhibitors of the B1 MBLs. Inhibition screening against NDM-1, VIM-2, and IMP-1 gave rise to IC_{50} values as low as 3 nM with compound 17 (Table 4.7). The potency of the indole carboxylates against all three of these enzyme families suggests that these compounds might have excellent utility in the potentiation of β-lactams against infections with resistance mediated by MBLs.

Compound	IC_{50} vs		
	NDM-1 (nM)	VIM-2 (nM)	IMP-1 (nM)
17	7.9 ± 0.4	3.2 ± 0.1	10.0 ± 0.5
18	290 ± 30	158 ± 8	500 ± 25
19	120 ± 20	7.9 ± 0.5	310 ± 10

Table 4.7: IC_{50} values for the inhibition of B1 metallo-β-lactamases by the indole carboxylates, 17-19. Inhibition assays were carried out at 25 °C and pH 7.5. Enzymes were incubated with the potential inhibitor for 10 minutes before initiation of the β-lactamase reaction by addition of FC5.

A structure of **17** in complex with VIM-2 has been solved to 1.45 Å and reveals a novel binding mode unlike any published MBL inhibitor complex structures to date (Figure 4.9). Interestingly, binding of **17** in the VIM-2 active site results in the loss of the apical water from the zinc ion in the DCH site, but does not cause displacement of the μ2 bridging water. Instead, the carboxylate moiety binds to the second zinc ion and interacts with Arg228, as seen in other inhibitor complexes (e.g. with the thioenolates above), while the nitrogen of the indole is positioned to hydrogen bond to the bridging water molecule. The dichlorophenyl substituent forms π interactions with Arg228 and Tyr67, the latter via a T-shaped interaction and the main core and isopropyl sidechain form additional hydrophobic interactions with Phe61, Trp87 and the backbones of His118 and Asp120.

The retention of the bridging water in the inhibitor complex supports the conclusion that the **17** is mimicking the binding of a substrate unhydrolysed β-lactam to the active site, with the carboxylate mimicking the C-3/C-4 carboxylate of the β-lactam and the indole nitrogen representing that of the closed lactam. Alternatively, since the indole nitrogen is likely to be protonated, this complex may represent the protonation of the ring opened anionic intermediate (EI in Figure 4.1).

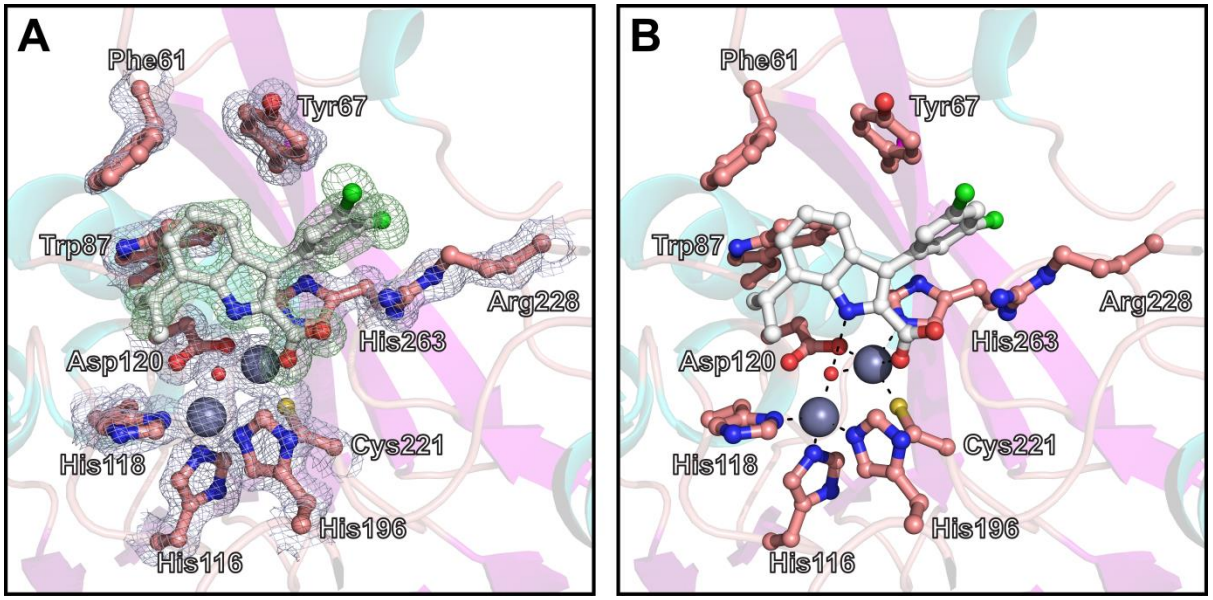

Figure 4.9: View from a crystal structure of the VIM-2:17 complex. A. Active site with representative electron density (3.0 σ *m*F_o-*D*F_c OMIT, blue mesh). Representative density for the ligand is also shown (3.0 σ *m*F_o-*D*F_c OMIT, green mesh). B. Interactions of 17 with active site residues. Dashed lines indicate metal coordination or potential hydrogen bonding interactions. Red spheres represent water molecules.

4.6.2. Inhibition of SBLs by Indole Carboxylates

The indole carboxylates were subsequently screened against example enzymes from all classes of SBL. Notably, at 200 μM compounds **17** and **18** gave residual activities of 13 ±1 and 3 ± 1%, respectively, *versus* TEM-1. **18** also showed mild inhibition of OXA-10, with a residual activity of 45 ± 5% at 200 μM. In all likelihood, the potencies of the indole carboxylates against the SBLs are not sufficient to be able to characterise the binding mode crystallographically, although it may be possible, in future studies, with TEM-1 and **18**.

Compound	% Residual Activity at 200 μM vs			
	TEM-1	CTX-M-15	AmpC	OXA-10
17	13 ± 1	100	100	100
18	3 ± 1	92 ± 7	69 ± 5	45 ± 5
19	44 ± 5	83 ± 4	92 ± 8	69 ± 2

Table 4.8: Residual activities for serine-β-lactamases after incubation with indole carboxylates at 200 μM. Residual activity measurements were carried out at 25 °C and pH 7.5. Enzymes were incubated with the potential inhibitor for 10 minutes before initiation of the β-lactamase reaction by addition of FC5.

4.6.3. Indole Carboxylates as Dual Action Inhibitors

The indole carboxylates are another class of molecule able to inhibit both the MBLs and SBLs, albeit weakly in the latter case. While activity against the SBLs is modest at present, this class of inhibitors may well reflect the most potent known against the MBLs. As with other inhibitors described above, these molecules are likely non-covalent inhibitors of the SBLs and might be an interesting scaffold to pursue in the development of such SBL inhibitors. The crystallographically determined binding mode to MBLs is remarkable in the retention of the bridging water, and as discussed above, may be a mimic of β-lactam substrate binding, or alternatively the process of protonation of the ring opened anionic intermediate seen in MBL catalysed β-lactam hydrolysis.

Given the opening premise of this chapter, in that chemically similar species along the β-lactam hydrolysis pathway should show inhibition of both MBLs and SBLs, the inhibition of the SBLs would suggest that the former proposal of indole carboxylates as substrate mimics would be correct, since no anionic intermediate species like EI in Figure 4.1 has been characterised with the SBLs. Further, the intermetallic distance of 3.5 Å in the indole carboxylate complex is identical to that seen in the VIM-2 apo enzyme(254), whereas this distance is generally seen to increase in anion intermediate or product complexes(259, 492), again suggesting mimicking of a substrate complex. With this being the case, the structure of **17** in complex with VIM-2 likely represents the closest thing to an MBL enzyme substrate complex to yet be determined, and further SAR studies aimed at creating indole carboxylates with more chemical features of β-lactams may prove highly fruitful in determining the exact residues and interactions responsible for the binding of β-lactams to the MBLs.

4.7. Discussion – Building a Picture of the MBL Reaction Pathway

The work in this chapter defines four chemical scaffolds, aside from the cyclic boronates described previously, that show inhibitory activity against both the MBLs and the SBLs. With a worldwide rise in antibiotic resistance(493) and, in particular, resistance to β-lactams mediated by both SBLs and MBLs likely to become more common in the future the development of dual action inhibitors is likely to be useful in the treatment of bacterial infections.

While these scaffolds are generally better inhibitors of the MBLs than the SBLs, the premise that one chemotype can inhibit two mechanistically distinct classes of enzyme though mimicking shared species in catalysis stands. Thus, in these cases, and likely others previously reported, inhibitors designed to mimic species in the mechanism of MBL mediated β-lactam hydrolysis can likely be developed to become SBL inhibitors as well through additional chemistry. Although knowledge of the SBL mechanism is a good starting

point for this development, structures of inhibitors in complex with MBLs, as well as computational docking studies with the SBLs, may prove to be useful tools in defining the chemistry required.

As discussed above, development of β-lactamase inhibitors is not only medicinally useful, but can find utility in the understanding of the mechanism of these enzymes. MBLs are very efficient enzymes with optimal turnover rates of 100s of molecules per second(283, 287, 326). This makes the structural characterisation of transient intermediates a near impossible task. Inhibitor complexes can inform about the binding modes and interactions of these transient species and help to build up a structural picture of β-lactam hydrolysis even in the absence of true substrate/intermediate complex structures. Figure 4.10 uses example structures from this chapter and the previous to demonstrate this principle and inform on the MBL mechanistic pathway. The continued development of new MBL inhibitors with diverse chemotypes, as supported by library screens and high throughput crystallography will only help with the fine details of β-lactamase mechanism and, thus, the development of the most potent clinically useful inhibitors in future.

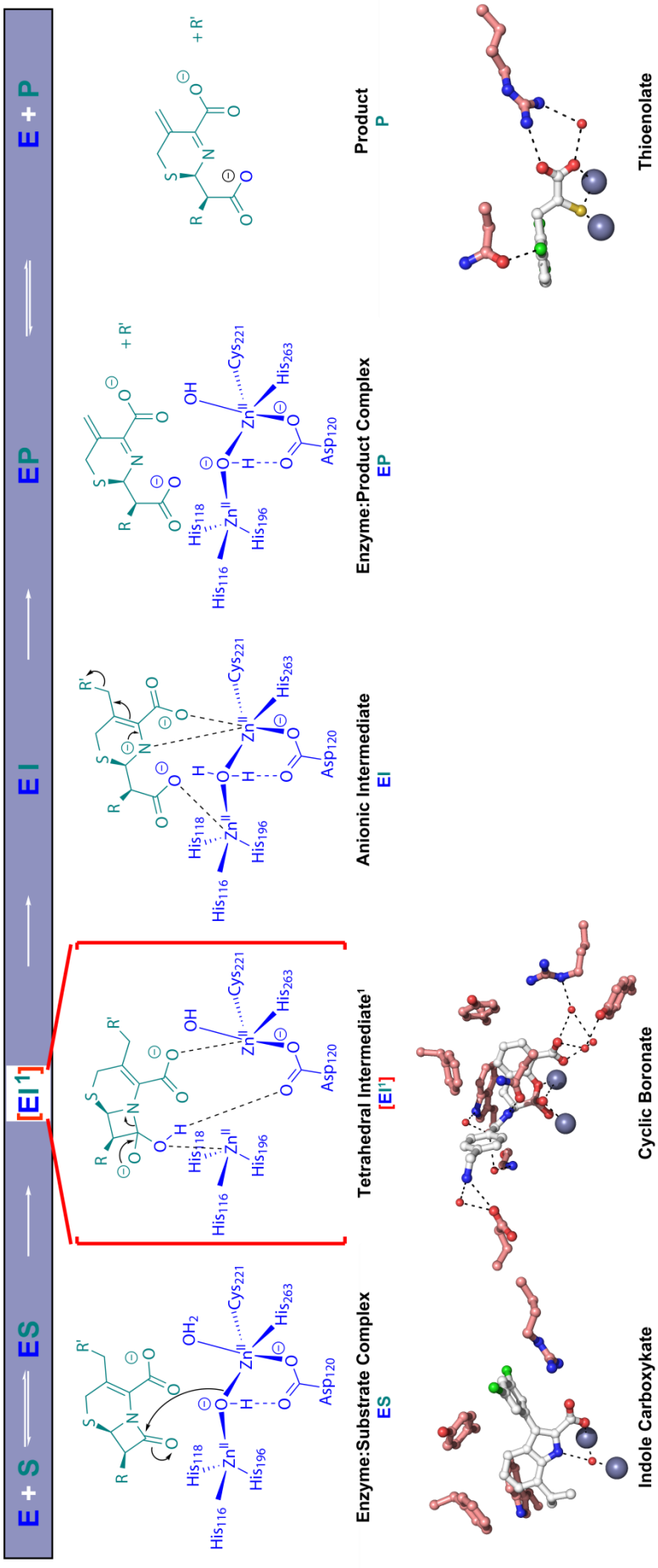

Figure 4.10: Outline mechanism for the hydrolysis of a cephalosporin by a metallo-β-lactamase. Crystallographically derived structures of inhibitors in complex with VIM-2 that may represent species along the reaction pathway are also shown.

Chapter 5: Towards a Fluorescence Assay for ETHE1

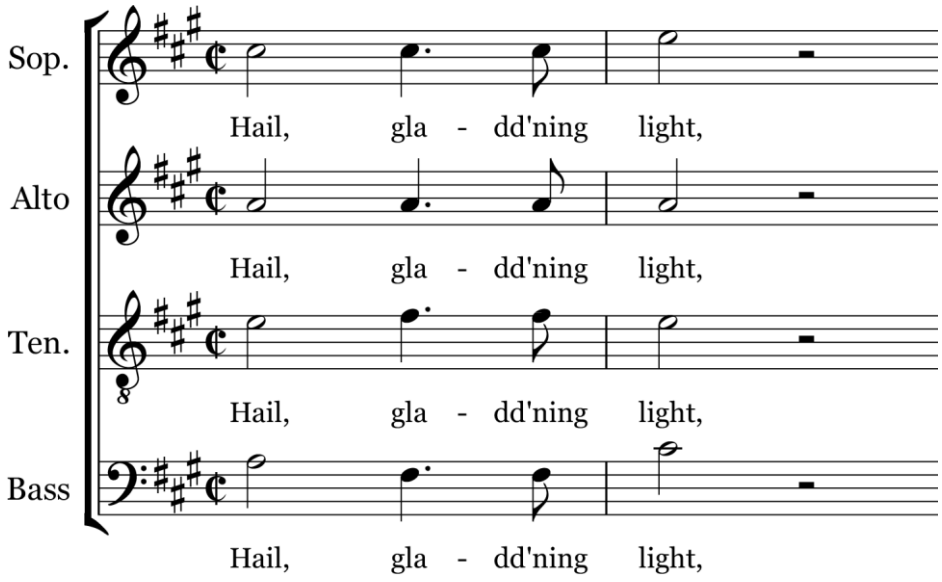

- *Charles Wood*

Contents

The work in this chapter was carried out in conjunction with Drs Ilaria Pettinati, who assisted with aspects of cloning and oxygen consumption assays, and Jürgen Brem, who advised on assay development. This work aims to build on the previous work of Dr Pettinati as reported in academic literature(220).

5.1. Introduction

As discussed in the General Introduction (Chapter 1), enzymes in the metallo-β-lactamase (MBL) superfamily, exhibiting the conserved MBL fold, are able to catalyse a number of different reactions including small molecule and DNA/RNA hydrolyses and oxidoreductase reactions (Figure 5.1)(216).

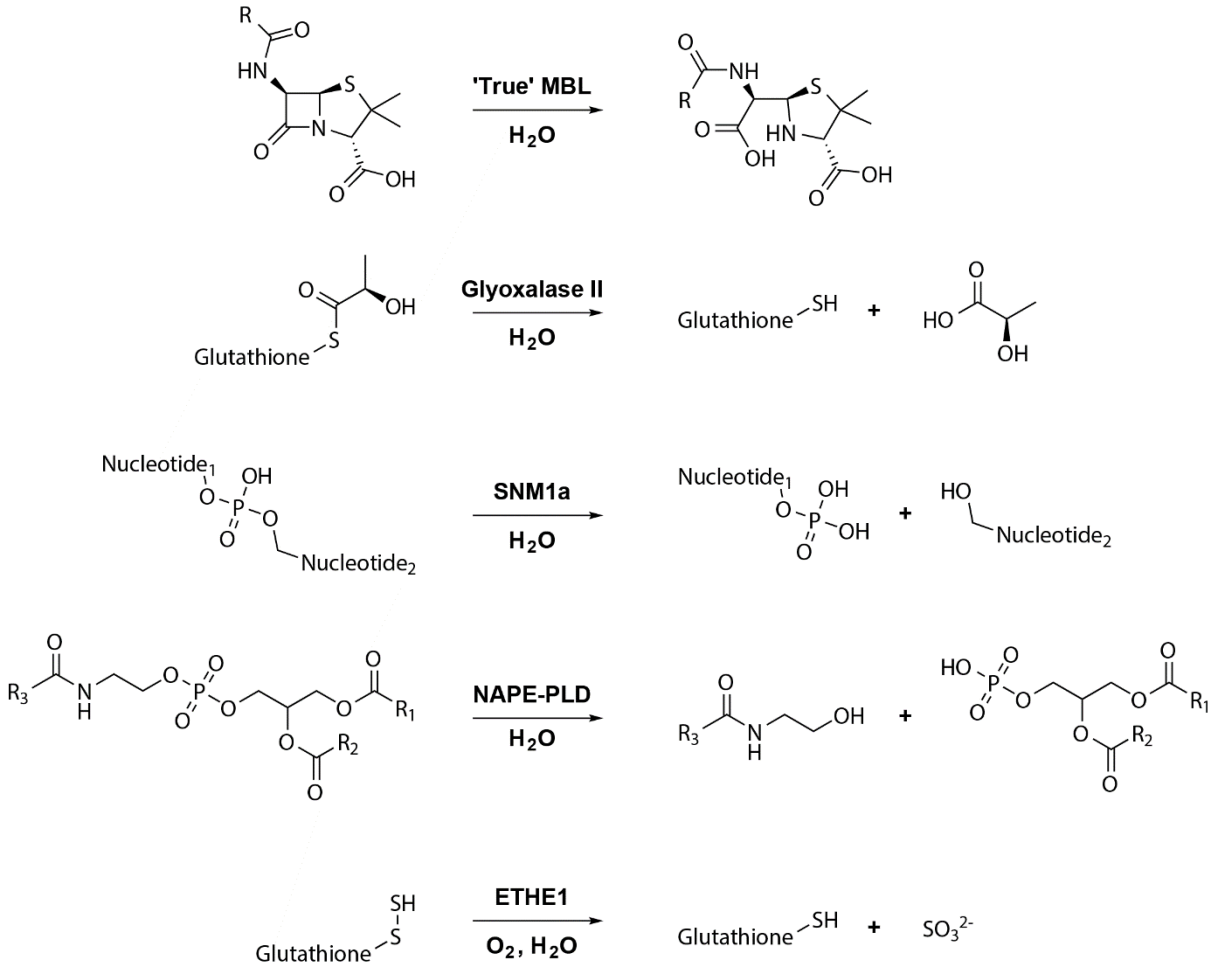

Figure 5.1: Known reactions catalysed by metallo-β-lactamase fold enzymes, with a focus on human enzymes. The reaction of a 'true' metallo-β-lactamase is provided for comparison. Note that the majority of the human enzymes are hydrolases, while ETHE1 is a sulfur dioxygenase.

A number of MBL fold enzymes are found in humans (at least 18)(217) and include, but are not limited to, Glyoxalase II(222), DNA cross-link repair enzyme 1A-C (DCLRE1A-C)(226),

N-acylphosphatidylethanolamine-hydrolysing phospholipase (NAPE-PLD)(494), ethylmalonic encephalopathy protein 1 (ETHE1)(220), and paroxysmal nonkinesiogenic dyskinesia protein (PNKD)(495). Those human MBL fold enzymes interacting with DNA (DCLRE1A-C, CPSF73, etc) exhibit a β-CASP domain in addition to their catalytic MBL domain(217, 225-227). With the human MBLs (hMBLs) being largely composed of hydrolases, the metal requirements of the human MBL (hMBL) are as expected, i.e. one or two Zn(II) ions are typically required as a cofactor. While distinct in the reactions that they catalyse, the hMBLs share five active site motifs, His84, His116XHis118XAsp120His121, His196, Asp221, and His263, using BBL numbering(496), with the first three being the most conserved(216, 497). Note that the His84 motif is not present in the 'true' β-lactamases, those hydrolysing β-lactam antibiotics, and that Asp221 replaces the prokaryotic Cys221 motif (Figure 5.2). Overall, the three dimensional structure of the hMBLs is well conserved across the family of enzymes, as exemplified by available crystal structures for many, but not all, of the hMBLs (Figure 5.2).

Since the hMBLs exhibit both a conserved three dimensional structure and an active site architecture that is comparable to the true MBLs, it is not unreasonable to suggest that inhibitors of the bacterial MBLs might also show potential as inhibitors of the hMBLs. This is, obviously, an undesirable characteristic, at least in the treatment of resistant bacterial infections, since the aim of such treatments is the selective inhibition of bacterial MBLs without disruption of the general metabolism of the human host. Thus, counter screens, testing inhibitors of the 'true' MBLs against hMBLs, may well expedite the development of inhibitors with clinical utility. With glyoxalase II perhaps being an exception(221, 222, 331), there are few activity assays for hMBLs that can be employed in a high throughput manner. Work in our group has resulted in the development of a high throughput assay for identifying inhibitors of the 'true' MBLs(433), and, if hMBL counter screens are to have high utility, it would be advantageous to employ hMBL screening methods with a similar rate of throughput.

5.1.1. Hydrogen Sulfide Metabolism and ETHE1

Hydrogen sulfide (H_2S) is a colourless, toxic, and flammable water analogue with the odour of rotten eggs(498). Until recently, the presence of H_2S in cells was dismissed as a metabolic waste product or a transient intermediate in the production of the sulfur containing amino acids, cysteine or methionine (at least in plants). The identification of H_2S production by animal tissues, as a result of cystathionine-β-synthase (CBS)(499), cystathionine-γ-lyase (CSE)(500) and 3-mercaptopyruvate sulfurtransferase (3-MST)(501) catalysis (Figure 5.3), has stimulated interest in its potential signalling roles. Alongside nitrogen monoxide and carbon monoxide(502, 503), H_2S is now considered a small molecule 'gasotransmitter',

which is implicated in multiple functions including regulation of vascular function, cellular energetics, and apoptosis(498, 504-506). Further, the possibility for therapeutic uses of H_2S is currently being explored(507).

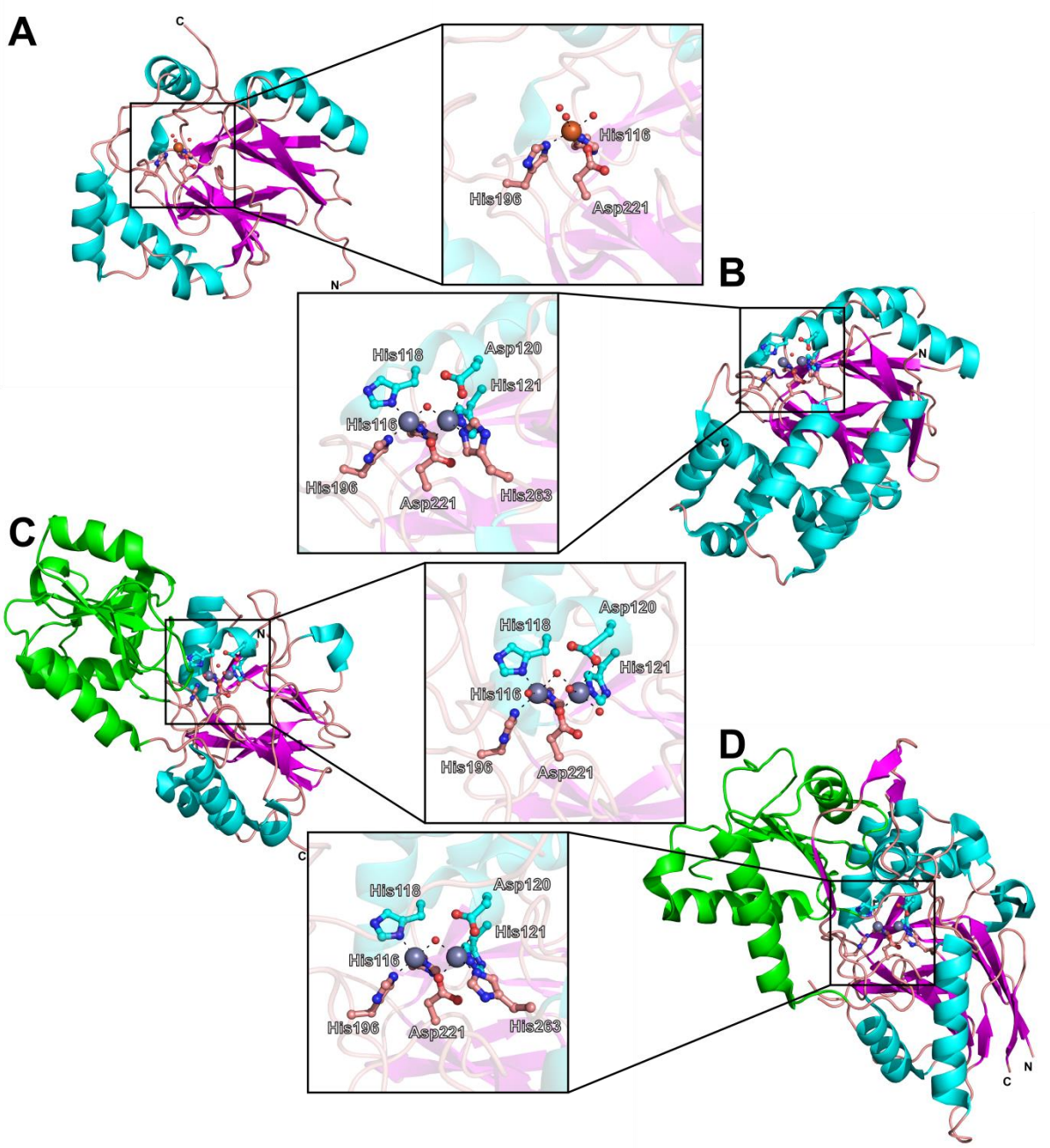

Figure 5.2: Crystal structures of human metallo-β-lactamase fold enzymes as exemplified by A. ETHE1, B. Glyoxalase II, C. SNM1B, and D. CPSF73 (PDB accession codes 4CHL, 2P18, 5AHO, and 2I7T, respectively)(220, 225, 227, 508). Active site views of each enzyme are also provided. Note that SNM1B and CPSF73 both exhibit a second β-CASP DNA binding domain (left side of each structure, green). BBL numbering of residues is used throughout(496).

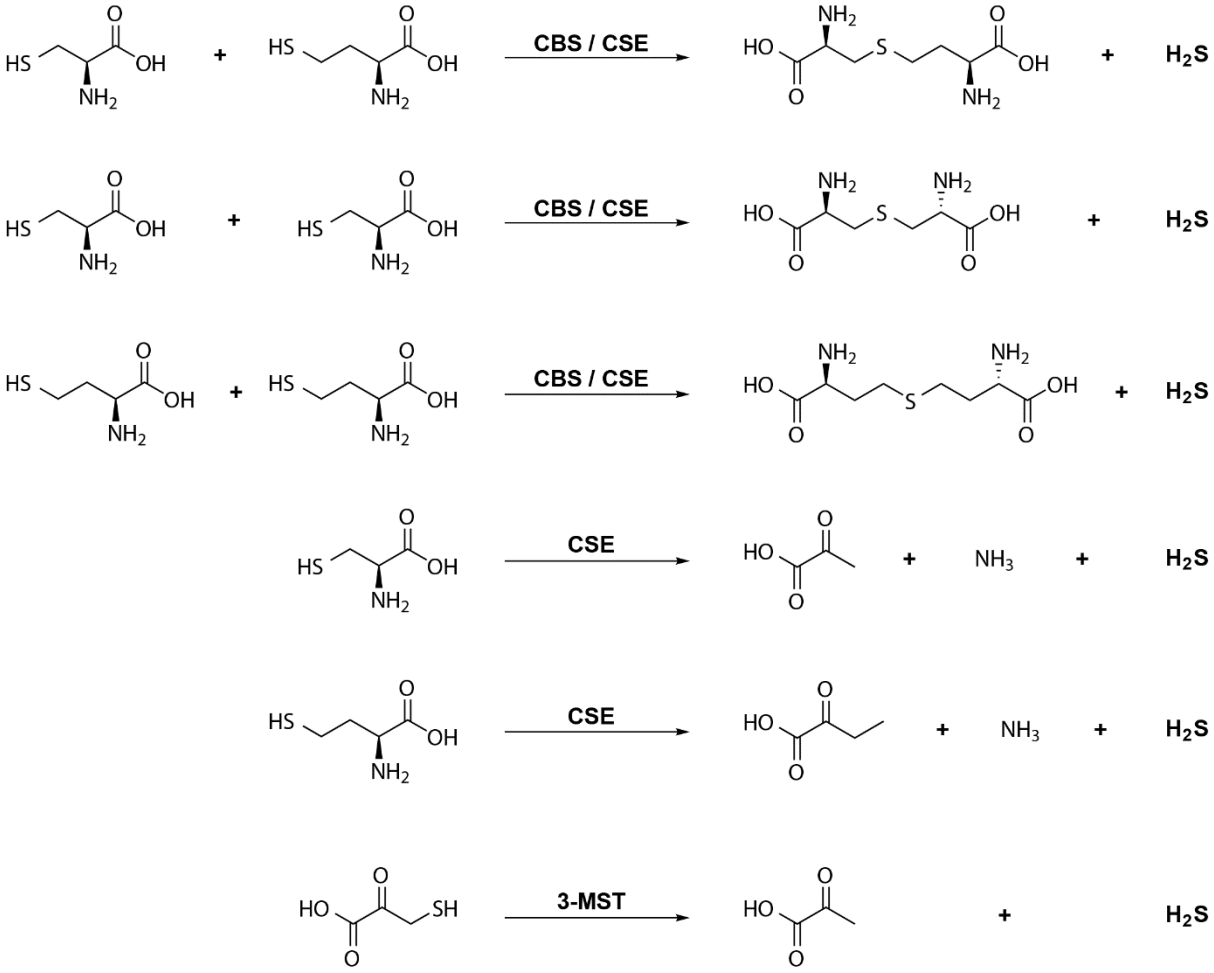

Figure 5.3: Metabolic sources of hydrogen sulfide. *In vivo* reactions producing hydrogen sulfide as catalysed by cystathionine-β-synthase (CBS), cystathionine-γ-lyase (CSE), and 3-mecaptopyruvate sulfur transferase (3-MST).

Much like nitric oxide and carbon monoxide, it is essential that H_2S concentrations are maintained below toxic thresholds(509). Reported measurements of *in vivo* H_2S concentrations range from the high micromolar in rate brain tissue to the low nanomolar in human red blood cells(510, 511), but it is now thought that the lower end of this scale is more representative(512). Once concentrations rise to around 10 to 30-fold higher levels, H_2S exerts a toxic effect by binding to the haem centre of cytochrome oxidase in mitochondrial Complex IV and inhibiting electron transport(513, 514), although it may also be used as a substrate at low concentrations, with electrons from H_2S being passed to oxygen via cyctochrome c oxidase(515-517). Despite the known inhibition of cytochrome oxidase, the exact method of H_2S cytotoxicity is still a matter of discussion, with suggestions ranging from the aforementioned electron transport chain inhibition, to direct induction of DNA damage, to generation of reactive oxygen species(518-520).

Catabolism of H_2S occurs via a single known oxidative pathway (Figure 5.4) involving a sulfurtransferase (rhodanese) and a mechanistically remarkable persulfide dioxygenase (ETHE1)(521). Multiple disease states are associated with elevated H_2S levels(522). It is proposed that H_2S exerts its signalling functions via post-translational S-sulfhydration of target proteins(523, 524). However, an understanding of how H_2S functions at the molecular level is still in its infancy and, as with many aspects of sulphur metabolism, is limited by available methods for studying, often reversible, sulfur biochemistry in cells.

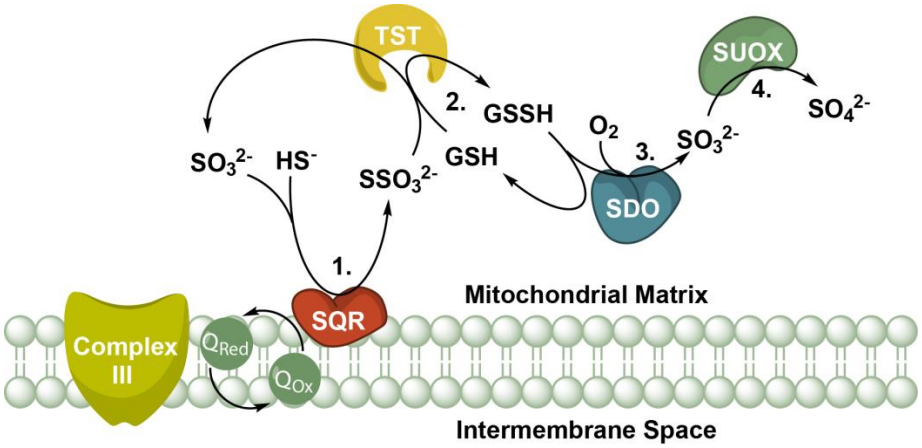

Figure 5.4: Pathway for hydrogen sulfide oxidation in many aerobes. 1. H_2S is initially oxidised and transferred to an acceptor molecule such as sulfite to form thiosulfate by a sulfide:quinone reductase (SQR). The electrons from this initial oxidation are passed on the respiratory chain via the quinone pool. 2. The sulfide sulfur is transferred to glutathione (GSH) via a thiosulfate sulfur transferase (TST) to form a persulfide (GSSH) before subsequent rounds of oxidation 3. by the sulfur dioxygenase (SDO) ETHE1 and 4. By further sulfite oxidases (SUOX).

Unlike most hMBLs which are zinc hydrolases(216), the hMBL, ETHE1, is an oxygenase that requires iron for catalytic activity(220). Knockouts of, or mutations in, the gene coding for ETHE1 in humans results in the distinct phenotype of ethylmalonic encephalopathy, a disease which is characterised by progressive encephalopathy, neurological symptoms, such as dystonia, and lesions in the brainstem grey matter leading to seizures(218, 340, 525).

5.1.2. Structure and Reaction of ETHE1

The exact reaction catalysed by ETHE1 is shown in Figure 5.5. Although the mechanism of this reaction is currently unknown, it most likely proceeds via initial oxidation of the terminal sulfide sulfur to a sulfinic acid before hydrolysis by water.

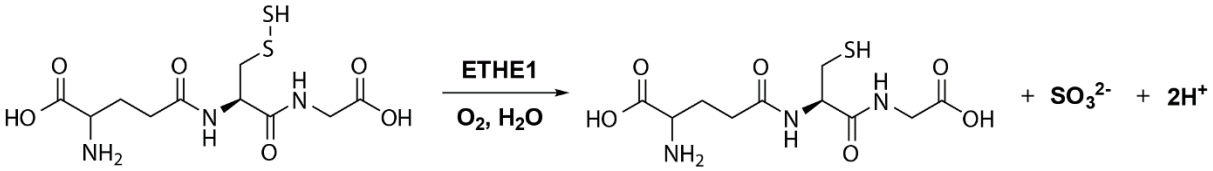

Figure 5.5: The oxidation of glutathione persulfide as catalysed by ETHE1.

This reaction shares some mechanistic similarities with both the cysteine dioxygenase (CDO) enzymes(526, 527) as well as isopenicillin N synthase (IPNS)(528), which are both examples of non-haem iron oxygenases that accept thiol substrates and that use the substrate as the electron source in the redox reaction. A comparison of the active sites of hETHE1, CDO, and IPNS, and mechanistic schemes for the reactions of IPNS and CDO are shown in Figures 5.6, and 5.7 and 5.8, respectively.

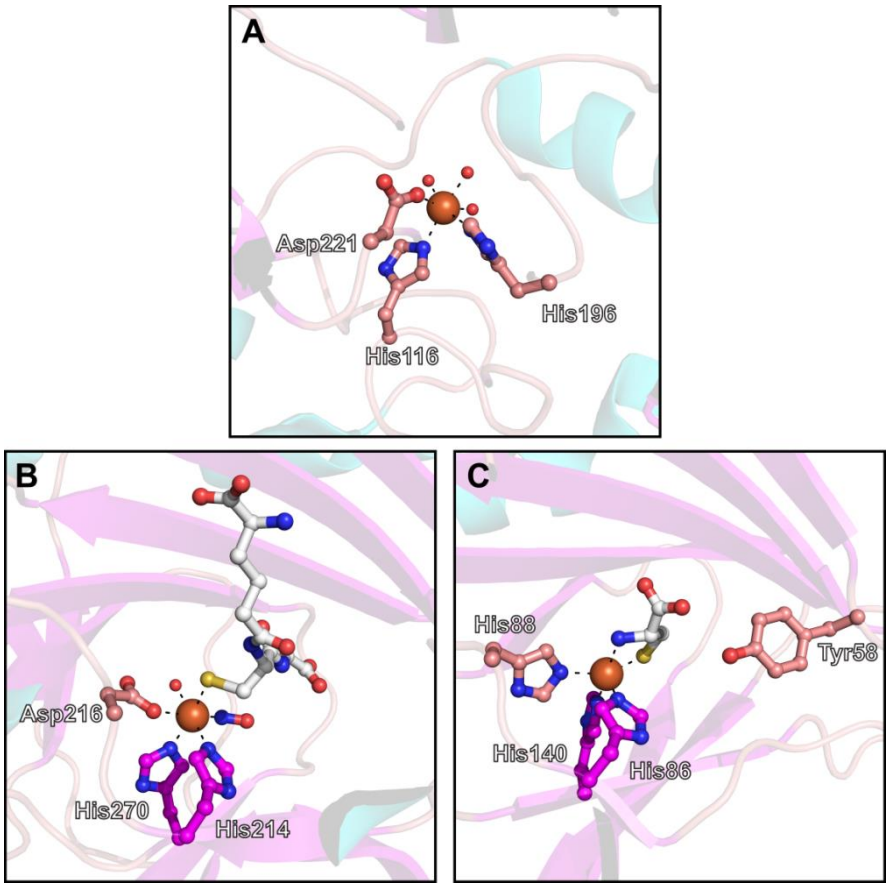

Figure 5.6: View from a crystal structure of A. hETHE1 (PDB accession code: 4CHL)(220), B. isopenicillin N synthase in complex with α-aminoadipoyl-cysteinyl-glycine and nitric oxide (PDB accession code: 1W04)(529), and C. cysteine dioxygenase in complex with L-cysteine (PDB accession code: 4JTO)(530).

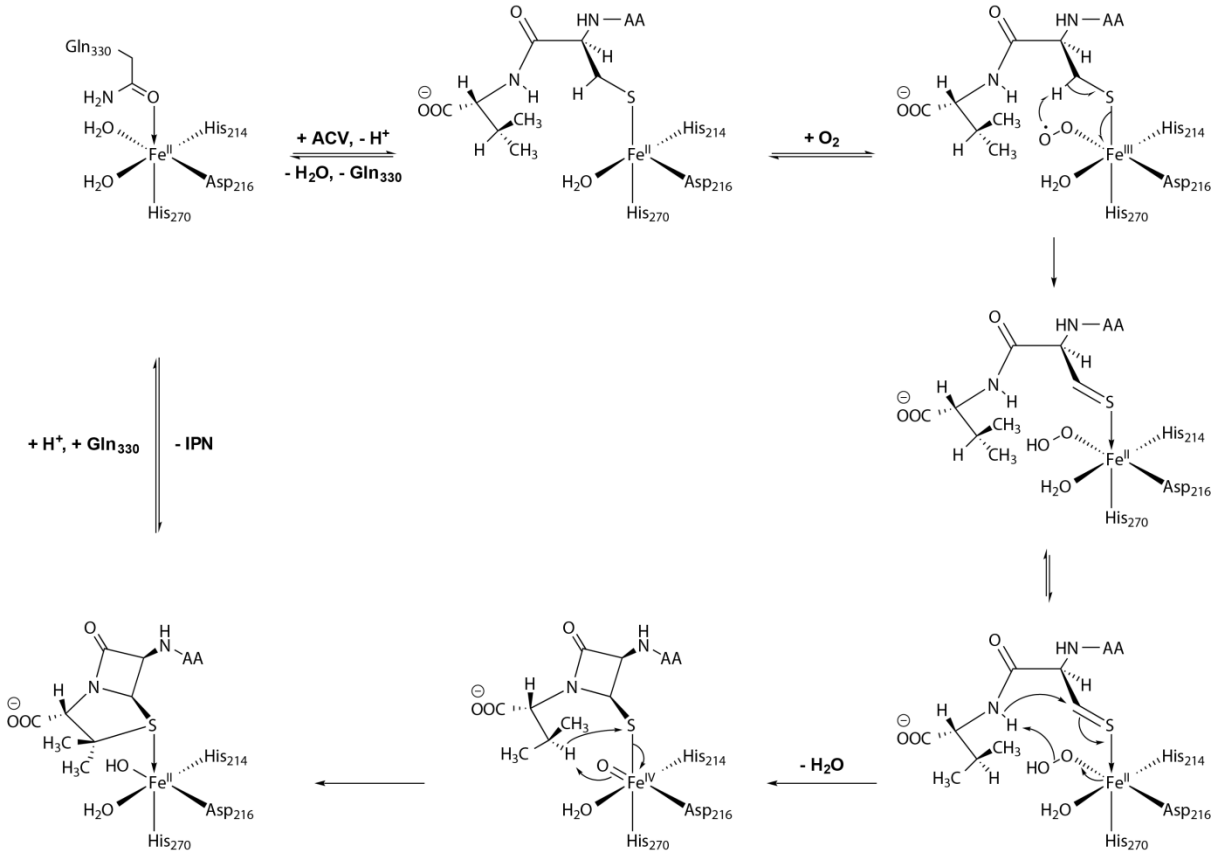

Figure 5.7: Mechanistic scheme for the reaction catalysed by isopenicillin N synthase. Given the active site structure and substrate chemistry of ETHE1, it is likely that the ETHE1 catalysed reaction shares mechanistic similarity with this enzyme. ACV - δ-(L-α-aminoadipoyl)-L-cysteinyl-D-valine, AA - L-α-aminoadipic acid, IPN – isopenicillin N.

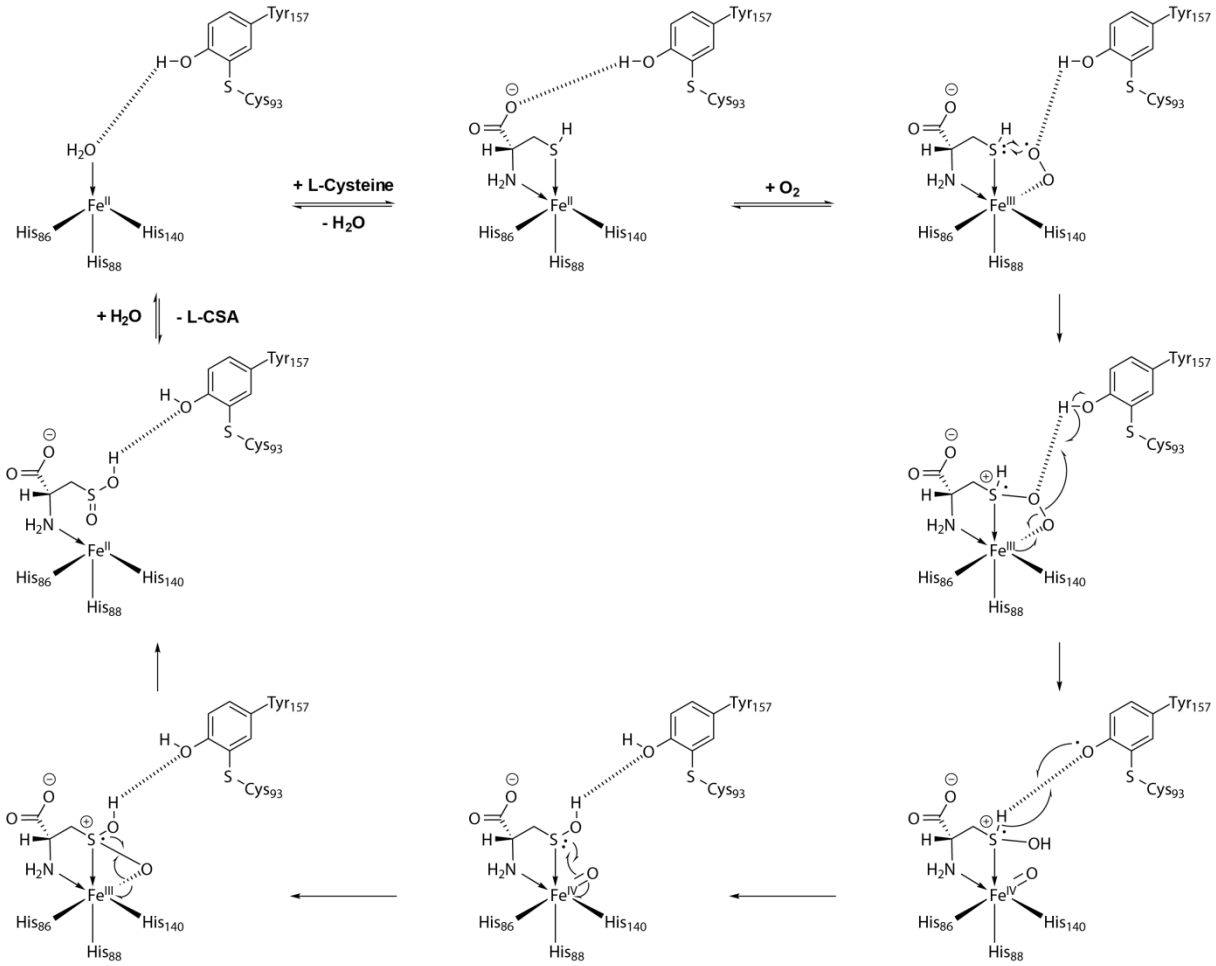

Figure 5.8: Mechanistic scheme for the reaction catalysed by cysteine dioxygenase. Given the active site structure and substrate chemistry of ETHE1, it is likely that the ETHE1 catalysed reaction shares mechanistic similarity with this enzyme. L-CSA – L-cysteine sulfenic acid.

To date, the structures of four ETHE1 homologues have been reported, those of the human and *Arabidopsis thaliana* enzymes (hETHE1 and AtETHE1, respectively)(220, 339), and two bacterial homologues, *Myxococcus xanthus* ETHE1 isoform 2 (Mx2ETHE1), and that from *Pseudomonas putida* (PpETHE1)(531). Despite variation in sequence identities (Figure 5.10), each of the enzymes exhibits the same active site structure and MBL fold (Figure 5.9)(220, 339, 531). In addition to structural characterisation, the activity of a number of bacterial ETHE1 homologues has been demonstrated, originating from species including *Pseudomonas aeruginosa*, *Burkholderia xenovorans*, and *Myxococcus xanthus*(532). Interestingly, the latter organism appears to produce three separate ETHE1 homologues, although the functional reason for this is not yet understood.

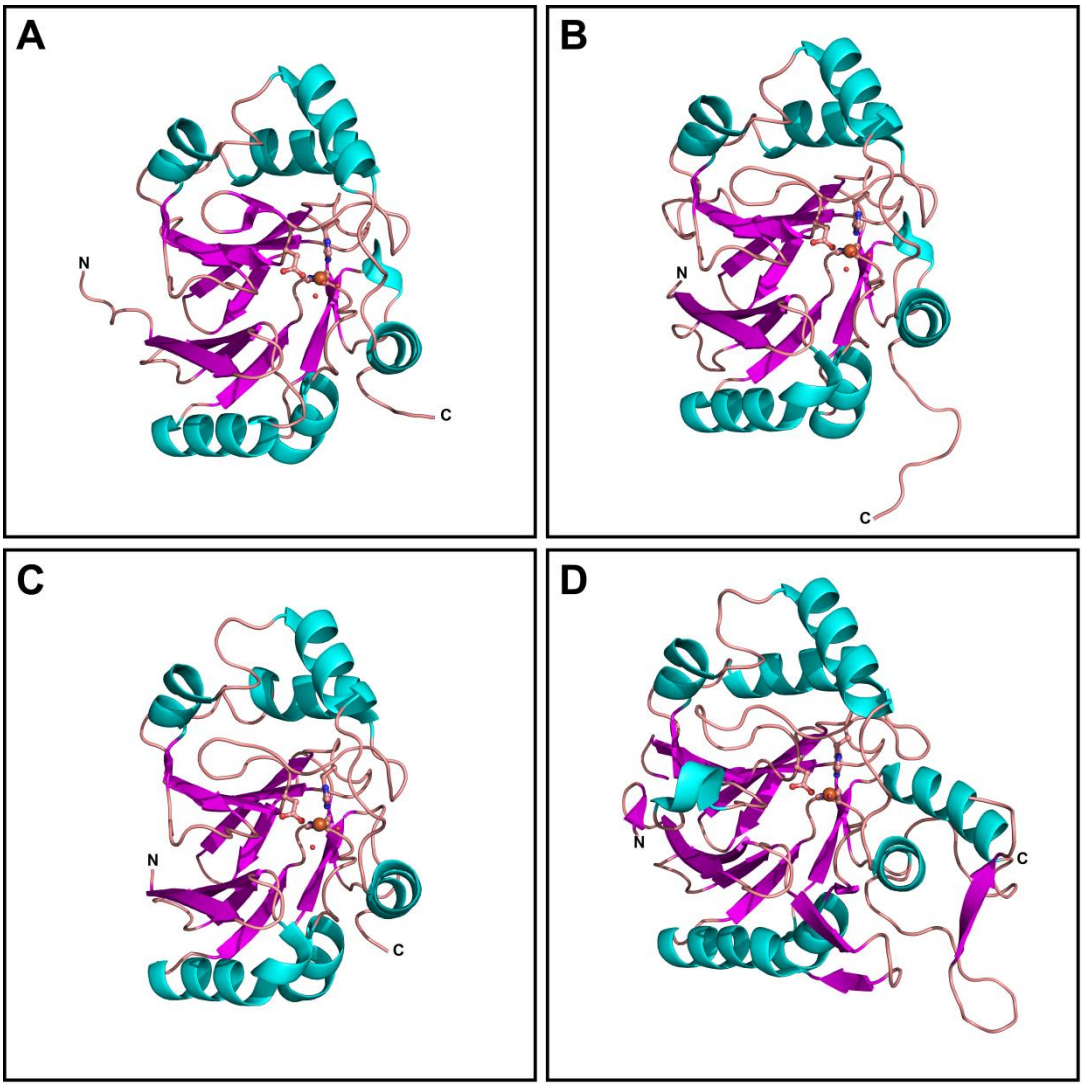

Figure 5.9: All determined crystal structures for ETHE1 homologues. Each enzyme exhibits the conserved metallo-β-lactamase fold, while the *Pseudomonas putida* homologue possesses an extended *C*-terminus. A. human (hETHE1). B. *Arabidopsis thaliana* (AtETHE1). C. *Myxococcus xanthus* isoform 2 (Mx2ETHE1). D. *Pseudomonas putida* (PpETHE1). PDB Accession codes: 4CHL, 2GCU, 4YSB, and 4YSL, respectively(220, 339, 531).

% Identity	h	At	Mx2	Pp
h	100	60	49	28
At	60	100	48	26
Mx2	49	48	100	32
Pp	28	26	32	100

Figure 5.10: Sequence similarities of crystallised ETHE1 homologues. Sequence alignments and identity calculations were performed using the Clustal Omega web service(158). h – human ETHE1, At – *Arabidopsis thaliana* ETHE1, Mx2 – *Myxococcus xanthus* ETHE1 isoform 2, Pp – *Pseudomonas putida* ETHE1.

5.1.3. Assaying ETHE1 – Production of Glutathione Persulfide

Two methods for the production of glutathione persulfide have been reported; firstly, by addition of an acetonic sulfur suspension to a solution of reduced glutathione(339), and, secondly, by the 1:1 reaction of oxidised glutathione with sodium sulfide(533). It should be noted that in both cases, the reaction mixture likely contains a number of polysulfide compounds in addition to the persulfide, which may cause interference with an ETHE1 assay, and both reactions are employed in this study to avoid this.

5.1.4. Assaying ETHE1 – Detection of Sulfite

Based on the ETHE1 catalysed reaction, two assays for ETHE1 activity have been published. The first, an assay based on a polarographic measurement of oxygen consumption(533), is able to demonstrate enzymatic activity, but has limited utility in obtaining reliable and repeatable data, particularly kinetic data. The second assay, based on high performance liquid chromatography (HPLC), involves the use of a fluorescent electrophilic molecule, monobromobimane, to chemically trap all nucleophiles in the enzymatic reaction mixture. The adducts are then separated using a gradient of methanol in water and quantified via standard samples of possible nucleophile-monobromobimane adducts of known concentration. This method is useful and has been used in multiple publications to obtain steady-state kinetic information on a number of ETHE1 homologues(531-533). However, as expressed above, the need for a more high-throughput method to support already existing assays for the 'true' MBLs suggests that this second assay method might not be the best for the particular task at hand.

More useful, perhaps, would be a plate reader based method utilising absorbance/fluorescence, either in real time or as an end-point assay, to follow multiple reactions in a 96 or 384 well format. Analysis of the ETHE1 reaction shows three potential

nucleophilic species that might be identifiable by fluorescence methods, glutathione persulfide, glutathione and sulfite. Since it is likely that glutathione and the corresponding persulfide have similar nucleophilic reactivity (although the persulfide is potentially a better nucleophile on account of the α-effect of the adjacent sulfur atom), it may be difficult to distinguish between these two species chemically. Thus development of a plate reader based assay focussed on methods to detect the formation sulfite anions during the ETHE1 catalysed reaction.

On account of its regulated use as a preservative in many wines and juices, and its generation at potentially toxic levels in sewage, multiple methods for the detection of sulfite anions in solutions have been reported. Examples of methods for the detection of sulfite ions via fluorescence are explored below. The publication of switch on/off fluorescent detectors of sulfite is of interest in the context of ETHE1, since such methods may be amenable to adaptation into a plate reader based assay, and also since fluorescence methods in this format typically have a greater signal-to-noise ratio than comparable absorbance assays (compare an FC5 fluorescence based MBL assay with a nitrocefin absorbance assay(433)).

Sulfite as a Deprotectant of Fluorophores. The use of levulinate esters as protecting groups for alcohols and their selective deprotection by sulfite anions has been reported previously(534). This deprotection has been utilised to develop sulfite detection assays using levulinate esters of resorufin, fluorescein, and umbelliferone, amongst others(535, 536). The deprotection likely occurs via nucleophilic attack of the sulfite anion onto the ketone of the levulinic acid side chain an subsequent cyclisation to cleave the ester, and this mechanism is supported by mass spectrometric analysis demonstrating that the a cyclised sulfite adduct can be detected (Figure 5.11 A).

Sulfite as a Chemical Switch to Induce Fluorescence. An anthracene based sulfite reporter molecule has been reported(537). The anthracene fluorophore in this molecule is linked to a para-formyl benzoic acid quencher, which prevents fluorescence via photoinduced electron transfer. The presence of sulfite is reported by deactivation of the adjacent quencher moiety, *via* the nucleophilic sulfite anions reacting with the aldehyde, which gives rise to a fluorescence signal (Figure 5.11 B).

A more complex sulfite reporter that utilises induced fluorescence is illustrated in Figure 5.11 C. This reporter comprises two molecules, a chemically modified polylysine chain decorated with para-formyl benzamide moieties and a tetraphenylethene bearing two quaternary amine cationic centres(538). In solution the tetraphenylethene does not give rise to fluorescence, however addition of sulfite induces fluorescence. This arises as a result of the reaction of the sulfite anions with the aldehyde moieties on the polylysine chain, thus

decorating it with negative charge; association of the cationic tetraphenylethene molecules with the negatively charged amino acid chain results in collapse of the two species together, giving rise to aggregation induced emission and, consequently, detection of the sulfite.

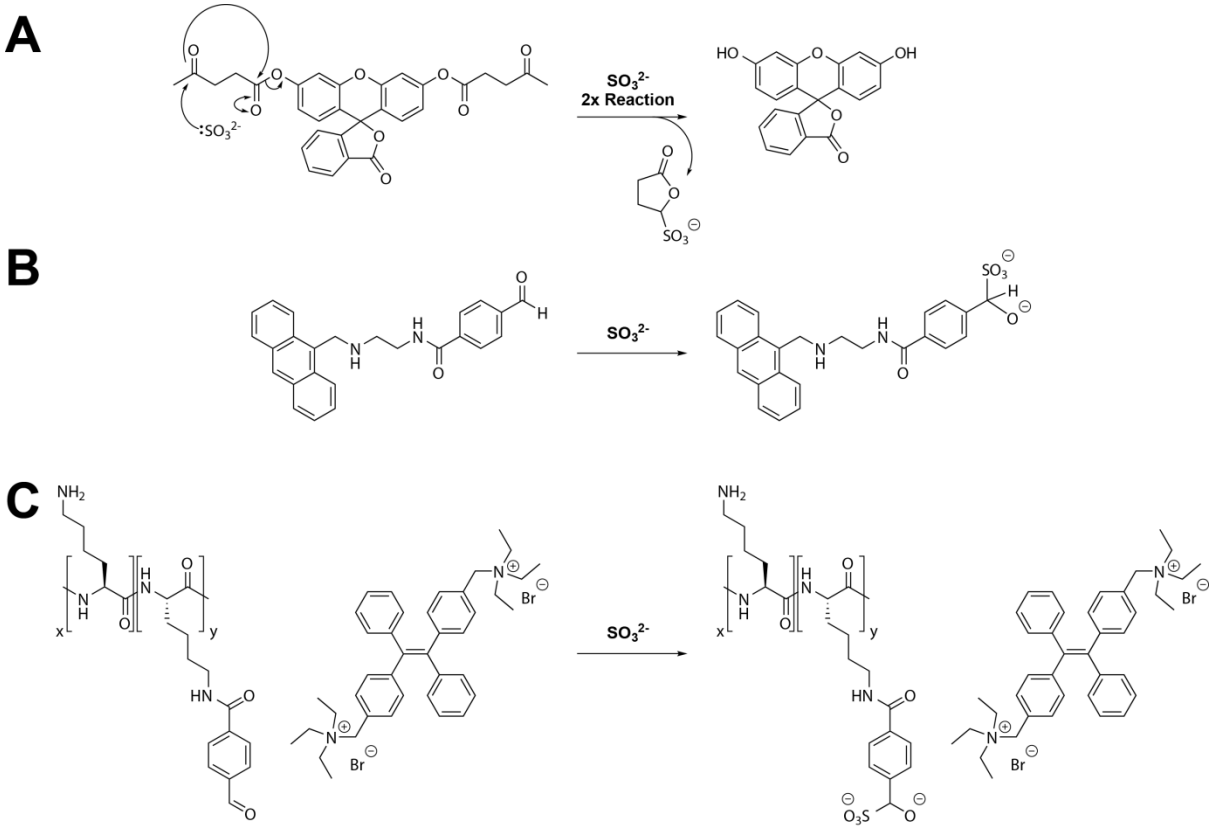

Figure 5.11: Example published methods for the chemical detection of sulfite anions.

5.2. Chapter Objectives

ETHE1 is a unique MBL fold enzyme with an unusual oxygenase mechanism(220). Further, its activity is essential for human health as exemplified by the highly debilitating disease, ethylmalonic encephalopathy, which arises from mutations in the *ETHE1* gene(218, 340, 533). Development of inhibitors of the 'true' bacterial MBL is likely to be essential to the continued use of β-lactams against antibiotic resistant bacterial infection(140), but, due to structural similarities between the bacterial enzymes and related human enzymes, there is a danger of off pathway targets in 'true' MBL inhibitor development. The goal of the work outlined in this chapter was to produce homologues of the ETHE1 enzyme and develop a medium to high throughput assay for ETHE1 activity. Such an assay, alongside assays for other human MBL fold enzymes, could be used to eliminate promiscuous inhibitors of the 'true' MBLs and expedite the development of bacterial MBL inhibitors in the future.

5.3. Production of ETHE1 Homologues

5.3.1. Cloning

Three ETHE1 homologues were chosen for study, the human ETHE1 (hETHE1) and two bacterial enzymes, one, isoform 1 from *Myxococcus xanthus* (MxETHE1), sharing the highest sequence identity of any single domain enzymes (an amino acid sequence similarity of 52%) and one from *Burkholderia cepacia* (BcETHE1), which shows a greater sequence similarity over the MBL domain (55% sequence similarity), but also features a second thiosulfate sulfur transferase (rhodanese) domain (Figures 5.12 & 5.13). Codon optimised synthetic gene constructs for these enzymes were purchased from ThermoFisher Scientific. All three genes were initially amplified from the supplied gene and cloned into a pCold vector (Takara). Primer sequences can be found in the General Methods.

% Identity	h	Bc	Mx
h	100	55	52
Bc	55	100	55
Mx	52	55	100

Figure 5.12: Sequence similarities of the ETHE1 homologues selected for this study. Sequence alignments and identity calculations were performed using the Clustal Omega web service(158). For the two domain *Burkholderia cepacia* enzyme, the identity shown accounts for the ETHE1 domain only. h – human ETHE1, Bc – *Burkholderia cepacia* ETHE1, Mx – *Myxococcus xanthus* ETHE1 isoform 1.

```
MxETHE1:    ---MLFRQLFDTTSSTYTYLLGDEEQGTALLIDPVAEKLDRDLTLLRELGLSLTHALDTH   57
 hETHE1:    MAPILLRQMFEPVSCTFTYLLGDRESREAVLIDPVLETAPRDAQLIKELGLRLLYAVNTH   60
BcETHE1:    ---MIFRQLFDPQSSTYTYLLADSASREALLIDPVFEQVRRDAALLDELGLRLVATVDTH   57

MxETHE1:    VHADHVTASGLLRARTGA-KVVSGITGAPCADIHVKHGDTLRAGTFTLQVLATPGHTDDS   116
 hETHE1:    CHADHITGSGLLRSLLPGCQSVISRLSGAQADLHIEDGDSIRFGRFALETRASPGHTPGC   120
BcETHE1:    VHADHVTGAWLLKQRTGSAIAISAASGAQGADRYLNDGDRCAFGSRYLTVRATPGHTSGC   117

MxETHE1:    VSYLLGDR--VFTGDALLIRGNGRTDFQNGNAGTLYDSITQVLFALPDETLVYPAHDYRG   174
 hETHE1:    VTFVLNDHSMAFTGDALLIRGCGRTDFQQGCAKTLYHSVHEKIFTLPGDCLIYPAHDYHG   180
BcETHE1:    ISLVLDDESMAFTGDCLLIRGTGRTDFQQGDPRALYRAVHGRLFTLPAACLLYPAHDYRG   177

MxETHE1:    LTVTTIGEEKRHNPRVAG-RSRDGFIQLMNNLGLPKPKLIDVAVPANRACGLTAPVRARG   233
 hETHE1:    FTVSTVEEERTLNPRLT--LSCEEFVKIMGNLNLPKPQQIDFAVPANMRCGVQTPTA---   235
BcETHE1:    LTVTSVGEERRFNPRLGGDLSEDDFAGYMRNLGLAHPRQIDVAVPANLQCGVAANASDAQ   237

MxETHE1:    SFTH-------------------------------------------------------   237
 hETHE1:    -------------------------------------------------------   235
BcETHE1:    AAADWAPLVYTFAGFWEIDPQWLEDHLPAVQVVDVREPDEFTGSLGHLPGATPIPLGELA   297

MxETHE1:    -------------------------------------------------------   237
 hETHE1:    -------------------------------------------------------   235
BcETHE1:    ARTGEIARDRPVVTVCRAGGRSAQATVILRKAGFDAVANLGGGMLRW           356
```

Figure 5.13: Multiple sequence alignment of ETHE1 homologues. Alignment was performed using Clustal Omega(158). The MBL domain is highlighted in purple, while the rhodanese domain of the Burkholderia cepacia homologue is highlighted in green. Metal binding residues in the MBL domain and the active site cysteine of the rhodanese domain are highlighted in red.

5.3.2. Expression Trials

Initially, expression of each pCold gene construct was investigated in *E. coli* BL21(DE3) cells. Cells were grown to an OD_{600} of 0.6 before cooling to 15 °C, inducing gene expression with a range of isopropyl β-D-1-thiogalactopyranoside (IPTG) concentrations, and continuing growth overnight. Successful production of both hETHE1 and BcETHE1 (Figure 5.14 A) was seen, and these constructs could be taken forward for large scale protein production and purification.

Production of MxETHE1 using the pCold vector construct was poor both in *E. coli* BL21(DE3) and in *E. coli* Rosetta DE3 cells, so an alternative construct with a 3C cleavable *N*-terminal hexahistidine tag was produced using the pET22b vector system. Production of MxETHE1 protein using this new construct was investigated at a number of temperatures and IPTG concentrations and the highest level of protein production was seen after an overnight growth at 25 °C with an IPTG concentration of 0.1 mM (Figure 5.14 B).

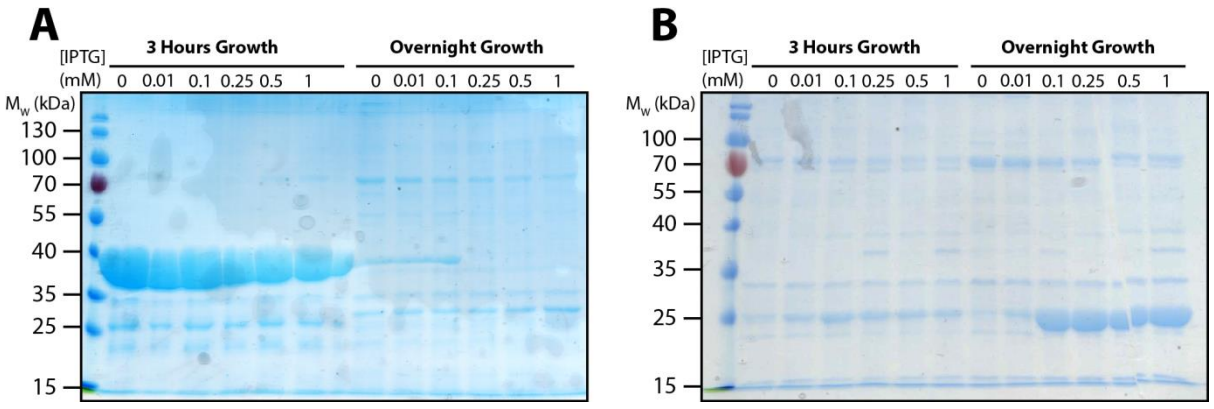

Figure 5.14: Expression trials of A. BcETHE1 and B. MxETHE1 with an *N*-terminal hexahistidine tag. After reaching an optical density of 0.6, cells were cooled to 15 (A) or 25 (B) °C and ETHE1 expression was induced with varying isopropyl β-D-1-thiogalactopyranoside. Cells were then grown overnight before lysis and purification of any expressed enzyme.

Large scale production of the MxETHE1 enzyme from this construct demonstrated that the *N*-terminal hexahistidine could not be cleaved by 3C protease, possibly due to structural obscuring of the cleavage site. Further, this construct was not particularly stable in solution (25 mM HEPES, pH 7.5, 100 mM NaCl), precipitating around one to two hours after a completed purification. Thus a third construct was created featuring a 3C-cleavable *C*-terminal hexahistidine tag in the pET22b vector. This construct was expressed similarly well in the conditions described for the *N*-terminally hexahistidine tagged enzyme (Figure 5.15) and was taken forward for large scale protein production and purification.

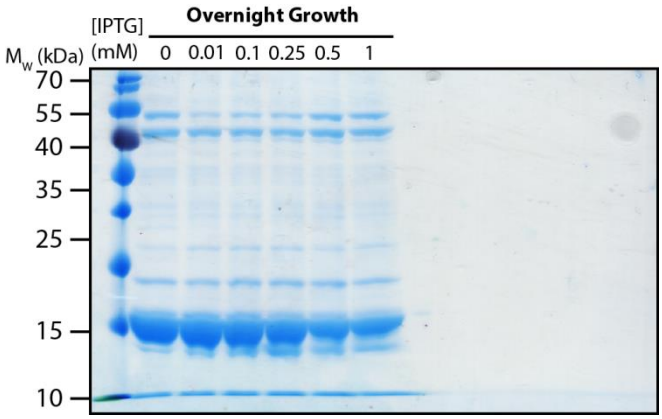

Figure 5.15: Expression trial of MxETHE1 with a *C*-terminal hexahistidine tag. After reaching an optical density of 0.6, cells were cooled to 25 °C and ETHE1 expression was induced with varying isopropyl β-D-1-thiogalactopyranoside. Cells were then grown overnight before lysis and purification of any expressed enzyme.

5.3.3. Large Scale Production and Purification of ETHE1 Homologues

Recombinant hETHE1, BcETHE1, both with an *N*-terminal hexahistidine tag, and MxETHE1 with a *C*-terminal hexahistidine tag were produced in *E. coli* BL21(DE3) cells and purified by immobilised metal ion affinity chromatography followed by size exclusion chromatography before removal of the *N*-terminal tag by 3C protease digestion, as described in the general methods. At each stage in the purification of these enzymes, their purity was determined by sodium dodecyl sulfate polyacrylamide gel electrophoresis (SDS-PAGE) (Figures 5.16-5.18).

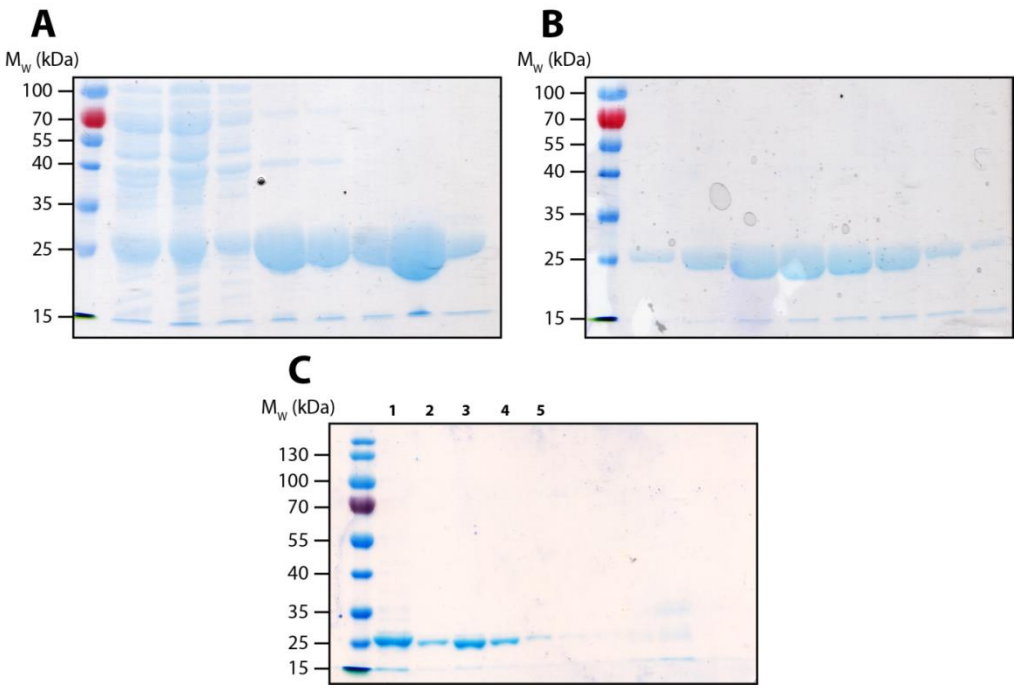

Figure 5.16: A-C. SDS-PAGE Gels of hETHE1 after successive rounds of metal ion affinity purification by elution from an immobilised nickel column with a gradient of 0-0.5 M imidazole, size exclusion chromatography using a Superdex 200 column, and 3C protease incubation followed by nickel ion affinity rebinding, respectively. All enzyme purification steps were carried out at 4 °C. (C1: hETHE1 before 3C incubation. C2: 3C protease. C3-5: Cleaved hETHE1).

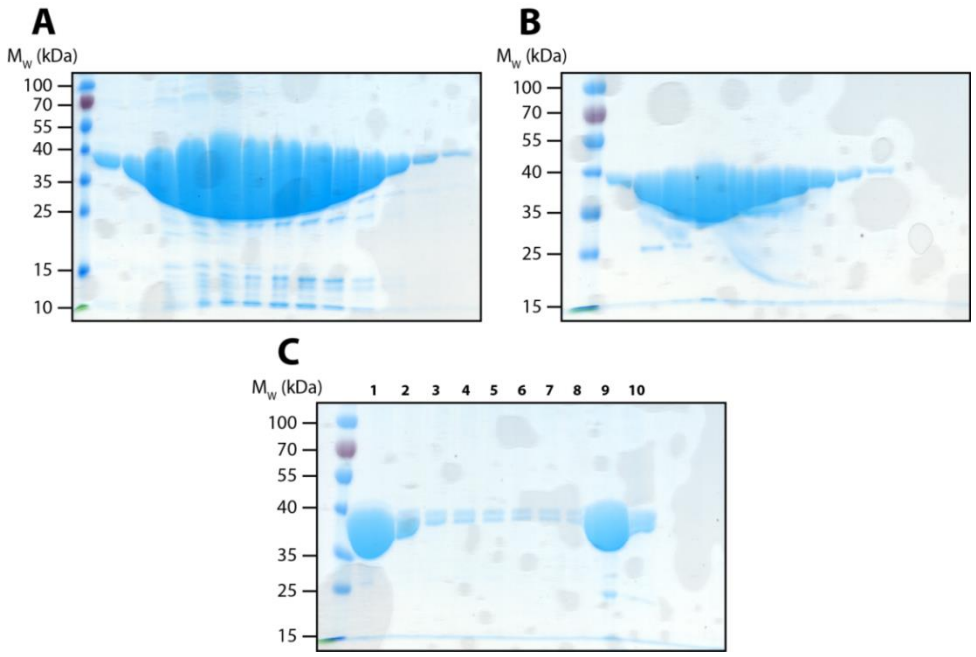

Figure 5.17: A-C. SDS-PAGE Gels of hETHE1 after successive rounds of metal ion affinity purification by elution from an immobilised nickel column with a gradient of 0-0.5 M imidazole, size exclusion chromatography using a Superdex 200 column, and 3C protease incubation followed by nickel ion affinity rebinding, respectively. All enzyme purification steps were carried out at 4 °C. (C1-8: 20 mM imidazole elutions. C9-10: 500 mM imidazole elutions).

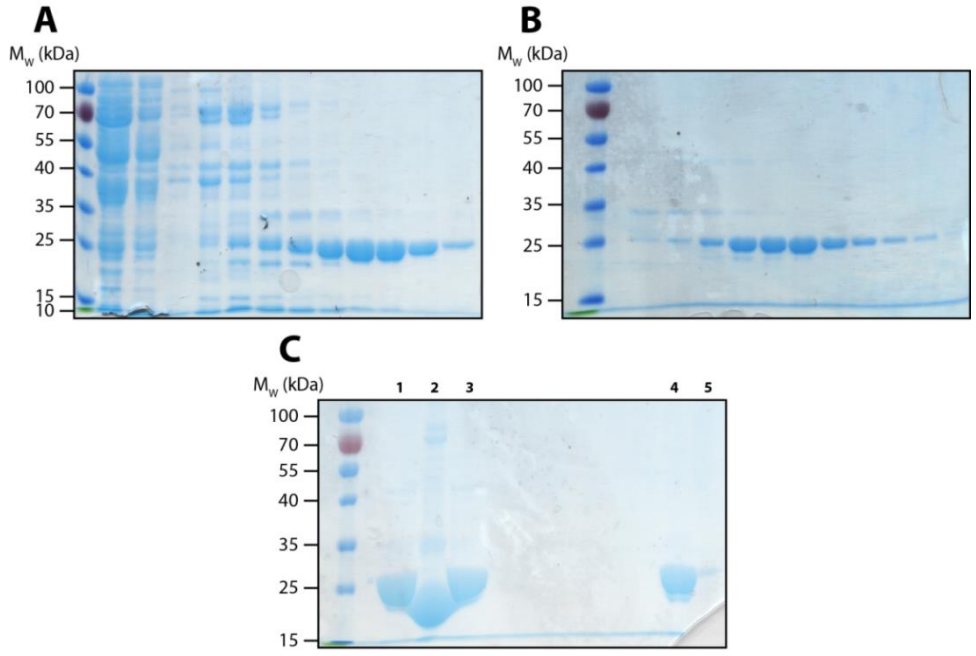

Figure 5.18: A-C. SDS-PAGE Gels of MxETHE1 after successive rounds of metal ion affinity purification by elution from an immobilised nickel column with a gradient of 0-0.5 M imidazole, size exclusion chromatography using a Superdex 200 column, and 3C protease incubation followed by nickel ion affinity rebinding, respectively. All enzyme purification steps were carried out at 4 °C. (C1: MxETHE1 before 3C incubation. C2: 3C protease. C3: Cleaved hETHE1. C4-5: 500 mM imidazole elutions).

5.4. Characterisation of ETHE1 Homologues

5.4.1. Circular Dichroism and Mass Spectrometry

Having successfully produced and purified the three ETHE1 homologues, their molecular masses were investigated using denaturing mass spectrometry and the extent of folding was monitored by circular dichroism (CD) spectroscopy (Figure 5.19 & Table 5.1).

CD spectroscopy demonstrated that the purified enzymes were successfully folded and measured molecular weights were in agreement with those predicted by each amino acid sequence. The thermal stability of each homologue was also examined (Figure 5.20 & Table 5.2). hETHE1 was found to be the most stable and MxETHE1 the least, with T_m values of 64.5 ± 0.1 and 54.4 ± 0.1 °C, respectively. BcETHE1 showed a biphasic melting curve. This curve shape likely results from one of the two domains, MBL or rhodanese, preferentially unfolding before the other. Given the melting temperatures of the two other homologues, which each consist of only an MBL domain, it is likely that the rhodanese domain unfolds first, since its melting temperature is lower than the range set by the other two homologues. The comparatively low melting temperature of the *Mxyococcus xanthus* homologue may be related to the reason for the precipitation of the *N*-terminally hexahistidine tagged construct after purification.

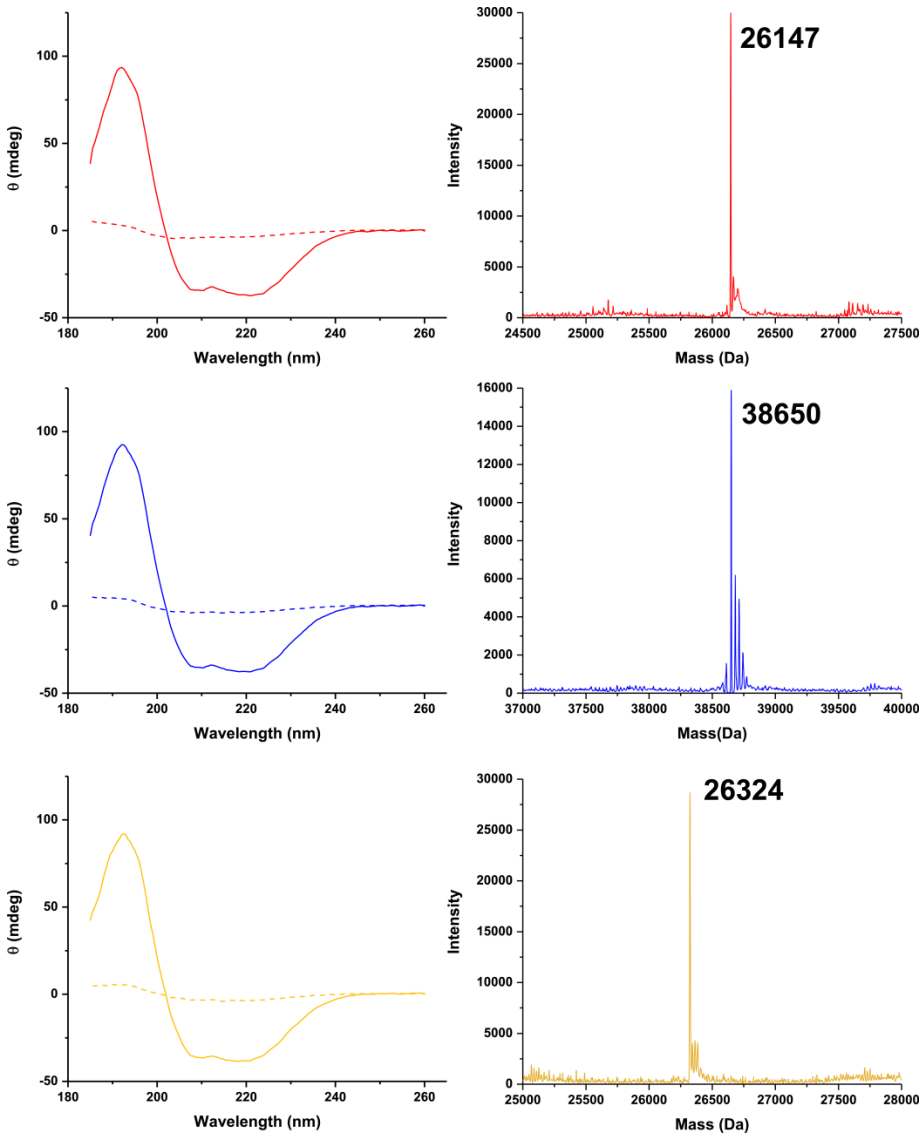

Figure 5.19: Circular dichroism and mass spectra for purified ETHE1 homologues. Solid lines in circular dichroism spectra represent measurements at 10 °C, while dashed lines represent those at 85 °C. Enzymes were assayed at 0.2 mg mL^{-1} in 10 mM sodium phosphate buffer, pH 7.5. Red: hETHE1. Blue: BcETHE1. Yellow: MxETHE1.

Enzyme	Predicted Mass (Da)	Measured Mass (Da)
hETHE1	26145	26147
BcETHE1	38660	38650
MxETHE1	26328	26324

Table 5.1: Masses purified ETHE1 homologues as determined by denaturing mass spectrometry. Enzymes were assayed at 0.2 mg mL^{-1} in 10 mM sodium phosphate buffer, pH 7.5. The predicted masses, based on amino acid sequence, are also provided.

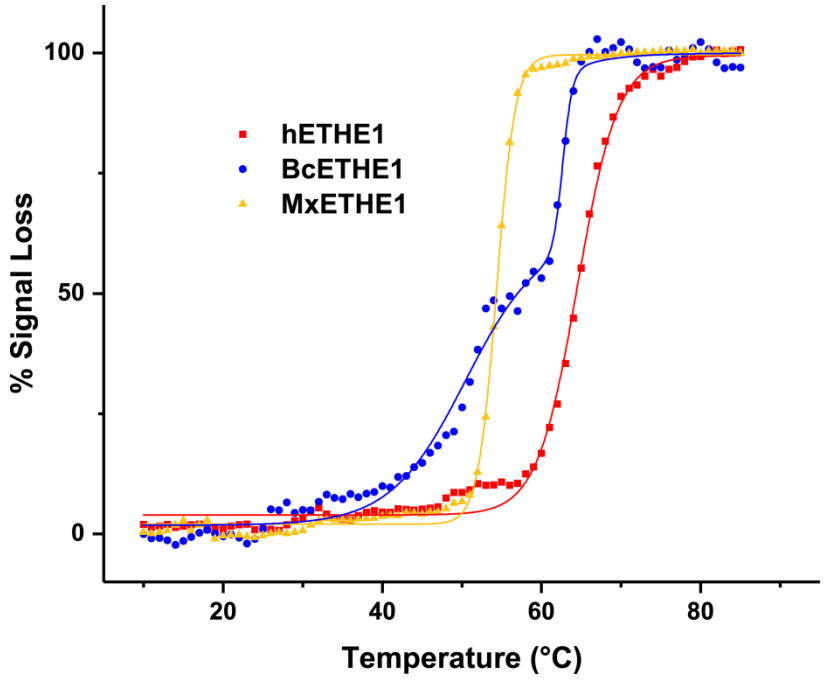

Figure 5.20: Melting curves for purified ETHE1 homologues as determined by circular dichroism. Enzymes were assayed at 0.2 mg mL^{-1} in 10 mM sodium phosphate buffer, pH 7.5. Curve fitting was performed using OriginPro(349).

Enzyme	T_m (°C)
hETHE1	64.5 ± 0.1
BcETHE1	50.4 ± 0.8
	62.7 ± 0.2
McETHE1	54.4 ± 0.1

Table 5.2: Melting temperatures of purified ETHE1 homologues as determined by circular dichroism. Enzymes were assayed at 0.2 mg mL^{-1} in 10 mM sodium phosphate buffer, pH 7.5.

5.4.2. Oligomerisation of ETHE1 Homologues

It is known that the human variant of ETHE1 can exist in dimeric and tetrameric forms in solution(220). To investigate the extent of oligomerisation of the new hETHE1 construct and other purified ETHE1 homologues, the enzymes were analysed by size exclusion chromatography with multi-angle light scattering (SEC-MALS, Figure 5.21). Note that these experiments were performed by Dr David Staunton of the Biophysical Service, Department of Biochemistry, University of Oxford.

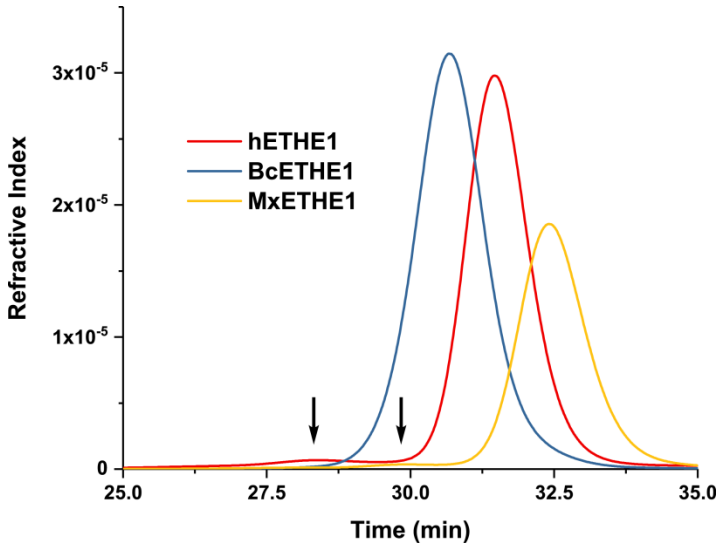

Figure 5.21: SEC-MALS analysis of purified ETHE1 homologues. Major peaks at 52.3, 77.3, and 52.6 kDa correspond to dimeric forms of hETHE1, BcETHE1, and MxETHE1, respectively. Smaller peaks around 28 and 30 min (indicated by arrows), reflect a small population of hETHE1 and MxETHE1 tetramer.

SEC-MALS analysis revealed that all three of the ETHE1 homologues adopt a dimeric state as their major population, corresponding to 52.3, 77.3, and 52.6 kDa for hETHE1, BcETHE1 and MxETHE1, respectively. A small population of tetrameric hETHE1 and MxETHE1 were also seen, but no such peak was observed with BcETHE1. Although the tetrameric state of hETHE1 has been reported previously(220), it constituted a minor population in that instance as well. This suggests that the tetrameric species may not be biologically relevant but comes as an artefact of isolation and purification of the human and *M. xanthus* enzymes.

5.4.3. Activity of Purified ETHE1 Homologues

Once the successful folding and correct masses of each purified homologue had been determined, the activity of the ETHE1 homologues was assessed using an oxygen consumption assay, as has been previously reported(533). This utilised a FOXY AL-300 probe (Ocean Optics), measuring oxygen induced changes in fluorescence after excitation at 450 nm. The glutathione persulfide substrate (GSSH) was prepared by addition of an acetonic sulfur suspension to a solution of reduced glutathione. Addition of the substrate alone made no difference to oxygen levels in solution, while all three homologues induced a drop in O_2 saturation. Both hETHE1 and MxETHE1 consumed around 90% of the available dissolved oxygen, while BcETHE1 did not consume as much under the same incubation conditions. Although not a direct explanation, it should be noted that the activity of the related ETHE1 homologue from *Burkholderia xenovorans* (80% sequence similarity) has been reported a 30-fold lower activity than *M. xanthus* isoform 1(532), and it may be that *Burkholderia sp.* ETHE1 homologues are less efficient in their sulfur dioxygenase catalysis.

It should be noted that in the reported crystal structures of both hETHE1 and AtETHE1 a conserved surface cysteine residue, Cys247, has been characterised a doubly oxidised(220, 339), much like the known oxidative modification of the active site Cys221 in the 'true' MBLs (see Chapter 2). The possibility of this modification occurring in solution may have implications for the use of an oxygen consumption assay to kinetically characterise ETHE1 enzymes. However, since this reaction is stoichiometric with the amount of enzyme assayed, it should have little effect on the basic test for sulfur dioxygenase activity described here.

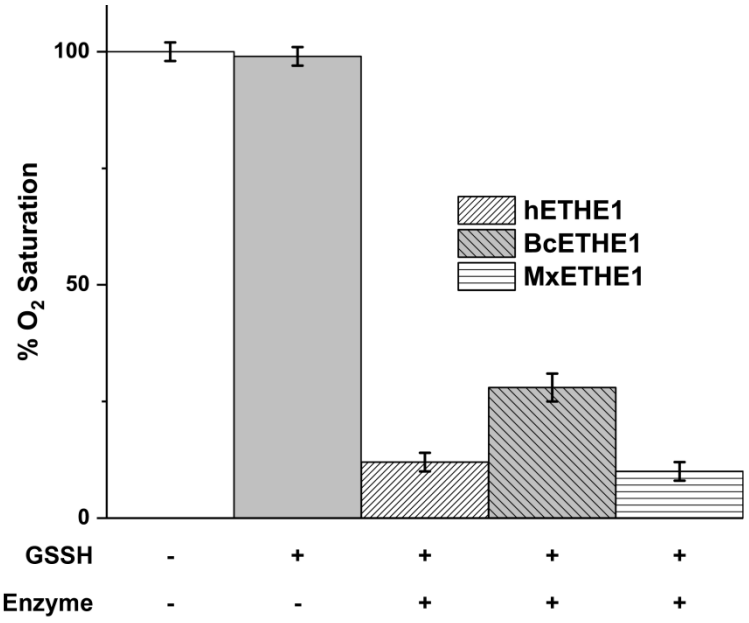

Figure 5.22: Oxygen consumption activity assay of purified ETHE1 homologues. Persulfide dioxygenase activity was measured as the percentage of oxygen consumed five minutes after addition of glutathione persulfide at 25 °C and pH 7.2. Enzymes were employed at a concentration of 0.5 μg mL^{-1}. Values are normalised to the maximum O_2 saturation of buffer at this temperature.

5.4.4. ETHE1 Crystallography

As previously stated, the structures of a number of ETHE1 homologues have been elucidated, including that of the human enzyme(220, 339, 531). It was reasoned that a good deal of information could be learned about the ETHE1 mechanism through crystallisation of an ETHE1 enzyme with its substrate or a substrate homologue, with or without the presence of oxygen. Multiple attempts were made to crystallise each of the three purified ETHE1 homologues, but none of these met with success. Crystals were generated with the *Burkholderia cepacia* enzyme, but X-ray analysis revealed that these diffracted poorly (to around 20 Å) and so no data were acquired.

5.5. Towards a Fluorescence Assay for ETHE1

5.5.1. Detector Synthesis

In order to investigate the utility of reported sulfite detectors, it was initially decided to synthesise two reported molecules relying on levulinate ester deprotection(536, 539). These molecules were synthesised by Steglich esterification (Figure 5.23), see the General Methods for full details.

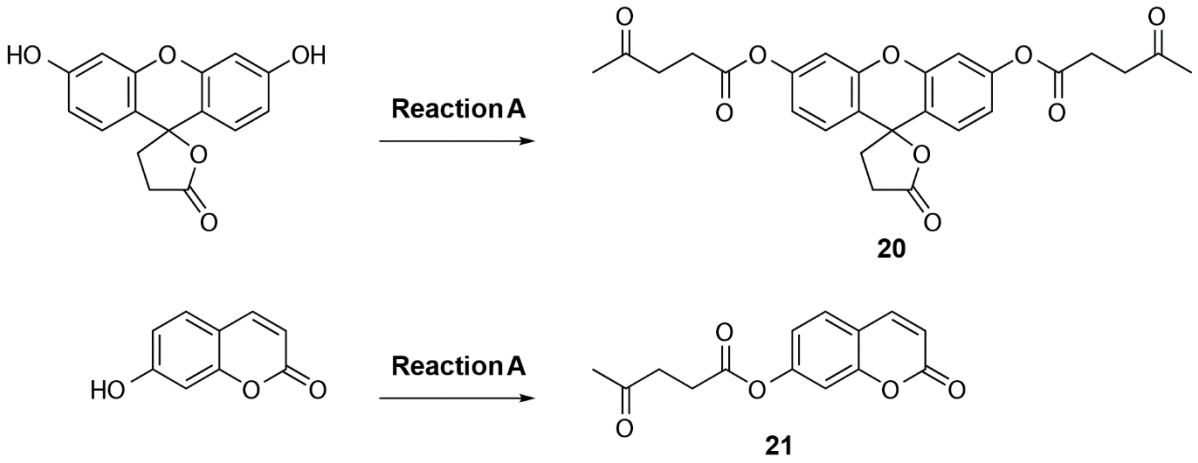

Figure 5.23: Structures and synthetic scheme for the production of levulinate based sulfite detector molecules. A: Levulinic acid, *N,N'*-dicyclohexylcarbodiimide, catalytic 4-dimethylaminopyridine, dry dichloromethane, 6 h, room temperature.

Fluorescence spectra of **20** and **21**, before and after incubation with a ten-fold excess of sulfite ions, confirmed that fluorescence emission is greatly enhanced by sulfite (Figure 5.24).

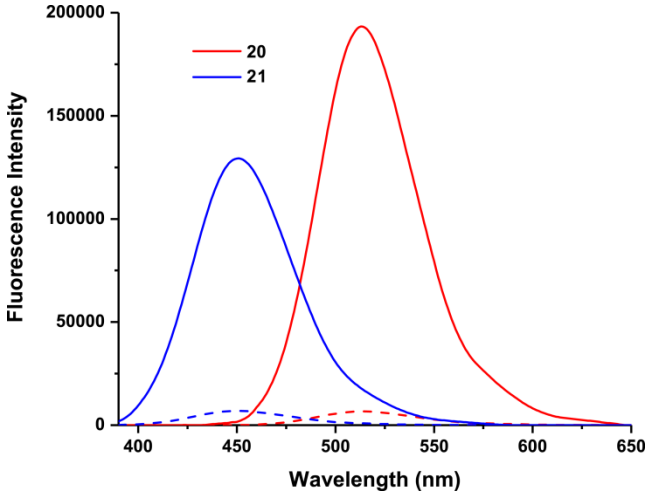

Figure 5.24: Emission spectra for sulfite detectors 20 (red) and 21 (blue). Detectors were employed at a concentration of 1 mM. Solid and dashed lines indicate the presence or absence of 10 mM sulfite ions, respectively. Measurements were carried out at 25 °C and pH 7.5.

5.5.2. Optimal Buffer for Sulfite Detection

Once it had been established that these compounds do, indeed, exhibit fluorescence after exposure to sulfite, the reaction of 1 mM **20**/**21** with 10 mM sodium sulfite was investigated in a number of buffers in order to establish which might give the best signal to noise ratio for further assay development.

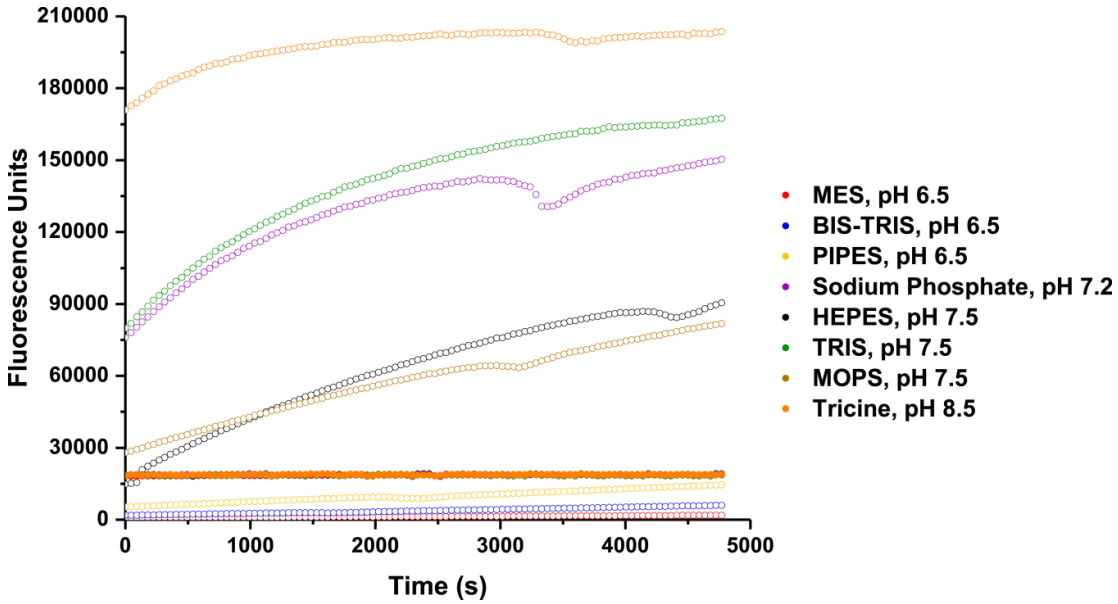

Figure 5.25: Time courses for the background hydrolysis of sulfite detectors in a range of buffers. Solid and hollow circles indicate compounds 20 and 21, respectively. Detectors were employed at a concentration of 1 mM and were activated through the addition of 100 mM sodium sulfite. All buffers were used at a concentration of 25 mM. Measurements were carried out at 25 °C and pH 7.5.

The levulinate protected umbelliferone, **21**, appears to be much more vulnerable to hydrolysis than the fluorescein counterpart, **20**. This may be as a result of the latter requiring two rounds of hydrolysis to restore the parent fluorophore. Optimum buffers for sulfite detection were determined based on the signal to noise ratio for the hydrolysis reaction after complete hydrolysis in the presence of sulfite was seen (Table 5.3). Compound **20** gave the best signal to noise ratio in TRIS and HEPES at pH 7.5, the latter being the reported condition in the original publication(536), while **21** gave the best signal to noise ratio in MES at pH 6.5, with BIS-TRIS being a less favourable second.

Buffer	pH	Signal to Noise Ratio	
		20	21
MES	6.5	21.3	19.2
BIS-TRIS	6.5	18.0	8.1
PIPES	6.5	18.6	4.1
Sodium Phosphate	7.2	21.8	1.1
HEPES	7.5	30.4	1.7
TRIS	7.5	33.4	1.1
MOPS	7.5	24.5	1.9
Tricine	8.5	26.7	1.0

Table 5.3: Signal to noise ratios for the hydrolysis of sulfite detectors in a range of buffers. The ratio is calculated by comparison of the fluorescence intensity after complete hydrolysis by sulfite, with that seen over the same timescale in buffer alone.

5.5.3. Assessing Selectivity for Nucleophiles

In order to confirm the selectivity of the detectors' reaction with sulfite ions, the fluorescence of **20** and **21** was measured after six hours of incubation with a number of sulfur nucleophiles, sodium salts, and typical assay reagents (Figure 5.26). The effect of the hETHE1 enzyme on the ester hydrolysis was also examined.

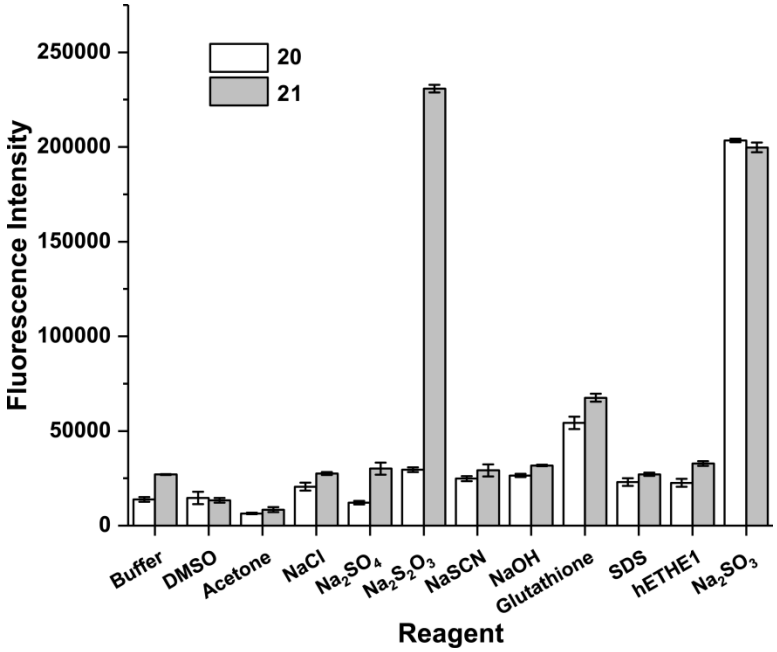

Figure 5.26: Hydrolysis of sulfite detectors 20 (white) and 21 (grey) by a range of added reagents as measured by fluorescence after six hours of incubation. Detectors were employed at a concentration of 1 mM and potential activators at 100 mM. Measurements were carried out at 25 °C and pH 7.5.

Most nucleophiles caused minimal detector hydrolysis for both **20** and **21**. A strong signal was seen with thiosulfate ions, and this likely derives from the acid catalysed decomposition

of the thiosulfate to sulfite in the pH 6.5 MES buffer(540). Glutathione did produce a greater signal with both **20** and **21**, when compared to the other added reagents, but the extent of hydrolysis did not appear significant enough to jeopardise the use of these detectors in an ETHE1 assay. The hydrolysis appears to be inhibited by the presence of acetone, which perhaps acts as a sink for potential nucleophiles. This suggests that the production of glutathione persulfide using an acetonic sulfur suspension may not be the best method for use with this assay. Notably, in all cases, **20** was once again less susceptible to hydrolysis than **21**, except in the presence of sulfite ions, suggesting that it is the more specific of the two detector molecules.

5.5.4. Reaction Time Course for Sulfite Detection

The time course for hydrolysis of **20** and **21** by sulfite was then examined (Figure 5.27). Notably, both detectors react at a rather slow rate. The fluorescence signal with **21** reached a plateau after about three hours of incubation, while a plateau in the signal of **20** was not obtainable even after six hours. Although a compound similar to **21** has been published as a real time detector of sulfite production(539), the results obtained here suggest that these molecules are only suitable for detection of sulfite in an end point assay.

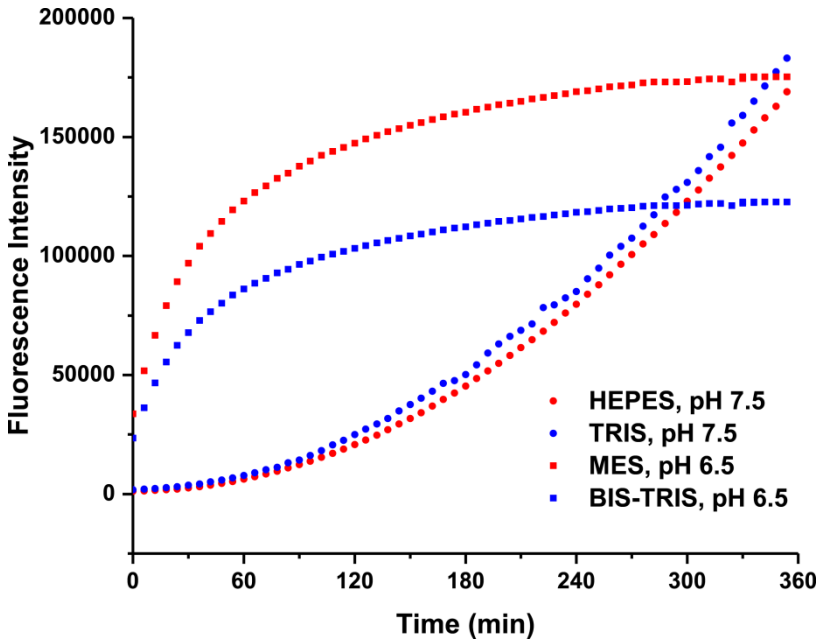

Figure 5.27: Time course for the sulfite induced hydrolysis of detectors 20 (circles) and 21 (squares) in their optimum buffer systems. The rate of hydrolysis of 21 is significantly faster than that of 20. Detectors were employed at a concentration of 1 mM and were activated through the addition of 100 mM sodium sulfite. All buffers were used at a concentration of 25 mM. Measurements were carried out at 25 °C and pH 7.5. Buffers were used at a concentration of 25 mM.

Despite the slow reaction of **20** and **21**, both molecules were able to give a fluorescence readout that was suitably linear with sulfite concentration, after six and three hours incubation, respectively (Figure 5.28).

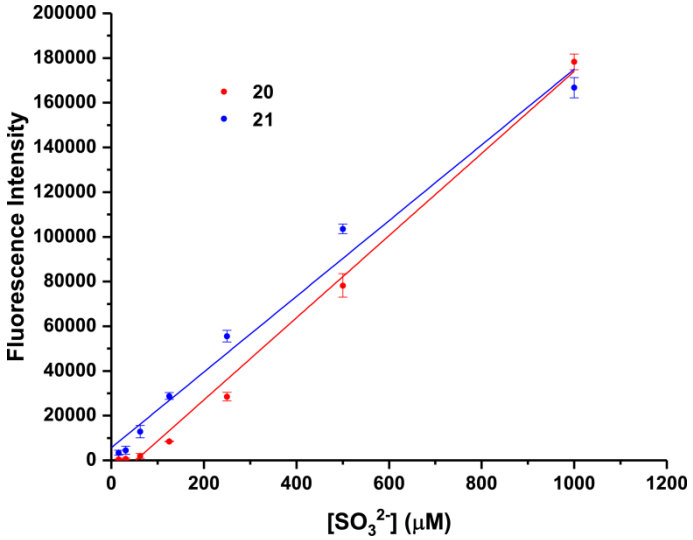

Figure 5.28: Fluorescence intensity of sulfite detectors 20 (red) and 21 (blue) with varying concentration of added sulfite. Detectors were employed at a concentration of 1 mM. Fluorescence measurements were acquired after six and three hours of incubation with sulfite for detectors 20 and 21, respectively. Incubation and measurements carried out at 25 °C and pH 7.5.

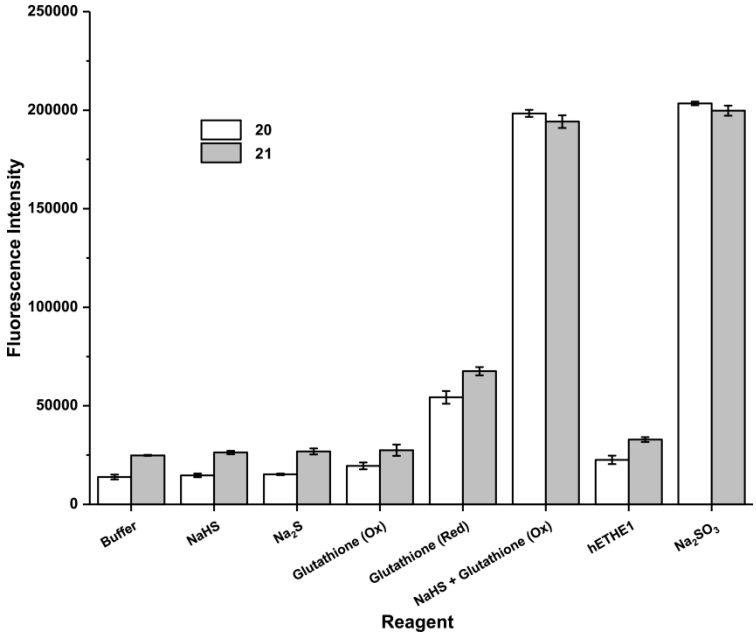

Figure 5.29: Hydrolysis of sulfite detectors 20 (white) and 21 (grey) by components of the ETHE1 enzymatic assay and the glutathione persulfide reaction mixture (NaHS & glutathione (Ox)). The persulfide mixture produces a similar fluorescence intensity to that seen with sulfite ions. Detectors were employed at a concentration of 1 mM and potential activators at 100 mM (hETHE1 was used at 100 μM). Measurements were carried out at 25 °C and pH 7.5.

5.5.5. Interference of Reaction Components

Despite encouraging results with the two synthesis sulfite detectors, attempts to use them to detect sulfite in a rudimentary enzyme assay met with failure. It was identified that, where hydrolysis was encouraged slightly by glutathione, it was much more extensive with glutathione persulfide, perhaps on account of the greater nucleophilicity of the substrate molecule (Figure 5.29). While individual reaction components did not induce significant hydrolysis of **20** and **21**, a strong fluorescence signal was seen with the glutathione persulfide reaction mixture, which was comparable to the signal induced by the addition of sulfite ions alone. Further work would need to be carried out in order to ascertain the reason for this, and whether it might be possible to avoid it.

5.6. Discussion

In this study three active homologues of ETHE1, those from human, *B. cepacia* and *M. xanthus*, were successfully produced and purified. Two sulfite detectors based on levulinate ester deprotection were produced and demonstrated to be selective for the detection of sulfite ions via fluorescence readout. Unfortunately, this selectivity did not extend to the substrate of the ETHE1 reaction, which appears to encourage the hydrolysis of both reporters with an efficiency comparable to sulfite ions. Thus, the attempt to develop a novel assay for ETHE1 via sulfite detection has been unsuccessful in this case. Despite this, the measured selectivity of **20** and **21** for sulfite over most other ions is encouraging, and more methods of sulfite detection, such as the anthracene based molecule shown in Figure 5.10, should be explored in case selectivity for sulfite over glutathione persulfide can be achieved. The need for robust ETHE1 assay with a moderate level of throughput remains. But with further exploration of sulfite detection may not be an unachievable goal. In the future, similar attempts at assay development with other known hMBLs may help to expedite the production of low toxicity inhibitors of the 'true' MBLs, a need that will only increase with the increased spread of MBL mediated antibiotic resistance(228).

ETHE1 itself is unique among the MBL fold enzymes on account of its mononuclear iron centre and non-haem oxygenase activity(218, 220). The production and purification of three homologues, as described in this chapter, should help to facilitate further studies into the, no doubt interesting, mechanism of ETHE1 and, more generally, its role in sulfur metabolism, a field ripe for exploration.

Chapter 6: Summary and Discussion

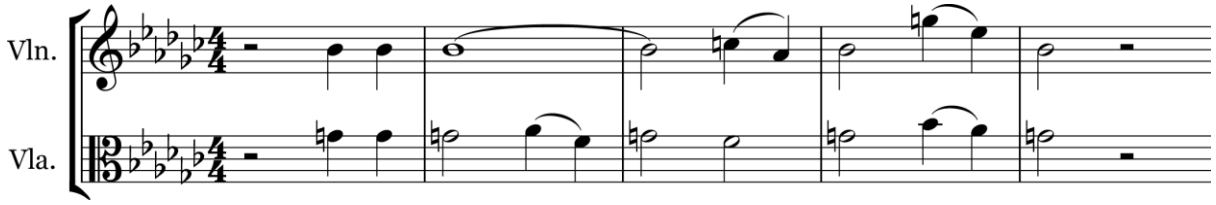

- *Dmitri Shostakovich*

Contents

The β-lactamases constitute one of the most prevalent methods of bacterial resistance to the β-lactam antibiotics(243). These enzymes are broadly divided into two mechanistic subclasses, the serine-β-lactamases (SBLs) and the metallo-β-lactamases (MBLs)(149, 216). Collectively, the β-lactamases are able to hydrolyse all classes of β-lactam antibiotics and their dissemination threatens the future clinical use of these widely utilised antibacterials(140). The MBLs are particularly worrisome on account of their ability to hydrolyse carbapenems(215), typically referred to as antibiotics of last resort, and the lack of any clinically available inhibitors of these enzymes(304).

Continued structural and mechanistic study of both the SBLs and the MBLs will, no doubt, aid in the development of inhibitors. In particular, shared mechanistic features provide the potential for dual action SBL/MBL inhibitors, which will likely prove useful in the future, as resistance mediated by the simultaneous production of SBLs and MBLs by a single bacterium continues to grow.

6.1. Use of Ferrous Iron by Metallo-β-Lactamases

The promiscuous binding of transition metals by the MBLs, either during purification or upon deliberate metal exchange is well documented(285, 327, 334). Previous work on the characterisation of iron bound MBLs has suggested that this particular metal does not support catalytic activityof MBLs(328). The results in Chapter 2, however, reveal that the class B1 metallo-β-lactamases are active when their native Zn(II) ions are replaced by Fe(II) ions, at least under low oxygen conditions(326). The differences between the results in Chapter 2 and previous reports likely stem from oxidation to the ferric iron state in those experiments.

Fe(II) bound *Bacillus cereus* β-lactamase II (BcII) and Verona integron-encoded metallo-β-lactamase 2 (VIM-2) are able to hydrolyse both nitrocefin and meropenem with similar catalytic efficiencies to the purified zinc(II) bound counterparts. The hexaaqua complexes of both Zn(II) and Fe(II) have highly comparable pKa values, 9.46 and 9.51, respectively(356), suggesting that their ability to provide a hydroxide nucleophile for β-lactam hydrolysis as well as a bound water as a proton source should be very similar. This would lend credence to both zinc(II) and iron(II)-bound MBLs exhibiting β-lactamase activity.

A crystal structure of BcII bound to ferrous ions shows only minor changes in the active site geometry. Indeed, the lack of substantial changes in the active site upon metal substitution may be a reason for the comparable activity of the differently metallated forms. The distance between the metal ion in the 3H site is shorter in the case of Fe(II) when compared to a native Zn(II)-bound structure, which suggests that the bridging water may be

bound more tightly to the Fe(II)-complexed enzyme. This would likely give rise to a poorer nucleophile, and hence one might expect a more poorly catalysed reaction with Fe(II)-BcII for this reason. The apical water, which likely acts a proton source in the hydrolysis, is also bound tighter in the di-Fe(II) enzyme. Despite their comparable pKa values in solution, this reduced metal-water distance in the case of Fe(II) might suggest that the pKa of the apical water is lower than in the Zn(II)-bound enzyme. This would lead to a faster protonation and hence a faster cleavage of the C-N bond during the hydrolysis. In the case where C-N bond cleavage and protonation were concurrent and rate limiting, the increased acidity of the Fe(II)-bound water would likely result in a more active enzyme than the native di-Zn(II) enzyme, especially at lower pH. Further studies of b-lactam hydrolysis under steady-state conditions and at different pH may shed further light on this matter.

Stopped-flow kinetics revealed that changes in active site metal, in this case the substitution of Zn(II) for Fe(II), can induce a change in the enzyme mechanism, despite little change in overall catalytic efficiency. With BcII, substitution of zinc(II) for iron(II), allowed an anionic intermediate to be observed in nitrocefin hydrolysis. The appearance of an anionic intermediate with di-Fe(II) BcII might be precedented by the difference in the reduction potentials of Zn(II) and Fe(II). The reduction of Fe(II) to its metallic form has a standard electrode potential of -0.44 V versus -0.763 V for Zn(II)(407). The difference in reduction potentials suggests that Fe(II) will accept electron donation (either complete or partially through ligation) more readily than Zn(II). Thus the stabilisation of an anionic intermediate with Fe(II) is likely greater than with Zn(II), leading to a longer lifetime of this species in the di-Fe(II) BcII catalysed reaction, and hence the ability to detect it. The opposite effect was, however, seen with VIM-2, where a detectable anionic intermediate with di-Zn(II) VIM-2 was lost with di-Fe(II) VIM-2. This observation is harder to explain and may simply come as a result of the enzyme employed – mutagenesis studies have demonstrated the appearance of an anionic species can be dependent, for example, on the identity of an active site loop(262). Thus, the particular, mechanistic impact of a metal substitution, at least with the MBLs, appears to depend on the particular enzyme being studied; this result is not too surprising given the sequence and structural variation among MBLs, even in the same subclass(215).

A potentially important result obtained in this chapter was the observation that in some, but not all cases, it is possible for an inhibitor to behave differently with Zn(II)- and Fe(II)-substituted MBL. Thus, the potent inhibitor **ML302F**(318) exhibited a higher IC_{50} against Fe(II) substituted BcII than against Zn(II) substituted BcII. Zinc is often described as a thiophile(541), so it is, perhaps, unsurprising that ML302F binds more tightly to di-Zn(II) BcII and has a greater inhibitory activity. Although not necessarily in its ferrous form, iron represents a metal ion with comparatively high bioavailability(542, 543). Thus, if iron bound

MBLs represent even a small population of enzymes produced by resistant bacteria, it may be prudent to test MBL inhibitors that are in clinical development against both Zn(II) and Fe(II) bound MBLs, so as to identify inhibitors with potency against both metallated forms. Finally, given the known promiscuity of the MBL fold(327), it may be possible that substitution of zinc ions for other transition metals may alter catalytic properties in a manner relevant to the further development of resistance by these enzymes.

6.2. Cyclic Boronates Inhibit All Classes of β-Lactamase

The inability of the MBLs to hydrolyse the monobactam aztreonam, has led the utility of the combination of aztreonam with avibactam. Avibactam is a more recent clinical inhibitor of Ambler class A, C, and some class D SBLs and, thus, can potentiate the use of aztreonam against resistant bacteria producing SBLs(154, 203), while the lack of aztreonam hydrolysis by MBLs allows it to bypass them in the treatment of MBL mediated resistant infections(372). However, the observation the MBLs are able to bind and hydrolyse avibactam, albeit slowly, jeopardises the future use of this β-lactam-inhibitor combination(207), particularly since continued use will likely contribute to the selection pressure for improved avibactam hydrolysis by MBLs. As a result, the development of dual action inhibitors of both the SBLs and MBLs would likely be a clinical boon.

In Chapter 3, studies on a collection of five cyclic boronates, which show inhibitory activity against all four Ambler classes of β-lactamase, including both SBLs and MBLs, are presented. Targets include clinically important B1 MBLs, such as New Delhi metallo-β-lactamase 1 (NDM-1), VIM-2, and MBL imipenemase 1 (IMP-1), the class A extended spectrum β-lactamase (ESBL), cefotaxime hydrolase from Munich 15 (CTX-M-15), and two oxacillinase (OXA) carbapenemases, OXA-23 and OXA-48. Potency against the B2 MBL, carbapenem hydrolase from *Aeromonas maltophilia* (CphA), and the OXA enzymes was not as high as against the other tested enzymes, suggesting that further optimisation of the scaffold is required. However, activity against both the SBLs and MBLs shows that this chemotype represents a useful starting point in the development of broad spectrum SBL/MBL inhibitors.

Crystal structures of the cyclic boronates in complex with representative enzymes from each Ambler class demonstrate that these compounds bind to the β-lactamases in a ring closed state with a tetrahedral anionic boron centre. The conformation of the fused bicyclic boronate ring system is remarkably conserved in all cases, with only minor changes seen in the conformation of the acetamido side chain. The observation of a closed boron ring system in all structures supports the proposal that the cyclic boronates inhibit both SBLs and MBLs by mimicking the first tetrahedral anionic intermediate in β-lactam hydrolysis.

Testing of cyclic boronate **2** against clinically resistant bacterial strains demonstrated that the cyclic boronates can potentiate the activity of all four classes of β-lactam against Gram-negative clinical isolates, with reduction in minimum inhibitory concentrations (MICs) seen against bacteria producing as many as six different β-lactamases. Further screening against multiple MBL producing isolates showed that supplementation with **2** could achieve around a 60% susceptibility rate. Thus, the cyclic boronates represent a promising class of compounds in treating bacterial infections with resistance mediated by both SBLs and MBLs. Further chemical development of this scaffold should help to increase the breadth of targets as well as increase potency against already susceptible β-lactamases.

6.3. Further Inhibitors Targeting Serine and Metallo-β-Lactamases

With the cyclic boronates inhibiting both SBLs and MBLs through mimicking of a common mechanistic intermediate, other inhibitors of the MBLs thought to behave as, for example, substrate or product mimics might also find utility in the inhibition of SBLs.

The work described in Chapter 4 explored four such instances where compounds identified as MBL inhibitors show some degree of activity against the SBLs. The classes of compound include the squaramides, thiol carboxylates, thioenolates, and indole carboxylates. The thiol carboxylates and thioenolates are likely candidates for MBL inhibition (both possessing free thiols). However, the squaramides and indole carboxylates perhaps represent more interesting chemotypes for MBL inhibition.

While squaric acid has pKa values of 0.54 and 3.58 for its two deprotonation events(485), squaramides are a little less acidic, with typical pKa values of between 5 and 10, depending on their substitution(544). Those towards the lower end of this range do still, however, have the ability to exist as a mono- or dianion in aqueous solution. This is the likely origin of their inhibition of MBLs, since the anionic form is a suitable chelating agent for binding to the active site zinc ions. Use of squaramides as mimics of phosphate may suggest, however tenuously, a mechanism for SBL inhibition, since there are numerous reports of SBLs crystallising with bound phosphate ions(545-547) and a recent report has characterised a phosphate binding site in BlaC for *M. tuberculosis* that may play a role in substrate/inhibitor recognition(545).

The indole carboxylates are, perhaps, unique among MBL inhibitors identified to date on account of their unusual binding mode. The ability of these molecules to inhibit the MBLs without displacing the bridging hydrolytic water – a feature common to the vast majority of MBL inhibitors – is highly novel and demonstrates that there is still scope for finding new chemotypes to inhibit even the most well studied of enzymes. In particular the identification of the indole carboxylate inhibitors highlights the use of library screening,

either through activity assays or crystallographically, is still a useful source of new leads against old targets.

While in each case activity is greater *versus* the MBLs compared to the SBLs, these results illustrate a variety of chemical scaffolds with the potential for development as dual inhibitors. Should further attempts to structurally characterise any of these compound classes in complex with a SBL prove successful, it would be interesting to investigate whether their interactions with SBLs do, indeed, mimic any possible intermediate species in catalysis, and, thus, whether their potency against both SBLs and MBLs is mechanistically derived.

6.4. Towards a Fluorescent Assay for ETHE1

Despite lending their name to the conserved structure, the MBL fold enzymes with β-lactamase activity constitute only a subsection of a much larger MBL superfamily(216), with members exhibiting activities ranging from small molecule hydrolysis(222) to DNA/RNA processing(226, 227) and oxidoreductase reactions(220, 337). Human MBL fold enzymes represent potential off pathway target for inhibitors of the 'true' MBLs, on account of their similar protein folds and active site architectures(217). As a result, the study of human MBL fold enzymes, and the development of assays with utility in the screening of potential inhibitors, will likely expedite the identification and optimisation of clinically useful 'true' MBL inhibitors.

Ethylmalonic encephalopathy 1 (ETHE1) is one such human MBL fold protein, which has a unique mono iron active site and persulfide dioxygenase activity(218, 220). Since ETHE1 functions in the metabolic removal of toxic hydrogen sulfide(533), and ETHE1 gene knockouts are known to result in highly debilitating symptoms and early death(218), the ability to remove ETHE1 inhibitors from identified hits against the 'true' MBLs would, no doubt, prove useful.

The work in Chapter 5 details the cloning and production of three ETHE1 homologues from human, *Myxococcus xanthus*, and *Burkholderia cepacia*. Preliminary oxygen consumption assays demonstrated the three purified enzymes to be active, while attempts at crystallisation have, to date, produced no notable results. Attempts were made to develop an assay for ETHE1 based on the fluorescent detection of sulfite. Two sulfite detector molecules, levulinic acid protected fluorophores, were synthesised and their utility in developing such an assay was explored. While both molecules demonstrated the generation of a fluorescent signal on exposure to sulfite, interference with a component of the ETHE1 substrate mixture suggests that these particular detectors may not be useful in this context. However, the ability to detect and titrate sulfite with these molecules is encouraging and suggests that further exploration of reported sulfite detectors may yet provide fruit in the development of a high throughput ETHE1 assay.

Chapter 7: General Methods

Contents

7.1. Sourcing of Materials

Where possible, and unless otherwise stated, all materials were obtained from Sigma-Aldrich Ltd., New England Biolabs, or Invitrogen at the highest purity available. Bacto tryptone, yeast extract and agar for cell growth media and antibiotic plates were obtained from Fisher Scientific Ltd. Isopropyl β-D-1-thiogalactopyranoside (IPTG) was obtained from Apollo Scientific Ltd.

Milli-Q water refers to water purified using a Millipore Elix Reverse Osmosis system followed by filtration through a 0.22 μm Millipore Milli-Q filter.

7.2. Competent Cells

The following strains of *E. coli* cells were used for cloning and protein expression:
XL10-GOLD competent cells
BL21(DE3)
BL21(DE3)pLysS
Rosetta-gami 2

7.3. pH Measurement for Buffer Solutions

The pH of solutions was determined using a Jenway pH Meter 3305, with an Aldrich glass/calomel combination electrode. Calibration was carried out prior to all measurements with buffer solutions of phthalate (pH 4.0), phosphate (pH 7.0) and borate (pH 10.0) (Fisher Scientific), with the former two used for calibration in the range of 4.0-7.0, and the latter two in the range of 7.0-10.0. Electrodes were stored in a 4 M saturated potassium chloride solution when not in use.

7.4. Centrifugation of Samples

Samples with a volume less than 1.5 mL, and suitable for handling room temperature, were centrifuged using a 1-14 microfuge (Sigma). Samples with a volume less than 1.5 mL requiring cold handling were centrifuged using a Microfuge 22R bench top centrifuge (Beckman Coulter Ltd.) at 4 °C. Pelleting of small scale cell growth cultures and protein concentration was performed using a Beckmann Allegra X-30R at 4 °C. Large scale cell growth cultures and cell lysates were centrifuged in a Beckmann Avanti J-25 at 4 °C.

7.5. 1000x Antibiotic Stocks for Cell Growth and Agar Plates

For ampicillin or kanamycin stocks, 500 mg or 340 mg, respectively, of antibiotic was dissolved in 10 mL Milli-Q water and the resultant solution was passed through a 0.22 μM filter before storage as aliquots at -20 °C. For chloramphenicol, 340 mg of antibiotic was dissolved in 10 mL of ethanol and stored as aliquots at -20 °C.

7.6. Media and Antibiotic Plate Preparation

7.6.1. Preparation of 2TY Medium

2TY Medium was made according to the following protocol. Solid components were dissolved in 900 mL of Milli-Q water and the pH was adjusted to 7.0 by addition of 1 M NaOH. The solution volume was then adjusted to 1 L before autoclaving.

Reagent	Mass
Bacto tryptone	16 g
Bacto yeast extract	10 g
Sodium chloride	5 g

7.6.2. Preparation of Auto-Induction Medium

Auto-Induction Medium was made according to the following protocol. 50x Salt and Sugar Solutions were placed in a water bath at 50 °C to ensure all components were fully dissolved before preparing the medium. Solid components and Salt and Sugar Solutions were dissolved in 900 mL of Milli-Q water and the pH was adjusted to 7.0. The volume was then adjusted to 1 L and the solution autoclaved.

Reagent	Mass/Volume
Bacto tryptone	16 g
Bacto yeast	10 g
Sodium chloride	5 g
50x Salt Solution	20 mL
50x Sugar Solution	20 mL
1M Magnesium sulfate	2 mL

Auto-Induction Medium (50x Salt Solution Recipe)

50x Salt Solution was made according to the following protocol. Solid components were mixed and 900 mL of Milli-Q water was added. The solution was stirred while heating to allow the solids to dissolve before the volume was adjusted to 1 L. The solution was stored at 4 °C for future use.

Reagent	Mass
Sodium phosphate dibasic	177.5 g
Potassium phosphate monobasic	170 g
Ammonium chloride	134 g
Sodium sulfate	35.4 g

Auto-Induction Medium (50x Sugar Solution Recipe)

50x Sugar Solution was made according to the following protocol. Solid components were dissolved in 900 mL of Milli-Q water. The volume was adjusted to 1 L and the solution was stored at 4 °C for future use.

Reagent	Volume
Glycerol	250 g
Glucose	25 g
α-Lactose	100 g

7.6.3. Preparation of Terrific Broth (TB) Medium

TB Medium was made according to the following protocol. Powdered medium and glycerol were dissolved in 900 mL Milli-Q water. The volume was then adjusted to 1 L and the solution was autoclaved.

Reagent	Mass/Volume
TB Medium powder	47.6 g
Glycerol	8 mL

7.6.4. Preparation of LB Agar Medium

LB Agar Medium was made according to the following recipe. Solid components were mixed before the addition of 1 L of Milli-Q water. The mixture was then autoclaved and stored at room temperature for future use.

Reagent	Mass
Bacto agar	15 g
Bacto tryptone	10 g
Sodium chloride	10 g
Bacto yeast extract	5 g

7.6.5. Preparation of Luria-Bertani (LB) Agar Antibiotic Plates

LB Agar Medium was melted by microwaving before being cooling to 55 °C via incubation in a water bath. 1 mL of the required antibiotic stocks was added for every 1 L of cooled agar before pouring into petri dishes. Once set the plates were sealed with parafilm (Bemis) and stored at 4 °C, for up to one month, before use.

7.6.6. Preparation of Super Optimal Catabolite Repression (SOC) Outgrowth Medium

SOC Outgrowth Medium was prepared according to the following recipe. SOC medium was made fresh in sterile Eppendorf tubes when required.

Reagent	Volume
2TY Medium	970 µL
2 M glucose (sterile)	20 µL
1 M Magnesium chloride (sterile)	10 µL

7.7. SDS-PAGE Electrophoresis

7.7.1. SDS-PAGE Gel Preparation

SDS-PAGE gels were made according to the following recipes. Polyacrylamide gels were made using the Mini-PROTEAN Tetra Cell system (Bio-Rad). In both running and stacking gel preparation, tetramethyleneethylenediamine (TEMED) was added as the last component. During production, the running buffer was covered with a layer of propan-2-ol to prevent it from drying out whilst setting. This was subsequently removed before pouring and setting of the stacking gel layer. SDS-PAGE gels were covered in wet tissue and stored at 4 °C until required.

Running Gel Recipe (Makes Four Gels)

Reagent	Volume
30% Bis-acrylamide	6.67 mL
Milli-Q water	5.06 mL
1.5 M Tris.HCl, pH 8.8	4 mL
10% (w/v) Ammonium persulfate	267 µL
10% (w/v) Sodium dodecyl sulfate	160 µL
Tetramethyleneethylenediamine	13.3 µL

Stacking Gel Recipe (Makes Four Gels)

Reagent	Volume
Milli-Q water	3.05 mL
0.5 M Tris.HCl, pH 6.8	1.25 mL
30% Bis-acrylamide	670 μL
10% (w/v) Sodium dodecyl sulfate	50 μL
10% (w/v) Ammonium persulfate	25 μL
Tetramethyleneethylenediamine	5 μL

7.7.2. Running of SDS-PAGE Experiments

20 μL of protein sample were mixed with 4 μL of SDS-PAGE Gel Loading Buffer. The samples were then heated at 100 °C on a hot block for 2 min before loading of up to 10 μL of each sample per well. Electrophoresis was carried out at a constant voltage of 160 V for 10 min followed by 180 V for 50 min using SDS-PAGE Running Buffer. Gels were subsequently stained for 10 minutes in SDS-PAGE Staining Solution and transferred into water. The gels were heated by microwaving until bands were visible before destaining overnight in water.

6x SDS-PAGE Gel Loading Buffer Recipe

6x SDS-PAGE gel loading buffer was made according to the following recipe. The components were combined and the solution was adjusted to 50 mL by addition of Milli-Q water. The final solution was stored at room temperature for future use.

Reagent	Mass/Volume
Sodium dodecyl sulfate	6 g
Dithiothreitol	4.65 g
Bromophenol blue	30 mg
Glycerol	23.5 mL
1 M Tris.HCl, pH 6.8	3 mL

10x SDS-PAGE Running Buffer Recipe

10x SDS-PAGE running buffer was made according to the following recipe. Components were dissolved in 900 mL before adjusting the final volume to 1 L. The solution was stored at room temperature for future use.

Reagent	Mass
Glycine	144 g
Tris base	30 g
Sodium dodecyl sulfate	10 g

SDS-PAGE Staining Solution Recipe

SDS-PAGE staining solution was made according to the following recipe. The solution was stored in a foil-wrapped bottle, to protect it from sources of light, and kept at room temperature for future use.

Reagent	Mass/Volume
Coomasie brilliant blue G250	0.4 g
Milli-Q water	800 mL
Ethanol	50 mL
70% Perchloric acid	34 mL

7.8. Cloning

7.8.1. Primers for Generation of ETHE1 Homologue Constructs

Construct	Primer Name	Primer Sequence	T_m (°C)
hETHE1-pCold	hETHE1_pC_Fw	CCCGGGGTCGACGCACCGATTCTGCTGCG	74
	hETHE1_pC_Rv	CCCGGGGCGGCCGCTTATGCGGTCGGGG	78
MxETHE1-pCold	MxETHE1_pC_Fw	CCCGGGGTCGACCTGTTTCGTCAGC	69
	MxETHE1_pC_Rv	CCCGGGGCGGCCGCTTAATGGGTAAAGC	72
BcETHE1-pCold	BcETHE1_pC_Fw	CCCGGGGTCGACATTTTTCGCCAGC	68
	BcETHE1_pC_Rv	CCCGGGGCGGCCGCTTAACTACGACCATCC	74
N-His-MxETHE1-pET-22b	N_MxETHE1_p22b_Fw_1	CAGGGCCCGCTGTTTCGTCAGCTGTTTGATACC	70
	N_MxETHE1_p22b_Fw_2	TCTGGAAGTGCTGTTTCAGGGCCCGCTGTTTCGTC	72
	N_MxETHE1_p22b_Fw_3	CATATGCATCATCATCATCATCTGGAAGTGC	63
	N_MxETHE1_p22b_Rv	CCCGGGCTCGAGTTAATGGGTAAAGCTACC	67
C-His-MxETHE1-pET-22b	C_MxETHE1_p22b_Fw	CCCGGGCATATGCTGTTTCGTCAGCTGTTTG	68
	C_MxETHE1_p22b_Rv_1	CCTGAAACAGCACTTCCAGATGGGTAAAGCTAC	66
	C_MxETHE1_p22b_Rv_2	GATGATGATGATGCGGGCCCTGAAACAAGC	67
	C_MxETHE1_p22b_Rv_3	CCCGGGCTCGAGTTAATGATGATGATGATGATGC	67

7.8.2. Preparation of Primers

Oligonucelotide primers were designed using the ApE (A Plasmid Editor) application(548). Primers were purchased from Sigma-Aldrich Ltd. as lyophilised pellets. Before use, the oligonucleotides were resuspended in 0.22 μm filter sterilised Milli-Q water to produce 100 μM stock solutions. These were then diluted to 10 μM with filter sterilised Milli-Q water for use in polymerase chain reaction (PCR) experiments.

7.8.3. PCR Reactions

For production of hETHE1, MxETHE1 and BcETHE1 pCold constructs, gene inserts were amplified from synthetic DNA constructs by a single round of PCR. MxETHE1 with an *N*- or *C*-terminal hexahistidine tag in pET-22b were amplified from the same synthetic construct, but the amplicon was subsequently modified by additional rounds of PCR in order to add the coding sequence for the tag. *PfuTurbo* polymerase was obtained from Agilent Technologies. A typical PCR reaction was set up with the following mixture of components. PCR reactions were carried out using 100 ng of template DNA in a final volume of 50 μL. The final volume was achieved by addition of 0.22 μM filter sterilised Milli-Q water. The polymerase was added as the final component of the mixture.

Reagent	Volume (μL)
10x Reaction buffer	5
10 mM Forward primer	2.5
10 mM Reverse primer	2.5
50 ng/μL Plasmid DNA	2
10 mM dNTP mix	1
PfuTurbo polymerase	1
Milli-Q water	36

Annealing temperature was typically taken to be 5 °C below the lowest melting temperature of the two primers, as predicted by ApE software. The length of the ligation step was dictated by the size of the gene, typically 60 s kb^{-1} is employed.

	PCR Step	Temperature (°C)	Time (s)
25 Cycles	Melting	98	10
	Annealing	70	30
	Ligation	72	60 per kb template
	Final Extension	72	600
	Final Hold	4	-

7.8.4. Purification of Amplified DNA

Amplified DNA was purified using agarose gel electrophoresis. The gel was loaded with 6 μL GeneRuler 1 kb DNA ladder (Thermo Fisher Scientific). DNA samples were mixed with 6x Purple Loading Buffer (Thermo Fisher Scientific) and added to wells with a maximum volume of 20 μL. The agarose gel was run at 60 V for 10 min, followed by a further 30 min at 70 V. DNA bands were visualised by fluorescence under UV light, excised using a clean scalpel, and placed in sterile Eppendorf tubes. Extraction was carried out using a Gel

Extraction Kit (Thermo Fisher Scientific) and the provided protocol. Plasmid DNA was eluted into 30 μL of 0.22 μm filter sterilised Milli-Q water.

50x TAE Buffer Preparation

50x TAE Buffer was made according to the following recipe. Tris base and ethylenediaminetetraacetic acid (EDTA) were dissolved in 700 mL Milli-Q water before addition of acetic acid. The solution volume was then adjusted to 1 L and stored at room temperature until required.

Reagent	Volume/Mass
Tris base	242 g
Disodium EDTA	18.6 g
Glacial acetic acid	57 mL

Agarose Gel Preparation

Agarose gels were freshly prepared when required. Agarose gels were made using the Clarit-E horizontal electrophoreses system (Alpha Laboratories). 0.8 % agarose gels were prepared according to the following recipe. Solutions were microwaved to ensure that all agarose was solubilised. SYBR Safe was added once all agarose was dissolved. The resultant solution was poured into a mould using an 8x 20 μL well comb and protected from light while allowed to set.

Reagent	Mass/Volume
Agarose	0.4 g
TAE Buffer	50 mL
SYBR Safe stain	2 μL

7.8.5. DNA Digestion

DNA digestion was carried out in a reaction volume of 20 μl using sterile 1.5 mL Eppendorf tubes and 0.22 μm filter sterilised Milli-Q water. The restriction enzymes were dictated by the primer design. For pCold constructs, NotI and $SalI_{HF}$ were used, while for pET-22b constructs, NdeI and XhoI were used. Typically 1000 ng of plasmid vector, or insert, DNA were digested in a single reaction. Reaction components were mixed and the solution was incubated in a water bath at 37 °C overnight. Digested DNA was subsequently purified by agarose gel electrophoresis.

Vector Components	Volume (μL)
DNA (e.g. 200 ng μL^{-1})	5
Buffer	2
5' Restriction enzyme	1
3' Restriction enzyme	1
BSA	0.2
Milli-Q water	10.8

7.8.6. Plasmid Ligation

Plasmid ligation was carried out in a reaction volume of 20 μL. The digested insert was added to a 10x molar excess compared to the digested vector DNA. Reaction components were added without mixing. The reaction was left at room temperature for 48 h.

Component	Volume (μL)
Digested vector (e.g. 5 ng μL^{-1})	8
Digested insert (e.g. 20 ng μL^{-1})	4
10x Ligation buffer	2
T4 Ligase	1
Milli-Q water	5

7.8.7. Transformation of Competent Cells

XL10-Gold and BL21(DE3) competent cells were stored at -80 °C. The cells were thawed on ice before placing 50 μL of the cell suspension into a 50 mL falcon tube. 2-3 μL of the DNA ligation mixture/purified plasmid was added to the cells without mixing and the cells were left on ice for 30 min. The cells were then heat shocked by placing them in a water bath at 42 °C for 30-45 seconds followed by 2 min on ice. Subsequently, 250 μL of SOC outgrowth medium was added and the cells were placed in a shaker at 37 °C for 45 min with shaking at 200 rpm. After incubation, 250 or 200 μL of the cells, for XL10-Gold or BL21(DE3) respectively, were plated on an appropriate antibiotic-containing plate and incubated at 37 °C overnight. Once colonies were seen, plates were sealed with parafilm and stored at 4 °C.

7.8.8. Plasmid Purification

A single colony from a successful transformation was picked and grown overnight in 5 mL of 2TY medium, supplemented with the appropriate antibiotic(s), at 37 °C with shaking at 200 rpm. Plasmid DNA was purified from the culture using a Miniprep Kit (Qiagen) following the manufacturer's protocol. Successfully cloned constructs were confirmed by DNA sequencing (Source Bioscience).

7.8.9. Glycerol Stock Preparation

A single colony from a successful BL21(DE3) or Rosetta-gami 2 transformation was picked and grown overnight in 5 mL of 2TY medium, supplemented with the appropriate antibiotic(s), at 37 °C with shaking at 200 rpm. 800 μL of the overnight growth was mixed with 200 μL of sterile glycerol before freezing on dry ice and subsequent storage at -80 °C.

7.9. Starter Culture Production

An agar plate, supplemented with the appropriate antibiotic(s), was streaked with the glycerol stock and incubated at 37 °C overnight. A single colony was picked from the plate and grown in 100 mL 2TY medium supplemented with the same antibiotic. The flask was incubated at 37 °C overnight with shaking at 200 rpm.

7.10. Protein Production & Purification

7.10.1. Buffers for Protein Purification

Buffers for protein purification were made according to the following protocol. (Recipes provided bellow all correspond to 1 L of buffer). Components were dissolved in 900 mL of Milli-Q and the pH adjusted accordingly. The volume of the buffers was then adjusted to 1 L and the solutions were passed through a 0.22 μm filter to sterilise them. Buffers was stored at 4 °C until required.

BcII Lysis Buffer Recipe, pH 6.5

Reagent	Mass
MES	7.80 g
Zinc chloride	54.6 mg

BcII High Salt Buffer Recipe, pH 6.5

Reagent	Mass
Sodium chloride	58.4 g
MES	3.90 g
Zinc chloride	27.3 mg

HisTrap Buffer A Recipe, pH 7.5

Reagent	Mass
Sodium chloride	29.2 g
HEPES	11.9 g
Imidazole	341 mg

HisTrap Buffer B Recipe, pH 7.5

Reagent	Mass
Imidazole	34.0 g
Sodium chloride	29.2 g
HEPES	11.9 g

HisTrap Wash Buffer Recipe, pH 7.5

Reagent	Mass
Sodium chloride	29.2 g
HEPES	11.9 g
Imidazole	1.36 g

Gel Filtration Buffer Recipe, pH 7.5

Reagent	Mass
Sodium chloride	29.2 g
HEPES	11.9 g

Exchange Buffer Recipe, pH 7.5

Reagent	Mass
HEPES	5.96 g
Sodium chloride	5.84 g

IPTG Stock Solution Preparation

IPTG stock solutions were freshly made when required. 47.7 mg IPTG were dissolved in 1 mL of 0.22 μm filter sterilised Milli-Q water to give a 200 mM solution. The resultant solution was then filter sterilised in the same way. The filtered solution was kept on ice until required.

Iron(II) Stock Solution Preparation

Iron(II) stock solutions were made immediately before use. 19.6 mg ammonium iron(II) sulfate hexahydrate, $(NH_4)_2Fe(SO_4)_2.6H_2O$, were dissolved in 1 mL of 0.22 μm filter sterilised Milli-Q water to give a 50 mM solution. The resultant solution was then filter sterilised in the same way.

Zn(II) Stock Solution Preparation

28.8 mg zinc(II) sulfate heptahydrate, $ZnSO_4.7H_2O$, were dissolved in 1 mL of 0.22 μm filter sterilised Milli-Q water to give a 100 mM solution. The resultant solution was then filter sterilised in the same way.

7.10.2. Expression Trials for His-Tagged Enzymes

Six flasks, containing 100mL 2TY supplemented with ampicillin were inoculated with 1 mL of starter culture and incubated at 37 °C, with shaking at 180 rpm, until an OD_{600} of 0.5-0.6 was reached (typically around 2-2.5 h).

Flask No.	[IPTG] (mM)
1	0
2	0.01
3	0.1
4	0.25
5	0.5
6	1

The flasks were then cooled to 15 °C and the cells were induced IPTG stock solution to give the final concentrations listed in the table. The flasks were also supplemented with iron(II), 50 μM final concentration. The flasks were incubated at 15 °C overnight, with shaking at 180 rpm. 50 mL of cells from each flask were spun down (3750 rpm, 10 min, 4°C), the supernatant was removed, and the pellet was allowed to dry.

Cell pellets were resuspended in 2 mL of HisTrap Buffer A, supplemented with DNAse I (20 mg L^{-1}) and stored on ice. The resuspended cells were sonicated using a Vibra-Cell VCX 130 microtip sonicator (SONICS) at 25% Amplitude, 3 mins, 10 s on, 10 s off, while on ice. 1 mL of each sonicated sample was transferred to a 1.5 mL Eppendorf and the cell debris was spun down (10 min, 13000 rpm, 4 °C). 200 μL of nickel resin, equilibrated with HisTrap buffer A, was added to the supernatant of each sample. The samples were then mixed at 4 °C for 45 min. The samples were spun down (3 min, 2000 rpm, 4 °C) and the supernatant collected as 'flow-through'. The resin was resuspended in 600 mL of HisTrap Buffer A, the tubes were spun down (3 min, 2000 rpm, 4 °C), and the supernatant was collected as 'Wash 1'. This step was then repeated. The resin was resuspended in 600 μL of HisTrap Wash Buffer and then spun down as previously described. The supernatant was collected as 'Wash 2'. The resin was washed a second time in this manner. His-tagged enzyme was eluted by resuspending the resin in 100 mL of HisTrap Buffer B and mixing the samples for 10 min at 4 °C. Samples were spun down (3 min, 2000 rpm, 4 °C) and the

supernatant collected as the 'Eluent'. Eluent samples were analysed by SDS-PAGE to assess the level of expression.

7.10.3. Large Scale Cell Growth Procedures

Recombinant BcII protein was produced in *E. coli* BL21 (DE3)pLysS cells grown at 37 °C using 2TY medium supplemented with ampicillin and chloramphenicol, as previously reported(345). The cells were grown until an OD_{600} of 0.6–0.7 was reached and induced with 0.5 mM isopropyl β-D-1-thiogalactopyranoside (IPTG). The cells were grown for a further 4 h after induction. Cells were harvested by centrifugation (10 min, 10000 *g*).

Recombinant VIM-2 with an *N*-terminal His-tag was produced in *E. coli* BL21 (DE3)pLysS cells at 37 °C using 2TY medium supplemented with 50 μg mL^{-1} ampicillin and 50 μg mL^{-1} chloramphenicol, as previously reported(433). Cells were grown until an OD_{600} of 0.6 - 0.7 was reached. At this point the temperature was lowered to 30 °C and expression was induced with IPTG (0.5 mM final concentration). The cells were incubated for a further 4 h at this temperature. Cells were harvested by centrifugation (10 min, 10000 *g*).

Recombinant CTX-M-15, AmpC, OXA-23, OXA-48, and BlaC, each with an *N*-terminal His-tag, were produced in *E. coli* BL21(DE3) cells using auto-induction medium supplemented with 50 μg mL^{-1} ampicillin. Cells were grown for four hours at 37 °C before cooling to 18 °C and continuing growth overnight. Cells were harvested by centrifugation (10 min, 10000 *g*).

Recombinant hETHE1 and BcETHE1, each with an *N*-terminal hexahistidine tag, were produced in *E. coli* BL21(DE3) cells using 2TY medium supplemented with 50 μg mL^{-1} ampicillin. Cells were grown until an OD_{600} of 0.6 - 0.7 was reached. At this point the temperature was lowered to 15 °C and the cultures were supplemented with ammonium iron(II) sulfate hexahydrate (50 μM final concentration) and IPTG (10 μM final concentration). The cells were incubated overnight and harvested by centrifugation (10 min, 10000 *g*).

Recombinant MxETHE1, with a *C*-terminal hexahistidine tag, was produced in *E. coli* BL21(DE3) cells using 2TY medium supplemented with 50 μg mL^{-1} ampicillin. Cells were grown until an OD_{600} of 0.6 - 0.7 was reached. At this point the temperature was lowered to 18 °C and the cultures were supplemented with ammonium iron(II) sulfate hexahydrate (50 μM final concentration) and IPTG (10 μM final concentration). The cells were incubated overnight and harvested by centrifugation (10 min, 10000 *g*).

7.10.4. BcII Purification

10 g of cell pellet were resuspended in 50 mL BcII Lysis Buffer, supplemented with DNase I and phenylmethylsulfonyl fluoride (PMSF, each 2 mg L^{-1} final concentration), and then lysed by sonication using a Vibra-Cell VCX 500 sonicator (SONICS, 10 min, 60% amplitude, 10 s pulse, 10 s rest). The lysate was loaded onto an SP-sepharose column (1.5 × 12 cm with a 25 mL bed volume), which had been pre-equilibrated with BcII Lysis Buffer. Bound proteins were eluted with a gradient of BcII High Salt Buffer in BcII Lysis Buffer (0-1 M NaCl). The purity of the fractions was determined using SDS-PAGE analysis and those fractions containing highly purified BcII (>95 % pure by SDS-PAGE) were concentrated by centrifugal ultrafiltration using an Amicon Ultra 15 mL centricon with a 10 kDa molecular weight cut off (Millipore). Concentrated BcII was rediluted into 50 mL BcII Lysis Buffer and purified a second time on the SP Sepharose column using the same protocol. Fractions containing purified BcII were concentrated by centrifugal ultrafiltration.

7.10.5. Hexahistidine Tagged Enzyme Purifications

20 g of VIM-2, CTX-M-15, AmpC, OXA-23, OXA-48, BlaC, hETHE1, MxETHE1a or BcETHE1 pellet were resuspended in 100 mL HisTrap Buffer A, supplemented with DNAse I and PMSF (2 g L^{-1} final concentration), and lysed by sonication using a Vibra-Cell VCX 500 sonicator (SONICS, 10 min, 60% amplitude, 10 s pulse, 10 s rest). The supernatant was loaded onto a 5 mL HisTrap HP column followed by extensive washing with HisTrap Buffer A before elution with a gradient of HisTrap Buffer B in HisTrap Buffer A (20-500 mM imidazole). Fractions containing purified enzyme were concentrated by centrifugal ultrafiltration using an Amicon Ultra 15 mL centricon with a 10 kDa molecular weight cut off (Millipore). The resultant solution was injected onto a Superdex S200 column (300 mL), pre-equilibrated with Gel Filtration Buffer, and eluted with an additional 300 mL of Gel Filtration Buffer. Fractions containing pure hexahistidine tagged enzyme were incubated overnight at 4 °C with Hexahistidine tagged 3C protease (1:100 w/w) to remove the *N*-terminal hexahistidine tag. The 3C protease together with any uncleaved protein was removed from the digestion mixture with a second 5 mL HisTrap HP column, pre-equilibrated with HisTrap Wash Buffer. Purified enzyme fractions, identified by SDS-PAGE analysis, were collected and concentrated by centrifugal ultrafiltration before buffer exchange into Exchange Buffer.

7.10.6. Protein Concentration Measurements

Protein extinction coefficients were determined from the amino acid sequence using the ExPASy Protparam online application (http://www.expasy.org/). Concentrations of enzymes were determined using a NanoDrop ND-1000 spectrophotometer (Thermo Scientific).

Protein	M_r (kDa)	ε (M^{-1} cm^{-1})
BcII	24.95	29450
VIM-2	25.67	31400
CTX-M-15	28.26	25440
BlaC	28.53	29910
AmpC	40.83	61310
OXA-23	28.3	43430
OXA-48	28.3	63940
hETHE1	26.15	7450
MxETHE1	26.33	8940
BcETHE1	38.66	40910

7.11. Production of Apo-Enzymes

Apo-BcII, apo-VIM-2 and apo-ETHE1 homologues were generated using an adaptation of a previous method(327). Solutions of purified enzyme were placed in 3 or 0.5 mL Slide-A-Lyzer Dialysis Cassettes (Thermo Scientific) for dialysis. Enzyme solutions were dialysed against three changes of >100 volumes of an EDTA-containing solution (10 mM HEPES, 200 mM NaCl, 20 mM EDTA, 2 mM TCEP.HCl, pH 7.5) over 24 hours. EDTA was removed by a second dialysis of three changes of >100 volumes of a metal-free solution (50 mM HEPES, 100 mM NaCl, 2 mM TCEP.HCl, Chelex 100, pH 7.5) over 24 hours. All dialyses were carried out at 4 °C. After dialysis, the concentrations of the apo-enzymes were determined using a NanoDrop spectrophotometer, as previously described.

7.12. Denaturing Mass-Spectrometry

Molecular masses of purified proteins were verified by denaturing mass spectrometry. Data were collected using an LCT Premier mass spectrometer (Waters) coupled to an Agilent 1100 Series HPLC using a Chromolith® FastGradient RP-18 endcapped column equipped with a 50-2 monolithic silica HPLC column (C18, 2 x 50 mm, 1.6 µm diameter macropores, Merck). Samples were diluted to 0.01 mg mL^{-1} before injection via a CTC-autosampler inlet system. Proteins were separated using a multi-step gradient over 10 min (Solvent A 94.9% (v/v) H_2O, 5% (v/v) CH_3CN, 0.1% (v/v) formic acid; Solvent B 99.9% (v/v) CH3CN, 0.1% (v/v) formic acid; 0-1 min 5% B, 1-5 min linear gradient to 100% B, 5-8 min 100% B, 8-10 min linear gradient to 5% B) with a flow rate of 0.4 mL min^{-1}. The ionisation source used a capillary voltage of 3.2 kV and cone voltage of 25 V. Nitrogen was used as the nebulizer and

desolvation gas at a flow rate of 600 L $hour^{-1}$. Calculated masses were determined from amino acid sequence using the ExPASy Protparam online application (http://www.expasy.org/).

7.13. Native Mass-Spectrometry

Enzymes were buffer exchanged into 15 mM ammonium acetate, pH 7.5, using Bio-Spin 6 columns (Bio-Rad) and diluted to 100 μM before measurements. Native mass-spectrometry data were acquired using a Q-TOF micro mass spectrometer (Waters) interfaced with a NanoMate (Advion Biosciences). Experiments utilised a chip voltage of 1.7 kV and a delivery pressure 3.45 kPa. The sample cone voltage was 50 V with a source temperature of 100 °C. The pressure at the interface between the atmospheric source and the high vacuum region was fixed at 6.30 mbar. Calibration and sample acquisition were performed in the positive ion mode in the range of 500-5,000 *m/z*. Data were processed using MassLynx 4.0 (Waters).

7.14. Preparation of Deoxygenated & Oxygen Saturated Solutions

To prepare O_2 free solutions, samples were deoxygenated by repeated rounds of vacuum/argon purging, then sealed with a rubber septum and parafilm. To prepare O_2 saturated solutions, samples were subjected to rounds of vacuum/oxygen purging.

7.15. X-ray Crystallography

7.15.1. Broad Screen and Optimisation Conditions

Broad screen and optimisation crystal solutions were stored as 96 well blocks in 96 well polypropylene V-bottomed Masterblocks (Greiner Bio One) with 2 mL of each solution per well. These blocks were sealed with Starseal aluminium foil sealing tape (Starlab) and stored at 4 °C.

7.15.2. Crystallisation Experiments

Protein solutions for crystallisation ranged between 10 and 40 mg mL^{-1} in concentration. Crystal plates were set up using a Phoenix/RE instrument (Art Robbins Instruments) equipped with a 96 syringe head and a single nano dispenser. Crystallisation experiments were set up in 96 well Intelli-Plates (Art Robbins Instruments) with three sitting drop experiments per condition. Plate reservoirs were filled with 80 mL of crystallisation condition solution with sitting drop experiments with crystallant:protein solution ratios of 0.1:0.2, 0.1:0.1, and 0.2:0.1 μL. The plates were sealed with Starseal advanced polyolefin film (Starlab)

7.15.3. Crystal Fishing

Cryoprotection solutions were made as 20%, by volume, glycerol in reservoir solution. Crystals were soaked in cryoprotection solution, fished using pin-mounted nylon loops (Hampton Research) and flash frozen in liquid nitrogen. Frozen crystals were stored in cryo vials (Hampton Research) under liquid nitrogen until required for diffraction experiments.

7.15.4. X-ray Diffraction Data Collection and Data Processing

Data were collected both in house and at the Diamond Light Source synchrotron. Data collected in house were integrated, scaled, indexed and merged using HKL-3000. Synchrotron data were processed using the CCP4i2 pipeline(549).

7.15.5. Structure Refinement

All structures were solved by molecular replacement using Phaser(550). Models were generated using iterative rounds of refinement in Phenix Refine(362) and model building in Coot(363).

7.15.6. Structure Deposition

Models and density maps of refined structures were deposited to the PDBe structural database.

7.16. Steady-State Kinetic Assays

7.16.1 Buffers for Steady-State Kinetic Assays

Buffers for steady-state kinetic assays were made according to the following protocol. (Recipes provided below all correspond to 1 L of buffer). Components were dissolved in 900 mL of Milli-Q and the pH adjusted accordingly. The volume of the buffers was then adjusted to 1 L and the solutions were passed through a 0.22 μm filter to sterilise them. Buffers were stored at 4 °C until required.

MBL Assay Buffer, pH 7.5

Reagent	Mass/Volume
HEPES	11.92 g
10 mg mL^{-1} BSA	100 μL
Triton X-100	100 μL
100 mM $ZnSO_4.7H_2O$	10 μL

CphA Assay Buffer, pH 6.5

Reagent	Mass
MES	2.93 g

SBL Assay Buffer, pH 7.2

Reagent	Mass/Volume
Phosphate buffer powder	17.19 g
Triton X-100	100 μL

OXA Assay Buffer Recipe

Reagent	Mass/Volume
Phosphate buffer powder	17.19 g
1 M $NaHCO_3$	50 mL
Triton X-100	100 μL

7.16.2. Nitrocefin/Meropenem Steady-State Kinetic Assays

Nitrocefin (Toku) was stored as a 100 mM solution in dimethyl sulfoxide (DMSO). Meropenem (Molekula Ltd.) was diluted directly into assay buffer as a 100 mM solution when required. Absorbance measurements were made using a PHERAstar multi-mode plate reader (BMG Labtech). All assays were carried out at 25 °C. Absorption assays were carried out using UV-star 96 well format μclear® transparent plates (Greiner Bio-One) with a final assay volume of 200 μL. Kinetics of nitrocefin and meropenem hydrolysis were followed by absorption at 485 or 295 nm, corresponding to hydrolysed nitrocefin formation or depletion of meropenem, respectively. The optimum concentration of enzyme for steady-state measurements was determined by examining the rate of substrate hydrolysis at varied concentrations of enzyme, with the concentration at which the initial rate remained constant for 5-10 min being selected as an appropriate enzyme concentration. Initial rates of substrate hydrolysis were determined at varying substrate concentrations. Steady-state kinetic parameters were determined by fitting of initial rates to the Michaelis-Menten equation using GraphPad Prism 5 software(347).

7.16.3. FC5 Steady-State Kinetic Assays

FC5 was stored as a 2.5 mM solution in assay buffer supplemented with 10 % (v/v) DMSO. Fluorescence measurements were made using a PHERAstar multi-mode plate reader (BMG Labtech). All assays were carried out at 25 °C. Fluorescence assays were carried out using black 96 well format half area μclear® plates (Greiner Bio-One) with a final assay volume of 100 μL. FC5 hydrolysis was followed by fluorescence (λ_{ex} = 380 nm, λ_{em} = 460 nm) corresponding to the release of the umbelliferone fluorophore. The optimum concentration of enzyme for steady-state measurements was determined by examining the rate of substrate hydrolysis at varied concentrations of enzyme, with the concentration at which the initial rate remained constant for 5-10 min being selected as an appropriate enzyme concentration. Initial rates of substrate hydrolysis were determined at varying substrate concentrations. Steady-state kinetic parameters were determined by fitting of initial rates to the Michaelis-Menten equation using GraphPad Prism 5 software(347).

7.17. Inhibition Assays

Inhibition assays were performed by monitoring the initial rate of FC5 hydrolysis via fluorescence at a range of inhibitor concentrations. Inhibitors were stored either as solids or as 100 mM stock solutions in DMSO, these were diluted to appropriate concentrations in the assay buffer. Typically inhibition assays were carried out using black 384 well format μclear® plates (Griener Bio-One) with a final assay volume of 25 μL. Enzyme concentrations were chosen to give a linear rate of FC5 hydrolysis over the first 5 min of the assay time with an FC5 concentration of 5 μM. Components were added in the following order and volumes:

Reagent	Inhibited Enzyme Volume (μL)	Free Enzyme Volume (μL)	Background Hydrolysis Volume (μL)
Inhibitor Solution	1	-	-
Assay Buffer	14	15	20
5x Enzyme Solution	5	5	-
25 μM FC5	5	5	5

Unless otherwise stated, the enzymes were incubated with the inhibitor for 10 min prior to initiation of the reaction by the addition of the substrate. The residual activities were calculated using the following formula: $\%RA = \frac{100 \times (V_{inhibited} - V_{background})}{(V_{uninhibited} - V_{background})}$. IC_{50} values were calculated by fitting of residual activity curves using GraphPad Prism 5 software(347).

7.18. Oxygen Consumption Assays

7.18.1. Preparation of Glutathione Persulfide

Glutathione persulfide substrate was prepared as previously described(533). Method one involved the reaction of NaHS and oxidized glutathione under anaerobic conditions. An oxygen depleted solution of 20 mM oxidised glutathione in 100 mM sodium phosphate, pH 7.2 was mixed with an excess of NaHS. The reaction was sealed and incubated at 37°C for 30 min. Method two involved the reaction of reduced glutathione with elemental sulfur. 20 μL of a saturated acetonic sulfur solution was added to 1 mL of 20 mM reduced glutathione in 100 mM sodium phosphate, pH 7.2. The reaction was sealed and incubated at RT for 30 min.

7.18.2. Oxygen Detection

A FOXY AL-300 probe and a USB2000/USB2000-LS-450 spectrophotometer (Ocean Optics) were used for oxygen detection. Variation in oxygen concentration was measured by changes in fluorescence (λ_{ex} = 450 nm, λ_{em} = 600 nm). Before each experiment, the probe was calibrated by taking readings in deoxygenated and oxygen saturated 100 mM sodium phosphate, pH 7.2. Samples were prepared by diluting 1 μg of ETHE1 homologue (in 25 mM HEPES, pH 7.5, 100 mM NaCl) into a sealed 2 mL vial of oxygen saturated 100 mM sodium phosphate buffer, pH 7.2. Glutathione persulfide substrate was added to a final concentration of 1 mM immediately before the measurement. Control samples were carried out in the absence of GSSH. Data is expressed as % relative oxygen saturation five minutes after glutathione persulfide addition.

7.19. UV/Vis Spectroscopy Studies

UV/Vis spectroscopy experiments were performed using a Varian Cary 4000 UV/Vis spectrophotometer (Agilent) with an excitation wavelength of 490 nm or 330 nm for sulfite detector **20** or **21**, respectively, and absorbance wavelength range of 200-800 nm. 3 mL quartz cuvettes with a path length of 1 cm were used for all measurements. Fluorescence spectra were recorded for sulfite detectors **20** and **21** in the presence and absence of sodium sulfite. Sulfite detector samples were diluted to 1 mM in 25 mM HEPES, pH 7.5. Sodium sulfite was then added to a final concentration of 10 mM.

7.20. Stopped-Flow Kinetics

An anaerobically prepared solution of 100 μM enzyme supplemented with 250 μM $ZnSO_4$ or $Fe(NH)(SO_4)\cdot 7H_2O$, in 50 mM HEPES, pH 7.5, was rapidly mixed with buffer/nitrocefin in a 1:1 ratio. Spectra were recorded over 1000 s using a photodiode array detector measuring absorbance changes over a wavelength range of 300-720 nm. Spectra for the buffer alone were obtained under analogous conditions. Kinetic traces were analysed using OriginPro 8.51(349) and KinTek Explorer software(352).

7.21. Circular Dichroism Spectroscopy

Circular dichroism spectra were recorded using a Chirascan CD/Fluorimeter spectrometer (Applied Photophysics). Measurements were performed at 10 °C in a quartz cuvette with a 0.1 cm path length. Enzymes were diluted to a final concentration of 0.2 mg mL^{-1} in 10 mM sodium phosphate buffer, pH 7.5, for measurements. Spectra were recorded for wavelengths in the range of 260 to 190 nm at 0.5 nm intervals. Each spectrum is an average of three scans. The baseline of all spectra was corrected by subtraction of the spectrum of the buffer. Thermal denaturation experiments were performed using the same conditions. The ellipticity at 220 nm was monitored between 10 and 90 °C. The data were fitted to a Boltzmann sigmoidal curve to estimate apparent T_m values using OriginPro software(349).

7.22. Nuclear Magnetic Resonance Spectroscopy

^{13}C nuclear magnetic resonance (NMR) experiments with OXA-10 used a Bruker AVIII 600 MHz spectrometer equipped with a Prodigy broadband cryoprobe. Spectra were acquired at 298 K using a standard Bruker ^{13}C pulse sequence. The experimental parameters used were as follows: 2,048 scans, 36,058 Hz spectral width, 2.0 s relaxation delay, and 65,536 data points. A line broadening of 10 Hz was applied to all spectra. NMR samples contained 560 μM OXA-10 and 10 mM $NaH^{13}CO_3$ and were supplemented with 10% D_2O. The impact of cyclic boronate **1** was tested at a concentration of 5 mM.

^{11}B-NMR spectra were acquired with a 600 MHz spectrometer equipped with a Prodigy N_2 broadband cryoprobe, using 5 mm quartz tubes. Experiments were performed at 298 K, with an acquisition time of 0.85 s and a relaxation delay of 0.5 s. Spectra consisted of 4096 scans for the pH experiments and 16384 scans for the enzyme experiments, and were processed with a line broadening of 5.0 Hz and manual multipoint baseline correction. The impact of pH was determined using 200 μM **2** in 50 mM sodium phosphate (pH 7.5 or pH 12.0) or 50 mM sodium acetate (pH 4.5), supplemented with 10% D_2O. The impact of TEM-1 was determined using 200 μM **2** in 50 mM sodium phosphate, pH 7.5, 10% D_2O, in the presence and the absence of 300 μM TEM-1.

7.23. Surface Plasmon Resonance

GE Healthcare Biacore T200 was used for all SPR experiments. The temperature was maintained at 4 °C to increase stability of the protein on the chip. VIM-2 was minimally biotinylated (1:1 ratio of protein was incubated with EZ link NHS-LCLC-Biotin for 2 h at 4 °C, excess of biotin was removed using a desalting column). Enzyme was captured on the streptavidin coated surface of a sensor chip in running buffer: 50 mM HEPES, pH 7.4, 150 mM NaCl, 0.05 % Tween 20, 3 % DMSO at ~ 3000 RU. Cyclic boronate **2** was screened at a concentration series ranging from 45 nM to 3.7 μM. **2** was injected from lowest to highest concentration. Traces were fitted using a 1:1 binding model with local R_{max} for each concentration due to saturation of the surface. All data were normalised to a blank surface and blank injections to account for non-specific binding and drift.

7.24. Antimicrobial Susceptibility Testing

The *in vitro* activity of cyclic boronate **2** was assessed using nine clinical isolates carrying multiple β-lactamases. The isolates selected included *Enterobacteriaceae* (*E. coli* ST 131, *Klebsiella pneumoniae* ST 258, and *Providencia stuartii*) producing class A ESBLs (CTX-M-15, CTX-M-27, SHV-5, and VEB-1), serine carbapenemase (KPC-2) and metallo-carbapenemases (VIM-1 and VIM-2), plasmid-mediated AmpC (CMY-2), and/or carbapenem-hydrolyzing OXA-48-like oxacillinases (OXA-181 and OXA-232) in various combinations. The activity against carbapenemase-producing strains of *Pseudomonas aeruginosa* (VIM-2) and *Acinetobacter baumannii* (OXA-23) was also investigated. All isolates have previously undergone extensive phenotypic and genotypic characterization(551). Bacterial susceptibility to β-lactams and standard β-lactam inhibitor (clavulanic acid, sulbactam, and tazobactam) combinations was determined by broth microtiter dilution (BMD) according to the Clinical and Laboratory Standards Institute (CLSI) methodology(552). Minimum inhibitory concentrations (MICs) were determined using commercial Sensititre GN4F panels (Thermo Scientific) and Mueller-Hinton II cation-adjusted broth (Oxoid), with and without the addition of cyclic boronate **2** at a fixed concentration of 10 μg/ml. Plates were incubated at 37 °C for 18 h and MICs read by eye following the addition of Alamar Blue (Trek Diagnostics). The inhibitory effects of cyclic boronate **2** on susceptibility to 19 β-lactam compounds was also assessed in Kirby-Bauer disc diffusion tests(451). Combination discs (Oxoid) were prepared with a fixed ratio of 2:1 between the β-lactam (μg) and cyclic boronate **2**. Zones of inhibition around combined and unsupplemented discs were compared following overnight incubation on MH II plates.

7.25. Chemical Synthesis

7.25.1. Synthesis of Sulfite Detector 20

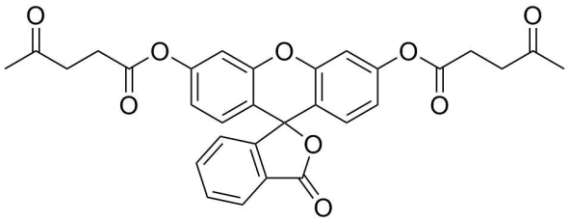

Fluorescein (1.0 g) was dissolved in dry methylene dichloride (50 mL). Levulinic acid (1.4 g), dicyclohexylcarbodiimide (3.1 g) and 4-dimethylaminopyridine (0.2 g) were added to the solution while stirring. The reaction mixture was allowed to stir for six hours at room temperature. The reaction mixture was subsequently filtered, and the solvent removed by rotary evaporation. The residue was purified by silica gel column chromatography (30% ethylacetate in cyclohexane) to give **20** as a pale yellow amorphous solid. (1.2 g, 72% yield). ^{1}H NMR (400 MHz, $CDCl_3$), δ (TMS, ppm) : 7.96 (d, *J* = 8.0 Hz, 1H), 7.55-7.60 (m, 2H), 7.09 (d, *J* = 8.0 Hz, 1H), 7.01 (s, 2H), 6.73 (d, *J* = 4 Hz, 4H), 2.78-2.82 (m, 4H), 2.72-2.77 (m, 4H), 2.16 (s, 6H); ^{13}CNMR(100 MHz, $CDCl_3$) *δ* (TMS, ppm): 206.68 (2C), 170.97 (2C), 169.19, 152.88, 152.04 (2C), 151.54 (2C), 135.31, 130.07, 128.94 (2C), 126.05, 125.21, 124.06, 117.73 (2C), 116.42 (2C), 110.37 (2C), 81.70, 37.80 (2C), 29.84 (2C), 28.15 (2C); ν_{max}/ cm^{-1}: 3352 s, 1679 s (note: shoulders were observed on either side of this peak); ESI(+)-HRMS (*m/z*): calculated for $C_{30}H_{24}NaO_9$: 551.1312 $[M+Na]^+$; measured 551.1313.

7.25.2. Synthesis of Sulfite Detector 21

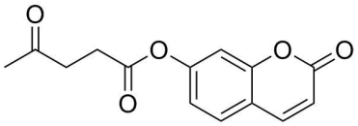

7-hydroxycoumarin (0.5 g) was dissolved in dry methylene dichloride (50 mL). Levulinic acid (1.4 g), dicyclohexylcarbodiimide (3.1 g) and 4-dimethylaminopyridine (0.2 g) were added to the solution while stirring. The reaction mixture was allowed to stir for six hours at room temperature. The reaction mixture was subsequently filtered, and the solvent removed by rotary evaporation. The residue was purified by silica gel column chromatography (40% ethylacetate in cyclohexane) to give **21** as an amorphous white solid. (0.6 g, 81% yield). ^{1}H NMR (400 MHz, $CDCl_3$), δ (TMS, ppm) : 7.62 (d, *J* = 8.0 Hz, 1H), 7.41 (d, *J* = 8.0 Hz, 1H), 7.05 (d, *J* = 4 Hz, 1H), 7.00 (dd, *J* = 8, 4 Hz, 1H), 6.32 (d, *J* = 8 Hz, 1H), 2.76-2.84 (m, 4H), 2.17 (s, 3H); ^{13}C NMR (400 MHz, $CDCl_3$) δ 207.4, 160.7, 153.6, 152.9, 171.0, 118.2, 116.4, 112.5, 110.1, 37.6, 27.3; ν_{max}/ cm^{-1}: 3350 s, 1724 s, 1701 s, 1679; ESI(+)-HRMS (*m/z*): calculated for $C_{14}H_{12}NaO_5$: 283.0576 $[M+Na]^+$; measured 283.0577.

Chapter 8: References

1. **Finch CE.** 2010. Evolution of the Human Lifespan and Diseases of Aging: Roles of Infection, Inflammation, and Nutrition. Proc Natl Acad Sci **107:**1718-1724.
2. **Zaffiri L, Gardner J, Toledo-Pereyra LH.** 2012. History of Antibiotics. From Salvarsan to Cephalosporins. J Invest Surg **25:**67-77.
3. **Hollis A, Ahmed Z.** 2013. Preserving Antibiotics, Rationally. New Engl J Med **369:**2474-2476.
4. **Clardy J, Fischbach M, Currie C.** 2009. The Natural History of Antibiotics. Curr Biol **19:**R437-R441.
5. **Pankey GA, Sabath LD.** 2004. Clinical Relevance of Bacteriostatic versus Bactericidal Mechanisms of Action in the Treatment of Gram-Positive Bacterial Infections. Clin Infect Dis **38:**864-870.
6. **Ehrlich P.** 1960. Experimental Researches on Specific Therapy: On Immunity with Special Reference to the Relationship Between Distribution and Action of Antigens, p 106-117, The Collected Papers of Paul Ehrlich. Pergamon.
7. **Williams KJ.** 2009. The Introduction of 'Chemotherapy' Using Arsphenamine – the First Magic Bullet. J R Soc Med **102:**343-348.
8. **Neu HC, Gootz TD.** 1996. Antimicrobial Chemotherapy In: Medical Microbiology 4th Edition Ed. Baron, S. Galveston (TX): University of Texas Medical Branch.
9. **Estee T, Ed M, Fiona C.** 2009. Oxford Handbook of Infectious Diseases and Microbiology. Oxford University Press, Oxford, UK.
10. **Brown GM.** 1962. The Biosynthesis of Folic Acid: II. Inhibition by Sulfonamides. J Biol Chem **237:**536-540.
11. **Silver LL.** 2011. Challenges of Antibacterial Discovery. Clin Microbiol Rev **24:**71-109.
12. **White RJ.** 2012. The Early History of Antibiotic Discovery: Empiricism Ruled, p 3-31. *In* Dougherty TJ, Pucci MJ (ed), Antibiotic Discovery and Development. Springer US, Boston, MA.
13. **Fleming A.** 1929. On the Antibacterial Action of Cultures of a *Penicillium*, with Special Reference to their Use in the Isolation of *B. influenzae*. Brit J Exp Pathol **10:**226-236.
14. **Grossman CM.** 2008. The First Use of Penicillin in the United States. Ann Intern Med **149:**135-136.
15. **Hinshaw HC, Feldman WH.** 1945. Streptomycin in Treatment of Clinical Tuberculosis: a Preliminary Report. Proc Staff Meet Mayo Clin **20:**313-318.
16. **Smadel JE.** 1949. Chloramphenicol (Chloromycetin) in the Treatment of Infectious Diseases. Am J Med **7:**671-685.

17. **Harris HJ.** 1949. Aureomycin and Chloromycetin in Brucellosis; with Special Reference to Chronic Brucellosis. Bull N Y Acad Med **25:**458.
18. **Geraci JE, Heilman FR, Nichols DR, Wellman EW, Ross GT.** 1956. Some Laboratory and Clinical Experiences with a New Antibiotic, Vancomycin. Antibiot Annu**:**90-106.
19. **Griffith RS.** 1956. Vancomycin; Continued Clinical Studies. Antibiot Annu**:**118-122.
20. **Sensi P, Margalith P, Timbal MT.** 1959. Rifomycin, a New Antibiotic; Preliminary Report. Farmaco Sci **14:**146-147.
21. **Kumazawa J, Yagisawa M.** 2002. The History of Antibiotics: The Japanese Story. J Infect Chemother **8:**125-133.
22. **Noall EWP, Sewards HFG, Waterworth PM.** 1962. Successful Treatment of a Case of *Proteus* Septicaemia. Br Med J **2:**1101-1102.
23. **Lesher GY, Froelich EJ, Gruett MD, Bailey JH, Brundage RP.** 1962. 1,8-Naphthyridine Derivatives. A New Class of Chemotherapeutic Agents. J Med Pharm Chem **91:**1063-1065.
24. **Autio S, Mäkelä P, Sunila R.** 1966. Experience with Nalidixic Acid in the Treatment of Urinary Tract Infections of Children. Arch Dis Child **41:**395-399.
25. **Rumsfield J, West DP, Aronson IK.** 1986. Topical Mupirocin in the Treatment of Bacterial Skin Infections. Drug Intell Clin Pharm **20:**943-948.
26. **Khosla R, Verma DD, Kapur A, Aruna RV, Khanna N.** 1999. Streptogramins: A New Class of Antibiotics. Indian J Med Sci **53:**111-119.
27. **Plouffe JF.** 2000. Emerging Therapies for Serious Gram-Positive Bacterial Infections: A Focus on Linezolid. Clin Infect Dis **31:**S144-S149.
28. **Steenbergen JN, Alder J, Thorne GM, Tally FP.** 2005. Daptomycin: A Lipopeptide Antibiotic for the Treatment of Serious Gram-Positive Infections. J Antimicrob Chemother **55:**283-288.
29. **Jacobs MR.** 2007. Retapamulin: A Semisynthetic Pleuromutilin Compound for Topical Treatment of Skin Infections in Adults and Children. Future Microbiol **2:**591-600.
30. **Novak R, Shlaes DM.** 2010. The Pleuromutilin Antibiotics: A New Class for Human Use. Curr Opin Investig Drugs **11:**182-191.
31. **Epstein IG, Nair KGS, Boyd LJ.** 1955. Cycloserine, a New Antibiotic in the Treatment of Human Pulmonary Tuberculosis: A Preliminary Report. Antibiotic Med **1:**80-93.
32. **Welch H, Putnam LE, Randall WA.** 1955. Antibacterial Activity and Blood and Urine Concentrations of Cycloserine, a New Antibiotic, Following Oral Administration. Antibiotic Med **1:**72-79.

33. **Kuehl FA, Wolf FJ, Trenner NR, Peck RL, Buhs RP, Howe E, Putter I, Hunnewell BD, Ormond R, Downing G, Lyons JE, Newstead E, Chaiet L, Folkers K.** 1955. *D*-4-Amino-3-isoxazolidone, a New Antibiotic. J Am Chem Soc **77:**2344-2345.
34. **Shinn DLS.** 1962. Metronidazole in Acute Ulcerative Gingivitis. Lancet **279:**1191.
35. **Clifton EB, Helena IMB, Cynthia SD.** 2004. Prospects for Clinical Introduction of Nitroimidazole Antibiotics for the Treatment of Tuberculosis. Curr Pharm Des **10:**3239-3262.
36. 1952. Erythromycin. Br Med J **2:**1085-1086.
37. **Lund E.** 1953. Erythromycin A New Antibiotic. Acta Pathol Microbiol Scandinavica **33:**393-400.
38. **Zuckerman JM, Qamar F, Bono BR.** 2011. Review of Macrolides (Azithromycin, Clarithromycin), Ketolids (Telithromycin) and Glycylcyclines (Tigecycline). Med Clin North Am **95:**761-791.
39. **Haight TH, Finland M.** 1952. Laboratory and Clinical Studies on Erythromycin. New Engl J Med **247:**227-232.
40. **Kohanski MA, Dwyer DJ, Collins JJ.** 2010. How Antibiotics Kill Bacteria: From Targets to Networks. Nat Rev Micro **8:**423-435.
41. **Cohen ML.** 2000. Changing Patterns of Infectious Disease. Nature **406:**762-767.
42. **Culotta E.** 1994. Funding Crunch Hobbles Antibiotic Resistance Research. Science **264:**362-363.
43. **Aminov RI.** 2010. A Brief History of the Antibiotic Era: Lessons Learned and Challenges for the Future. Front Microbiol **1:**134.
44. **Ventola CL.** 2015. The Antibiotic Resistance Crisis: Part 1: Causes and Threats. P T **40:**277-283.
45. **Davies J, Davies D.** 2010. Origins and Evolution of Antibiotic Resistance. Microbiol Mol Biol Rev **74:**417-433.
46. **Lewis K.** 2012. Antibiotics: Recover the Lost Art of Drug Discovery. Nature **485:**439-440.
47. **Payne DJ, Gwynn MN, Holmes DJ, Pompliano DL.** 2007. Drugs for Bad Bugs: Confronting the Challenges of Antibacterial Discovery. Nat Rev Drug Discov **6:**29-40.
48. **Garber K.** 2015. A β-Lactamase Inhibitor Revival Provides New Hope for Old Antibiotics. Nat Rev Drug Discov **14:**445-447.
49. **Ling LL, Schneider T, Peoples AJ, Spoering AL, Engels I, Conlon BP, Mueller A, Schaberle TF, Hughes DE, Epstein S, Jones M, Lazarides L, Steadman VA, Cohen DR, Felix CR, Fetterman KA, Millett WP, Nitti AG,**

Zullo AM, Chen C, Lewis K. 2015. A New Antibiotic Kills Pathogens Without Detectable Resistance. Nature **517:**455-459.

50. **Zipperer A, Konnerth MC, Laux C, Berscheid A, Janek D, Weidenmaier C, Burian M, Schilling NA, Slavetinsky C, Marschal M, Willmann M, Kalbacher H, Schittek B, Brötz-Oesterhelt H, Grond S, Peschel A, Krismer B.** 2016. Human Commensals Producing a Novel Antibiotic Impair Pathogen Colonization. Nature **535:**511-516.
51. **Livermore DM, Woodford N.** 2006. The β-Lactamase Threat in *Enterobacteriaceae*, *Pseudomonas* and *Acinetobacter*. Trends Microbiol **14:**413-420.
52. **Versporten A, Bolokhovets G, Ghazaryan L, Abilova V, Pyshnik G, Spasojevic T, Korinteli I, Raka L, Kambaralieva B, Cizmovic L, Carp A, Radonjic V, Maqsudova N, Celik HD, Payerl-Pal M, Pedersen HB, Sautenkova N, Goossens H.** 2014. Antibiotic Use in Eastern Europe: A Cross-National Database Study in Coordination with the WHO Regional Office for Europe. Lancet Infect Dis **14:**381-387.
53. **Demain AL, Elander RP.** 1999. The β-Lactam Antibiotics: Past, Present, and Future. Antonie Van Leeuwenhoek **75:**5-19.
54. **Elander RP.** 2003. Industrial Production of Beta-lactam Antibiotics. Appl Microbiol Biotechnol **61:**385-392.
55. **Stewart GT.** 1964. Toxicity of the Penicillins. Postgrad Med J **40:**160-165.
56. **Selwyn S.** 1979. Pioneer Work on the 'Penicillin Phenomenon', 1870-1876. J Antimicrob Chemother **5:**249-255.
57. **Brunel J.** 1951. Antibiosis from Pasteur to Fleming. J Hist Med Allied Sci **6:**287-301.
58. **Sanderson JB.** 1871. Appendix No. 5 - Further Report of Researches Concerning the Intimate Pathology of Contagion. The Origin and Distribution of Microzymes (Bacteria) in Water, and the Circumstances which Determine Their Existence in the Tissue and Liquids of the Living Body. 13th Report of the Medical Officer of the Privy Council, with Appendix, 1870, Her Majesty's Stationery Office, London**:**56-66.
59. **Lister JB.** 1871. On Bacteria, vol 1. Royal College of Surgeons of England, London.
60. **Lister JB.** 1875. A Contribution to the Germ Theory of Putrefaction and Other Fermentative Changes: And to the Natural History of Torulae and Bacteria. Neill.
61. **Lister JB.** 1872. In Correspondence with Arthur Lister (Cited by W. Fraser-Moodie, 1971).
62. **Fraser-Moodie W.** 1971. Struggle Against Infection. Proc R Soc Med **64:**87-94.
63. **Roberts W.** 1874. Studies on Biogenesis. Phil Trans R Soc Lond **164:**457-477.

64. **Tyndall J.** 1876. The Optical Deportment of the Atmosphere in Relation to the Phenomena of Putrefaction and Infection. Phil Trans R Soc Lond **166:**27-74.
65. **Pasteur L, Joubert JF.** 1877. Charbon et Septicémie. Gauthier-Villars.
66. **Duchesne E.** 1897. Contribution à l'Etude de la Concurrence Vitale chez les Microorganismes: Antagonisme Entre les Moisissures et les Microbes. Alexandre Rey, Imprimeur de la Faculté de Médecine.
67. **Chain E, Florey HW, Gardner AD, Heatley NG, Jennings MA, Orr-Ewing J, Sanders AG.** 1940. Penicillin as a Chemotherapeutic Agent. Lancet **236:**226-228.
68. **Florey H.** 1949. Antibiotics: A Survey of Penicillin, Streptomycin, and Other Antimicrobial Substances from Fungi, Actinomycotes, Bacteria and Plants. Oxford University Press.
69. **Macfarlane G.** 1979. Howard Florey: The Making of a Great Scientist. Oxford University Press.
70. **American Chemical Society.** 1999. The Discovery and Development of Penicillin 1928-1945.
71. **Richards AN.** 1964. Production of Penicillin in the United States (1941-1946). Nature **201:**441-445.
72. **Crowfoot D, Bunn CW, Rogers-Low BW, Turner-Jones A.** 1949. The X-ray Crystallographic Investigation of the Structure of Penicillin, p 310-366, Chemistry of Penicillin. Princeton University Press.
73. **Sheehan JC, Logan KRH.** 1959. A General Synthesis of the Penicillins. J Am Chem Soc **81:**5838-5839.
74. **Sheehan JC, Henery-Logan KR.** 1962. The Total and Partial General Syntheses of the Penicillins. J Am Chem Soc **84:**2983-2990.
75. **Batchelor FR, Doyle FP, Nayler JHC, Rolinson GN.** 1959. Synthesis of Penicillin: 6-Aminopenicillanic Acid in Penicillin Fermentations. Nature **183:**257-258.
76. **Huang HT, English AR, Seto TA, Shull GM, Sobin BA.** 1960. Enzymatic Hydrolysis of the Side Chain of Penicillins. J Am Chem Soc **82:**3790-3791.
77. **Oshiro BT.** 1999. The Semisynthetic Penicillins. Prim Care Update Ob Gyns **6:**56-60.
78. **Sheehan JC.** 1967. The Chemistry of Synthetic and Semisynthetic Penicillins. Ann N Y Acad Sci **145:**216-223.
79. **Acred P, Brown DM, Knudsen ET, Rolinson GN, Sutherland R.** 1967. New Semi-Synthetic Penicillin Active Against *Pseudomonas pyocyanea*. Nature **215:**25-30.

80. **Abraham EP.** 1979. A Glimpse of the Early History of the Cephalosporins. Rev Infect Dis **1:**99-105.
81. **Brotzu G.** 1948. Ricerche su di un Nuovo Antibiotico. Lavori dell'Instituto d'Igiene di Cagliari **1948:**1-11.
82. **Newton GGF, Abraham EP.** 1956. Isolation of Cephalosporin C, a Penicillin-Like Antibiotic Containing *D*-α-Aminoadipic Acid. Biochem J **62:**651-658.
83. **Abraham EP, Newton GGF.** 1961. The Structure of Cephalosporin C. Biochem J **79:**377-393.
84. **Hodgkin DC, Maslen EN.** 1961. The X-ray Analysis of the Structure of Cephalosporin C. Biochem J **79:**393-402.
85. **Eriksen NL, Blanco JD.** 1992. Extended-Spectrum (Second- and Third-Generation) Cephalosporins. Obstet Gynecol Clin North Am **19:**461-474.
86. **Giamarellou H.** 1999. Fourth Generation Cephalosporins in the Antimicrobial Chemotherapy of Surgical Infections. J Chemother **11:**486-493.
87. **Aoki H, Sakai H, Kohsaka M, Konomi T, Hosoda J.** 1976. Nocardicin A, a New Monocyclic Beta-Lactam Antibiotic. I. Discovery, Isolation and Characterization. J Antibiot (Tokyo) **29:**492-500.
88. **Imada A, Kitano K, Kintaka K, Muroi M, Asai M.** 1981. Sulfazecin and Isosulfazecin, Novel Beta-Lactam Antibiotics of Bacterial Origin. Nature **289:**590-591.
89. **Katayama N, Nozaki Y, Okonogi K, Ono H, Harada S, Okazaki H.** 1985. Formadicins, New Monocyclic Beta-Lactam Antibiotics of Bacterial Origin. I. Taxonomy, Fermentation and Biological Activities. J Antibiot (Tokyo) **38:**1117-1127.
90. **Sykes RB, Bonner DP.** 1985. Aztreonam: The First Monobactam. Am J Med **78:**2-10.
91. **Fuchs PC, Jones RN, Barry AL.** 1988. *In Vitro* Antimicrobial Activity of Tigemonam, a New Orally Administered Monobactam. Antimicrob Agents Chemother **32:**346-349.
92. **Fass RJ, Helsel VL.** 1985. *In Vitro* Activity of Carumonam. Antimicrob Agents Chemother **28:**834-836.
93. **McNulty CA, Garden GM, Ashby J, Wise R.** 1985. Pharmacokinetics and Tissue Penetration of Carumonam, a New Synthetic Monobactam. Antimicrob Agents Chemother **28:**425-427.
94. **Kahan J, Kahan F, Goegelman R, Currie S, Jackson M, Stapley E, Miller T, Miller A, Hendlin D, Mochales S.** Thienamycin. A New β-Lactam Antibiotic. I. Discovery and Isolation. 16th Interscience Conference on Antimicrob Agents Chemother, Chicago.

95. **Kropp H, Kahan J, Kahan F, Sundelof J, Darland G, Birnbaum J.** Thienamycin. A New β-Lactam Antibiotic. II *In Vitro* and *In Vivo* Evaluation. Program and Abstracts of the 16th Interscience Conference on Antimicrob Agents Chemother, Chicago.
96. **Kesado T, Hashizume T, Asahi Y.** 1980. Antibacterial Activities of a New Stabilized Thienamycin, *N*-Formimidoyl Thienamycin, in Comparison with Other Antibiotics. Antimicrob Agents Chemother **17:**912-917.
97. **Kahan FM, Kropp H, Sundelof JG, Birnbaum J.** 1983. Thienamycin: Development of Imipenem-Cilastatin. J Antimicrob Chemother **12 Suppl D:**1-35.
98. **Zhanel GG, Wiebe R, Dilay L, Thomson K, Rubinstein E, Hoban DJ, Noreddin AM, Karlowsky JA.** 2007. Comparative Review of the Carbapenems. Drugs **67:**1027-1052.
99. **Edwards JR, Turner PJ, Wannop C, Withnell ES, Grindey AJ, Nairn K.** 1989. *In Vitro* Antibacterial Activity of SM-7338, a Carbapenem Antibiotic with Stability to Dehydropeptidase I. Antimicrob Agents Chemother **33:**215-222.
100. **Greer ND.** 2008. Doripenem (Doribax): The Newest Addition to the Carbapenems. Proc Baylor Univ Med Center **21:**337-341.
101. **Shah PM, Isaacs RD.** 2003. Ertapenem, the First of a New Group of Carbapenems. J Antimicrob Chemother **52:**538-542.
102. **Papp-Wallace KM, Endimiani A, Taracila MA, Bonomo RA.** 2011. Carbapenems: Past, Present, and Future. Antimicrob Agents Chemother **55:**4943-4960.
103. **Wise EM, Park JT.** 1965. Penicillin: Its Basic Site of Action as an Inhibitor of a Peptide Cross-Linking Reaction in Cell Wall Mucopeptide Synthesis. Proc Natl Acad Sci USA **54:**75-81.
104. **Yocum RR, Rasmussen JR, Strominger JL.** 1980. The Mechanism of Action of Penicillin. Penicillin Acylates the Active Site of *Bacillus stearothermophilus D*-Alanine Carboxypeptidase. J Biol Chem **255:**3977-3986.
105. **Sauvage E, Kerff F, Terrak M, Ayala JA, Charlier P.** 2008. The Penicillin-Binding Proteins: Structure and Role in Peptidoglycan Biosynthesis. FEMS Microbiol Rev **32:**234-258.
106. **Yocum RR, Waxman DJ, Rasmussen JR, Strominger JL.** 1979. Mechanism of Penicillin Action: Penicillin and Substrate Bind Covalently to the Same Active Site Serine in Two Bacterial *D*-Alanine Carboxypeptidases. Proc Natl Acad Sci USA **76:**2730-2734.

107. **Tipper DJ, Strominger JL.** 1965. Mechanism of Action of Penicillins: A Proposal Based on Their Structural Similarity to Acyl-*D*-Alanyl-*D*-Alanine. Proc Natl Acad Sci USA **54:**1133-1141.
108. **Lee B.** 1971. Conformation of Penicillin as a Transition-State Analog of the Substrate of Peptidoglycan Transpeptidase. J Mol Biol **61:**463-469.
109. **Josephine HR, Kumar I, Pratt RF.** 2004. The Perfect Penicillin? Inhibition of a Bacterial *DD*-Peptidase by Peptidoglycan-Mimetic Beta-Lactams. J Am Chem Soc **126:**8122-8123.
110. **Silvaggi NR, Josephine HR, Kuzin AP, Nagarajan R, Pratt RF, Kelly JA.** 2005. Crystal Structures of Complexes Between the R61 *DD*-Peptidase and Peptidoglycan-Mimetic Beta-Lactams: A Non-Covalent Complex with a "Perfect Penicillin". J Mol Biol **345:**521-533.
111. **de Pedro MA, Holtje JV, Schwarz H.** 2002. Fast Lysis of *Escherichia coli* Filament Cells Requires Differentiation of Potential Division Sites. Microbiology **148:**79-86.
112. **Chung HS, Yao Z, Goehring NW, Kishony R, Beckwith J, Kahne D.** 2009. Rapid Beta-Lactam-Induced Lysis Requires Successful Assembly of the Cell Division Machinery. Proc Natl Acad Sci USA **106:**21872-21877.
113. **Yao Z, Kahne D, Kishony R.** 2012. Distinct Single-Cell Morphological Dynamics Under Beta-Lactam Antibiotics. Mol Cell **48:**705-712.
114. **Aminov RI.** 2009. The Role of Antibiotics and Antibiotic Resistance in Nature. Environ Microbiol **11:**2970-2988.
115. **Hall BG, Barlow M.** 2004. Evolution of the Serine β-Lactamases: Past, Present and Future. Drug Resist Updat **7:**111-123.
116. **Barlow M, Hall BG.** 2002. Phylogenetic Analysis Shows that the OXA β-Lactamase Genes Have Been on Plasmids for Millions of Years. J Mol Evol **55:**314-321.
117. **Aminov RI, Mackie RI.** 2007. Evolution and Ecology of Antibiotic Resistance Genes. FEMS Microbiol Lett **271:**147-161.
118. **Bhullar K, Waglechner N, Pawlowski A, Koteva K, Banks ED, Johnston MD, Barton HA, Wright GD.** 2012. Antibiotic Resistance is Prevalent in an Isolated Cave Microbiome. PLOS ONE **7:**e34953.
119. **Allen HK, Moe LA, Rodbumrer J, Gaarder A, Handelsman J.** 2008. Functional Metagenomics Reveals Diverse Beta-Lactamases in a Remote Alaskan Soil. ISME J **3:**243-251.
120. **Vaidya VK.** 2011. Horizontal Transfer of Antimicrobial Resistance by Extended-Spectrum β Lactamase-Producing *Enterobacteriaceae*. J Lab Physicians **3:**37-42.

121. **Doi Y, Adams-Haduch JM, Peleg AY, D'Agata EMC.** 2012. The Role of Horizontal Gene Transfer in the Dissemination of Extended-Spectrum Beta-Lactamase–Producing *Escherichia coli* and *Klebsiella pneumoniae* Isolates in an Endemic Setting. Diagn Microbiol Infect Dis **74:**34-38.

122. **Conly JM, Johnston BL.** 2005. Where Are All the New Antibiotics? The New Antibiotic Paradox. Can J Infect Dis Med Microbiol **16:**159-160.

123. **Gaude G, Hattiholli J.** 2013. Rising Bacterial Resistance to Beta-Lactam Antibiotics: Can There Be Solutions? J Dr NTR Univ Health Sci **2:**4-9.

124. **Hede K.** 2014. Antibiotic Resistance: An Infectious Arms Race. Nature **509:**S2-S3.

125. **Zhanel GG, Lawson CD, Adam H, Schweizer F, Zelenitsky S, Lagace-Wiens PR, Denisuik A, Rubinstein E, Gin AS, Hoban DJ, Lynch JP, 3rd, Karlowsky JA.** 2013. Ceftazidime-Avibactam: A Novel Cephalosporin/Beta-Lactamase Inhibitor Combination. Drugs **73:**159-177.

126. **Bush LM, Johnson CC.** 2000. Ureidopenicillins and Beta-Lactam/Beta-Lactamase Inhibitor Combinations. Infect Dis Clin North Am **14:**409-433.

127. **Sensakovic JW, Smith LG.** 1995. Beta-Lactamase Inhibitor Combinations. Med Clin North Am **79:**695-704.

128. **Lodise TP, Jr., Lomaestro B, Drusano GL.** 2007. Piperacillin-Tazobactam for *Pseudomonas aeruginosa* Infection: Clinical Implications of an Extended-Infusion Dosing Strategy. Clin Infect Dis **44:**357-363.

129. **Munita JM, Arias CA.** 2016. Mechanisms of Antibiotic Resistance. Microbiol Spect **4:**VMBF-0016-2015.

130. **Blair JMA, Webber MA, Baylay AJ, Ogbolu DO, Piddock LJV.** 2015. Molecular Mechanisms of Antibiotic Resistance. Nat Rev Microbiol **13:**42-51.

131. **Lin J, Nishino K, Roberts MC, Tolmasky M, Aminov RI, Zhang L.** 2015. Mechanisms of Antibiotic Resistance. Front Microbiol **6:**34.

132. **Tenover FC.** 2006. Mechanisms of Antimicrobial Resistance in Bacteria. Am J Infect Control **34:**S3-S10.

133. **Dever LA, Dermody TS.** 1991. Mechanisms of Bacterial Resistance to Antibiotics. Arch Intern Med **151:**886-895.

134. **Ubukata K, Nonoguchi R, Matsuhashi M, Konno M.** 1989. Expression and Inducibility in *Staphylococcus aureus* of the *mecA* Gene, which Encodes a Methicillin-Resistant *S. aureus*-Specific Penicillin-Binding Protein. J Bacteriol **171:**2882-2885.

135. **Siroy A, Molle V, Lemaître-Guillier C, Vallenet D, Pestel-Caron M, Cozzone AJ, Jouenne T, Dé E.** 2005. Channel Formation by CarO, the

Carbapenem Resistance-Associated Outer Membrane Protein of *Acinetobacter baumannii*. Antimicrob Agents Chemother **49:**4876-4883.

136. **Tomás M, Doumith M, Warner M, Turton JF, Beceiro A, Bou G, Livermore DM, Woodford N.** 2010. Efflux Pumps, OprD Porin, AmpC β-Lactamase, and Multiresistance in *Pseudomonas aeruginosa* Isolates from Cystic Fibrosis Patients. Antimicrob Agents Chemother **54:**2219-2224.
137. **Farra A, Islam S, Stralfors A, Sorberg M, Wretlind B.** 2008. Role of Outer Membrane Protein OprD and Penicillin-Binding Proteins in Resistance of *Pseudomonas aeruginosa* to Imipenem and Meropenem. Int J Antimicrob Agents **31:**427-433.
138. **Köhler T, Michea-Hamzehpour M, Epp SF, Pechere J-C.** 1999. Carbapenem Activities Against *Pseudomonas aeruginosa*: Respective Contributions of OprD and Efflux Systems. Antimicrob Agents Chemother **43:**424-427.
139. **Li XZ, Ma D, Livermore DM, Nikaido H.** 1994. Role of Efflux Pump(s) in Intrinsic Resistance of *Pseudomonas aeruginosa*: Active Efflux as a Contributing Factor to Beta-Lactam Resistance. Antimicrob Agents Chemother **38:**1742-1752.
140. **Drawz SM, Bonomo RA.** 2010. Three Decades of β-Lactamase Inhibitors. Clin Microbiol Rev **23:**160-201.
141. **Abraham EP, Chain E.** 1940. An Enzyme from Bacteria Able to Destroy Penicillin. Nature **146:**837.
142. **Sabath LD, Abraham EP.** 1965. Cephalosporinase and Penicillinase Activity of *Bacillus cereus*. Antimicrob Agents Chemother **5:**392-397.
143. **Sabath LD, Abraham EP.** 1966. Zinc as a Cofactor for Cephalosporinase from *Bacillus cereus* 569. Biochem J **98:**11C-13C.
144. **Barber M, Rozwadowska-Dowzenko M.** 1948. Infection by Penicillin-Resistant *Staphylococci*. Lancet **2:**641-644.
145. **Kirby WM.** 1944. Extraction of a Highly Potent Penicillin Inactivator from Penicillin Resistant *Staphylococci*. Science **99:**452-453.
146. **Bush K.** 2013. Proliferation and Significance of Clinically Relevant Beta-Lactamases. Ann N Y Acad Sci **1277:**84-90.
147. **G. Jacoby KB.** β-Lactamase Classification and Amino Acid Sequences for TEM, SHV and OXA Extended-Spectrum and Inhibitor Resistant Enzymes. http://www.lahey.org/Studies/webt.asp.
148. **Massova I, Mobashery S.** 1999. Structural and Mechanistic Aspects of Evolution of Beta-Lactamases and Penicillin-Binding Proteins. Curr Pharm Des **5:**929-937.
149. **Ghuysen JM.** 1991. Serine Beta-Lactamases and Penicillin-Binding Proteins. Annu Rev Microbiol **45:**37-67.

150. **Meroueh SO, Minasov G, Lee W, Shoichet BK, Mobashery S.** 2003. Structural Aspects for Evolution of Beta-Lactamases from Penicillin-Binding Proteins. J Am Chem Soc **125:**9612-9618.

151. **Bush K, Jacoby GA.** 2010. Updated Functional Classification of β-Lactamases. Antimicrob Agents Chemother **54:**969-976.

152. **Papp-Wallace KM, Bethel CR, Distler AM, Kasuboski C, Taracila M, Bonomo RA.** 2010. Inhibitor Resistance in the KPC-2 β-Lactamase, a Preeminent Property of this Class A β-Lactamase. Antimicrob Agents Chemother **54:**890-897.

153. **Chaïbi EB, Sirot D, Paul G, Labia R.** 1999. Inhibitor-Resistant TEM β-Lactamases: Phenotypic, Genetic and Biochemical Characteristics. J Antimicrob Chemother **43:**447-458.

154. **Ehmann DE, Jahić H, Ross PL, Gu R-F, Hu J, Durand-Réville TF, Lahiri S, Thresher J, Livchak S, Gao N, Palmer T, Walkup GK, Fisher SL.** 2013. Kinetics of Avibactam Inhibition against Class A, C, and D β-Lactamases. J Biol Chem **288:**27960-27971.

155. **Choi H, Paton RS, Park H, Schofield CJ.** 2016. Investigations on Recyclisation and Hydrolysis in Avibactam Mediated Serine β-Lactamase Inhibition. Org Biomol Chem **14:**4116-4128.

156. **Moews PC, Knox JR, Dideberg O, Charlier P, Frere JM.** 1990. Beta-Lactamase of *Bacillus licheniformis* 749/C at 2 Å Resolution. Proteins **7:**156-171.

157. **Lahiri SD, Mangani S, Durand-Reville T, Benvenuti M, De Luca F, Sanyal G, Docquier J-D.** 2013. Structural Insight into Potent Broad-Spectrum Inhibition with Reversible Recyclization Mechanism: Avibactam in Complex with CTX-M-15 and *Pseudomonas aeruginosa* AmpC β-Lactamases. Antimicrob Agents Chemother **57:**2496-2505.

158. **Sievers F, Wilm A, Dineen D, Gibson TJ, Karplus K, Li W, Lopez R, McWilliam H, Remmert M, Söding J, Thompson JD, Higgins DG.** 2011. Fast, Scalable Generation of High-Quality Protein Multiple Sequence Alignments Using Clustal Omega. Mol Syst Biol **7:**539-539.

159. **Jacoby GA.** 2009. AmpC β-Lactamases. Clin Microbiol Rev **22:**161-182.

160. **Bulychev A, Mobashery S.** 1999. Class C β-Lactamases Operate at the Diffusion Limit for Turnover of Their Preferred Cephalosporin Substrates. Antimicrob Agents Chemother **43:**1743-1746.

161. **Monnaie D, Frere J-M.** 1993. Interaction of Clavulanate with Class C β-Lactamases. FEBS Lett **334:**269-271.

162. **Kazmierczak A, Cordin X, Duez JM, Siebor E, Pechinot A, Sirot J.** 1990. Differences Between Clavulanic Acid and Sulbactam in Induction and Inhibition of Cephalosporinases in *Enterobacteria*. J Int Med Res **18 Suppl 4:**67d-77d.

163. **Bush K, Macalintal C, Rasmussen BA, Lee VJ, Yang Y.** 1993. Kinetic Interactions of Tazobactam with Beta-Lactamases from All Major Structural Classes. Antimicrob Agents Chemother **37:**851-858.

164. **Galleni M, Amicosante G, Frère JM.** 1988. A Survey of the Kinetic Parameters of Class C Beta-Lactamases. Cephalosporins and Other Beta-Lactam Compounds. Biochem J **255:**123-129.

165. **Doi Y, Paterson DL, Adams-Haduch JM, Sidjabat HE, O'Keefe A, Endimiani A, Bonomo RA.** 2009. Reduced Susceptibility to Cefepime Among *Escherichia coli* Clinical Isolates Producing Novel Variants of CMY-2 β-Lactamase. Antimicrob Agents Chemother **53:**3159-3161.

166. **Nordmann P, Mammeri H.** 2007. Extended-Spectrum Cephalosporinases: Structure, Detection and Epidemiology. Future Microbiol **2:**297-307.

167. **Mammeri H, Nordmann P, Berkani A, Eb F.** 2008. Contribution of Extended-Spectrum AmpC (ESAC) β-Lactamases to Carbapenem Resistance in *Escherichia coli*. FEMS Microbiol Lett **282:**238-240.

168. **Antunes NT, Lamoureaux TL, Toth M, Stewart NK, Frase H, Vakulenko SB.** 2014. Class D β-Lactamases: Are They All Carbapenemases? Antimicrob Agents Chemother **58:**2119-2125.

169. **Evans BA, Amyes SGB.** 2014. OXA β-Lactamases. Clin Microbiol Rev **27:**241-263.

170. **Poirel L, Bonnin RA, Nordmann P.** 2012. Genetic Features of the Widespread Plasmid Coding for the Carbapenemase OXA-48. Antimicrob Agents Chemother **56:**559-562.

171. **Stojanoski V, Chow D-C, Fryszczyn B, Hu L, Nordmann P, Poirel L, Sankaran B, Prasad BVV, Palzkill T.** 2015. Structural Basis for Different Substrate Profiles of Two Closely Related Class D β-Lactamases and their Inhibition by Halogens. Biochemistry **54:**3370-3380.

172. **Golemi D, Maveyraud L, Vakulenko S, Samama JP, Mobashery S.** 2001. Critical Involvement of a Carbamylated Lysine in Catalytic Function of Class D Beta-Lactamases. Proc Natl Acad Sci USA **98:**14280-14285.

173. **Baurin S, Vercheval L, Bouillenne F, Falzone C, Brans A, Jacquamet L, Ferrer J-L, Sauvage E, Dehareng D, Frère J-M, Charlier P, Galleni M, Kerff F.** 2009. Critical Role of Tryptophan 154 for the Activity and Stability of Class D β-Lactamases. Biochemistry **48:**11252-11263.

174. **Oliva M, Dideberg O, Field MJ.** 2003. Understanding the Acylation Mechanisms of Active-Site Serine Penicillin-Recognizing Proteins: A Molecular Dynamics Simulation Study. Proteins **53:**88-100.

175. **Hata M, Fujii Y, Tanaka Y, Ishikawa H, Ishii M, Neya S, Tsuda M, Hoshino T.** 2006. Substrate Deacylation Mechanisms of Serine-Beta-Lactamases. Biol Pharm Bull **29:**2151-2159.

176. **Chambers HF, Sachdeva MJ, Hackbarth CJ.** 1994. Kinetics of Penicillin Binding to Penicillin-Binding Proteins of *Staphylococcus aureus*. Biochem J **301:**139-144.

177. **Hermann JC, Ridder L, Mulholland AJ, Höltje H-D.** 2003. Identification of Glu166 as the General Base in the Acylation Reaction of Class A β-Lactamases through QM/MM Modeling. J Am Chem Soc **125:**9590-9591.

178. **Hata M, Fujii Y, Ishii M, Hoshino T, Tsuda M.** 2000. Catalytic Mechanism of Class A β-Lactamases. I. The Role of Glu166 and Ser130 in the Deacylation Reaction. Chem Pharm Bull (Tokyo) **48:**447-453.

179. **Ishiguro M, Imajo S.** 1996. Modeling Study on a Hydrolytic Mechanism of Class A β-Lactamases. J Med Chem **39:**2207-2218.

180. **Goldberg SD, Iannuccilli W, Nguyen T, Ju J, Cornish VW.** 2003. Identification of Residues Critical for Catalysis in a Class C β-Lactamase by Combinatorial Scanning Mutagenesis. Protein Sci **12:**1633-1645.

181. **Tripathi R, Nair NN.** 2013. Mechanism of Acyl–Enzyme Complex Formation from the Henry–Michaelis Complex of Class C β-Lactamases with β-Lactam Antibiotics. J Am Chem Soc **135:**14679-14690.

182. **Chen Y, McReynolds A, Shoichet BK.** 2009. Re-Examining the Role of Lys67 in Class C β-Lactamase Catalysis. Protein Sci **18:**662-669.

183. **Dubus A, Ledent P, Lamotte-Brasseur J, Frere JM.** 1996. The Roles of Residues Tyr150, Glu272, and His314 in Class C Beta-Lactamases. Proteins **25:**473-485.

184. **Chen Y, Minasov G, Roth TA, Prati F, Shoichet BK.** 2006. The Deacylation Mechanism of AmpC β-Lactamase at Ultrahigh Resolution. J Am Chem Soc **128:**2970-2976.

185. **Lamotte-Brasseur J, Dubus A, Wade RC.** 2000. pK_a Calculations for Class C Beta-Lactamases: The Role of Tyr-150. Proteins **40:**23-28.

186. **Gherman BF, Goldberg SD, Cornish VW, Friesner RA.** 2004. Mixed Quantum Mechanical/Molecular Mechanical (QM/MM) Study of the Deacylation Reaction in a Penicillin Binding Protein (PBP) Versus in a Class C β-Lactamase. J Am Chem Soc **126:**7652-7664.

187. **Li J, Cross JB, Vreven T, Meroueh SO, Mobashery S, Schlegel HB.** 2005. Lysine Carboxylation in Proteins: OXA-10 Beta-Lactamase. Proteins **61:**246-257.

188. **King DT, Sobhanifar S, Strynadka NC.** 2016. One Ring to Rule them All: Current Trends in Combating Bacterial Resistance to the Beta-Lactams. Protein Sci **25:**787-803.

189. **Reading C, Cole M.** 1977. Clavulanic Acid: A Beta-Lactamase-Inhibiting Beta-Lactam from *Streptomyces clavuligerus*. Antimicrob Agents Chemother **11:**852-857.

190. **Leigh DA, Bradnock K, Marriner JM.** 1981. Augmentin (Amoxycillin and Clavulanic Acid) Therapy in Complicated Infections due to β-Lactamase Producing Bacteria. J Antimicrob Chemother **7:**229-236.

191. **Appelbaum PC, Spangler SK, Jacobs MR.** 1990. Beta-Lactamase Production and Susceptibilities to Amoxicillin, Amoxicillin-Clavulanate, Ticarcillin, Ticarcillin-Clavulanate, Cefoxitin, Imipenem, and Metronidazole of 320 Non-*Bacteroides fragilis Bacteroides* isolates and 129 *Fusobacteria* from 28 U.S. Centers. Antimicrob Agents Chemother **34:**1546-1550.

192. **Brown AG.** 1986. Clavulanic Acid, a Novel Beta-Lactamase Inhibitor - A Case Study in Drug Discovery and Development. Drug Des Deliv **1:**1-21.

193. **Gutmann L, Kitzis MD, Yamabe S, Acar JF.** 1986. Comparative Evaluation of a New Beta-Lactamase Inhibitor, YTR 830, Combined with Different Beta-Lactam Antibiotics Against Bacteria Harboring Known Beta-Lactamases. Antimicrob Agents Chemother **29:**955-957.

194. **Benson JM, Nahata MC.** 1988. Sulbactam/Ampicillin, a New Beta-Lactamase Inhibitor/Beta-Lactam Antibiotic Combination. Drug Intell Clin Pharm **22:**534-541.

195. **Schoonover LL, Occhipinti DJ, Rodvold KA, Danziger LH.** 1995. Piperacillin/Tazobactam: A New Beta-Lactam/Beta-Lactamase Inhibitor Combination. Ann Pharmacother **29:**501-514.

196. **Appelbaum PC, Jacobs MR, Spangler SK, Yamabe S.** 1986. Comparative Activity of Beta-Lactamase Inhibitors YTR 830, Clavulanate, and Sulbactam Combined with Beta-Lactams Against Beta-Lactamase-Producing Anaerobes. Antimicrob Agents Chemother **30:**789-791.

197. **Jacobs MR, Aronoff SC, Johenning S, Shlaes DM, Yamabe S.** 1986. Comparative Activities of the Beta-Lactamase Inhibitors YTR 830, Clavulanate, and Sulbactam Combined with Ampicillin and Broad-Spectrum Penicillins Against Defined Beta-Lactamase-Producing Aerobic Gram-Negative *Bacilli*. Antimicrob Agents Chemother **29:**980-985.

198. **Brown RP, Aplin RT, Schofield CJ.** 1996. Inhibition of TEM-2 Beta-Lactamase from *Escherichia coli* by Clavulanic Acid: Observation of Intermediates by Electrospray Ionization Mass Spectrometry. Biochemistry **35:**12421-12432.

199. **Padayatti PS, Helfand MS, Totir MA, Carey MP, Carey PR, Bonomo RA, van den Akker F.** 2005. High Resolution Crystal Structures of the Trans-Enamine Intermediates Formed by Sulbactam and Clavulanic Acid and E166A SHV-1 β-Lactamase. J Biol Chem **280:**34900-34907.

200. **Therrien C, Levesque RC.** 2000. Molecular Basis of Antibiotic Resistance and β-Lactamase Inhibition by Mechanism-Based Inactivators: Perspectives and Future Directions. FEMS Microbiol Rev **24:**251-262.

201. **Labia R, Peduzzi J.** 1978. Kinetics of Beta-Lactamase Inhibition by Clavulanic Acid. Biochim Biophys Acta **526:**572-579.

202. **Burns CJ, Goswami R, Jackson RW, Lessen T, Li W, Pevear D, Tirunahari PK, Xu H.** 2010. Beta-Lactamase Inhibitors. WO 2010/130708 A1.

203. **Ehmann DE, Jahić H, Ross PL, Gu R-F, Hu J, Kern G, Walkup GK, Fisher SL.** 2012. Avibactam is a Covalent, Reversible, Non-β-Lactam β-Lactamase Inhibitor. Proc Natl Acad Sci **109:**11663-11668.

204. **Mosley JF, Smith LL, Parke CK, Brown JA, Wilson AL, Gibbs LV.** 2016. Ceftazidime-Avibactam (Avycaz): For the Treatment of Complicated Intra-Abdominal and Urinary Tract Infections. P T **41:**479-483.

205. **Papp-Wallace KM, Winkler ML, Taracila MA, Bonomo RA.** 2015. Variants of β-Lactamase KPC-2 that are Resistant to Inhibition by Avibactam. Antimicrob Agents Chemother **59:**3710-3717.

206. **Smith Moland E, Hanson ND, Herrera VL, Black JA, Lockhart TJ, Hossain A, Johnson JA, Goering RV, Thomson KS.** 2003. Plasmid-Mediated, Carbapenem-Hydrolysing Beta-Lactamase, KPC-2, in *Klebsiella pneumoniae* Isolates. J Antimicrob Chemother **51:**711-714.

207. **Abboud MI, Damblon C, Brem J, Smargiasso N, Mercuri P, Gilbert B, Rydzik AM, Claridge TDW, Schofield CJ, Frère J-M.** 2016. Interaction of Avibactam with Class B Metallo-β-Lactamases. Antimicrob Agents Chemother **60:**5655-5662.

208. **Blizzard TA, Chen H, Kim S, Wu J, Bodner R, Gude C, Imbriglio J, Young K, Park Y-W, Ogawa A, Raghoobar S, Hairston N, Painter RE, Wisniewski D, Scapin G, Fitzgerald P, Sharma N, Lu J, Ha S, Hermes J, Hammond ML.** 2014. Discovery of MK-7655, a β-Lactamase Inhibitor for Combination with Primaxin®. Bioorg Med Chem Lett **24:**780-785.

209. **Lucasti C, Vasile L, Sandesc D, Venskutonis D, McLeroth P, Lala M, Rizk ML, Brown ML, Losada MC, Pedley A, Kartsonis NA, Paschke A.** 2016. Phase 2, Dose-Ranging Study of Relebactam with Imipenem-Cilastatin in Subjects with Complicated Intra-Abdominal Infection. Antimicrob Agents Chemother **60:**6234-6243.

210. **Lob SH, Hackel MA, Kazmierczak KM, Young K, Motyl MR, Karlowsky JA, Sahm DF.** 2017. *In Vitro* Activity of Imipenem-Relebactam against Gram-Negative ESKAPE Pathogens Isolated by Clinical Laboratories in the United States in 2015 – Results from the SMART Global Surveillance Program. Antimicrob Agents Chemother.

211. **Lapuebla A, Abdallah M, Olafisoye O, Cortes C, Urban C, Landman D, Quale J.** 2015. Activity of Imipenem with Relebactam against Gram-Negative Pathogens from New York City. Antimicrob Agents Chemother **59:**5029-5031.

212. **Hecker SJ, Reddy KR, Totrov M, Hirst GC, Lomovskaya O, Griffith DC, King P, Tsivkovski R, Sun D, Sabet M, Tarazi Z, Clifton MC, Atkins K, Raymond A, Potts KT, Abendroth J, Boyer SH, Loutit JS, Morgan EE, Durso S, Dudley MN.** 2015. Discovery of a Cyclic Boronic Acid β-Lactamase Inhibitor (RPX7009) with Utility vs Class A Serine Carbapenemases. J Med Chem **58:**3682-3692.

213. **Castanheira M, Rhomberg PR, Flamm RK, Jones RN.** 2016. Effect of the β-Lactamase Inhibitor Vaborbactam Combined with Meropenem when Tested Against Serine-Carbapenemase-Producing *Enterobacteriaceae*. Antimicrob Agents Chemother **60:**5454-5458.

214. **Bull SD, Davidson MG, van den Elsen JMH, Fossey JS, Jenkins ATA, Jiang Y-B, Kubo Y, Marken F, Sakurai K, Zhao J, James TD.** 2013. Exploiting the Reversible Covalent Bonding of Boronic Acids: Recognition, Sensing, and Assembly. Acc Chem Res **46:**312-326.

215. **Palzkill T.** 2013. Metallo-β-Lactamase Structure and Function. Ann N Y Acad Sci **1277:**91-104.

216. **Bebrone C.** 2007. Metallo-β-Lactamases (Classification, Activity, Genetic Organization, Structure, Zinc Coordination) and their Superfamily. Biochem Pharmacol **74:**1686-1701.

217. **Pettinati I, Brem J, Lee SY, McHugh PJ, Schofield CJ.** 2016. The Chemical Biology of Human Metallo-β-Lactamase Fold Proteins. Trends Biochem Sci **41:**338-355.

218. **Tiranti V, Viscomi C, Hildebrandt T, Di Meo I, Mineri R, Tiveron C, D Levitt M, Prelle A, Fagiolari G, Rimoldi M, Zeviani M.** 2009. Loss of ETHE1,

a Mitochondrial Dioxygenase, Causes Fatal Sulfide Toxicity in Ethylmalonic Encephalopathy. Nat Med **15:**200-205.

219. **Varki A.** 2009. Multiple Changes in Sialic Acid Biology During Human Evolution. Glycoconj J **26:**231-245.
220. **Pettinati I, Brem J, McDonough MA, Schofield CJ.** 2015. Crystal Structure of Human Persulfide Dioxygenase: Structural Basis of Ethylmalonic Encephalopathy. Hum Mol Genet **24:**2458-2469.
221. **Cameron AD, Ridderström M, Olin B, Mannervik B.** 1999. Crystal Structure of Human Glyoxalase II and its Complex with a Glutathione Thiolester Substrate Analogue. Structure **7:**1067-1078.
222. **Vander Jagt DL.** 1993. Glyoxalase II: Molecular Characteristics, Kinetics and Mechanism. Biochem Soc Trans **21:**522-527.
223. **Garau G, Lemaire D, Vernet T, Dideberg O, Di Guilmi AM.** 2005. Crystal Structure of Phosphorylcholine Esterase Domain of the Virulence Factor Choline-Binding Protein E from *Streptococcus pneumoniae*: New Structural Features Among the Metallo-β-Lactamase Superfamily. J Biol Chem **280:**28591-28600.
224. **Vollmer W, Tomasz A.** 2001. Identification of the Teichoic Acid Phosphorylcholine Esterase in *Streptococcus pneumoniae*. Mol Microbiol **39:**1610-1622.
225. **Allerston CK, Lee SY, Newman JA, Schofield CJ, McHugh PJ, Gileadi O.** 2015. The Structures of the SNM1A and SNM1B/Apollo Nuclease Domains Reveal a Potential Basis for their Distinct DNA Processing Activities. Nucleic Acids Res **43:**11047-11060.
226. **Sengerova B, Allerston CK, Abu M, Lee SY, Hartley J, Kiakos K, Schofield CJ, Hartley JA, Gileadi O, McHugh PJ.** 2012. Characterization of the Human SNM1A and SNM1B/Apollo DNA Repair Exonucleases. J Biol Chem **287:**26254-26267.
227. **Mandel CR, Kaneko S, Zhang H, Gebauer D, Vethantham V, Manley JL, Tong L.** 2006. Polyadenylation Factor CPSF-73 is the Pre-mRNA 3'-End Processing Endonuclease. Nature **444:**953-956.
228. **Walsh TR, Toleman MA, Poirel L, Nordmann P.** 2005. Metallo-β-Lactamases: The Quiet Before the Storm? Clin Microbiol Rev **18:**306-325.
229. **Fujii T, Sato K, Miyata K, Inoue M, Mitsuhashi S.** 1986. Biochemical Properties of Beta-Lactamase Produced by *Legionella gormanii*. Antimicrob Agents Chemother **29:**925-926.

230. **Saino Y, Kobayashi F, Inoue M, Mitsuhashi S.** 1982. Purification and Properties of Inducible Penicillin Beta-Lactamase Isolated from *Pseudomonas maltophilia*. Antimicrob Agents Chemother **22:**564-570.

231. **Sato K, Fujii T, Okamoto R, Inoue M, Mitsuhashi S.** 1985. Biochemical Properties of Beta-Lactamase Produced by *Flavobacterium odoratum*. Antimicrob Agents Chemother **27:**612-614.

232. **Watanabe M, Iyobe S, Inoue M, Mitsuhashi S.** 1991. Transferable Imipenem Resistance in *Pseudomonas aeruginosa*. Antimicrob Agents Chemother **35:**147-151.

233. **Rossolini GM, Franceschini N, Riccio ML, Mercuri PS, Perilli M, Galleni M, Frere JM, Amicosante G.** 1998. Characterization and Sequence of the *Chryseobacterium* (*Flavobacterium*) *meningosepticum* Carbapenemase: A New Molecular Class B Beta-Lactamase Showing a Broad Substrate Profile. Biochem J **332 (Pt 1):**145-152.

234. **Bandoh K, Watanabe K, Muto Y, Tanaka Y, Kato N, Ueno K.** 1992. Conjugal Transfer of Imipenem Resistance in *Bacteroides fragilis*. J Antibiot (Tokyo) **45:**542-547.

235. **Johnson AP, Woodford N.** 2013. Global Spread of Antibiotic Resistance: The Example of New Delhi Metallo-Beta-Lactamase (NDM)-Mediated Carbapenem Resistance. J Med Microbiol **62:**499-513.

236. **Walsh TR.** 2010. Emerging Carbapenemases: A Global Perspective. Int J Antimicrob Agents **36:**S8-S14.

237. **Grundmann H, Livermore DM, Giske CG, Canton R, Rossolini GM, Campos J, Vatopoulos A, Gniadkowski M, Toth A, Pfeifer Y, Jarlier V, Carmeli Y.** 2010. Carbapenem-Non-Susceptible *Enterobacteriaceae* in Europe: Conclusions from a Meeting of National Experts. Euro Surveill **15**.

238. **Diene SM, Rolain JM.** 2014. Carbapenemase Genes and Genetic Platforms in Gram-Negative *Bacilli*: *Enterobacteriaceae, Pseudomonas* and *Acinetobacter* Species. Clin Microbiol Infect **20:**831-838.

239. **Miriagou V, Cornaglia G, Edelstein M, Galani I, Giske CG, Gniadkowski M, Malamou-Lada E, Martinez-Martinez L, Navarro F, Nordmann P, Peixe L, Pournaras S, Rossolini GM, Tsakris A, Vatopoulos A, Canton R.** 2010. Acquired Carbapenemases in Gram-Negative Bacterial Pathogens: Detection and Surveillance Issues. Clin Microbiol Infect **16:**112-122.

240. **Saavedra MJ, Peixe L, Sousa JC, Henriques I, Alves A, Correia A.** 2003. Sfh-I, a Subclass B2 Metallo-Beta-Lactamase from a *Serratia fonticola* Environmental Isolate. Antimicrob Agents Chemother **47:**2330-2333.

241. **Rossolini GM, Condemi MA, Pantanella F, Docquier JD, Amicosante G, Thaller MC.** 2001. Metallo-Beta-Lactamase Producers in Environmental Microbiota: New Molecular Class B Enzyme in *Janthinobacterium lividum*. Antimicrob Agents Chemother **45:**837-844.

242. **Stoczko M, Frere JM, Rossolini GM, Docquier JD.** 2006. Postgenomic Scan of Metallo-Beta-Lactamase Homologues in *Rhizobacteria*: Identification and Characterization of BJP-1, a Subclass B3 Ortholog from *Bradyrhizobium japonicum*. Antimicrob Agents Chemother **50:**1973-1981.

243. **Frère J-M.** 1995. Beta-Lactamases and Bacterial Resistance to Antibiotics. Mol Microbiol **16:**385-395.

244. **Felici A, Amicosante G, Oratore A, Strom R, Ledent P, Joris B, Fanuel L, Frere JM.** 1993. An Overview of the Kinetic Parameters of Class B Beta-Lactamases. Biochem J **291:**151-155.

245. **Rafiee R, Eftekhar F, Tabatabaei SA, Minaee Tehrani D.** 2014. Prevalence of Extended-Spectrum and Metallo β-Lactamase Production in AmpC β-Lactamase Producing *Pseudomonas aeruginosa* Isolates from Burns. Jundishapur J Microbiol **7:**e16436.

246. **Oberoi L, Singh N, Sharma P, Aggarwal A.** 2013. ESBL, MBL and AmpC β Lactamase Producing Superbugs – Havoc in the Intensive Care Units of Punjab India. J Clin Diagn Res **7:**70-73.

247. **Safari M, Mozaffari Nejad AS, Bahador A, Jafari R, Alikhani MY.** 2015. Prevalence of ESBL and MBL Encoding Genes in *Acinetobacter baumannii* Strains Isolated from Patients of Intensive Care Units (ICUs). Saudi J Biol Sci **22:**424-429.

248. **Fomda BA, Khan A, Zahoor D.** 2014. NDM-1 (New Delhi Metallo-Beta-Lactamase 1) Producing Gram-Negative *Bacilli*: Emergence & Clinical Implications. Indian J Med Res **140:**672-678.

249. **Yong D, Toleman MA, Giske CG, Cho HS, Sundman K, Lee K, Walsh TR.** 2009. Characterization of a New Metallo-β-Lactamase Gene, bla(NDM-1), and a Novel Erythromycin Esterase Gene Carried on a Unique Genetic Structure in *Klebsiella pneumoniae* Sequence Type 14 from India. Antimicrob Agents Chemother **53:**5046-5054.

250. **Aschbacher R, Doumith M, Livermore DM, Larcher C, Woodford N.** 2008. Linkage of Acquired Quinolone Resistance (qnrS1) and Metallo-Beta-Lactamase (blaVIM-1) Genes in Multiple Species of *Enterobacteriaceae* from Bolzano, Italy. J Antimicrob Chemother **61:**515-523.

251. **Hall BG, Barlow M.** 2005. Revised Ambler Classification of β-Lactamases. J Antimicrob Chemother **55:**1050-1051.

252. **Brindisi M, Brogi S, Giovani S, Gemma S, Lamponi S, De Luca F, Novellino E, Campiani G, Docquier J-D, Butini S.** 2016. Targeting Clinically-Relevant Metallo-β-Lactamases: From High-Throughput Docking to Broad-Spectrum Inhibitors. J Enzyme Inhib Med Chem **31:**98-109.

253. **Pfeifer Y, Cullik A, Witte W.** 2010. Resistance to Cephalosporins and Carbapenems in Gram-Negative Bacterial Pathogens. Int J Med Microbiol **300:**371-379.

254. **Brem J, van Berkel SS, Zollman D, Lee SY, Gileadi O, McHugh PJ, Walsh TR, McDonough MA, Schofield CJ.** 2016. Structural Basis of Metallo-β-Lactamase Inhibition by Captopril Stereoisomers. Antimicrob Agents Chemother **60:**142-150.

255. **Garau G, Bebrone C, Anne C, Galleni M, Frere JM, Dideberg O.** 2005. A Metallo-Beta-Lactamase Enzyme in Action: Crystal Structures of the Monozinc Carbapenemase CphA and its Complex with Biapenem. J Mol Biol **345:**785-795.

256. **Nauton L, Kahn R, Garau G, Hernandez JF, Dideberg O.** 2008. Structural Insights into the Design of Inhibitors for the L1 Metallo-Beta-Lactamase from *Stenotrophomonas maltophilia*. J Mol Biol **375:**257-269.

257. **Carfi A, Pares S, Duée E, Galleni M, Duez C, Frère JM, Dideberg O.** 1995. The 3-D Structure of a Zinc Metallo-β-Lactamase from *Bacillus cereus* Reveals a New Type of Protein Fold. EMBO J **14:**4914-4921.

258. **Carfi A, Duee E, Galleni M, Frere JM, Dideberg O.** 1998. 1.85 Å Resolution Structure of the Zinc (II) Beta-Lactamase from *Bacillus cereus*. Acta Crystallogr D Biol Crystallogr **54:**313-323.

259. **King DT, Worrall LJ, Gruninger R, Strynadka NC.** 2012. New Delhi Metallo-Beta-Lactamase: Structural Insights into Beta-Lactam Recognition and Inhibition. J Am Chem Soc **134:**11362-11365.

260. **Chiou J, Leung TY-C, Chen S.** 2014. Molecular Mechanisms of Substrate Recognition and Specificity of New Delhi Metallo-β-Lactamase. Antimicrob Agents Chemother **58:**5372-5378.

261. **Brem J, Struwe WB, Rydzik AM, Tarhonskaya H, Pfeffer I, Flashman E, van Berkel SS, Spencer J, Claridge TDW, McDonough MA, Benesch JLP, Schofield CJ.** 2015. Studying the Active-Site Loop Movement of the São Paolo Metallo-β-Lactamase-1. Chem Sci **6:**956-963.

262. **Moali C, Anne C, Lamotte-Brasseur J, Groslambert S, Devreese B, Van Beeumen J, Galleni M, Frère J-M.** 2003. Analysis of the Importance of the Metallo-β-Lactamase Active Site Loop in Substrate Binding and Catalysis. Chem Biol **10:**319-329.

263. **Concha NO, Janson CA, Rowling P, Pearson S, Cheever CA, Clarke BP, Lewis C, Galleni M, Frere JM, Payne DJ, Bateson JH, Abdel-Meguid SS.** 2000. Crystal Structure of the IMP-1 Metallo Beta-Lactamase from *Pseudomonas aeruginosa* and its Complex with a Mercaptocarboxylate Inhibitor: Binding Determinants of a Potent, Broad-Spectrum Inhibitor. Biochemistry **39:**4288-4298.

264. **Rossolini GM, Zanchi A, Chiesurin A, Amicosante G, Satta G, Guglielmetti P.** 1995. Distribution of CphA or Related Carbapenemase-Encoding Genes and Production of Carbapenemase Activity in Members of the Genus *Aeromonas*. Antimicrob Agents Chemother **39:**346-349.

265. **Fonseca F, Arthur CJ, Bromley EHC, Samyn B, Moerman P, Saavedra MJ, Correia A, Spencer J.** 2011. Biochemical Characterization of Sfh-I, a Subclass B2 Metallo-β-Lactamase from *Serratia fonticola* UTAD54. Antimicrob Agents Chemother **55:**5392-5395.

266. **Segatore B, Massidda O, Satta G, Setacci D, Amicosante G.** 1993. High Specificity of CphA-Encoded Metallo-Beta-Lactamase from *Aeromonas hydrophila* AE036 for Carbapenems and its Contribution to Beta-Lactam Resistance. Antimicrob Agents Chemother **37:**1324-1328.

267. **Hernandez Valladares M, Felici A, Weber G, Adolph HW, Zeppezauer M, Rossolini GM, Amicosante G, Frère J-M, Galleni M.** 1997. Zn(II) Dependence of the *Aeromonas hydrophila* AE036 Metallo-β-Lactamase Activity and Stability. Biochemistry **36:**11534-11541.

268. **Costello AL, Sharma NP, Yang K-W, Crowder MW, Tierney DL.** 2006. X-ray Absorption Spectroscopy of the Zinc-Binding Sites in the Class B2 Metallo-β-lactamase ImiS from *Aeromonas veronii bv. sobria*. Biochemistry **45:**13650-13658.

269. **Bebrone C, Delbrück H, Kupper MB, Schlömer P, Willmann C, Frère J-M, Fischer R, Galleni M, Hoffmann KMV.** 2009. The Structure of the Dizinc Subclass B2 Metallo-β-Lactamase CphA Reveals that the Second Inhibitory Zinc Ion Binds in the Histidine Site. Antimicrob Agents Chemother **53:**4464-4471.

270. **Hall BG, Salipante SJ, Barlow M.** 2004. Independent Origins of Subgroup B1 + B2 and Subgroup B3 Metallo-Beta-Lactamases. J Mol Evol **59:**133-141.

271. **Hall BG, Salipante SJ, Barlow M.** 2003. The Metallo-Beta-Lactamases Fall into Two Distinct Phylogenetic Groups. J Mol Evol **57:**249-254.

272. **Walsh TR, Hall L, Assinder SJ, Nichols WW, Cartwright SJ, MacGowan AP, Bennett PM.** 1994. Sequence Analysis of the L1 Metallo-Beta-Lactamase from *Xanthomonas maltophilia*. Biochim Biophys Acta **1218:**199-201.

273. **Boschi L, Mercuri PS, Riccio ML, Amicosante G, Galleni M, Frere JM, Rossolini GM.** 2000. The *Legionella* (*Fluoribacter*) *gormanii* Metallo-Beta-

Lactamase: A New Member of the Highly Divergent Lineage of Molecular-Subclass B3 Beta-Lactamases. Antimicrob Agents Chemother **44:**1538-1543.

274. **Bellais S, Aubert D, Naas T, Nordmann P.** 2000. Molecular and Biochemical Heterogeneity of Class B Carbapenem-Hydrolyzing Beta-Lactamases in *Chryseobacterium meningosepticum*. Antimicrob Agents Chemother **44:**1878-1886.
275. **Morán-Barrio J, González JM, Lisa MN, Costello AL, Peraro MD, Carloni P, Bennett B, Tierney DL, Limansky AS, Viale AM, Vila AJ.** 2007. The Metallo-β-Lactamase GOB is a Mono-Zn(II) Enzyme with a Novel Active Site. J Biol Chem **282:**18286-18293.
276. **Moran-Barrio J, Lisa MN, Larrieux N, Drusin SI, Viale AM, Moreno DM, Buschiazzo A, Vila AJ.** 2016. Crystal Structure of the Metallo-Beta-Lactamase GOB in the Periplasmic Dizinc Form Reveals an Unusual Metal Site. Antimicrob Agents Chemother **60:**6013-6022.
277. **Ullah JH, Walsh TR, Taylor IA, Emery DC, Verma CS, Gamblin SJ, Spencer J.** 1998. The Crystal Structure of the L1 Metallo-β-Lactamase from *Stenotrophomonas maltophilia* at 1.7 Å Resolution. J Mol Biol **284:**125-136.
278. **Crowder MW, Walsh TR, Banovic L, Pettit M, Spencer J.** 1998. Overexpression, Purification, and Characterization of the Cloned Metallo-β-Lactamase L1 from *Stenotrophomonas maltophilia*. Antimicrob Agents Chemother **42:**921-926.
279. **Page MI, Badarau A.** 2008. The Mechanisms of Catalysis by Metallo β-Lactamases. Bioinorg Chem Appl **2008:**576297.
280. **Fast W, Sutton LD.** 2013. Metallo-β-Lactamase: Inhibitors and Reporter Substrates. Biochim Biophys Acta **1834:**1648-1659.
281. **Rasia RM, Vila AJ.** 2003. Mechanistic Study of the Hydrolysis of Nitrocefin Mediated by *B. cereus* Metallo-β-Lactamase. Arkivoc **10:**507-516.
282. **Spencer J, Clarke AR, Walsh TR.** 2001. Novel Mechanism of Hydrolysis of Therapeutic β-Lactams by *Stenotrophomonas maltophilia* L1 Metallo-β-Lactamase. J Biol Chem **276:**33638-33644.
283. **Aitha M, Marts AR, Bergstrom A, Møller AJ, Moritz L, Turner L, Nix JC, Bonomo RA, Page RC, Tierney DL, Crowder MW.** 2014. Biochemical, Mechanistic, and Spectroscopic Characterization of Metallo-β-Lactamase VIM-2. Biochemistry **53:**7321-7331.
284. **Badarau A, Damblon C, Page Michael I.** 2007. The Activity of the Dinuclear Cobalt-β-Lactamase from *Bacillus cereus* in Catalysing the Hydrolysis of β-Lactams. Biochem J **401:**197-203.

285. **Tioni MF, Llarrull LI, Poeylaut-Palena AA, Martí MA, Saggu M, Periyannan GR, Mata EG, Bennett B, Murgida DH, Vila AJ.** 2008. Trapping and Characterization of a Reaction Intermediate in Carbapenem Hydrolysis by *B. cereus* Metallo-β-Lactamase. J Am Chem Soc **130:**15852-15863.

286. **Mock WL, Tsay JT.** 1988. pK_a Values for Active Site Residues of Carboxypeptidase A. J Biol Chem **263:**8635-8641.

287. **Meini M-R, Llarrull LI, Vila AJ.** 2015. Overcoming Differences: The Catalytic Mechanism of Metallo-β-Lactamases. FEBS Lett **589:**3419-3432.

288. **Wang Z, Fast W, Benkovic SJ.** 1999. On the Mechanism of the Metallo-Beta-Lactamase from *Bacteroides fragilis*. Biochemistry **38:**10013-10023.

289. **Yang H, Aitha M, Hetrick AM, Richmond TK, Tierney DL, Crowder MW.** 2012. Mechanistic and Spectroscopic Studies of Metallo-β-lactamase NDM-1. Biochemistry **51:**3839-3847.

290. **McManus-Munoz S, Crowder MW.** 1999. Kinetic Mechanism of Metallo-β-Lactamase L1 from *Stenotrophomonas maltophilia*. Biochemistry **38:**1547-1553.

291. **Hawk MJ, Breece RM, Hajdin CE, Bender KM, Hu Z, Costello AL, Bennett B, Tierney DL, Crowder MW.** 2009. Differential Binding of Co(II) and Zn(II) to Metallo-β-Lactamase Bla2 from *Bacillus anthracis*. J Am Chem Soc **131:**10753-10762.

292. **O'Callaghan CH, Morris A, Kirby SM, Shingler AH.** 1972. Novel Method for Detection of β-Lactamases by Using a Chromogenic Cephalosporin Substrate. Antimicrob Agents Chemother **1:**283-288.

293. **Oelschlaeger P, Aitha M, Yang H, Kang JS, Zhang AL, Liu EM, Buynak JD, Crowder MW.** 2015. Meropenem and Chromacef Intermediates Observed in IMP-25 Metallo-β-Lactamase-Catalyzed Hydrolysis. Antimicrob Agents Chemother **59:**4326-4330.

294. **Garrity JD, Carenbauer AL, Herron LR, Crowder MW.** 2004. Metal Binding Asp-120 in Metallo-β-lactamase L1 from *Stenotrophomonas maltophilia* Plays a Crucial Role in Catalysis. J Biol Chem **279:**920-927.

295. **Llarrull LI, Fabiane SM, Kowalski JM, Bennett B, Sutton BJ, Vila AJ.** 2007. Asp-120 Locates Zn2 for Optimal Metallo-Beta-Lactamase Activity. J Biol Chem **282:**18276-18285.

296. **Zhang H, Hao Q.** 2011. Crystal Structure of NDM-1 Reveals a Common Beta-Lactam Hydrolysis Mechanism. FASEB J **25:**2574-2582.

297. **Fonseca F, Bromley EH, Saavedra MJ, Correia A, Spencer J.** 2011. Crystal Structure of *Serratia fonticola* Sfh-I: Activation of the Nucleophile in Mono-Zinc Metallo-Beta-Lactamases. J Mol Biol **411:**951-959.

298. **Sharma NP, Hajdin C, Chandrasekar S, Bennett B, Yang KW, Crowder MW.** 2006. Mechanistic Studies on the Mononuclear Zn(II)-Containing Metallo-Beta-Lactamase ImiS from *Aeromonas sobria*. Biochemistry **45:**10729-10738.

299. **Franz KJ.** 2013. Clawing Back: Broadening the Notion of Metal Chelators in Medicine. Curr Opin Chem Biol **17:**143-149.

300. **Lienard BM, Garau G, Horsfall L, Karsisiotis AI, Damblon C, Lassaux P, Papamicael C, Roberts GC, Galleni M, Dideberg O, Frere JM, Schofield CJ.** 2008. Structural Basis for the Broad-Spectrum Inhibition of Metallo-Beta-Lactamases by Thiols. Org Biomol Chem **6:**2282-2294.

301. **Minond D, Saldanha SA, Subramaniam P, Spaargaren M, Spicer T, Fotsing JR, Weide T, Fokin VV, Sharpless KB, Galleni M, Bebrone C, Lassaux P, Hodder P.** 2009. Inhibitors of VIM-2 by Screening Pharmacologically Active and Click-Chemistry Compound Libraries. Bioorg Med Chem **17:**5027-5037.

302. **Johnson JW.** 2011. Cyclobutanone Analogues of β-Lactam Antibiotics as Inhibitors of Serine- and Metallo-β-Lactamases. UWSpace.

303. **Toney JH, Moloughney JG.** 2004. Metallo-Beta-Lactamase Inhibitors: Promise for the Future? Curr Opin Investig Drugs **5:**823-826.

304. **Faridoon, Ul Islam N.** 2013. An Update on the Status of Potent Inhibitors of Metallo-β-Lactamases. Scientia Pharmaceutica **81:**309-327.

305. **Toney JH, Fitzgerald PM, Grover-Sharma N, Olson SH, May WJ, Sundelof JG, Vanderwall DE, Cleary KA, Grant SK, Wu JK, Kozarich JW, Pompliano DL, Hammond GG.** 1998. Antibiotic Sensitization Using Biphenyl Tetrazoles as Potent Inhibitors of *Bacteroides fragilis* Metallo-Beta-Lactamase. Chem Biol **5:**185-196.

306. **Toney JH, Hammond GG, Fitzgerald PM, Sharma N, Balkovec JM, Rouen GP, Olson SH, Hammond ML, Greenlee ML, Gao YD.** 2001. Succinic Acids as Potent Inhibitors of Plasmid-Borne IMP-1 Metallo-Beta-Lactamase. J Biol Chem **276:**31913-31918.

307. **Moloughney JG, J DT, Toney JH.** 2005. Novel IMP-1 Metallo-Beta-Lactamase Inhibitors Can Reverse Meropenem Resistance in *Escherichia coli* Expressing IMP-1. FEMS Microbiol Lett **243:**65-71.

308. **Horsfall LE, Garau G, Liénard BMR, Dideberg O, Schofield CJ, Frère JM, Galleni M.** 2007. Competitive Inhibitors of the CphA Metallo-β-Lactamase from *Aeromonas hydrophila*. Antimicrob Agents Chemother **51:**2136-2142.

309. **Roll DM, Yang Y, Wildey MJ, Bush K, Lee MD.** 2010. Inhibition of Metallo-β-Lactamases by Pyridine Monothiocarboxylic Acid Analogs. J Antibiot **63:**255-257.

310. **Walter MW, Felici A, Galleni M, Soto RP, Adlington RM, Baldwin JE, Frère J-M, Gololobov M, Schofield CJ.** 1996. Trifluoromethyl Alcohol and Ketone Inhibitors of Metallo-β-Lactamases. Bioorg Med Chem Lett **6:**2455-2458.

311. **Hiraiwa Y, Morinaka A, Fukushima T, Kudo T.** 2009. Metallo-Beta-Lactamase Inhibitory Activity of Phthalic Acid Derivatives. Bioorg Med Chem Lett **19:**5162-5165.

312. **Lienard BM, Horsfall LE, Galleni M, Frere JM, Schofield CJ.** 2007. Inhibitors of the FEZ-1 Metallo-Beta-Lactamase. Bioorg Med Chem Lett **17:**964-968.

313. **Damblon C, Jensen M, Ababou A, Barsukov I, Papamicael C, Schofield CJ, Olsen L, Bauer R, Roberts GCK.** 2003. The Inhibitor Thiomandelic Acid Binds to Both Metal Ions in Metallo-β-lactamase and Induces Positive Cooperativity in Metal Binding. J Biol Chem **278:**29240-29251.

314. **Siemann S, Clarke AJ, Viswanatha T, Dmitrienko GI.** 2003. Thiols as Classical and Slow-Binding Inhibitors of IMP-1 and Other Binuclear Metallo-Beta-Lactamases. Biochemistry **42:**1673-1683.

315. **Lassaux P, Hamel M, Gulea M, Delbruck H, Mercuri PS, Horsfall L, Dehareng D, Kupper M, Frere JM, Hoffmann K, Galleni M, Bebrone C.** 2010. Mercaptophosphonate Compounds as Broad-Spectrum Inhibitors of the Metallo-Beta-Lactamases. J Med Chem **53:**4862-4876.

316. **Mollard C, Moali C, Papamicael C, Damblon C, Vessilier S, Amicosante G, Schofield CJ, Galleni M, Frère J-M, Roberts GCK.** 2001. Thiomandelic Acid, a Broad Spectrum Inhibitor of Zinc β-Lactamases: Kinetic and Spectroscopic Studies. J Biol Chem **276:**45015-45023.

317. **Yusof Y, Tan DTC, Arjomandi OK, Schenk G, McGeary RP.** 2016. Captopril Analogues as Metallo-β-Lactamase Inhibitors. Bioorg Med Chem Lett **26:**1589-1593.

318. **Brem J, van Berkel SS, Aik W, Rydzik AM, Avison MB, Pettinati I, Umland K-D, Kawamura A, Spencer J, Claridge TDW, McDonough MA, Schofield CJ.** 2014. Rhodanine Hydrolysis Leads to Potent Thioenolate Mediated Metallo-β-Lactamase Inhibition. Nat Chem **6:**1084-1090.

319. **Payne DJ, Bateson JH, Gasson BC, Proctor D, Khushi T, Farmer TH, Tolson DA, Bell D, Skett PW, Marshall AC, Reid R, Ghosez L, Combret Y, Marchand-Brynaert J.** 1997. Inhibition of Metallo-Beta-Lactamases by a Series of Mercaptoacetic Acid Thiol Ester Derivatives. Antimicrob Agents Chemother **41:**135-140.

320. **Buynak JD, Chen H, Vogeti L, Gadhachanda VR, Buchanan CA, Palzkill T, Shaw RW, Spencer J, Walsh TR.** 2004. Penicillin-Derived Inhibitors that Simultaneously Target Both Metallo- and Serine-β-lactamases. Bioorg Med Chem Lett **14:**1299-1304.

321. **Tsang WY, Dhanda A, Schofield CJ, Frere JM, Galleni M, Page MI.** 2004. The Inhibition of Metallo-Beta-Lactamase by Thioxo-Cephalosporin Derivatives. Bioorg Med Chem Lett **14:**1737-1739.

322. **Badarau A, Llinas A, Laws AP, Damblon C, Page MI.** 2005. Inhibitors of Metallo-Beta-Lactamase Generated from Beta-Lactam Antibiotics. Biochemistry **44:**8578-8589.

323. **Beharry Z, Chen H, Gadhachanda VR, Buynak JD, Palzkill T.** 2004. Evaluation of Penicillin-Based Inhibitors of the Class A and B Beta-Lactamases from *Bacillus anthracis*. Biochem Biophys Res Commun **313:**541-545.

324. **Ganta SR, Perumal S, Pagadala SR, Samuelsen O, Spencer J, Pratt RF, Buynak JD.** 2009. Approaches to the Simultaneous Inactivation of Metallo- and Serine-Beta-Lactamases. Bioorg Med Chem Lett **19:**1618-1622.

325. **Johnson JW, Gretes M, Goodfellow VJ, Marrone L, Heynen ML, Strynadka NC, Dmitrienko GI.** 2010. Cyclobutanone Analogues of Beta-Lactams Revisited: Insights into Conformational Requirements for Inhibition of Serine- and Metallo-Beta-Lactamases. J Am Chem Soc **132:**2558-2560.

326. **Cahill ST, Tarhonskaya H, Rydzik AM, Flashman E, McDonough MA, Schofield CJ, Brem J.** 2016. Use of Ferrous Iron by Metallo-β-Lactamases. J Inorg Biochem **163:**185-193.

327. **Badarau A, Page MI.** 2006. The Variation of Catalytic Efficiency of *Bacillus cereus* Metallo-β-Lactamase with Different Active Site Metal Ions. Biochemistry **45:**10654-10666.

328. **Baier F, Chen J, Solomonson M, Strynadka NCJ, Tokuriki N.** 2015. Distinct Metal Isoforms Underlie Promiscuous Activity Profiles of Metalloenzymes. ACS Chemical Biology **10:**1684-1693.

329. **Crawford PA, Yang KW, Sharma N, Bennett B, Crowder MW.** 2005. Spectroscopic Studies on Cobalt(II)-Substituted Metallo-Beta-Lactamase ImiS from *Aeromonas veronii bv. sobria*. Biochemistry **44:**5168-5176.

330. **Hu Z, Periyannan G, Bennett B, Crowder MW.** 2008. Role of the Zn1 and Zn2 sites in Metallo-β-lactamase L1. J Am Chem Soc **130:**14207-14216.

331. **Crowder MW, Maiti MK, Banovic L, Makaroff CA.** 1997. Glyoxalase II from *A. thaliana* Requires Zn(II) for Catalytic Activity. FEBS Lett **418:**351-354.

332. **Vogel A, Schilling O, Niecke M, Bettmer J, Meyer-Klaucke W.** 2002. ElaC Encodes a Novel Binuclear Zinc Phosphodiesterase. J Biol Chem **277:**29078-29085.

333. **Hu Z, Gunasekera TS, Spadafora L, Bennett B, Crowder MW.** 2008. Metal Content of Metallo-β-Lactamase L1 is Determined by the Bioavailability of Metal Ions. Biochemistry **47:**7947-7953.

334. **Thomas PW, Zheng M, Wu S, Guo H, Liu D, Xu D, Fast W.** 2011. Characterization of Purified New Delhi Metallo-β-Lactamase-1. Biochemistry **50:**10102-10113.

335. **Doherty CP.** 2007. Host-Pathogen Interactions: The Role of Iron. J Nutr **137:**1341-1344.

336. **Skaar EP.** 2010. The Battle for Iron Between Bacterial Pathogens and Their Vertebrate Hosts. PLoS Path **6:**e1000949.

337. **Frazao C, Silva G, Gomes CM, Matias P, Coelho R, Sieker L, Macedo S, Liu MY, Oliveira S, Teixeira M, Xavier AV, Rodrigues-Pousada C, Carrondo MA, Le Gall J.** 2000. Structure of a Dioxygen Reduction Enzyme from *Desulfovibrio gigas*. Nat Struct Mol Biol **7:**1041-1045.

338. **Silaghi-Dumitrescu R, Kurtz DM, Ljungdahl LG, Lanzilotta WN.** 2005. X-ray Crystal Structures of *Moorella thermoacetica* FprA. Novel Diiron Site Structure and Mechanistic Insights into a Scavenging Nitric Oxide Reductase. Biochemistry **44:**6492-6501.

339. **McCoy JG, Bingman CA, Bitto E, Holdorf MM, Makaroff CA, Phillips GN, Jr.** 2006. Structure of an ETHE1-Like Protein from *Arabidopsis thaliana*. Acta Crystallogr Sect D Biol Crystallogr **62:**964-970.

340. **Tiranti V, D'Adamo P, Briem E, Ferrari G, Mineri R, Lamantea E, Mandel H, Balestri P, Garcia-Silva M-T, Vollmer B, Rinaldo P, Hahn SH, Leonard J, Rahman S, Dionisi-Vici C, Garavaglia B, Gasparini P, Zeviani M.** 2004. Ethylmalonic Encephalopathy is Caused by Mutations in ETHE1, a Gene Encoding a Mitochondrial Matrix Protein. Am J Hum Genet **74:**239-252.

341. **Makris TM, Knoot CJ, Wilmot CM, Lipscomb JD.** 2013. Structure of a Dinuclear Iron Cluster-Containing Beta Hydroxylase Active in Antibiotic Biosynthesis. Biochemistry **52:**10.1021/bi400845b.

342. **Arts IS, Gennaris A, Collet J-F.** 2015. Reducing Systems Protecting the Bacterial Cell Envelope from Oxidative Damage. FEBS Lett **589:**1559-1568.

343. **Holmgren A, Fagerstedt M.** 1982. The *In Vivo* Distribution of Oxidized and Reduced Thioredoxin in *Escherichia coli*. J Biol Chem **257:**6926-6930.

344. **Minsky A, Summers RG, Knowles JR.** 1986. Secretion of Beta-Lactamase into the Periplasm of *Escherichia coli*: Evidence for a Distinct Release Step Associated with a Conformational Change. Proc Natl Acad Sci USA **83:**4180-4184.

345. **de Seny D, Prosperi-Meys C, Bebrone C, Rossolini GM, Page MI, Noel P, Frère J-M, Galleni M.** 2002. Mutational Analysis of the Two Zinc-Binding Sites of the *Bacillus cereus* 569/H/9 Metallo-Beta-Lactamase. Biochem J **363:**687-696.

346. **Makena A, van Berkel SS, Lejeune C, Owens RJ, Verma A, Salimraj R, Spencer J, Brem J, Schofield CJ.** 2013. Chromophore-Linked Substrate (CLS405): Probing Metallo-β-Lactamase Activity and Inhibition. ChemMedChem **8:**1923-1929.

347. **GraphPadPrism.** v5.04. GraphPad Software, San Diego, California, USA. www.graphpad.com.

348. **Davies AM, Rasia RM, Vila AJ, Sutton BJ, Fabiane SM.** 2005. Effect of pH on the Active Site of an Arg121Cys Mutant of the Metallo-β-Lactamase from *Bacillus cereus*: Implications for the Enzyme Mechanism. Biochemistry **44:**4841-4849.

349. **OriginPro.** v8.5.1. OriginLab, Northampton, Massachusetts, USA. www.originlab.com.

350. **Wang Z, Fast W, Benkovic SJ.** 1998. Direct Observation of an Enzyme-Bound Intermediate in the Catalytic Cycle of the Metallo-β-Lactamase from *Bacteroides fragilis*. J Am Chem Soc **120:**10788-10789.

351. **Johnson KA, Simpson ZB, Blom T.** 2009. Global Kinetic Explorer: A New Computer Program for Dynamic Simulation and Fitting of Kinetic Data. Anal Biochem **387:**20-29.

352. **Kintek Explorer.** v2.03. KinTek Corporation, Snow Shoe, Pennsylvania, USA. www.kintekexplorer.com.

353. **Ohsuka S, Arakawa Y, Horii T, Ito H, Ohta M.** 1995. Effect of pH on Activities of Novel Beta-Lactamases and Beta-Lactamase Inhibitors Against these Beta-Lactamases. Antimicrob Agents Chemother **39:**1856-1858.

354. **Mercuri PS, Bouillenne F, Boschi L, Lamotte-Brasseur J, Amicosante G, Devreese B, van Beeumen J, Frère J-M, Rossolini GM, Galleni M.** 2001. Biochemical Characterization of the FEZ-1 Metallo-β-Lactamase of *Legionella gormanii* ATCC 33297T Produced in *Escherichia coli*. Antimicrob Agents Chemother **45:**1254-1262.

355. **Karsisiotis AI, Damblon CF, Roberts GCK.** 2013. Solution Structures of the *Bacillus cereus* Metallo-β-Lactamase BcII and its Complex with the Broad Spectrum Inhibitor *R*-Thiomandelic Acid. Biochem J **456:**397-407.

356. **Smith RM, Martell AE.** 1976. Critical Stability Constants. Plenum Press, New York.

357. **González JM, Meini M-R, Tomatis PE, Martín FJM, Cricco JA, Vila AJ.** 2012. Metallo-β-Lactamases Withstand Low Zn(II) Conditions by Tuning Metal-Ligand Interactions. Nat Chem Biol **8:**698-700.

358. **Roach PL, Clifton IJ, Hensgens CMH, Shibata N, Long AJ, Strange RW, Hasnain SS, Schofield CJ, Baldwin JE, Hajdu J.** 1996. Anaerobic

Crystallisation of an Isopenicillin N Synthase · Fe(II) · Substrate Complex Demonstrated by X-ray Studies. Eur J Biochem **242:**736-740.

359. **González JM, Buschiazzo A, Vila AJ.** 2010. Evidence of Adaptability in Metal Coordination Geometry and Active-Site Loop Conformation Among B1 Metallo-β-Lactamases. Biochemistry **49:**7930-7938.
360. **Battye TGG, Kontogiannis L, Johnson O, Powell HR, Leslie AGW.** 2011. iMOSFLM: A New Graphical Interface for Diffraction-Image Processing with MOSFLM. Acta Crystallogr Sect D Biol Crystallogr **67:**271-281.
361. **Evans PR, Murshudov GN.** 2013. How Good are my Data and What is the Resolution? Acta Crystallogr Sect D Biol Crystallogr **69:**1204-1214.
362. **Adams PD, Grosse-Kunstleve RW, Hung L-W, Ioerger TR, McCoy AJ, Moriarty NW, Read RJ, Sacchettini JC, Sauter NK, Terwilliger TC.** 2002. PHENIX: Building New Software for Automated Crystallographic Structure Determination. Acta Crystallogr Sect D Biol Crystallogr **58:**1948-1954.
363. **Emsley P, Lohkamp B, Scott WG, Cowtan K.** 2010. Features and Development of Coot. Acta Crystallogr Sect D Biol Crystallogr **66:**486-501.
364. **Kruidenier L, Chung C-W, Cheng Z, Liddle J, Che K, Joberty G, Bantscheff M, Bountra C, Bridges A, Diallo H, Eberhard D, Hutchinson S, Jones E, Katso R, Leveridge M, Mander PK, Mosley J, Ramirez-Molina C, Rowland P, Schofield CJ, Sheppard RJ, Smith JE, Swales C, Tanner R, Thomas P, Tumber A, Drewes G, Oppermann U, Patel DJ, Lee K, Wilson DM.** 2012. A Selective Jumonji H3K27 Demethylase Inhibitor Modulates the Proinflammatory Macrophage Response. Nature **488:**404-408.
365. **Hopkinson RJ, Tumber A, Yapp C, Chowdhury R, Aik W, Che KH, Li XS, Kristensen JBL, King ONF, Chan MC, Yeoh KK, Choi H, Walport LJ, Thinnes CC, Bush JT, Lejeune C, Rydzik AM, Rose NR, Bagg EA, McDonough MA, Krojer TJ, Yue WW, Ng SS, Olsen L, Brennan PE, Oppermann U, Muller S, Klose RJ, Ratcliffe PJ, Schofield CJ, Kawamura A.** 2013. 5-Carboxy-8-Hydroxyquinoline is a Broad Spectrum 2-Oxoglutarate Oxygenase Inhibitor Which Causes Iron Translocation. Chemical Science **4:**3110-3117.
366. **Oelschlaeger P, Schmid RD, Pleiss J.** 2003. Insight into the Mechanism of the IMP-1 Metallo-β-Lactamase by Molecular Dynamics Simulations. Protein Eng **16:**341-350.
367. **Breece RM, Hu Z, Bennett B, Crowder MW, Tierney DL.** 2009. Motion of the Zinc Ions in Catalysis by a Dizinc Metallo-β-Lactamase. J Am Chem Soc **131:**11642-11643.

368. **Lau CKY, Krewulak KD, Vogel HJ.** 2015. Bacterial Ferrous Iron Transport: The Feo System. FEMS Microbiol Rev.

369. **Krewulak KD, Vogel HJ.** 2008. Structural Biology of Bacterial Iron Uptake. Biochim Biophys Acta **1778:**1781-1804.

370. **Brem J, Cain R, Cahill S, McDonough MA, Clifton IJ, Jimenez-Castellanos J-C, Avison MB, Spencer J, Fishwick CWG, Schofield CJ.** 2016. Structural Basis of Metallo-β-Lactamase, Serine-β-Lactamase and Penicillin-Binding Protein Inhibition by Cyclic Boronates. Nat Commun **7**.

371. **Cahill ST, Cain R, Wang DY, Lohans CT, Wareham DW, Oswin HP, Mohammed J, Spencer J, Fishwick CWG, McDonough MA, Schofield CJ, Brem J.** 2017. Cyclic Boronates Inhibit All Classes of β-Lactamase. Antimicrob Agents Chemother.

372. **Marshall S, Hujer AM, Rojas LJ, Papp-Wallace KM, Humphries RM, Spellberg B, Hujer KM, Marshall EK, Rudin SD, Perez F, Wilson BM, Wasserman RB, Chikowski L, Paterson DL, Vila AJ, van Duin D, Kreiswirth BN, Chambers HF, Fowler VG, Jacobs MR, Pulse ME, Weiss WJ, Bonomo RA.** 2017. Can Ceftazidime/Avibactam and Aztreonam Overcome β-Lactam Resistance Conferred by Metallo-β-Lactamases in *Enterobacteriaceae*? Antimicrob Agents Chemother.

373. **Biedenbach DJ, Kazmierczak K, Bouchillon SK, Sahm DF, Bradford PA.** 2015. *In Vitro* Activity of Aztreonam-Avibactam Against a Global Collection of Gram-Negative Pathogens from 2012-2013. Antimicrob Agents Chemother **59:**4239-4248.

374. **Vasoo S, Cunningham SA, Cole NC, Kohner PC, Menon SR, Krause KM, Harris KA, De PP, Koh TH, Patel R.** 2015. *In Vitro* Activities of Ceftazidime-Avibactam, Aztreonam-Avibactam, and a Panel of Older and Contemporary Antimicrobial Agents against Carbapenemase-Producing Gram-Negative *Bacilli*. Antimicrob Agents Chemother **59:**7842-7846.

375. **Wang X, Zhang F, Zhao C, Wang Z, Nichols WW, Testa R, Li H, Chen H, He W, Wang Q, Wang H.** 2014. *In Vitro* Activities of Ceftazidime-Avibactam and Aztreonam-Avibactam against 372 Gram-Negative *Bacilli* Collected in 2011 and 2012 from 11 Teaching Hospitals in China. Antimicrob Agents Chemother **58:**1774-1778.

376. **Krishnan NP, Nguyen NQ, Papp-Wallace KM, Bonomo RA, van den Akker F.** 2015. Inhibition of *Klebsiella* β-Lactamases (SHV-1 and KPC-2) by Avibactam: A Structural Study. PLOS ONE **10:**e0136813.

377. **Queenan AM, Bush K.** 2007. Carbapenemases: The Versatile β-Lactamases. Clin Microbiol Rev **20:**440-458.

378. **Walther-Rasmussen J, Høiby N.** 2006. OXA-Type Carbapenemases. J Antimicrob Chemother **57:**373-383.
379. **Taibi P, Mobashery S.** 1995. Mechanism of Turnover of Imipenem by the TEM β-Lactamase Revisited. J Am Chem Soc **117:**7600-7605.
380. **Maveyraud L, Mourey L, Kotra LP, Pedelacq J-D, Guillet V, Mobashery S, Samama J-P.** 1998. Structural Basis for Clinical Longevity of Carbapenem Antibiotics in the Face of Challenge by the Common Class A β-Lactamases from the Antibiotic-Resistant Bacteria. J Am Chem Soc **120:**9748-9752.
381. **Beadle BM, Shoichet BK.** 2002. Structural Basis for Imipenem Inhibition of Class C β-Lactamases. Antimicrob Agents Chemother **46:**3978-3980.
382. **Nukaga M, Bethel CR, Thomson JM, Hujer AM, Distler A, Anderson VE, Knox JR, Bonomo RA.** 2008. Inhibition of Class A β-Lactamases by Carbapenems: Crystallographic Observation of Two Conformations of Meropenem in SHV-1. J Am Chem Soc **130:**12656-12662.
383. **Usher KC, Blaszczak LC, Weston GS, Shoichet BK, Remington SJ.** 1998. Three-Dimensional Structure of AmpC Beta-Lactamase from *Escherichia coli* Bound to a Transition-State Analogue: Possible Implications for the Oxyanion Hypothesis and for Inhibitor Design. Biochemistry **37:**16082-16092.
384. **Murphy BP, Pratt RF.** 1988. Evidence for an Oxyanion Hole in Serine Beta-Lactamases and *DD*-Peptidases. Biochem J **256:**669-672.
385. **Pernot L, Frenois F, Rybkine T, L'Hermite G, Petrella S, Delettre J, Jarlier V, Collatz E, Sougakoff W.** 2001. Crystal Structures of the Class D Beta-Lactamase OXA-13 in the Native Form and in Complex with Meropenem. J Mol Biol **310:**859-874.
386. **Schneider KD, Karpen ME, Bonomo RA, Leonard DA, Powers RA.** 2009. The 1.4 Å Crystal Structure of the Class D β-Lactamase OXA-1 Complexed with Doripenem. Biochemistry **48:**11840-11847.
387. **Bush K, Freudenberger JS, Sykes RB.** 1982. Interaction of Azthreonam and Related Monobactams with Beta-Lactamases from Gram-Negative Bacteria. Antimicrob Agents Chemother **22:**414-420.
388. **Sykes RB, Bonner DP, Bush K, Georgopapadakou NH.** 1982. Azthreonam (SQ 26,776), a Synthetic Monobactam Specifically Active Against Aerobic Gram-Negative Bacteria. Antimicrob Agents Chemother **21:**85-92.
389. **Knott-Hunziker V, Petursson S, Waley SG, Jaurin B, Grundström T.** 1982. The Acyl-Enzyme Mechanism of Beta-Lactamase Action. The Evidence for Class C Beta-Lactamases. Biochem J **207:**315-322.

390. **Hubschwerlen C, Angehrn P, Gubernator K, Page MG, Specklin JL.** 1998. Structure-Based Design of Beta-Lactamase Inhibitors. 2. Synthesis and Evaluation of Bridged Sulfactams and Oxamazins. J Med Chem **41:**3972-3975.

391. **Heinze-Krauss I, Angehrn P, Charnas RL, Gubernator K, Gutknecht E-M, Hubschwerlen C, Kania M, Oefner C, Page MGP, Sogabe S, Specklin J-L, Winkler F.** 1998. Structure-Based Design of β-Lactamase Inhibitors. 1. Synthesis and Evaluation of Bridged Monobactams. J Med Chem **41:**3961-3971.

392. **Strynadka NCJ, Adachi H, Jensen SE, Johns K, Sielecki A, Betzel C, Sutoh K, James MNG.** 1992. Molecular Structure of the Acyl-Enzyme Intermediate in β-Lactam Hydrolysis at 1.7 Å Resolution. Nature **359:**700-705.

393. **Bulychev A, Bellettini JR, O'Brien M, Crocker PJ, Samama J-P, Miller MJ, Mobashery S.** 2000. *N*-Sulfonyloxy-β-lactam Inhibitors for β-Lactamases. Tetrahedron **56:**5719-5728.

394. **Farmer TH, Page JW, Payne DJ, Knowles DJ.** 1994. Kinetic and Physical Studies of Beta-Lactamase Inhibition by a Novel Penem, BRL 42715. Biochem J **303:**825-830.

395. **Pattanaik P, Bethel CR, Hujer AM, Hujer KM, Distler AM, Taracila M, Anderson VE, Fritsche TR, Jones RN, Pagadala SR, van den Akker F, Buynak JD, Bonomo RA.** 2009. Strategic Design of an Effective Beta-Lactamase Inhibitor: LN-1-255, a 6-Alkylidene-2'-Substituted Penicillin Sulfone. J Biol Chem **284:**945-953.

396. **Matagne A, Ledent P, Monnaie D, Felici A, Jamin M, Raquet X, Galleni M, Klein D, François I, Frère JM.** 1995. Kinetic Study of Interaction Between BRL 42715, Beta-Lactamases, and *D*-Alanyl-*D*-Alanine Peptidases. Antimicrob Agents Chemother **39:**227-231.

397. **Tabei K, Feng X, Venkatesan AM, Abe T, Hideki U, Mansour TS, Siegel MM.** 2004. Mechanism of Inactivation of β-Lactamases by Novel 6-Methylidene Penems Elucidated Using Electrospray Ionization Mass Spectrometry. J Med Chem **47:**3674-3688.

398. **Michaux C, Charlier P, Frere JM, Wouters J.** 2005. Crystal Structure of BRL 42715, C6-(N1-Methyl-1,2,3-triazolylmethylene)penem, in Complex with *Enterobacter cloacae* 908R Beta-Lactamase: Evidence for a Stereoselective Mechanism from Docking Studies. J Am Chem Soc **127:**3262-3263.

399. **Nukaga M, Abe T, Venkatesan AM, Mansour TS, Bonomo RA, Knox JR.** 2003. Inhibition of Class A and Class C β-Lactamases by Penems: Crystallographic Structures of a Novel 1,4-Thiazepine Intermediate. Biochemistry **42:**13152-13159.

400. **Venkatesan AM, Gu Y, Santos OD, Abe T, Agarwal A, Yang Y, Petersen PJ, Weiss WJ, Mansour TS, Nukaga M, Hujer AM, Bonomo RA, Knox JR.** 2004. Structure–Activity Relationship of 6-Methylidene Penems Bearing Tricyclic Heterocycles as Broad-Spectrum β-Lactamase Inhibitors: Crystallographic Structures Show Unexpected Binding of 1,4-Thiazepine Intermediates. J Med Chem **47:**6556-6568.

401. **Nagano R, Adachi Y, Imamura H, Yamada K, Hashizume T, Morishima H.** 1999. Carbapenem Derivatives as Potential Inhibitors of Various Beta-Lactamases, Including Class B Metallo-Beta-Lactamases. Antimicrob Agents Chemother **43:**2497-2503.

402. **Dobozy O, Mile I, Ferencz I, Csanyi V.** 1971. Effect of Electrolytes on the Activity and Iodine Sensitivity of Penicillinase from *B. cereus*. Acta Biochim Biophys Acad Sci Hung **6:**97-105.

403. **Kiener PA, Waley SG.** 1978. Reversible Inhibitors of Penicillinases. Biochem J **169:**197-204.

404. **Lindquist RN, Terry C.** 1974. Inhibition of Subtilisin by Boronic Acids, Potential Analogs of Tetrahedral Reaction Intermediates. Arch Biochem Biophys **160:**135-144.

405. **Bone R, Shenvi AB, Kettner CA, Agard DA.** 1987. Serine Protease Mechanism: Structure of an Inhibitory Complex of α-Lytic Protease and a Tightly Bound Peptide Boronic Acid. Biochemistry **26:**7609-7614.

406. **Lienhard GE, Koehler KA.** 1971. 2-Phenylethaneboronic Acid, a Possible Transition-State Analog for Chymotrypsin. Biochemistry **10:**2477-2483.

407. **Lide DR.** 2016. CRC Handbook of Chemistry and Physics, 97th ed. CRC Press, Boca Raton, Florida.

408. **Cama E, Shin H, Christianson DW.** 2003. Design of Amino Acid Sulfonamides as Transition-State Analogue Inhibitors of Arginase. J Am Chem Soc **125:**13052-13057.

409. **Smoum R, Rubinstein A, Dembitsky VM, Srebnik M.** 2012. Boron Containing Compounds as Protease Inhibitors. Chem Rev **112:**4156-4220.

410. **Beesley T, Gascoyne N, Knott-Hunziker V, Petursson S, Waley SG, Jaurin B, Grundström T.** 1983. The Inhibition of Class C Beta-Lactamases by Boronic Acids. Biochem J **209:**229-233.

411. **Crompton IE, Cuthbert BK, Lowe G, Waley SG.** 1988. Beta-Lactamase Inhibitors. The Inhibition of Serine Beta-Lactamases by Specific Boronic Acids. Biochem J **251:**453-459.

412. **Winkler ML, Rodkey EA, Taracila MA, Drawz SM, Bethel CR, Papp-Wallace KM, Smith KM, Xu Y, Dwulit-Smith JR, Romagnoli C, Caselli E,**

Prati F, van den Akker F, Bonomo RA. 2013. Design and Exploration of Novel Boronic Acid Inhibitors Reveals Important Interactions with a Clavulanic Acid-Resistant Sulfhydryl-Variable (SHV) β-Lactamase. J Med Chem **56:**1084-1097.

413. **Werner JP, Mitchell JM, Taracila MA, Bonomo RA, Powers RA.** 2017. Exploring the Potential of Boronic Acids as Inhibitors of OXA-24/40 β-Lactamase. Protein Sci **26:**515-526.
414. **Rojas LJ, Taracila MA, Papp-Wallace KM, Bethel CR, Caselli E, Romagnoli C, Winkler ML, Spellberg B, Prati F, Bonomo RA.** 2016. Boronic Acid Transition State Inhibitors Active Against KPC and Other Class A Beta-Lactamases: Structure-Activity Relationships as a Guide to Inhibitor Design. Antimicrob Agents Chemother **60:**1751-1759.
415. **Thomson JM, Prati F, Bethel CR, Bonomo RA.** 2007. Use of Novel Boronic Acid Transition State Inhibitors To Probe Substrate Affinity in SHV-Type Extended-Spectrum β-Lactamases. Antimicrob Agents Chemother **51:**1577-1579.
416. **Chen Y, Shoichet B, Bonnet R.** 2005. Structure, Function, and Inhibition along the Reaction Coordinate of CTX-M β-Lactamases. J Am Chem Soc **127:**5423-5434.
417. **Drawz SM, Babic M, Bethel CR, Taracila M, Distler AM, Ori C, Caselli E, Prati F, Bonomo RA.** 2010. Inhibition of the Class C β-Lactamase from *Acinetobacter spp*: Insights into Effective Inhibitor Design. Biochemistry **49:**329-340.
418. **Adams J, Kauffman M.** 2004. Development of the Proteasome Inhibitor Velcade (Bortezomib). Cancer Invest **22:**304-311.
419. **Curran MP, McKeage K.** 2009. Bortezomib: A Review of its Use in Patients with Multiple Myeloma. Drugs **69:**859-888.
420. **Bonvini P, Zorzi E, Basso G, Rosolen A.** 2007. Bortezomib-Mediated 26S Proteasome Inhibition Causes Cell-Cycle Arrest and Induces Apoptosis in CD-30+ Anaplastic Large Cell Lymphoma. Leukemia **21:**838-842.
421. **Groll M, Berkers CR, Ploegh HL, Ovaa H.** 2006. Crystal Structure of the Boronic Acid-Based Proteasome Inhibitor Bortezomib in Complex with the Yeast 20S Proteasome. Structure **14:**451-456.
422. **Cox JD, Kim NN, Traish AM, Christianson DW.** 1999. Arginase-Boronic Acid Complex Highlights a Physiological Role in Erectile Function. Nat Struct Mol Biol **6:**1043-1047.
423. **Di Costanzo L, Sabio G, Mora A, Rodriguez PC, Ochoa AC, Centeno F, Christianson DW.** 2005. Crystal Structure of Human Arginase I at 1.29-Å Resolution and Exploration of Inhibition in the Immune Response. Proc Natl Acad Sci U S A **102:**13058-13063.

424. **Winum JY, Innocenti A, Scozzafava A, Montero JL, Supuran CT.** 2009. Carbonic Anhydrase Inhibitors. Inhibition of the Human Cytosolic Isoforms I and II and Transmembrane, Tumor-Associated Isoforms IX and XII with Boronic Acids. Bioorg Med Chem **17:**3649-3652.

425. **Innocenti A, Winum JY, Hall RA, Muhlschlegel FA, Scozzafava A, Supuran CT.** 2009. Carbonic Anhydrase Inhibitors. Inhibition of the Fungal Beta-Carbonic Anhydrases from *Candida albicans* and *Cryptococcus neoformans* with Boronic Acids. Bioorg Med Chem Lett **19:**2642-2645.

426. **Alterio V, Cadoni R, Esposito D, Vullo D, Fiore AD, Monti SM, Caporale A, Ruvo M, Sechi M, Dumy P, Supuran CT, Simone GD, Winum J-Y.** 2016. Benzoxaborole as a New Chemotype for Carbonic Anhydrase Inhibition. Chem Commun (Camb) **52:**11983-11986.

427. **Matthews DA, Alden RA, Birktoft JJ, Freer ST, Kraut J.** 1975. X-ray Crystallographic Study of Boronic Acid Adducts with Subtilisin BPN' (Novo). A Model for the Catalytic Transition State. J Biol Chem **250:**7120-7126.

428. **D'Antonio EL, Ullman B, Roberts SC, Dixit UG, Wilson ME, Hai Y, Christianson DW.** 2013. Crystal Structure of Arginase from *Leishmania mexicana* and Implications for the Inhibition of Polyamine Biosynthesis in Parasitic Infections. Arch Biochem Biophys **535:**163-176.

429. **Nguyen NQ, Krishnan NP, Rojas LJ, Prati F, Caselli E, Romagnoli C, Bonomo RA, van den Akker F.** 2016. Crystal Structures of KPC-2 and SHV-1 β-Lactamases in Complex with the Boronic Acid Transition State Analog S02030. Antimicrob Agents Chemother **60:**1760-1766.

430. **Bebrone C, Anne C, De Vriendt K, Devreese B, Rossolini GM, Van Beeumen J, Frère J-M, Galleni M.** 2005. Dramatic Broadening of the Substrate Profile of the *Aeromonas hydrophila* CphA Metallo-β-Lactamase by Site-Directed Mutagenesis. J Biol Chem **280:**28195-28202.

431. **Griffin DH, Richmond TK, Sanchez C, Moller AJ, Breece RM, Tierney DL, Bennett B, Crowder MW.** 2011. Structural and Kinetic Studies on Metallo-β-Lactamase IMP-1. Biochemistry **50:**9125-9134.

432. **Green VL, Verma A, Owens RJ, Phillips SEV, Carr SB.** 2011. Structure of New Delhi Metallo-β-Lactamase 1 (NDM-1). Acta Crystallogr Sect F Struct Biol Cryst Commun **67:**1160-1164.

433. **van Berkel SS, Brem J, Rydzik AM, Salimraj R, Cain R, Verma A, Owens RJ, Fishwick CWG, Spencer J, Schofield CJ.** 2013. Assay Platform for Clinically Relevant Metallo-β-Lactamases. J Med Chem **56:**6945-6953.

434. **Inglis SR, Strieker M, Rydzik AM, Dessen A, Schofield CJ.** 2012. A Boronic-Acid-Based Probe for Fluorescence Polarization Assays with Penicillin Binding Proteins and β-Lactamases. Anal Biochem **420:**41-47.

435. **Sainsbury S, Bird L, Rao V, Shepherd SM, Stuart DI, Hunter WN, Owens RJ, Ren J.** 2011. Crystal Structures of Penicillin-Binding Protein 3 from *Pseudomonas aeruginosa*: Comparison of Native and Antibiotic-Bound Forms. J Mol Biol **405:**173-184.

436. **Kalp M, Totir MA, Buynak JD, Carey PR.** 2009. Different Intermediate Populations Formed by Tazobactam, Sulbactam, and Clavulanate Reacting with SHV-1 β-Lactamases: Raman Crystallographic Evidence. J Am Chem Soc **131:**2338-2347.

437. **Imtiaz U, Billings EM, Knox JR, Mobashery S.** 1994. A Structure-Based Analysis of the Inhibition of Class A β-Lactamases by Sulbactam. Biochemistry **33:**5728-5738.

438. **Ruzin A, Petersen PJ, Jones CH.** 2010. Resistance Development Profiling of Piperacillin in Combination with the Novel β-Lactamase Inhibitor BLI-489. J Antimicrob Chemother **65:**252-257.

439. **Petersen PJ, Jones CH, Venkatesan AM, Bradford PA.** 2009. Efficacy of Piperacillin Combined with the Penem β-Lactamase Inhibitor BLI-489 in Murine Models of Systemic Infection. Antimicrob Agents Chemother **53:**1698-1700.

440. **Hermanek S.** 1992. Boron-11 NMR Spectra of Boranes, Main-Group Heteroboranes, and Substituted Derivatives. Factors Influencing Chemical Shifts of Skeletal Atoms. Chem Rev **92:**325-362.

441. **Ness S, Martin R, Kindler AM, Paetzel M, Gold M, Jensen SE, Jones JB, Strynadka NCJ.** 2000. Structure-Based Design Guides the Improved Efficacy of Deacylation Transition State Analogue Inhibitors of TEM-1 β-Lactamase. Biochemistry **39:**5312-5321.

442. **Maveyraud L, Golemi D, Kotra LP, Tranier S, Vakulenko S, Mobashery S, Samama JP.** 2000. Insights into Class D Beta-Lactamases are Revealed by the Crystal Structure of the OXA-10 Enzyme from *Pseudomonas aeruginosa*. Structure **8:**1289-1298.

443. **Vshyvenko S, Clapson ML, Suzuki I, Hall DG.** 2016. Characterization of the Dynamic Equilibrium between Closed and Open Forms of the Benzoxaborole Pharmacophore. ACS Medicinal Chemistry Letters.

444. **Paetzel M, Danel F, de Castro L, Mosimann SC, Page MG, Strynadka NC.** 2000. Crystal Structure of the Class D Beta-Lactamase OXA-10. Nat Struct Biol **7:**918-925.

445. **Sauvage E, Powell AJ, Heilemann J, Josephine HR, Charlier P, Davies C, Pratt RF.** 2008. Crystal Structures of Complexes of Bacterial *DD*-Peptidases with Peptidoglycan-Mimetic Ligands: The Substrate Specificity Puzzle. J Mol Biol **381:**383-393.

446. **Nicola G, Tomberg J, Pratt RF, Nicholas RA, Davies C.** 2010. Crystal Structures of Covalent Complexes of Beta-Lactam Antibiotics with *Escherichia coli* Penicillin-Binding Protein 5: Toward an Understanding of Antibiotic Specificity. Biochemistry **49:**8094-8104.

447. **Nicola G, Peddi S, Stefanova M, Nicholas RA, Gutheil WG, Davies C.** 2005. Crystal Structure of *Escherichia coli* Penicillin-Binding Protein 5 Bound to a Tripeptide Boronic Acid Inhibitor: A Role for Ser-110 in Deacylation. Biochemistry **44:**8207-8217.

448. **Nicholas RA, Krings S, Tomberg J, Nicola G, Davies C.** 2003. Crystal Structure of Wild-Type Penicillin-Binding Protein 5 from *Escherichia coli*: Implications for Deacylation of the Acyl-Enzyme Complex. J Biol Chem **278:**52826-52833.

449. **Banerjee S, Pieper U, Kapadia G, Pannell LK, Herzberg O.** 1998. Role of the Omega-Loop in the Activity, Substrate Specificity, and Structure of Class A Beta-Lactamases. Biochemistry **37:**3286-3296.

450. **Brown NG, Horton LB, Huang W, Vongpunsawad S, Palzkill T.** 2011. Analysis of the Functional Contributions of Asn233 in Metallo-Beta-Lactamase IMP-1. Antimicrob Agents Chemother **55:**5696-5702.

451. **Hudzicki J.** 2009. Kirby-Bauer Disc Diffusion Susceptibility Test Protocol.

452. **ChemBioDraw3DUltra.** PerkinElmer, Waltham, Massachusetts, USA. www.cambridgesoft.com.

453. **Gentile I, Maraolo AE, Borgia G.** 2016. What is the Role of the New β-Lactam/β-Lactamase Inhibitors Ceftolozane/Tazobactam and Ceftazidime/Avibactam? Expert Review of Anti-infective Therapy **14:**875-878.

454. **Elewski BE, Aly R, Baldwin SL, González Soto RF, Rich P, Weisfeld M, Wiltz H, Zane LT, Pollak R.** 2015. Efficacy and Safety of Tavaborole Topical Solution, 5%, a Novel Boron-Based Antifungal Agent, for the Treatment of Toenail Onychomycosis: Results from 2 Randomized Phase-III Studies. Journal of the American Academy of Dermatology **73:**62-69.

455. **Trippier PC, McGuigan C.** 2010. Boronic Acids in Medicinal Chemistry: Anticancer, Antibacterial and Antiviral Applications. MedChemComm **1:**183-198.

456. **Nazarian R, Weinberg JM.** 2009. AN-2728, a PDE4 Inhibitor for the Potential Topical Treatment of Psoriasis and Atopic Dermatitis. Curr Opin Investig Drugs **10:**1236-1242.

457. **Mendes RE, Alley MRK, Sader HS, Biedenbach DJ, Jones RN.** 2013. Potency and Spectrum of Activity of AN3365, a Novel Boron-Containing Protein Synthesis Inhibitor, Tested against Clinical Isolates of *Enterobacteriaceae* and Nonfermentative Gram-Negative *Bacilli*. Antimicrob Agents Chemother **57:**2849-2857.

458. **Johnson SL, Pellecchia M.** 2006. Structure- and Fragment-Based Approaches to Protease Inhibition. Curr Top Med Chem **6:**317-329.

459. **Quiñonero D, Garau C, Frontera A, Ballester P, Costa A, Deyà PM.** 2002. Quantification of Aromaticity in Oxocarbons: The Problem of the Fictitious "Nonaromatic" Reference System. Chemistry – A European Journal **8:**433-438.

460. **Rotger C, Soberats B, Quiñonero D, Frontera A, Ballester P, Benet-Buchholz J, Deyà PM, Costa A.** 2008. Crystallographic and Theoretical Evidence of Anion–π and Hydrogen-Bonding Interactions in a Squaramide–Nitrate Salt. Eur J Org Chem **2008:**1864-1868.

461. **Malerich JP, Hagihara K, Rawal VH.** 2008. Chiral Squaramide Derivatives are Excellent Hydrogen Bond Donor Catalysts. J Am Chem Soc **130:**14416-14417.

462. **Sato K, Tawarada R, Seio K, Sekine M.** 2004. Synthesis and Structural Properties of New Oligodeoxynucleotide Analogues Containing a 2′,5′-Internucleotidic Squaryldiamide Linkage Capable of Formation of a Watson–Crick Base Pair with Adenine and a Wobble Base Pair with Guanine at the 3′-Downstream Junction Site. Eur J Org Chem **2004:**2142-2150.

463. **Sato K, Seio K, Sekine M.** 2002. Squaryl Group as a New Mimic of Phosphate Group in Modified Oligodeoxynucleotides: Synthesis and Properties of New Oligodeoxynucleotide Analogues Containing an Internucleotidic Squaryldiamide Linkage. J Am Chem Soc **124:**12715-12724.

464. **Lee C-W, Cao H, Ichiyama K, Rana TM.** 2005. Design and Synthesis of a Novel Peptidomimetic Inhibitor of HIV-1 Tat–TAR Interactions: Squaryldiamide as a New Potential Bioisostere of Unsubstituted Guanidine. Bioorg Med Chem Lett **15:**4243-4246.

465. **Butera JA, Antane MM, Antane SA, Argentieri TM, Freeden C, Graceffa RF, Hirth BH, Jenkins D, Lennox JR, Matelan E, Norton NW, Quagliato D, Sheldon JH, Spinelli W, Warga D, Wojdan A, Woods M.** 2000. Design and SAR of Novel Potassium Channel Openers Targeted for Urge Urinary

Incontinence. 1. N-Cyanoguanidine Bioisosteres Possessing *In Vivo* Bladder Selectivity. J Med Chem **43:**1187-1202.

466. **Gilbert AM, Antane MM, Argentieri TM, Butera JA, Francisco GD, Freeden C, Gundersen EG, Graceffa RF, Herbst D, Hirth BH, Lennox JR, McFarlane G, Norton NW, Quagliato D, Sheldon JH, Warga D, Wojdan A, Woods M.** 2000. Design and SAR of Novel Potassium Channel Openers Targeted for Urge Urinary Incontinence. 2. Selective and Potent Benzylamino Cyclobutenediones. J Med Chem **43:**1203-1214.
467. **Urbahns K, Härter M, Albers M, Schmidt D, Stelte-Ludwig B, Brüggemeier U, Vaupel A, Keldenich J, Lustig K, Tsujishita H, Gerdes C.** 2007. Biphenyls as Potent Vitronectin Receptor Antagonists. Part 3: Squaric Acid Amides. Bioorg Med Chem Lett **17:**6151-6154.
468. **Xie YF, Lake K, Ligsay K, Komandla M, Sircar I, Nagarajan G, Li J, Xu K, Parise J, Schneider L, Huang D, Liu J, Dines K, Sakurai N, Barbosa M, Jack R.** 2007. Structure-Activity Relationships of Novel, Highly Potent, Selective, and Orally Active CCR1 Antagonists. Bioorg Med Chem Lett **17:**3367-3372.
469. **McCleland BW, Davis RS, Palovich MR, Widdowson KL, Werner ML, Burman M, Foley JJ, Schmidt DB, Sarau HM, Rogers M, Salyers KL, Gorycki PD, Roethke TJ, Stelman GJ, Azzarano LM, Ward KW, Busch-Petersen J.** 2007. Comparison of *N*,*N*'-Diarylsquaramides and *N*,*N*'-Diarylureas as Antagonists of the CXCR2 Chemokine Receptor. Bioorg Med Chem Lett **17:**1713-1717.
470. **Fan E, Zhang Z, Minke WE, Hou Z, Verlinde CLMJ, Hol WGJ.** 2000. High-Affinity Pentavalent Ligands of *Escherichia coli* Heat-Labile Enterotoxin by Modular Structure-Based Design. J Am Chem Soc **122:**2663-2664.
471. **Pickens JC, Mitchell DD, Liu J, Tan X, Zhang Z, Verlinde CL, Hol WG, Fan E.** 2004. Nonspanning Bivalent Ligands as Improved Surface Receptor Binding Inhibitors of the Cholera Toxin B Pentamer. Chem Biol **11:**1205-1215.
472. **Merritt EA, Zhang Z, Pickens JC, Ahn M, Hol WG, Fan E.** 2002. Characterization and Crystal Structure of a High-Affinity Pentavalent Receptor-Binding Inhibitor for Cholera Toxin and *E. coli* Heat-Labile Enterotoxin. J Am Chem Soc **124:**8818-8824.
473. **Costa TA, Rotger MC, Fernandez de Mattos S, Villalonga P.** 2010. Use of Cyclosquaramide Compounds as Anti-Tumour Agents. WO2010066933 A1.
474. **Castelhano AL, Crew A, Dong H, Li AH, Qiu L, Smith A, Tardibono L, Zhang T.** 2010. (Arylamidoaryl)squaramide Compounds. US7829717 B2.
475. **Busschaert N, Park S-H, Baek K-H, Choi YP, Park J, Howe ENW, Hiscock JR, Karagiannidis LE, Marques I, Félix V, Namkung W, Sessler JL, Gale**

PA, Shin I. 2017. A Synthetic Ion Transporter that Disrupts Autophagy and Induces Apoptosis by Perturbing Cellular Chloride Concentrations. Nat Chem **9:**667-675.

476. **Quintana M, Alegre-Requena JV, Marques-Lopez E, Herrera RP, Triola G.** 2016. Squaramides with Cytotoxic Activity Against Human Gastric Carcinoma Cells HGC-27: Synthesis and Mechanism of Action. MedChemComm **7:**550-561.
477. **Sampedro A, Villalonga-Planells R, Vega M, Ramis G, Fernández de Mattos S, Villalonga P, Costa A, Rotger C.** 2014. Cell Uptake and Localization Studies of Squaramide Based Fluorescent Probes. Bioconj Chem **25:**1537-1546.
478. **Kitson S.** 2017. Squaryl Molecular Metaphors – Application to Rational Drug Design and Imaging Agents. J Diagn Imaging Ther **4:**35-75.
479. **Buurman ET, Foulk MA, Gao N, Laganas VA, McKinney DC, Moustakas DT, Rose JA, Shapiro AB, Fleming PR.** 2012. Novel Rapidly Diversifiable Antimicrobial RNA Polymerase Switch Region Inhibitors with Confirmed Mode of Action in *Haemophilus influenzae*. J Bacteriol **194:**5504-5512.
480. **Ma C, Yang X, Lewis PJ.** 2016. Bacterial Transcription as a Target for Antibacterial Drug Development. Microbiol Mol Biol Rev **80:**139-160.
481. **Tantry SJ, Markad SD, Shinde V, Bhat J, Balakrishnan G, Gupta AK, Ambady A, Raichurkar A, Kedari C, Sharma S, Mudugal NV, Narayan A, Naveen Kumar CN, Nanduri R, Bharath S, Reddy J, Panduga V, Prabhakar KR, Kandaswamy K, Saralaya R, Kaur P, Dinesh N, Guptha S, Rich K, Murray D, Plant H, Preston M, Ashton H, Plant D, Walsh J, Alcock P, Naylor K, Collier M, Whiteaker J, McLaughlin RE, Mallya M, Panda M, Rudrapatna S, Ramachandran V, Shandil R, Sambandamurthy VK, Mdluli K, Cooper CB, Rubin H, Yano T, Iyer P, Narayanan S, Kavanagh S, Mukherjee K, Balasubramanian V, et al.** 2017. Discovery of Imidazo[1,2-a]pyridine Ethers and Squaramides as Selective and Potent Inhibitors of Mycobacterial Adenosine Triphosphate (ATP) Synthesis. J Med Chem **60:**1379-1399.
482. **Onaran MB, Comeau AB, Seto CT.** 2005. Squaric Acid-Based Peptidic Inhibitors of Matrix Metalloprotease-1. J Org Chem **70:**10792-10802.
483. **Charton J, Déprez BP, Déprez-Poulain RF.** 2008. Synthesis of a 200-Member Library of Squaric Acid *N*-Hydroxylamide Amides. Bioorg Med Chem Lett **18:**4968-4971.
484. **European Lead Factory.** www.europeanleadfactory.eu.
485. **Ian Storer R, Aciro C, Jones LH.** 2011. Squaramides: Physical Properties, Synthesis and Applications. Chem Soc Rev **40:**2330-2346.

486. **Marciano DC, Brown NG, Palzkill T.** 2009. Analysis of the Plasticity of Location of the Arg244 Positive Charge within the Active Site of the TEM-1 Beta-Lactamase. Protein Sci **18:**2080-2089.

487. **Bebrone C, Lassaux P, Vercheval L, Sohier JS, Jehaes A, Sauvage E, Galleni M.** 2010. Current Challenges in Antimicrobial Chemotherapy: Focus on β-Lactamase Inhibition. Drugs **70:**651-679.

488. **Grant EB, Guiadeen D, Baum EZ, Foleno BD, Jin H, Montenegro DA, Nelson EA, Bush K, Hlasta DJ.** 2000. The Synthesis and SAR of Rhodanines as Novel Class C Beta-Lactamase Inhibitors. Bioorg Med Chem Lett **10:**2179-2182.

489. **Zervosen A, Lu WP, Chen Z, White RE, Demuth TP, Jr., Frere JM.** 2004. Interactions Between Penicillin-Binding Proteins (PBPs) and Two Novel Classes of PBP Inhibitors, Arylalkylidene Rhodanines and Arylalkylidene Iminothiazolidin-4-ones. Antimicrob Agents Chemother **48:**961-969.

490. **Zervosen A, Sauvage E, Frere JM, Charlier P, Luxen A.** 2012. Development of New Drugs for an Old Target: The Penicillin Binding Proteins. Molecules **17:**12478-12505.

491. 2010. Probe Reports from the NIH Molecular Libraries Program. National Center for Biotechnology Information (US), Bethesda (MD).

492. **Spencer J, Read J, Sessions RB, Howell S, Blackburn GM, Gamblin SJ.** 2005. Antibiotic Recognition by Binuclear Metallo-Beta-Lactamases Revealed by X-ray Crystallography. J Am Chem Soc **127:**14439-14444.

493. 2016. Tackling Drug-Resistant Infections Globally: Final Report and Recommendations. O'Neill J (ed), Resistance RoA.

494. **Magotti P, Bauer I, Igarashi M, Babagoli M, Marotta R, Piomelli D, Garau G.** 2015. Structure of Human *N*-Acylphosphatidylethanolamine-Hydrolyzing Phospholipase D: Regulation of Fatty Acid Ethanolamide Biosynthesis by Bile Acids. Structure **23:**598-604.

495. **Lee HY, Xu Y, Huang Y, Ahn AH, Auburger GW, Pandolfo M, Kwiecinski H, Grimes DA, Lang AE, Nielsen JE, Averyanov Y, Servidei S, Friedman A, Van Bogaert P, Abramowicz MJ, Bruno MK, Sorensen BF, Tang L, Fu YH, Ptacek LJ.** 2004. The Gene for Paroxysmal Non-Kinesigenic Dyskinesia Encodes an Enzyme in a Stress Response Pathway. Hum Mol Genet **13:**3161-3170.

496. **Garau G, García-Sáez I, Bebrone C, Anne C, Mercuri P, Galleni M, Frère J-M, Dideberg O.** 2004. Update of the Standard Numbering Scheme for Class B β-Lactamases. Antimicrob Agents Chemother **48:**2347-2349.

497. **Daiyasu H, Osaka K, Ishino Y, Toh H.** 2001. Expansion of the Zinc Metallo-Hydrolase Family of the β-Lactamase Fold. FEBS Lett **503:**1-6.

498. **Wang R.** 2012. Physiological Implications of Hydrogen Sulfide: A Whiff Exploration that Blossomed. Physiol Rev **92:**791-896.

499. **Chen X, Jhee KH, Kruger WD.** 2004. Production of the Neuromodulator H_2S by Cystathionine Beta-Synthase via the Condensation of Cysteine and Homocysteine. J Biol Chem **279:**52082-52086.

500. **Renga B.** 2011. Hydrogen Sulfide Generation in Mammals: The Molecular Biology of Cystathionine-Beta-Synthase (CBS) and Cystathionine-Gamma-Lyase (CSE). Inflamm Allergy Drug Targets **10:**85-91.

501. **Shibuya N, Tanaka M, Yoshida M, Ogasawara Y, Togawa T, Ishii K, Kimura H.** 2009. 3-Mercaptopyruvate Sulfurtransferase Produces Hydrogen Sulfide and Bound Sulfane Sulfur in the Brain. Antioxid Redox Signal **11:**703-714.

502. **Heinrich TA, da Silva RS, Miranda KM, Switzer CH, Wink DA, Fukuto JM.** 2013. Biological Nitric Oxide Signalling: Chemistry and Terminology. Br J Pharmacol **169:**1417-1429.

503. **Kim HP, Ryter SW, Choi AM.** 2006. CO as a Cellular Signaling Molecule. Annu Rev Pharmacol Toxicol **46:**411-449.

504. **KIMURA Y, KIMURA H.** 2004. Hydrogen Sulfide Protects Neurons from Oxidative Stress. FASEB J **18:**1165-1167.

505. **Zhao W, Zhang J, Lu Y, Wang R.** 2001. The Vasorelaxant Effect of H_2S as a Novel Endogenous Gaseous K_{ATP} Channel Opener. EMBO J **20:**6008-6016.

506. **Abe K, Kimura H.** 1996. The Possible Role of Hydrogen Sulfide as an Endogenous Neuromodulator. J Neurosci **16:**1066-1071.

507. **Bełtowski J.** 2015. Hydrogen Sulfide in Pharmacology and Medicine – An Update. Pharmacol Rep **67:**647-658.

508. **Silva MS, Barata L, Ferreira AE, Romao S, Tomas AM, Freire AP, Cordeiro C.** 2008. Catalysis and Structural Properties of *Leishmania infantum* Glyoxalase II: Trypanothione Specificity and Phylogeny. Biochemistry **47:**195-204.

509. **Jiang J, Chan A, Ali S, Saha A, Haushalter KJ, Lam W-LM, Glasheen M, Parker J, Brenner M, Mahon SB, Patel HH, Ambasudhan R, Lipton SA, Pilz RB, Boss GR.** 2016. Hydrogen Sulfide - Mechanisms of Toxicity and Development of an Antidote. Sci Rep **6:**20831.

510. **Ubuka T.** 2002. Assay Methods and Biological Roles of Labile Sulfur in Animal Tissues. J Chromatogr B **781:**227-249.

511. **Shen X, Peter EA, Bir S, Wang R, Kevil CG.** 2012. Analytical Measurement of Discrete Hydrogen Sulfide Pools in Biological Specimens. Free Radical Biol Med **52:**2276-2283.

512. **Stein A, Bailey SM.** 2013. Redox Biology of Hydrogen Sulfide: Implications for Physiology, Pathophysiology, and Pharmacology. Redox Biology **1:**32-39.

513. **Cooper CE, Brown GC.** 2008. The Inhibition of Mitochondrial Cytochrome Oxidase by the Gases Carbon Monoxide, Nitric Oxide, Hydrogen Cyanide and Hydrogen Sulfide: Chemical Mechanism and Physiological Significance. J Bioenerg Biomembr **40:**533-539.

514. **Nicholls P, Marshall DC, Cooper CE, Wilson MT.** 2013. Sulfide Inhibition of and Metabolism by Cytochrome C Oxidase. Biochem Soc Trans **41:**1312-1316.

515. **Goubern M, Andriamihaja M, Nubel T, Blachier F, Bouillaud F.** 2007. Sulfide, the First Inorganic Substrate for Human Cells. FASEB J **21:**1699-1706.

516. **Modis K, Coletta C, Erdelyi K, Papapetropoulos A, Szabo C.** 2013. Intramitochondrial Hydrogen Sulfide Production by 3-Mercaptopyruvate Sulfurtransferase Maintains Mitochondrial Electron Flow and Supports Cellular Bioenergetics. FASEB J **27:**601-611.

517. **Szabo C, Ransy C, Modis K, Andriamihaja M, Murghes B, Coletta C, Olah G, Yanagi K, Bouillaud F.** 2014. Regulation of Mitochondrial Bioenergetic Function by Hydrogen Sulfide. Part I. Biochemical and Physiological Mechanisms. Br J Pharmacol **171:**2099-2122.

518. **Truong DH, Eghbal MA, Hindmarsh W, Roth SH, O'Brien PJ.** 2006. Molecular Mechanisms of Hydrogen Sulfide Toxicity. Drug Metab Rev **38:**733-744.

519. **Attene-Ramos MS, Wagner ED, Gaskins HR, Plewa MJ.** 2007. Hydrogen Sulfide Induces Direct Radical-Associated DNA Damage. Mol Cancer Res **5:**455-459.

520. **Eghbal MA, Pennefather PS, O'Brien PJ.** 2004. H_2S Cytotoxicity Mechanism Involves Reactive Oxygen Species Formation and Mitochondrial Depolarisation. Toxicology **203:**69-76.

521. **Libiad M, Yadav PK, Vitvitsky V, Martinov M, Banerjee R.** 2014. Organization of the Human Mitochondrial Hydrogen Sulfide Oxidation Pathway. J Biol Chem **289:**30901-30910.

522. **Whiteman M, Le Trionnaire S, Chopra M, Fox B, Whatmore J.** 2011. Emerging Role of Hydrogen Sulfide in Health and Disease: Critical Appraisal of Biomarkers and Pharmacological Tools. Clin Sci (Lond) **121:**459-488.

523. **Paul BD, Snyder SH.** 2012. H_2S Signalling through Protein Sulfhydration and Beyond. Nat Rev Mol Cell Biol **13:**499-507.

524. **Paul BD, Snyder SH.** H_2S: A Novel Gasotransmitter that Signals by Sulfhydration. Trends Biochem Sci **40:**687-700.

525. **Burlina A, Zacchello F, Dionisi-Vici C, Bertini E, Sabetta G, Bennet MJ, Hale DE, Schmidt-Sommerfeld E, Rinaldo P.** 1991. New Clinical Phenotype of Branched-Chain Acyl-CoA Oxidation Defect. Lancet **338:**1522-1523.

526. **Joseph CA, Maroney MJ.** 2007. Cysteine Dioxygenase: Structure and Mechanism. Chem Commun **28:**3338-3349.

527. **Ye S, Wu Xa, Wei L, Tang D, Sun P, Bartlam M, Rao Z.** 2007. An Insight into the Mechanism of Human Cysteine Dioxygenase: Key Roles of the Thioether-Bonded Tyrosine-Cysteine Cofactor. J Biol Chem **282:**3391-3402.

528. **Roach PL, Clifton IJ, Hensgens CMH, Shibata N, Schofield CJ, Hajdu J, Baldwin JE.** 1997. Structure of Isopenicillin N Synthase Complexed with Substrate and the Mechanism of Penicillin Formation. Nature **387:**827-830.

529. **Long AJ, Clifton IJ, Roach PL, Baldwin JE, Rutledge PJ, Schofield CJ.** 2005. Structural Studies on the Reaction of Isopenicillin N Synthase with the Truncated Substrate Analogues Delta-(L-Alpha-Aminoadipoyl)-L-Cysteinyl-Glycine and Delta-(L-Alpha-Aminoadipoyl)-L-Cysteinyl-D-Alanine. Biochemistry **44:**6619-6628.

530. **Driggers CM, Cooley RB, Sankaran B, Hirschberger LL, Stipanuk MH, Karplus PA.** 2013. Cysteine Dioxygenase Structures from pH 4 to 9: Consistent Cys-Persulfenate Formation at Intermediate pH and a Cys-Bound Enzyme at Higher pH. J Mol Biol **425:**3121-3136.

531. **Sattler SA, Wang X, Lewis KM, DeHan PJ, Park C-M, Xin Y, Liu H, Xian M, Xun L, Kang C.** 2015. Characterizations of Two Bacterial Persulfide Dioxygenases of the Metallo-β-lactamase Superfamily. J Biol Chem **290:**18914-18923.

532. **Liu H, Xin Y, Xun L.** 2014. Distribution, Diversity, and Activities of Sulfur Dioxygenases in Heterotrophic Bacteria. Appl Environ Microbiol **80:**1799-1806.

533. **Kabil O, Banerjee R.** 2012. Characterization of Patient Mutations in Human Persulfide Dioxygenase (ETHE1) Involved in H_2S Catabolism. J Biol Chem **287:**44561-44567.

534. **Mitsunori O, Isamu I.** 1988. A New Deprotection Method for Levulinyl Protecting Groups under Neutral Conditions. Chem Lett **17:**585-588.

535. **Choi MG, Hwang J, Eor S, Chang S-K.** 2010. Chromogenic and Fluorogenic Signaling of Sulfite by Selective Deprotection of Resorufin Levulinate. Org Lett **12:**5624-5627.

536. **Ma X, Liu C, Shan Q, Wei G, Wei D, Du Y.** 2013. A Fluorescein-Based Probe with High Selectivity and Sensitivity for Sulfite Detection in Aqueous Solution. Sensors Actuators B: Chem **188:**1196-1200.

537. **Yu C, Luo M, Zeng F, Wu S.** 2012. A Fast-Responding Fluorescent Turn-On Sensor for Sensitive and Selective Detection of Sulfite Anions. Anal Methods **4:**2638-2640.

538. **Xie H, Zeng F, Yu C, Wu S.** 2013. A Polylysine-Based Fluorescent Probe for Sulfite Anion Detection in Aqueous Media *via* Analyte-Induced Charge Generation and Complexation. Polym Chem **4:**5416-5424.

539. **Paritala H, Carroll KS.** 2013. A Continuous Spectrophotometric Assay for APS Reductase Activity with Sulfite-Selective Probes. Anal Biochem **440:**32-39.

540. **Hashwa F, Pfennig N.** 1972. The Reductive Enzymatic Cleavage of Thiosulfate. Methods and Applictions. Arch Mikrobiol **81:**36-44.

541. **Maret W, Krężel A.** 2007. Cellular Zinc and Redox Buffering Capacity of Metallothionein/Thionein in Health and Disease. Mol Med **13:**371-375.

542. **Messenger AJM, Barclay R.** 1983. Bacteria, Iron and Pathogenicity. Biochemical Education **11:**54-63.

543. **Ratledge C, Dover LG.** 2000. Iron Metabolism in Pathogenic Bacteria. Annu Rev Microbiol **54:**881-941.

544. **Busschaert N, Elmes RBP, Czech DD, Wu X, Kirby IL, Peck EM, Hendzel KD, Shaw SK, Chan B, Smith BD, Jolliffe KA, Gale PA.** 2014. Thiosquaramides: pH switchable anion transporters. Chemical science (Royal Society of Chemistry : 2010) **5:**3617-3626.

545. **Elings W, Tassoni R, van der Schoot SA, Luu W, Kynast JP, Dai L, Blok AJ, Timmer M, Florea BI, Pannu NS, Ubbink M.** 2017. Phosphate Promotes the Recovery of Mycobacterium tuberculosis beta-Lactamase from Clavulanic Acid Inhibition. **56:**6257-6267.

546. **Wang X, Minasov G, Shoichet BK.** 2002. Evolution of an Antibiotic Resistance Enzyme Constrained by Stability and Activity Trade-offs. J Mol Biol **320:**85-95.

547. **Na J-H, Cha S-S.** 2016. Structural Basis for the Extended Substrate Spectrum of AmpC BER and Structure-Guided Discovery of the Inhibition Activity of Citrate Against the Class C β-Lactamases AmpC BER and CMY-10. Acta Crystallogr D Biol Crystallogr **72:**976-985.

548. ApE: A Plasmid Editor, v1.06. www.biologylabs.utah.edu/jorgensen/wayned/ape.

549. **Winn MD, Ballard CC, Cowtan KD, Dodson EJ, Emsley P, Evans PR, Keegan RM, Krissinel EB, Leslie AGW, McCoy A, McNicholas SJ, Murshudov GN, Pannu NS, Potterton EA, Powell HR, Read RJ, Vagin A, Wilson KS.** 2011. Overview of the CCP4 Suite and Current Developments. Acta Crystallogr Sect D **67:**235-242.

550. **Bunkoczi G, Echols N, McCoy AJ, Oeffner RD, Adams PD, Read RJ.** 2013. Phaser.MRage: Automated Molecular Replacement. Acta Crystallogr Sect D **69:**2276-2286.

551. **Hornsey M, Phee L, Stubbings W, Wareham DW.** 2013. *In Vitro* Activity of the Novel Monosulfactam BAL30072 Alone and in Combination with Meropenem Versus a Diverse Collection of Important Gram-Negative Pathogens. Int J Antimicrob Agents **42:**343-346.

552. **CLSI.** 2012. Methods for Dilution Antimicrobial Susceptibility Tests for Bacteria that Grow Aerobically, Approved Standard, 9th ed. CLSI document M07-A9.

Appendix 1: Kirby-Bauer Disc Diffusion Assays

Supplemental Disc Diffusion Test Images: Plate Plan

CAR: Carbenacillin PRL: Piperacillin TZP: Piperacillin/Tazobactam KF: Cephalothin

C/T: Ceftolazone/Tazobactam

TEM: Temocillin MEL: Mecillinam CTX: Cefotaxime CAZ: Ceftazidime

SAM:Ampicillin/Sulbactam

CPT: Ceftaroline FEP: Cefipime AZT: Aztreonam IPM: Imipenem

CAZ/AVI: Ceftazidime/Avibactam

AUG: Amoxicillin/Clavulanate ERT: Ertapenem FOX: Cefoxitin MEM: Meropenem

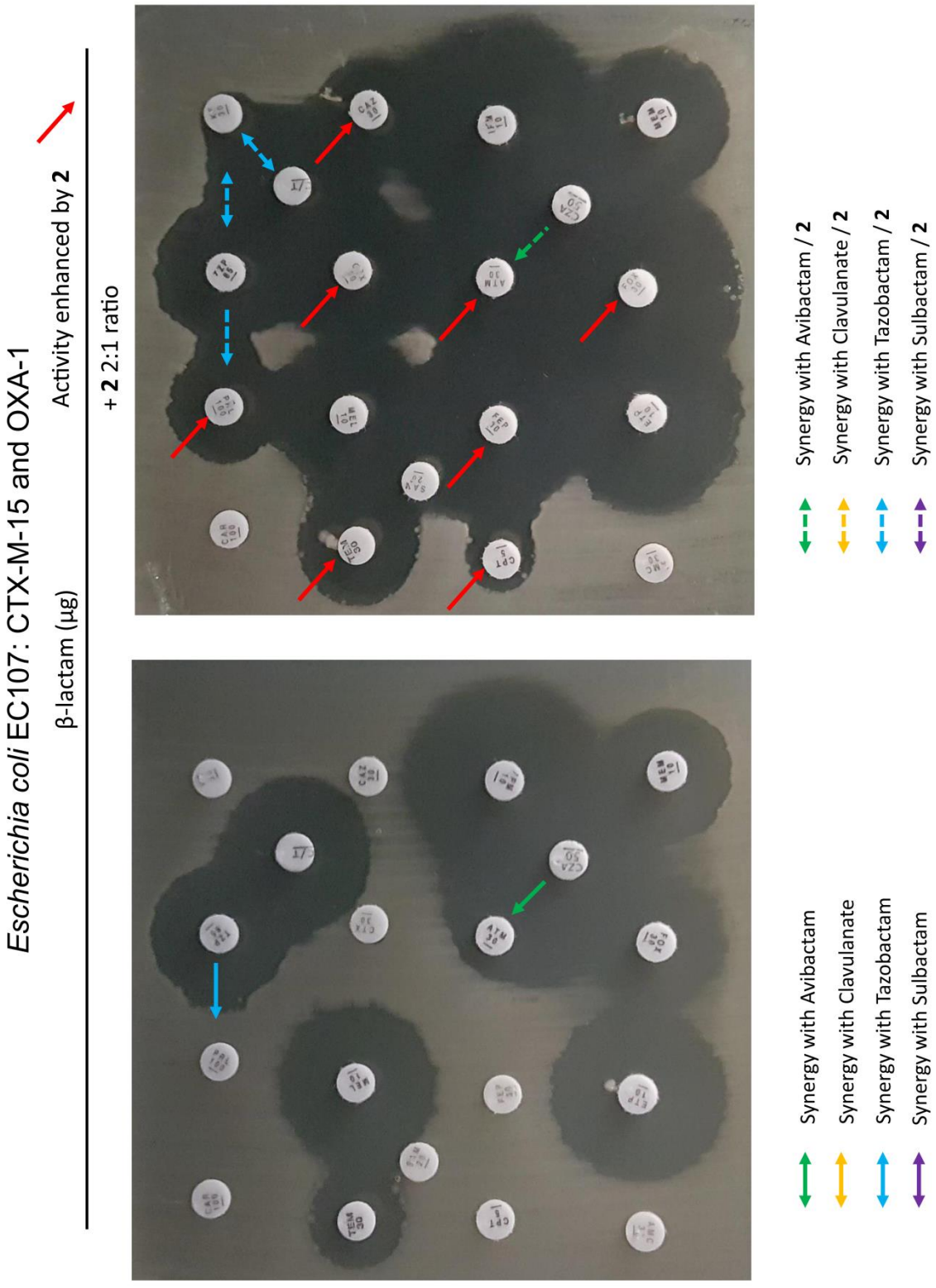
Escherichia coli EC107: CTX-M-15 and OXA-1
β-lactam (μg)
Activity enhanced by **2**
+ **2** 2:1 ratio
Synergy with Avibactam / **2**
Synergy with Clavulanate / **2**
Synergy with Tazobactam / **2**
Synergy with Sulbactam / **2**
Synergy with Avibactam
Synergy with Clavulanate
Synergy with Tazobactam
Synergy with Sulbactam

Escherichia coli EC114: TEM-1, CTX-M-15 and OXA-1
β-lactam (μg)
Activity enhanced by **2**
+ **2** 2:1 ratio
Synergy with Avibactam
Synergy with Clavulanate
Synergy with Tazobactam
Synergy with Sulbactam
Synergy with Avibactam / **2**
Synergy with Clavulanate / **2**
Synergy with Tazobactam / **2**
Synergy with Sulbactam / **2**

Escherichia coli EC86: CTX-M-15,CMY-4 and OXA-181
β-lactam (μg)
Activity enhanced by **2**
+ **2** 2:1 ratio
Synergy with Avibactam
Synergy with Clavulanate
Synergy with Tazobactam
Synergy with Sulbactam
Synergy with Avibactam / **2**
Synergy with Clavulanate / **2**
Synergy with Tazobactam / **2**
Synergy with Sulbactam / **2**

Escherichia coli EC113: CTX-M-27
β-lactam (μg)
Activity enhanced by **2**
+ **2** 2:1 ratio
Synergy with Avibactam / **2**
Synergy with Clavulanate / **2**
Synergy with Tazobactam / **2**
Synergy with Sulbactam / **2**
Synergy with Avibactam
Synergy with Clavulanate
Synergy with Tazobactam
Synergy with Sulbactam

Klebsiella pneumoniae KP15: TEM-1, SHV-11, KPC-2
β-lactam (μg)
Activity enhanced by **2**
+ **2** 2:1 ratio
Synergy with Avibactam
Synergy with Clavulanate
Synergy with Tazobactam
Synergy with Sulbactam
Synergy with Avibactam / **2**
Synergy with Clavulanate / **2**
Synergy with Tazobactam / **2**
Synergy with Sulbactam / **2**

Klebsiella pneumoniae KP41:TEM-1, SHV-1,5,11, CTX-M-15, OXA-232
β-lactam (μg)
Activity enhanced by **2**
+ **2** 2:1 ratio
Synergy with Avibactam
Synergy with Clavulanate
Synergy with Tazobactam
Synergy with Sulbactam
Synergy with Avibactam / **2**
Synergy with Clavulanate / **2**
Synergy with Tazobactam / **2**
Synergy with Sulbactam / **2**

Klebsiella pneumoniae KP58: SHV-11, VIM-4
β-lactam (μg)
Activity enhanced by **2**
+ **2** 2:1 ratio
Synergy with Avibactam / **2**
Synergy with Clavulanate / **2**
Synergy with Tazobactam / **2**
Synergy with Sulbactam / **2**
Synergy with Avibactam
Synergy with Clavulanate
Synergy with Tazobactam
Synergy with Sulbactam

Providencia stuartii PS71: TEM-1, SHV-5, VEB-1, VIM-1
β-lactam (μg)
Activity enhanced by **2**
+ **2** 2:1 ratio
Synergy with Avibactam
Synergy with Clavulanate
Synergy with Tazobactam
Synergy with Sulbactam
Synergy with Avibactam / **2**
Synergy with Clavulanate / **2**
Synergy with Tazobactam / **2**
Synergy with Sulbactam / **2**

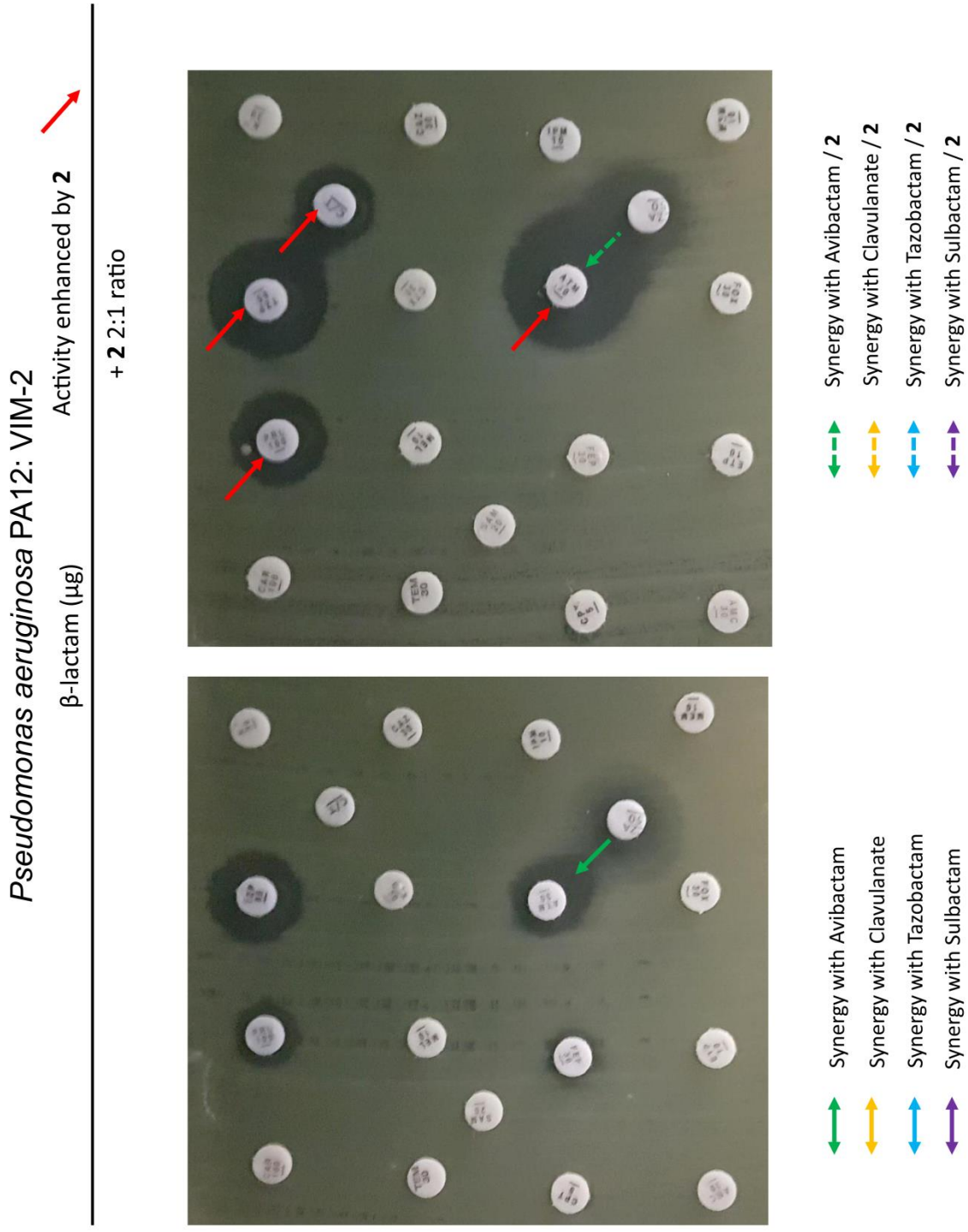
Pseudomonas aeruginosa PA12: VIM-2
β-lactam (μg)
Activity enhanced by **2**
+ **2** 2:1 ratio
Synergy with Avibactam
Synergy with Clavulanate
Synergy with Tazobactam
Synergy with Sulbactam
Synergy with Avibactam / **2**
Synergy with Clavulanate / **2**
Synergy with Tazobactam / **2**
Synergy with Sulbactam / **2**

Acinetobacter baumannii AB14: OXA-51, OXA-23
β-lactam (μg)
Activity enhanced by **2**
+ **2** 2:1 ratio
Synergy with Avibactam
Synergy with Clavulanate
Synergy with Tazobactam
Synergy with Sulbactam
Synergy with Avibactam / **2**
Synergy with Clavulanate / **2**
Synergy with Tazobactam / **2**
Synergy with Sulbactam / **2**